The Dissertation Committee for Gabrielle Antoinette Russo Certifies that this is the approved version of the following dissertation:

FUNCTIONAL MORPHOLOGY OF MAMMALIAN SACRA AND CAUDAL VERTEBRAE: IMPLICATIONS FOR TAIL LOSS AND POSITIONAL BEHAVIORS IN EXTINCT PRIMATES

Committee:

Liza Shapiro, Supervisor

E. Christopher Kirk

John Kappelman

Roberto Fajardo

Laurie Godfrey

Carol Ward

FUNCTIONAL MORPHOLOGY OF MAMMALIAN SACRA AND CAUDAL VERTEBRAE: IMPLICATIONS FOR TAIL LOSS AND POSITIONAL BEHAVIORS IN EXTINCT PRIMATES

by

Gabrielle Antoinette Russo, B.A.; M.A.

Dissertation

Presented to the Faculty of the Graduate School of

The University of Texas at Austin

in Partial Fulfillment

of the Requirements

for the Degree of

Doctor of Philosophy

The University of Texas at Austin

August 2013

Dedication

For my parents, JoAnn, Joseph, and Martha

Acknowledgements

I extend my deepest appreciation to my advisor Liza Shapiro. I am grateful for her patience, kindness, support, honesty, and friendship over the past 5 years. To her I owe the substantial improvement of my writing style, careful attention to detail, and love for spinal functional morphology. I look forward to collaborating on future "dream team" projects. I thank Chris Kirk for encouraging me to incorporate the comparative method into my research, Laurie Godfrey for sharing with me her excitement and expertise about subfossil lemurs, Roberto Fajardo for his patience and assistance while I learned about trabecular bone structure and analyses, Carol Ward for sharing her knowledge of spinal anatomy and Miocene hominoids, and John Kappelman for asking the big picture questions.

I can't imagine my time at UT without the friendship of Amber N. Heard-Booth, Andrew Barr, Brett Nachman, Carrie Veilleux, Angel Zeininger, and the other UT graduate students. I feel fortunate to have been surrounded by a group of such fun, talented and hard-working folks.

Matt Colbert and Jessie Maisano were gracious hosts, and provided me with months of time and space (and an endless supply of candy) in the UTCT computer lab to analyze scans.

Thanks are also owed to Bill Stanley (FMNH), Eileen Westwig and Gisselle Garcia (AMNH), Linda Gordon and Darrin Lunde (NMNH), Loic Costeur (NHMB), Laura Nightengale (TARL) and Gregg Gunnell (DUPC) for providing access to the museum collections in their care. Special thanks are owed to the Naturhistorisches

Museum Basel, for generously providing me with the *Oreopithecus* and *Epipliopithecus* sacral scans, and to Masato Nakatsukasa who provided me with the *Nacholapithecu*s scans. I also thank Vanesa De Pietri, for her assistance during my time in Basel.

This research was supported by the National Science Foundation grant BCS 1156016, A Leakey Foundation General Research Grant, and two College of Liberal Arts Graduate Research Fellowships from The University of Texas at Austin.

.

Functional Morphology of Mammalian Sacra and Caudal Vertebrae: Implications for tail loss and positional behaviors in extinct primates

Gabrielle Antoinette Russo, Ph.D.

The University of Texas at Austin, 2013

Supervisor: Liza Shapiro

All living hominoids are characterized by taillessness and adaptations to orthograde (upright) trunk posture. Accordingly, these features have importance for our understanding of ape origins, evolutionary relationships and positional behaviors. Despite extensive study of the hominoid postcranial skeleton, researchers continue to face difficulty identifying taillessness and orthogrady from fossil material. In part, difficulties persist because although the Miocene fossil record indicates that the evolution of tail loss and orthogrady was decoupled, previous research has focused primarily on how the skeletal anatomy of extinct apes resembles that of living apes, in which these traits appear in conjunction. The remarkable diversity in tail lengths and positional behaviors exhibited by other mammals presents a valuable opportunity to employ the strength of the comparative method for testing functional hypotheses.

The goal of this dissertation is to identify anatomical correlates of tail length and positional behaviors from sacral and caudal vertebral morphology among primates and other mammals in three studies. The first study examines the relationship between trabecular structure in the first sacral vertebra and positional behaviors (N= 78 primates).

The second study quantifies aspects of internal (N=78 primates) and external (N= 472 mammals) sacral anatomy for correlates of relative tail length. The third study evaluates the functional morphology of caudal vertebrae among nonprehensile-tailed primates and other mammals that vary in relative tail length, offering additional insight into the anatomy associated with tail loss (N=333).

The relationship between trabecular structure in the proximal sacrum and positional behaviors among living primates is somewhat unclear. Some trabecular parameters in the distal sacrum appear to have a relationship with tail length. Results support the functional links between previously and newly defined metrics from the external morphology of sacra and caudal vertebrae, and relative tail length, among primates and other mammals. Identified anatomical correlates from the extant primate sample are used to reconstruct the tail lengths of extinct primates. From the sacral data, *Proconsul* is reconstructed as tailless, *Archaeolemur* likely possessed a long tail, and *Palaeopropithecus*, *Megaladapis* and *Epipliopithecus* had short tails. From the caudal vertebrae data, *Archaeolemur* is reconstructed as possessing a long tail and *Palaeopropithecus* is reconstructed as having a short tail.

Table of Contents

List of Tables

List of Figures

Chapter 1: Introduction

INTRODUCTION

The spine is the structural core of the body and links together the head, arms, legs, and tail (or coccyx). Among living primates, the spine exhibits prominent morphological and functional variation (e.g., Shapiro, 1993a, 2007; Shapiro and Simons, 2002; Shapiro et al., 2005). Evaluation of how spinal anatomy varies among living primates has the potential to inform anatomical and behavioral reconstructions of extinct primates. Such an endeavor is of particular importance to physical anthropologists as fundamental shifts in vertebral anatomy throughout the course of primate evolution are often associated with the evolutionary origin of new primate groups and novel adaptations.

The dissertation study presented here investigates the fundamental shifts in spinal anatomy that occurred during the course of hominoid (apes and humans) evolution, including the loss of an external tail and adoption of more orthograde (upright) trunk postures and locomotion. In contrast to monkeys, all living hominoids lack external tails. Thus, it is assumed that taillessness also characterized all extinct hominoids (Ward et al., 1991; Fleagle, 2013). Therefore, tail loss is a key feature marking the origins of the hominoid clade. Also in contrast to monkeys, which exhibit horizontal (pronograde) trunk posture, living hominoids share adaptations to more upright (orthograde) positional behaviors. Notably, not all extinct apes exhibit orthograde trunk postures (e.g., *Nacholapithecus kerioi*; Nakatsukasa and Kunimatsu, 2009), but those that do are presumably most closely related to living apes (Pilbeam and Young, 2004). The adoption of more orthograde positional behaviors thus marks the evolutionary appearance of apes

of a modern aspect (i.e., crown hominoids) (Keith, 1923; Benefit and McCrossin, 1995; Pilbeam and Young, 2004; but see Larson, 1998).

Though taillessness and adaptations to orthograde trunk posture are features of the postcranial axial skeleton shared by living apes and humans, evidence from the Miocene fossil record indicates that their evolution was probably decoupled. Tail loss may have appeared first, in the context of pronograde posture, and before the adoption of modern ape-like orthograde posture and locomotion (e.g., *Nacholapithecus kerioi*, Nakatsukasa and Kunimatsu, 2009). Moreover, the positional behaviors of extinct apes were probably characterized by combinations of posture and locomotion not found in living apes (Rose, 1993; Moyà-Solà et al., 2004). Nonetheless, previous research seeking to attribute tail lengths and orthograde positional behaviors to extinct hominoids has focused primarily on examining the extent to which their postcranial axial anatomy resembles that of living apes, in which these traits appear in conjunction.

Taken collectively, there are a number of reasons why the approach this study takes to identify correlates of tail loss and orthograde posture departs from previous works. This study examines the sacrum, a much understudied skeletal element. The sacrum occupies a functionally important anatomical position as part of both the vertebral column and pelvis, and serves as the tail's sole bony link to the rest of the body, making it ideal for studying tail length and posture. Moreover, the sacrum is preserved for a number of extinct primates (e.g., *Proconsul, Nacholapithecus, Epipliopithecus, Oreopithecus,* subfossil lemurs). However, perhaps because the sacrum's irregular and complex shape makes its anatomy difficult to quantify (Figure 1.1), sacral functional morphology is

poorly understood. The methodology employed in this study addresses this issue by drawing from both external and internal (e.g., trabecular bone) bony morphological analyses. Using basic biomechanical principles and the results of past research on vertebrae in other regions of the spine, the study delineates specific expectations for how sacral anatomy should relate to trunk posture, locomotion and tail length. Additionally, because bone's internal architecture responds to dynamic loading over an individual's lifetime (Ruff et al., 2006), the use of high resolution and micro- computed tomography scanning to quantify trabecular bone parameters permits analysis of more nuanced morphology associated with the forces induced by tail movement and positional behaviors than can be achieved by external morphometrics alone. Further, this study evaluates changes in nonprehensile tail anatomy associated with tail reduction to gain additional insight into the anatomy associated with tail loss. Previous studies of primate tail morphology have focused almost entirely on prehensile tails (Dor, 1937; German, 1982; Youlatos, 2003; Organ, 2007, 2010). However, the majority of primates have nonprehensile tails, and we know relatively little about how caudal vertebral anatomy changes in relation to tail length. Finally, this study employs a comparative mammalian anatomical approach. Although tail reduction independently evolved in a number of nonhominoid primates (e.g., macaques, subfossil lemurs) and nonprimate mammals (e.g., koalas, lynxes), the strength of a comparative sample to test functional hypotheses has previously been largely ignored.

The objectives of this dissertation are twofold:

1) *Identify* anatomical correlates of tail length and positional behaviors from the external and internal bony morphology of the sacrocaudal region using a broad, comparative mammalian sample.

2) *Apply* the identified anatomical correlates to reconstructions of the tail lengths and positional behaviors of extinct primates.

The following section of this introductory chapter provides general background information about the anatomical evidence for tail loss and the adoption of upright posture in hominoid evolution, sacral and caudal vertebral anatomy, and trabecular bone structure.

Anatomical Evidence for Tail Loss and Orthogrady in the Hominoid Fossil Record

Tail Loss

The absence of an external tail is one of the first identifiable ape-like traits of the postcranial skeleton in the hominoid fossil record. Features consistent with the morphology of the first coccygeal vertebra in living apes (e.g., a dorsoventrally narrow and caudally tapering body bearing a shallow dorsal groove instead of a neural canal, and the absence of zygapophyseal joints) characterize a vertebral element belonging to *Nacholapithecus kerioi* (KNM-BG 40949; Nakatsukasa et al., 2003), suggesting that hominoids possessed a coccyx, and thus lacked an external tail, by at least 15 Ma (Nakatsukasa et al., 2003, 2004; Nakatsukasa and Kunimatsu, 2009). Potential evidence for an earlier occurrence of tail loss (e.g., *Proconsul,* 18Ma, Ward et al., 1991; Ward et al., 1999) closer to the estimated divergence date of cercopithecoids and hominoids exists (23-25 Ma; Pilbeam and Young, 2004; but see Steiper et al., 2006 for an earlier date), but

this evidence remains controversial (Harrison, 1998; see also Fleagle, 2013). KNM-KPS V42 is a fragmented vertebra belonging to a subadult *Proconsul heseloni* individual (Walker et al., 1983). Walker et al. (1983) identified the specimen as a last sacral vertebra. The last sacral vertebra in living apes tapers caudally (i.e., mediolateral dimension of the caudal articular surface is narrower than that of the cranial articular surface area) to articulate with a coccyx, rather than a robust first caudal vertebra (Ward et al., 1991). Ward and colleagues (1991) reported that the degree of tapering of V42 falls within the range of extant apes, indicating that *Proconsul heseloni* lacked an external tail. However, Harrison (1998) argued that the specimen is better identified as a caudal vertebra because its cranial articular surface shape resembles that of Old World monkey proximal caudal vertebrae. Harrison (1998) maintained that not only did *Proconsul* probably have a tail, but that its tail may have been long. Nakatsukasa and colleagues (2004) reevaluated V42 and agreed with Ward and colleagues (1991) that V42 was a sacral vertebra and that it probably articulated distally with a coccyx**.** However, Nakatsukasa and colleagues (2004) only reexamined V42 qualitatively.

Postcranial evidence from Early to Middle Miocene hominoids (e.g., *Proconsul, Afropithecus, Sivapithecus, Nacholapithecus*) suggests that their axial skeletons generally retained the primitive catarrhine morphological condition (Ward, 1993; see below). In addition to primitive catarrhine lumbar vertebral morphology, at least one fossil hominoid (*Nacholapithecus*) probably retained a sacrum with anthropoid-like numbers of vertebrae (3-4 sacral vertebrae, Nakatsukasa and Kunimatsu, 2009). Therefore, tail loss probably

occurred in the context of the pronograde posture and primitive catarrhine axial morphology.

Orthogrady

Early Miocene hominoids (e.g., *Proconsul* and *Nacholapithecus*) had relatively long lumbar vertebral regions (6-7 lumbar vertebrae) with craniocaudally elongated vertebral bodies bearing rudimentary accessory processes, ventral median keels, and transverse processes arising from the vertebral body or body-pedicle junction (Ward, 1993, 1997; Nakatsukasa and Kunimatsu, 2009). These features characterize most living mammals, and permit sagittal lumbar mobility during pronograde, quadrupedal behaviors (Slijper, 1946; Schultz, 1953, 1961; Benton, 1967; Hildebrand et al., 1974; Jenkins, 1974; Ward, 1993; Shapiro and Simons, 2002). In contrast, the axial morphology of living apes is characterized by fewer lumbar vertebrae with craniocaudally shorter vertebral bodies that lack accessory processes and ventral median keels, and have transverse processes arising from the pedicle or pedicle-lamina junction (Benton, 1967; Jungers, 1984; Shapiro, 1993; Ward, 1993). Functionally, these features provide sagittal lumbar stability during orthograde, suspensory behaviors by reducing intervertebral bending movements (Ankel, 1972; Cartmill and Milton, 1977; Hunt, 1989; Ward, 1993; Johnson and Shapiro, 1998; Lovejoy, 2005). Although too few sacral elements are known to accurately determine sacral numbers for *Proconsul* (Pilbeam, 2004), the sacrum articulated with a cercopithecoid-like pelvis, with the blades oriented in the parasagittal planes (Ward, 1991).

Some derived modern ape-like features of the fore- and hind limb suggest orthograde positional behaviors were employed by Early-Mid Miocene taxa to varying extents. *Proconsul* exhibited a slightly inflated humeral capitulum separated from the trochlea by a shallow zona conoidea, a high femoral neck-shaft angle, and circular femoral condyles (Ward, 1997). These features are found in living apes and functionally serve to enhance mobility at the elbow, hip, and knee joints during climbing activities (Rose, 1993; Ward, 1997). While hip and knee joint morphology in *Nacholapithecus* is similar to that of *Proconsul*, the elbow joint has more pronounced mobility-enhancing features (e.g., more inflated capitulum, keeled trochlea, lateral radial notch) which, along with a long, modern ape-like clavicle and large manual phalanges relative to pedal phalanges, have been used to infer that it probably relied on forelimb-dominated activities (e.g., orthograde clambering, bridging) to a greater extent (Rose et al., 1996; Nakatsukasa et al., 2007, Nakatsukasa and Kunimatsu, 2009). From the Middle Miocene, *Sivapithecus* (12.5 -8.5 Ma) shares with living apes more features of the hind limb (e.g., extensive femoral head articular surface area) than does *Proconsul*, indicating a greater reliance on orthograde climbing behaviors (Rose, 1993). Yet, *Sivapithecus* exhibits a humeral shaft that is more primitive than that of *Proconsul* (Rose, 1993), which, along with a pear-shaped scapular glenoid fossa, indicates that arboreal pronograde quadrupedalism was its predominant locomotor mode (but see Begun and Kivell, 2011).

Orthograde suspensory behaviors may appear in the hominoid fossil record by the Early or Middle Miocene (Deane and Begun, 2010), but this argument is contested (Alba et al., 2010). *Pierolapithecus catalaunicus* (~12.5 - 13Ma) shares with great apes

increased rib angulation and lumbar vertebrae that have wide, short pedicles, somewhat caudally-oriented spinous processes, no ventral body keeling, and transverse processes that originate from the vertebral body-pedicle junction (Moyà-Solà et al., 2004). A fragmented glenoid fossa and middle lumbar vertebra belonging to *Morotopithecus* (~20Ma) provide possible evidence for suspensory behaviors in the Early Miocene (MacLatchy et al., 2000). Like extant apes, the glenoid fossa fragment is ovoid and shallow, indicative of a highly mobile shoulder joint (MacLatchy et al., 2000). The middle lumbar vertebra has transverse processes that arise from the pedicle as in living great apes, suggesting an emphasis on lower lumbar stability (Shapiro, 1993; Sanders and Bodenbender, 1994; MacLatchy et al., 2000). However, a more cranial lumbar vertebra also attributed to *Morotopithecus* has transverse processes that originate ventrally on the vertebral body-pedicle junction, and the lumbar vertebral bodies are craniocaudally elongate (Nakatsukasa and Kinumatsu, 2009). This latter line of evidence suggests that *Morotopithecus* may have retained a relatively long (6-7 lumbar vertebrae) and flexible lumbar vertebral column (Nakatsukasa and Kinumatsu, 2009). The acquisition of the crown hominoid body plan (assuming it did not evolve in parallel; but see Larson, 1998; Begun et al., 1997) may have been more related to generalized orthogrady than specifically to suspensory behaviors (Almécija et al., 2009). The most convincing evidence for frequent use of orthograde postures and suspensory behaviors appears in the late Middle to Late Miocene (Moyà–Solà and Kohler, 1996). *Hispanopithecus laietanus* (9-12 Ma, Moyà–Solà and Kohler, 1996) shares with great apes lumbar vertebrae that have transverse processes arising from the pedicle, a fully extendable elbow joint, and

highly curved manual phalanges (Begun, 2007; Almecija et al., 2007). *Oreopithecus* (6-7 Ma; Begun, 2007) shares with apes long forelimbs relative to hind limbs and broad scapulae having deep glenoid fossae, permitting locomotor activities that require full circumduction at the shoulder joint (Begun, 2007).

Sacral and Caudal Vertebral Anatomy

The sacrum is a vertebral element formed in all amniotes by the ankylosis of two or more vertebrae, one or more of which articulates with the innominates (the exception is cetaceans, for which the iliac blades are absent and no vertebrae are modified into a sacrum) (Flower, 1876). The sacrum articulates cranially with the ultimate lumbar vertebrae and caudally with the first postsacral vertebra (caudal or coccygeal). In his extensive monograph on the comparative osteology of mammals, Flower (1876) speculated that the primitive sacral number for mammals is two. Schultz and Straus (1945) observed three sacral vertebrae in most specimens of *Tupaia*. The modal number for primates is three (Schultz and Straus, 1945; see also Chapter 4).

The mammalian tail can be divided into three distinct regions based on external caudal vertebral morphology: proximal, transitional, and distal (Figure 4.1; Flower, 1876; German, 1982; Lemelin, 1995; Argot, 2003; Schmitt et al., 2005; Organ, 2007, 2010; Organ et al., 2009; Russo and Young, 2011). Caudal vertebrae in the proximal region possess one or two pair of transverse processes and bear neural arches, articulating with one another via zygapophyseal joints. Proceeding distally in the proximal region, neural arches, spinous processes, and transverse processes become reduced (transverse processes may also bifurcate) until reaching the last proximal vertebra, or transition

vertebra (TV in Figure 4.1; Ankel, 1972). The morphology of the transition vertebra is distinct as it bears zygapophyseal joints on its cranial end, but lacks them on its caudal end, reflecting the fact that this vertebra demarcates the proximal and transitional caudal vertebral sequences. Distal to the transition vertebra, all caudal vertebrae possess one or two pairs of relatively reduced transverse processes and lack neural arches, such that the vertebrae are joined only by intervertebral body joint surfaces. Caudal vertebral bodies increase in craniocaudal length from the transition vertebra until reaching a longest vertebra (LV in Figure 4.1), marking the end of the transitional region. All vertebrae thereafter comprise the distal tail region and decrease in craniocaudal length until reaching the tail's end. Chevron bones are variably present among mammals and humans (see Schultz, 1941). Tail-bearing mammals may possess as many as 46 caudal vertebrae (e.g., *Manis tetradactyla*; Pholidota; Flower, 1876).

The sacrococcygeal joint is a fibrocartilaginous symphsial joint (Woon and Stringer, 2012). In some cases, fused sacrococcygeal joints have been documented (Saluja, 1988; Maigne et al., 1992). Use of the term "coccygeal" is typically reserved for describing the rudimentary internal (i.e., in contrast to an externally protruding tail) caudal vertebrae, which may ankylose to form a coccyx (cuckoo: Greek κόκκυξ) in hominoid primates. Coccygeal vertebrae are distinct from caudal vertebrae in that they lack neural arches (pedicles, laminae, and spinous processes) and zygapophyseal articulating facet joints (as does the distal sacrum in hominoids). Instead of zygapophyses, coccygeal vertebrae often possess cornuae, marking the distal boundary of the sacral hiatus and forming the passageway for the posterior division of the fifth sacral

nerve. Thus, the sacrococcygeal articulation occurs primarily via the vertebral bodies as the distal sacrum and coccygeal vertebrae. The first coccygeal vertebra can be somewhat robust compared to more distal coccygeal vertebrae and it often possesses transverse processes, thus resembling the last sacral vertebra in these respects (Woon and Stringer, 2012). Travelling distally, there is gradual diminution in the size of the coccygeal bodies until reaching its apex (Woon and Stringer, 2012). Among hominoids, there are generally between two and five coccygeal vertebrae, although as few as one or none (e.g., *Hylobates*) have been reported (Schultz and Straus, 1945; Woon and Stringer, 2012).

Trabecular Bone Structure

It has long been recognized that trabecular bone responds to dynamic functional loads during life by altering its structural properties (Wolff, 1892; Thompson, 1919; Wainwright et al., 1976; Currey, 1984; Biewener et al., 1996; Burr et al., 2002). For example, trabecular bone's primary orientation usually reflects the principal direction of the applied loads (Wolff, 1892; Gibson, 1985; Goldstein et al., 1993) because bone is strongest (i.e., bending moments are reduced) when loaded on-axis (Wainwright et al., 1976; Currey, 1984; Gibson, 1985; Goldstein et al., 1991; Biewener et al. 1996; Ulrich et al., 1999; Huiskes et al., 2000; Keaveny et al., 2001). Trabeculae also tend to orient themselves more strongly (i.e., they are more anisotropic) in a particular direction in response to loads that are repetitive or stereotypical, whereas trabeculae assume a more random orientation (i.e., they are more isotropic) in response to loads that are more varied (Gibson, 1985; Goldstein et al., 1991, 1993; Fajardo and Müller, 2001). Trabecular struts also respond to the magnitude of the typical load (Carter et al., 1987). Higher bone

densities, approximated by measures of bone volume fraction (bone volume / total volume) (Rice et al., 1988), increase bone strength in areas of high loading (Keaveny et al., 2001). Bone volume fraction may also increase in response to strains that are low in magnitude but high in frequency (Rubin et al., 1985). Overall, the mechanical behavior of cancellous bone is largely dependent on the interplay between bone density, degree of anisotropy and trabecular orientation (Goldstein et al., 1993). In fact, bone density and degree of anisotropy can account for over 92% of the variance in trabecular bone yield strength (Turner, 1992a,b; Ulrich et al., 1999). Trabecular morphology and mechanical usage are thus related (Huiskes et al, 2000; Macchiarelli et al., 2001).

Researchers have demonstrated that some aspects of trabecular bone structure in regions of the postcranial skeleton, such as the humerus (Fajardo and Müller, 2001), femur (MacLatchy and Müller, 2002), os coxa (Rook et al., 1999; Macchiarelli et al., 2001), calcaneus (Maga et al., 2006), and thoracic and lumbar vertebrae (Oxnard and Yang, 1981; Robson-Brown et al., 2002; Cotter et al., 2009) may relate to differences in positional behaviors among extant primates (see also Rafferty and Ruff, 1994; Rafferty, 1998; but see Fajardo et al., 2007; Ryan and Walker, 2010). Nevertheless, it is important to acknowledge that bone structure may be influenced by factors other than external loading, including growth and development (Ding and Hvid, 2000; Gosman and Ketcham, 2009; Ryan and Krovitz, 2006), sex, anatomical region (Lieberman et al., 2004; Pearson and Lieberman, 2004; Ruff et al., 2006), genetics (Judex et al., 2004; Wallace et al., 2012) diet, disease (Lanyon, 1996; Ruff, 1999, 2008), and body size (Swartz et al., 1998; Fajardo et al., 2007; Cotter et al., 2009; Doube et al., 2011; Ryan and Shaw, 2013)

(see also Goldstein et al., 1993; Fajardo and Müller, 2001; Lovejoy et al., 2003; Welch et al., 2008). As such, bone morphology should be viewed broadly as a compromise between the influences of mechanical demands and other factors (Ruff, 2008). However, separating the effects of genetics and loading history would prove difficult and, while bone's response to loading is slower in adults than in juveniles (Pearson and Lieberman, 2004), remodeling does not stop at the end of the juvenile growth period (Ruff et al., 2006). Because bone's internal architecture clearly responds to dynamic loading over an individual's lifetime, locomotion is considered a principal mechanical stimulator of bone structure (Ruff et al., 2006).

Organization of Chapters

The three main studies presented flow from cranial to caudal in the sacrocaudal region. Starting with the proximal sacrum, Chapter 2 examines the relationship between trabecular bone structure in the first sacral vertebra and positional behaviors among living primates. Progressing to the sacrum's distal end, Chapter 3 quantifies aspects of external and internal sacral anatomy for correlates of relative tail length/presence among living primates and other mammals. Finally, Chapter 4 evaluates the functional morphology of caudal vertebrae in living nonprehensile-tailed primates and other mammals that vary in relative tail length, offering additional insight into the anatomy associated with tail loss. For all three chapters, identified correlates of tail length and positional behaviors from the extant primate sample are applied to reconstructions of these features in extinct primates.

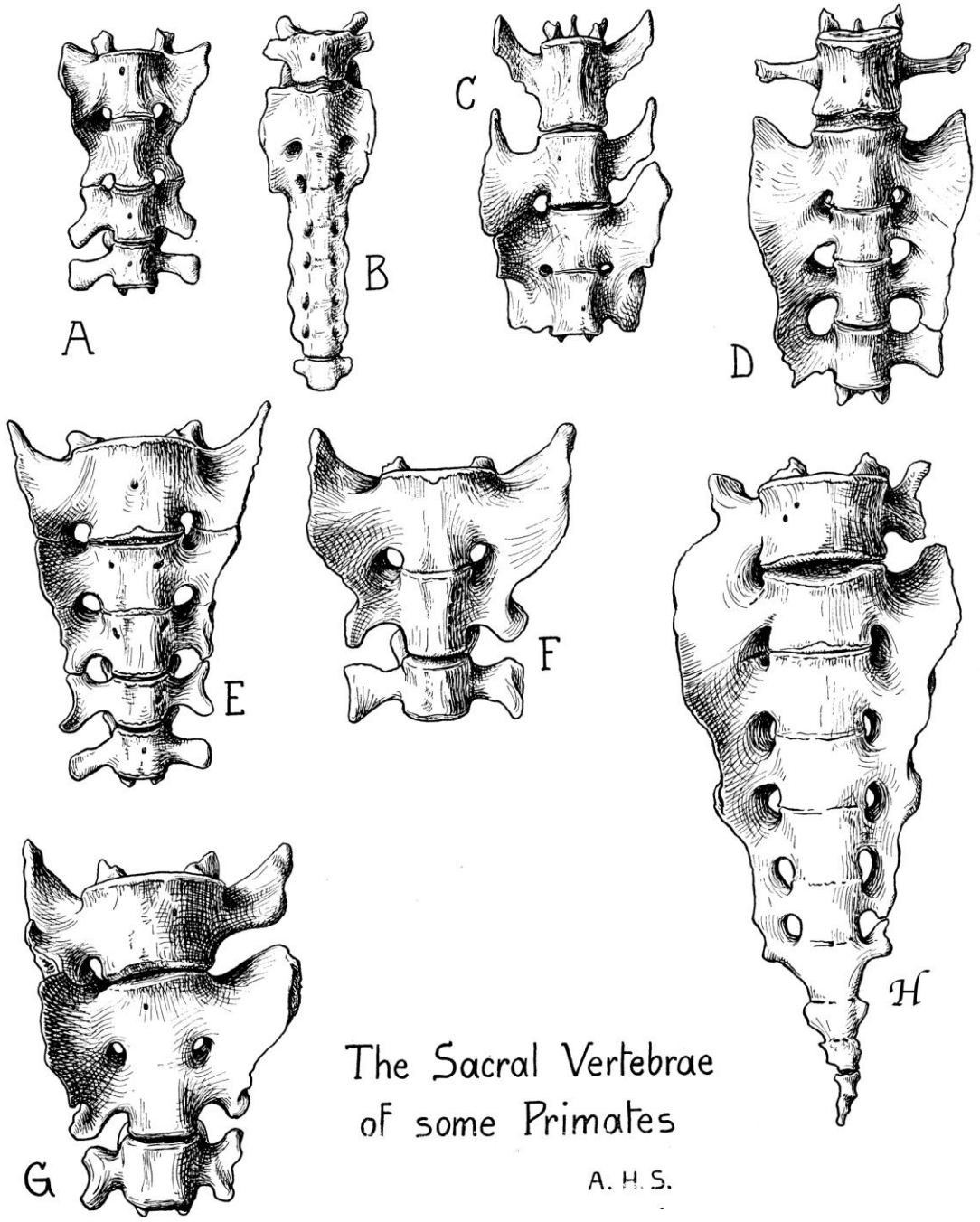

Figure 1.1 Diversity in primate sacral anatomy (as drawn by A.H. Schultz). A= *Galago,* B=*Nycticebus*, C= *Saguinus* ; D= *Alouatta*; E and F= *Cercocebus*; G = *Macaca;* H= *Pan*. Modified from Schultz and Straus (1945).

REFERENCES

Alba, D.M., Almécija, S., and Moyà-Solà, S. 2010. Locomotor inferences in Pierolapithecus and Hispanopithecus: Reply to Deane and Begun (2008). J. Hum. Evol. 59, 143–149.

Almécija, S., Alba, D.M., Moyà-Solà, S., and Kohler. 2007. Orang-like manual adaptations in the fossil hominoid Hispanopithecus laietanus: first steps towards great ape suspensory behaviours. Proc. R. Soc. 274:2375–2384.

Ankel, F. 1972. Vertebral morphology of fossil and extant prima- tes. In: Tuttle R, editor. The functional and evolutionary biol- ogy of primates. Chicago: Aldine. p 223–240.

Argot, C. 2003. Functional-adaptive anatomy of the axial skeleton of some extant marsupials and the paleobiology of the paleocene marsupials Mayulestes ferox and Pucadelphys andinus. J. Morph. 255, 279–300.

Begun, D.R. 2007. Fossil Record of Miocene Hominoids. In: Tattersall, I., Henke, W. (eds.) Handbook of Paleoanthropology. pp. 921-977.

Begun, D.R., Ward, C.V., and Rose, M.D. (eds.) 1997. Function, Phylogeny and Fossils: Miocene Hominoid Origins and Adaptations. Plenum Press, New York.

Begun, D. R., and Tracy L. Kivell. 2011. Knuckle-walking in *Sivapithecus*? The combined effects of homology and homoplasy with possible implications for pongine dispersals. J. Hum. Evol. 60, 158-170.

Benefit, B.R., and McCrossin, M.L. 1995. Miocene Hominoids and Hominid Origins. Ann. Rev. Anthropol. 24, 237–256.

Benton, R. 1967. Morphological evidence for adaptations within the epaxial region of the primates. In: Vagtborg H, editor. The baboon in medical research, Vol. 2. p 201–216.

Biewener, A., Fazzalari, N., Konieczynski, D., Baudinette, R. 1996. Adaptive changes in trabecular architecture in relation to functional strain patterns and disuse. Bone 19,1–8.

Burr, D.B., Robling, A.G., C.H. Turner. 2002. Effects of Biomechanical Stress on Bones in Animals. Bone 30(5), 781-786.

Cartmill, M/, Milton, K. 1977. The lorisiform wrist joint and the evolution of ‘‘brachiating’’ adaptations in the Hominoidea. Am. J. Phys. Anthropol. 47,249–272.

Cotter, M.M., Simpson, S.W., Latimer, B.M., Hernandez, C.J. 2009. Trabecular microarchitecture of hominoid thoracic vertebrae. Anat. Rec. 292, 1098–1106.

Currey, J.D. 1984. The mechanical adaptations of bones. Princeton University Press Princeton, NJ.

Deane, A.S., and Begun, D.R. 2010. Pierolapithecus locomotor adaptations: a reply to Alba et al.'s comment on Deane and Begun (2008). J. Hum. Evol. 59,150–154.

Ding, M., Hvid, I. 2000. Quantification of age-related changes in the structure model type and trabecular thickness of human tibial cancellous bone. Bone 26, 291–295.

Dor, M. 1937. La morphologie de la queue des mammiferes. Paris: Pierre Andre.

Doube, M., Klosowski, M.M, Wiktorowicz-Conroy, A.M.,Hutchinson, J.R., Shefelbine, S.J. 2011 Trabecular bone scales allometrically in mammals and birds. Proc. R. Soc.B 278, 3067–3073.

Fajardo, R.J, and Müller, R. 2001. Three dimensional analysis of nonhuman primate trabecular architecture using micro computed tomography. Am. J. Phys. Anthropol. 115,327–336.

Fajardo, R.J., Muller, R., Ketcham, R.A, Colbert, M. 2007. Nonhuman anthropoid primate femoral neck trabecular architecture and its relationship to locomotor mode. Anat. Rec. 290, 422–436.

Fleagle, J. G. 2013. *Primate Adaptation and Evolution: 3rd Edn*. Academic Press.

Flower, W.H. 1876. An Introduction to the Osteology of the Mammalia: Being the Substance of the Course of Lectures Delivered at the Royal College of Surgeons of England in 1870. Macmillan.

German, R.Z. 1982. The functional morphology of caudal vertebrae in New World monkeys. Am. J. Phys. Anthropol. 58, 453–459.

Gibson, L.J. 1985. The mechanical behaviour of cancellous bone. J. Biomech. 18:317.

Goldstein, S.A., Matthews, L.S., Kuhn, J.L., and Hollister, S.J. 1991. Trabecular bone remodeling: an experimental model. J. Biomech. 24,135–150.

Goldstein, S.A., Goulet, R., and McCubbrey, D. 1993. Measurement and significance of three-dimensional architecture to the mechanical integrity of trabecular bone. Cal. Tiss. Intl. 53, S127–S133.

Gosman, J.H., Ketcham, R.A. 2009 Patterns in ontogeny of human trabecular bone from SunWatch Village in the prehistoric Ohio Valley: general features of microarchitectural change. Am. J. Phys. Anthropol. 138, 318–332.

Harrison, T. 1998. Evidence for a tail in Proconsul heseloni. Am. J. Phys. Anthropol. 26,93–94.

Hildebrand, M., Goslow, G.. 1974. Analysis of vertebrate structure. New York: Wiley.

Huiskes, R., Ruimerman, R., van Lenthe, G.H., and Janssen, J.D. 2000. Effects of mechanical forces on maintenance and adaptation of form in trabecular bone. Nature 405:704–706.

Hunt, K. 1989. Positional behavior in Pan troglodytes at the Mahale Mountains and the Gombe stream national parks, Tanzania, Ph.D. dissertation, University of Michigan, Ann Arbor, Michigan.

Jenkins, F.A. 1974. Tree shrew locomotion and the origins of arborealism. In: Jenkins F Jr., editor. Primate locomotion. New York: Academic Press. p 85–116.

Johnson, S., Shapiro, L.J. 1998. Positional behavior and vertebral morphology in atelines and cebines. Am. J. Phys. Anthropol. 105,333–354.

Jungers, W. 1984. Aspects of size and scaling in primate biology with special reference to the locomotor skeleton. Yrbk. Phys. Anthropol. 27,73–97.

Judex, S., Garman, R., Squire, M., Donahue, L.R., Rubin, C., 2004. Genetically based influences on the site-specific regulation of trabecular and cortical bone morphology. J. Bone Miner. Res. 19, 600-606.

Keaveny, T.M, Morgan, E.F., Niebur, G.L., and Yeh, O.C. 2001. Biomechanics of trabecular bone. Ann. Rec. Biomed. Eng. 3, 307–333.

Keith, A. 1923. Man's posture: its evolution and disorders. Br. Med. J. 1,451–454.

Larson, S. 1998. Parallel evolution in the hominoid trunk and forelimb. Evolutionary Anthropology Issues News and Reviews 6,87–99.

Lemelin, P. 1995. Comparative and functional myology of the prehensile tail in New World monkeys. J. Morphol. 224,351– 368.

Lieberman, D.E., Polk, J.D., Demes B. 2004. Predicting long bone loading from cross-sectional geometry. Am. J. Phys. Anthropol. 123, 156-171.

Lovejoy, C.O., McCollum, M.A., Reno, P.L., and Rosenman, B.A. 2003. Developmental biology and human evolution. Ann. Rev. Anthropol. 32,5–109.

Lovejoy, C.O. 2005. The natural history of human gait and posture, Part 1: Spine and pelvis. Gait Posture 21,95– 112.

Macchiarelli, R., Rook, L., Bondioli, L. 2001. Comparative analysis of the iliac trabecular architecture in extant and fossil primates by means of digital image processing techniques: implications for the reconstruction of fossil locomotor behaviours. In: Agusti, J., Rook, L., Andrews, P. (Eds.), Hominoid Evolution and Climatic Change in Europe. Cambridge University Press, U.K. pp 60–101.

MacLatchy, L., Gebo, D., Kityo, R., and Pilbeam, D. 2000. Postcranial functional morphology of Morotopithecus bishopi, with implications for the evolution of modern ape locomotion. J. Hum. Evol. 39,159–183.

MacLatchy, L., Müller, R. 2002 A comparison of the femoral head and neck trabecular architecture of Galago and Perodicticus using micro-computed tomography (mCT). J. Hum. Evol. 43, 89–105.

Maga, M., Kappelman, J., Ryan, T.M., and Ketcham, R.A. 2006. Preliminary Observations on the Calcaneal Trabecular Microarchitecture of Extant Large-Bodied Hominoids. Am. J. Phys. Anthropol. 129,410–417.

Maigne, J-Y, and Tamalet, B. 1996. Standardized radiologic protocol for the study of common coccygodynia and characteristics of the lesions observed in the sitting position: Clinical elements differentiating luxation, hypermobility, and normal mobility. Spine 21,2588–2593.

Moyà-Solà S, Kohler M, Alba DM, Casanovas-Vilar I, and Galindo J. 2004. *Pierolapithecus catalaunicus*, a new Middle Miocene great ape from Spain. Science 306:1339.

Moyà-Solà S, and Kohler M. 1996. A *Dryopithecus* skeleton and the origins of great-ape locomotion. Nature 379,156–159.

Nakatsukasa, M., Tsujikawa, H., Shimizu, D., Takano, T., Kunimatsu, Y., Nakano, Y., and Ishida, H. 2003. Definitive evidence for tail loss in Nacholapithecus, an East African Miocene hominoid. J. Hum. Evol. 45,179–186.

Nakatsukasa, M., Ward, C.V., Walker, A, Teaford, M., Kunimatsu, Y., and Ogihara, N. 2004. Tail loss in *Proconsul heseloni*. J. Hum. Evol. 46,777–784.

Nakatsukasa, M., Kunimatsu, Y., Nakano, Y., and Ishida, H. 2007. Vertebral morphology of *Nacholapithecus kerioi* based on KNM-BG 35250. J. Hum. Evo. 52,347–369.

Nakatsukasa, M., and Kunimatsu, Y. 2009. Nacholapithecus and its importance for understanding hominoid evolution. Evolutionary Anthropology: Issues, News, and Reviews 18,103–119.

Organ, J.M. 2007. The functional anatomy of prehensile and non- prehensile tails of the Platyrrhini (Primates) and Procyonidae (Carnivora). PhD Dissertation. The Johns Hopkins University, Baltimore, MD.

Organ, J.M., Teaford, M.F, Taylor AB. 2009. Functional correlates of fiber architecture of the lateral caudal musculature in pre- hensile and nonprehensile tails of the Platyrrhini (Primates) and Procyonidae (Carnivora). Anat. Rec. 292, 827–841.

Organ, J.M. 2010. Structure and function of platyrrhine caudal vertebrae. Anat. Rec. 293,730–745.

Oxnard, C.E., and Yang, H.C.L. 1981. Beyond biometrics: studies of complex biological patterns. In: Symp Zool Soc Lond. Vol. 46. . p 127–167.

Pearson, O.M., Lieberman, D.E. 2004. The aging of Wolff's "law": ontogeny and responses to mechanical loading in cortical bone. Am. J. Phys. Anthropol. 125, 63-99.

Pilbeam, D. 2004. The anthropoid postcranial axial skeleton: comments on development, variation, and evolution. J. Exp. Zool. Part B. Molec. and Dev. Evol. 302,241–267.

Pilbeam, D., and Young, N. 2004. Hominoid evolution: synthesizing disparate data. Comptes rendus-Palevol. 3,305–321.

Rafferty, K.L. 1998. Structural design of the femoral neck in primates. J. Hum. Evol. 34:361–383.

Rafferty, K., and Ruff, C. 1994. Articular structure and function in Hylobates, Colobus, and Papio. Am. J. Phys. Anthropol. 94,395–408.

Robson-Brown, K., Katharine, A., Davies, E.N., and McNally, D.S. 2002. The angular distribution of vertebral trabeculae in modern humans, chimpanzees and the Kebara 2 Neanderthal. J. Hum. Evo. 43,189–205.

Rice, J.C., Cowin, S.C., and Bowman, J.A. 1988. On the dependence of the elasticity and strength of cancellous bone on apparent density. J. Biomech. 21,155-168.

Rook, L., Bondioli, L., Köhler, M., Moyà-Solà, S., and Macchiarelli, R. 1999. *Oreopithecus* was a bipedal ape after all: evidence from the iliac cancellous architecture. Proc. Natl. Acad. Sci. 96, 8795-8799.

Rose, M.D. 1993. Locomotor anatomy of Miocene hominoids. In: Gebo, D. (Ed.) Postcranial Adaptation in Nonhuman Primates. pp 252–272.

Rose, M.D., Nakano, Y., and Ishida, H. 1996. *Kenyapithecus* postcranial specimens from Nachola, Kenya. Afr. Stud. Monogr 24,3–56.

Rubin, C.T., and Lanyon, L.E. 1985. Regulation of bone mass by mechanical strain magnitude. Cal. Tiss. Intl. 37, 411–417.

Ruff, C.B. 1999. Skeletal structure and behavioral patterns of prehistoric Great Basin populations. In: Hemphill, B.E., Larsen, C.S. (eds) Prehistoric Lifeways in the Great Basin Wetlands: Bioarchaeological Reconstruction and Interpretation. Salt Lake city: Universityu Utah Press. Pp. 290-320.

Ruff, C.B. 2008. Biomechanical analyses of archaeological human skeletons.In: M.A. Katzenberg, S.R. Saunders (eds). *Biological Anthropology of the Human Skeleton, Second Edition*. John Wiley & Sons, Inc. Pp 183-206.

Ruff, C.B., Holt B, and Trinkaus E. 2006. Whos afraid of the big bad Wolff?:“ Wolffs law” and bone functional adaptation. Am. J. Phys. Anthropol. 129,484-498.

Russo, G.A., and Young, J.W. 2011. Tail growth tracks the ontogeny of prehensile tail use in capuchin monkeys (*Cebus albifrons* and *C. apella*). Am. J. Phys. Anthropol. 146, 465–473.

Ryan, T.M., Krovitz, G.E. 2006. Trabecular bone ontogeny in the human proximal femur. J. Hum. Evol. 51, 591–602.

Ryan, TM, Shaw C.N. 2013. Trabecular bone microstructure scales allometrically in the primate humerus and femur. Proc. R. Soc. B: Biological Sciences, 280, 1758.

Ryan, T.M., Walker, A. 2010 Trabecular bone structure in the humeral and femoral heads of anthropoid primates. Anat. Rec. 293, 719–729.

Saluja, P.G. 1988. The incidence of ossification of the sacrococcygeal joint. J. Anat. 156:11-15.

Sanders, W.J., and Bodenbender, B.E. 1994. Morphometric analysis of lumbar vertebra UMP 67-28: Implications for spinal function and phylogeny of the Miocene Moroto hominoid. J. Hum. Evol. 26,203–237.

Schultz, A.H. 1941. Chevron bones in adult man. Am. J. Phys. Anthropol. 28,91–97.

Schultz, A.H. 1953. The relative thickness of the long bones and the vertebrae in primates. Am. J. Phys. Anthropol. 11,277–311.

Schultz, A.H. 1961. Vertebral column and thorax. Primatologica 5, 1–66.

Schultz, A.H., and Straus, Jr W. 1945. The numbers of vertebrae in primates. Proc. Am. Phil. Soc. 601–626.

Schmitt, D., Rose, M.D., Turnquist, J.E., Lemelin, P., 2005. Role of the prehensile tail during ateline locomotion: experimental and osteological evidence. Am. J. Phys. Anthropol. 126, 435-446.

Shapiro, L.J. 1993. Functional morphology of the vertebral column in primates. In: Gebo, D. (ed.). Postcranial adaptation in nonhuman primates. DeKalb: Northern Illinois University Press. pp. 121–149.

Shapiro, L.J. 2007. Morphological and functional differentiation in the lumbar spine of lorisids and galagids. Am. J. Primatol. 69,86–102.

Shapiro, L.J., and Simons C. 2002. Functional aspects of strepsirrhine lumbar vertebral bodies and spinous processes. Journal of Human Evolution 42:753–783.

Shapiro, L.J., Seiffer, C., Godfrey L, Jungers W, Simons E, and Randria G. 2005. Morphometric Analysis of Lumbar Vertebrae in Extinct Malagasy Strepsirrhines. Am. J. Phys. Anthropol. 128:823-839.

Slijper, E. 1946. Comparative biologic-anatomical investigations on the vertebral column and spinal musculature of mammals. Verh. K. Ned. Akad. Wet. Afd. Natuurkd. Tweede. Reeks 42,1–128.

Steiper, M., Young, N., and Sukarna, T. 2004. Genomic data support the hominoid slowdown and an Early Oligocene estimate for the hominoid-cercopithecoid divergence. Proc. Nat. Acad. Sci. 101,17021–17026.

Swartz, S.M., Parker, A., Huo, C. 1998 Theoretical and empirical scaling patterns and topological homology in bone trabeculae. J. Exp. Biol. 201, 573–590.

Thompson, D.W. 1919. On Growth and Form. University Press, Cambridge.

Turner, C.H. 1992a. On Wolff's law of trabecular architecture. J Biomech 25:1–9.

Turner, C.H. 1992b. Functional determinants of bone structure: beyond Wolff's law of bone transformation. Bone 13:403.

Ulrich, D., van Rietbergen, B., Laib A, Ru¨egsegger P. 1999. The ability of three-dimensional structural indices to reflect mechanical aspects of trabecular bone. Bone 25:55–60.

Wainwright, S. A., Biggs, W. D., Currey, J. D., and J. M. Gosline. 1976. Mechanical Design in Organisms. Princeton University Press, Princeton, NJ.

Wallace, I.J., Tommasini, S.M., Judex, S., Garland Jr., T., Demes, B., 2012. Genetic variations and physical activity as determinants of limb bone morphology: an experimental approach using a mouse model. Am. J. Phys. Anthropol. 148, 24-35.

Walker, A.C., and Pickford, M. 1983. New postcranial fossils of Proconsul africanus and *Proconsul nyanzae*. In: Ciochon, R.L. and Corrucini, R.S. New interpretations of ape and human ancestry. Pp. 325–351.

Ward, C.V. 1991. Functional Anatomy of the Lower Back and Pelvis of the Miocene Hominoid Proconsul nyanzae. Ph.D. Dissertation. Johns Hopkins University School of Medicine.

Ward, C.V., Walker, A. and M. F. Teaford. *Proconsul* did not have a tail. J. Hum. Evo. 21, 215-220.

Ward, C.V. 1993. Torso morphology and locomotion in *Proconsul nyanzae*. Am. J. Phys. Anthropol. 92,291–328.

Ward, C.V. Hominoid trunk and hind limb evolution. In: Begun, D.R., C.V. Ward & M.D. Rose (eds). Function, Phylogeny and Fossils: Miocene Hominoids and Great Ape and Human Origins. New York: Plenum Press, pp. 389-415.

Woon, J. T., and Stringer, M. D. 2012. Clinical anatomy of the coccyx: a systematic review. Clin. Anat. 25(2), 158-167.

Youlatos, D. 2003. Osteological correlates of tail prehensility in carnivorans. J. Zool. 259, 423-430.

Chapter 2: Trabecular bone structure in the proximal sacrum and its relationship to positional behaviors

ABSTRACT

Among primates, the external morphology of the human sacrum is distinct and clearly reflects adaptations to our unique practice of habitual orthograde posture and bipedal locomotion. However, the relationship between variation in external sacral morphology and differences in positional behaviors among nonhuman primates is less clear. As an alternative approach to examining external sacral morphology, this study investigates whether the sacrum's internal morphology (i.e., trabecular bone) is functionally informative with respect to differences in positional behaviors. This study quantified trabecular bone structure in a volume of interest positioned in the first sacral vertebra in 78 primate individuals (5 hominoid genera, 2 cercopithecoid genera, 3 platyrrhine genera, and 3 strepsirrhine genera) that vary in trunk posture and locomotion. Results suggest that some aspects of trabecular bone structure may be related to positional behaviors, but the morphological trends are not always consistent with functional expectations. In some cases, modern humans differed from other extant primates. There was substantial intra-taxonomic variation with respect to trabecular bone orientation in S1 with no clear indicators of differences in loading patterns. When multiple trabecular bone variables are considered together as a functional suite in multivariate principal component analyses, it was possible to distinguish among some extant primate taxa. Results from the extant primate analyses may provide a functionally

informative context for reconstructing the positional behaviors of extinct primate taxa, although more work is needed to understand trabecular morphological patterns.

INTRODUCTION

External Sacral Anatomy

The sacrum occupies a functionally important anatomical position as part of both the pelvic girdle and vertebral column. Proximally, the sacrum is subjacent to the lumbar vertebrae from which it receives the weight of the upper body. Bilaterally, the sacrum articulates with the os coxae, where weight is transferred to, and joint forces are received from, the hind limbs. As such, the orientation of an animal's spine relative to the substrate (i.e., posture) and which limbs are responsible for supporting the majority of the animal's body weight during movement (i.e., locomotion) likely influence the type of loads imposed on the sacrum. For example, in pronograde quadrupedal stance, body weight is distributed somewhat evenly between the fore- and hind limbs, both of which work to propel the body; during bouts of vertical clinging and leaping, the trunk is orthograde, and the hind limbs provide propulsive force; in bimanual suspension, the trunk is orthograde, but only the forelimbs support the body's weight and provide propulsive force; and, in habitual bipedal stance (striding or hopping), the trunk is orthograde and the entire weight of the head, trunk and forelimbs bears upon the hind limbs, which solely propel the body as the forelimbs are freed from a locomotor role (see also Schultz, 1930). Accordingly, the morphology of the sacrum may be informative with respect to positional behaviors among extant primates.

The sacrum is also well-preserved in fossil samples, with partial or complete elements known for a number of extinct primates, including subfossil lemurs (*Hadropithecus* [see Godfrey et al., 2006]; *Megaladapis* [e.g., DLC 7950]; *Palaeopropithecus* [e.g., DLC 24778]*; Archaeolemur* [e.g., BMNH M7909, Godfrey et al., 2006; DLC 11823, DUPC 11835, DLC 9905]), early catarrhines and hominoids (e.g., *Epipliopithecus* [O.E. 304-45, Zapfe, 1958, 1960]; *Proconsul* [e.g., KNM-KPS V42, KNM-MV 13142M, Walker et al., 1983; Ward et al., 1993]; *Nacholapithecus* [e.g., KNM-BG 17822, Rose et al., 1996; Ishida et al., 2004]; *Oreopithecus* [e.g., BA#50, BA#72, Hürzeler, 1958; Straus, 1963), and hominins (*Australopithecus* [Sts 14, Robinson, 1972; A.L.288-1, Johanson et al., 1982]; *Homo* [KNM-WT 15000, Walker and Leakey, 1993; Pelvis 1 Atapuerca, Arsuaga et al., 1999; BSN49/P27, Simpson et al., 2008]). Our understanding of sacral functional morphology in extant primates thus has potential significance for making inferences about the positional behaviors of extinct primates.

Among primates, the external morphology of the human sacrum is distinct and clearly reflects adaptations to the substantial axial compressive forces generated by our unique practice of habitual orthograde posture and bipedal locomotion. For example, compared to apes, human sacra are more horizontally oriented (relative to the long axis of the spine), bringing the trunk's line of gravity closer to, and reducing moments around, the femoral heads (Stern and Susman, 1983; Abitbol, 1987a, b). Additionally, human sacra are more ventrally curved, resulting from the pull of the sacro-tuberous and -spinous ligaments that prevent excessive nutation as a result of the lordotic spine’s

tendency for forward displacement (Weidenreich, 1913; Abitbol, 1989). Human sacra are also greater in transverse width, which increases the coronal distance between the sacroiliac joints and vertically aligns them with the hips joints, thereby resisting the tendency for the pelvic bones to rotate around the sacroiliac joints and reducing stresses on the pubic symphysis (Leutenegger, 1977). A wide sacrum also accommodates the anteromedial rotation of the iliac blades into the sagittal plane (without impinging on pelvic visceral space) (Lovejoy, 1988) and provides increased surface area for the attachment of the erector spinae musculature that maintains upright posture (Gregory, 1928). Finally, human sacra have relatively larger articular surfaces (first sacral cranial, zygapophyseal, and auricular) that serve to dissipate high loads generated by habitual upright posture and bipedal locomotion over a more extensive area (Schultz, 1930; Jungers, 1988; Whitcome, 2006; Russo and Shapiro, 2013). By contrast, the relationship between variation in external sacral morphology and differences in positional behaviors among nonhuman primates is less clear. Compared to monkeys, all apes share a suite of adaptations that reflect a greater reliance on orthograde positional behaviors (though neither their adaptations nor their behaviors are identical [Young, 2003]). However, ape ranges for measures of the lumbosacral angle and sacral curvature overlap those of pronograde, quadrupedal monkeys (Abitbol, 1987a, b). Further, relative transverse sacral width is greatest in the highly suspensory *Hylobates*, among apes, and that of pronograde, quadrupedal cercopithecoids exceeds all apes (Rosenman, 2008). Moreover, apes generally have relatively smaller sacral articular surfaces (e.g., first sacral cranial, Ward,

1991; sacroiliac, Schultz, 1961) than monkeys, suggesting that despite their adaptations to more orthograde posture, smaller loads may be transmitted across these joint surfaces.

Objectives

As an alternative approach to examining external sacral morphology, this study investigates whether the sacrum's internal morphology (i.e., trabecular bone) is functionally informative with respect to differences in positional behaviors. Researchers have demonstrated that variation in some aspects of trabecular bone structure in other regions of the skeleton, such as the humerus (Fajardo and Müller, 2001), femur (MacLatchy and Müller, 2002), os coxa (Rook et al., 1999; Macchiarelli et al., 2001), calcaneus (Maga et al., 2006), and thoracic and lumbar vertebrae (Oxnard and Yang, 1981; Robson-Brown et al., 2002; Cotter et al., 2009) may relate to differences in positional behaviors among extant primates (see also Rafferty and Ruff, 1994; Rafferty, 1998; but see Fajardo et al., 2007; Ryan and Walker, 2010). Therefore, it is possible that the use of high resolution X-ray computed tomography (CT) scans to quantify sacral trabecular bone parameters may permit analysis of more nuanced morphology associated with posture and locomotion than can be achieved by external morphometrics alone.

The specific objectives of this study are twofold. First, this study seeks to determine whether trabecular bone structure in a volume of interest located in the first sacral vertebra (henceforth referred to as S1) (Figure 2.1) reflects differences in positional behaviors among extant primates (Table 2.1). The extant primates sampled in this study vary in posture and locomotion, and were chosen to best represent taxonomic breadth (i.e., number of species) and intraspecific depth (i.e., number of individuals per

species). If identified, functionally relevant patterns in trabecular bone structure among living primates have the potential to inform our interpretations of trabecular bone in fossil sacra for understanding extinct primate positional behaviors. Thus, the second objective of the study is to evaluate S1 trabecular structure in six extinct primates, including *Archaeolemur, Megaladapis, Palaeopropithecus, Epipliopithecus, Nacholapithecus* and *Oreopithecus* (Figure 2.2) with the goal of reconstructing their positional behaviors.

Background & Predictions

Expectations for internal sacral morphology can be delineated based on what is known about the trabecular structure in skeletal elements adjacent to the sacrum. Axial compression and sagittal plane bending are the primary and secondary loads acting on the lumbar vertebral column (Ashton-Miller and McGlashen, 1989; Wilke et al., 1997; Smit, 2002), produced by contraction of the dorsal extensor musculature and passive tensile forces in ventral abdominal structures (e.g., the linea alba resists sagittal bending moments imposed by gravity). Accordingly, researchers have shown that trabeculae in lumbar vertebral bodies form a cruciate pattern by coursing primarily in the craniocaudal direction and secondarily in the dorsoventral direction across mammals, regardless of trunk posture (Ashton-Miller and McGlashen, 1989; Wilke et al., 1997; Smit, 2002; see also Smit et al., 1997). However, among apes, Oxnard and Yang (1981) found that humans exhibited the *strongest* craniocaudal orientation among all apes, African apes exhibited additional off-orthogonal orientations, and orangutans exhibited no orthogonality. In the latter two groups, these differences may reflect additional lateral-bending loads induced by suspensory activity, which are resisted by a shortened lumbar

vertebral column comprised of fewer lumbar vertebrae (in comparison to the primitive catarrhine condition) (Cartmill and Milton, 1977; Ward, 1993). Fajardo et al. (2010) found that both trabecular bone orientation and anisotropy distinguished between the lumbar vertebrae of leaping galagines and those of anti-pronograde lorisines, and reflected the more stereotypical locomotor mode of the former, and the more non-stereotypical locomotor mode of the latter. Finally, Machida and Inoue (1994) demonstrated that bone density is higher in the lumbar vertebrae of bipedal rodents compared to quadrupedal rodents, supporting the idea that orthograde posture places greater axial compressive forces on the spine than pronograde posture. Indeed, weight-gain and weight-lifting activities known to increase axial compressive forces are associated with increased vertebral trabecular bone density in humans (Granhed et al., 1987).

Differences in mammalian positional behaviors may also be detected in hip joint morphology, including, to some extent, the trabecular structure of the femoral head (Rafferty and Ruff, 1994; MacLatchy and Müller, 2002; Ryan and Ketcham, 2005; but see Fajardo et al., 2007) and neck (Rafferty, 1998), and os coxae (Rook et al., 1999; Macchiarelli et al., 2001). Human os coxae exhibit anisotropic, dense sacropubic and ilioischial trabecular bundles (and accordingly the supra-acetabular region where these bundles intersect), reflecting their role in receiving high, repetitive stresses generated during habitual terrestrial bipedalism (Rook et al., 1999; Macchiarelli et al., 2001). By contrast, the os coxae of predominantly suspensory arboreal apes (e.g., *Hylobates*) exhibit more isotropic, less dense sacropubic and ilioischial trabecular bundles, reflecting the use

of more varied limb postures in which a greater portion of the body's weight is supported by the fore-limbs (Rook et al., 1999; Macchiarelli et al., 2001). If the internal architecture of lumbar vertebrae and ossa coxae distinguishes among mammals that vary in positional behaviors, then it is reasonable to expect that the internal architecture of sacra will as well.

This study tests the hypothesis that trabecular morphology in S1 (subjacent to the lumbosacral joint) will differ among primates and that these morphological differences will relate to behavioral differences in posture and locomotion (see Table 2.1). In humans, trabeculae in the sacrum's proximal end generally course in a mediolateral direction from the body-alae junctions toward the central first sacral vertebral body, a trajectory that accords with the route of weight transmission between the lumbosacral joint and the sacroiliac joints during habitual orthograde bipedal stance and locomotion (Pal, 1989; Ebraheim et al., 2000; Peretz et al., 1998; Mahato, 2010). Since the proximal end of the sacrum in all mammals is responsible for receiving some body weight via the lumbosacral joint and transmitting it to the sacroiliac joints, and trabeculae in lumbar vertebral bodies form a cruciate pattern regardless of trunk posture (Ashton-Miller and McGlashen, 1989; Wilke et al., 1997; Smit, 2002; see also Smit et al., 1997), it is expected that S1trabeculae in all primates should be oriented primarily in a mediolateral direction.

In habitual bipedal stance, the trunk is orthograde and the entire weight of the head, trunk and forelimbs bears upon the hind limbs, which solely propel the body as the forelimbs are freed from a locomotor role. As such, the sacrum should be subjected to,

and thus structured to resist, the greatest loads in humans. Therefore, values for parameters associated with trabecular bone strength (e.g., bone volume fraction, degree of anisotropy, trabecular number and trabecular thickness) should be highest in humans. As Oxnard and Yang (1981) noted for lumbar vertebrae, humans exhibit the *strongest* craniocaudal orientation among all apes, and so it is also predicted that values for the elongation index should be closest to 1 in humans, which would indicate rod-like trabecular shape (i.e., higher magnitude of primary axis/secondary axis). Following humans, it is expected that values for parameters describing trabecular bone strength and shape will be next highest in vertical clingers and leapers (*Indri* and *Propithecus*) as the trunk is also held orthograde and, like bipeds, the hind limbs in these taxa provide the primary propulsive force during locomotion. This form of locomotion is also considered more stereotypical than suspensory (inverted quadrupedal) behaviors exhibited by lorises (Fajardo et al., 2010). In pronograde quadrupedalism (*Macaca, Mandrillus, Sapajus*, *Saimiri* and *Varecia*), body weight is distributed somewhat evenly between the fore- and hind limbs, both of which work to propel the body with limbs moving in the parasagittal planes. Because, like bipedalism, pronograde quadrupedalism is also a stereotypical form of locomotion (though notably limb posture is more varied in arboreal quadrupedalism versus terrestrial quadrupedalism), it is expected that parameters associated with trabecular strength and shape will be third highest in taxa that rely on pronograde quadrupedal positional behaviors. *Pan* and *Gorilla* are orthograde-adapted and employ some arm swinging and suspensory behaviors (Doran, 1991), however, they rely predominantly on terrestrial quadrupedal knuckle-walking and climbing (Tuttle and

Watts, 1985). The (more arboreal) bimanual suspensors like *Hylobates*, *Pongo*, *Ateles* are also orthograde-adapted, but the forelimbs support the animal's body weight and the hind limbs may not support any body weight. As noted by Oxnard and Yang (1981), African apes exhibited additional off-orthogonal orientations and orangutans exhibited no orthogonality in comparison to humans. Low values for degree of anisotropy would indicate little trabecular organization and low values for the elongation index would indicate more plate-like trabeculae (i.e, similar magnitudes of the primary and secondary trabecular axes). These trabecular morphologies may be associated with highly suspensory behaviors in which the spine encounters and receives more varied loads and degrees of hind limb support. Therefore, following pronograde quadrupeds, values for parameters describing trabecular bone strength and shape should be next highest in the orthograde-adapted quadrupeds, and lowest among all groups in orthograde bimanual suspensors.

Significance

Postcranial similarities among extant hominoids suggest to some researchers that orthogrady was present in the crown hominoid last common ancestor (Benefit and McCrossin, 1995; Pilbeam and Young, 2004; but see Larson, 1998). Thus, the ability to confidently identify morphological markers of orthogrady is key to understanding both postcranial functional anatomy and evolutionary relationships among extinct apes. However, postcranial evidence suggests that Miocene hominoids employed a wide range of orthograde positional behaviors to varying extents. For example, Early to Middle Miocene hominoids had apparently pronograde posture, but also engaged in some

climbing (e.g., *Proconsul*) and forelimb- dominated (e.g., *Nacholapithecus*) behaviors. Evidence for orthograde suspensory behaviors appear by at least the Middle Miocene (e.g., *Pierolapithecus*; Deane and Begun, 2010; but see Alba et al., 2010), though material belonging to *Morotopithecus* (~20Ma) provides evidence for suspensory behaviors in the earlier part of the epoch (MacLatchy et al., 2000). The most convincing evidence for the frequent use of orthograde postures and suspensory behaviors appears in the late Middle to Late Miocene (e.g., *Hispanopithecus*, Moyà–Solà and Köhler, 1996; *Oreopithecus,* Harrison and Rook, 1997). It is increasingly clear that the positional behaviors of many extinct hominoids may have been characterized by combinations of posture and locomotion not found in living apes (Rose, 1993). Further, it seems likely that the acquisition of the crown hominoid body plan was more related to some form of generalized orthogrady than specifically to suspensory behaviors (Almécija et al., 2009). As a result, it is difficult to determine from skeletal material how, and to what extent, various orthograde positional behaviors were practiced (Rose, 1993). By employing high resolution X-ray CT scanning to examine the sacrum's internal architecture, this study may provide new insight about how morphology relates to function in an important region of the locomotor skeleton. If differences beyond a simple pronograde-orthograde dichotomy can be detected in the sacrum's trabecular bone structure in extant primates, then an examination of the internal bone of sacra belonging to extinct primates can improve our ability to make inferences about their postural and locomotor adaptations.

This study examines the sacra of extinct primates, including extinct hominoids, in order to independently test inferences about their positional behaviors. The extinct

primates examined in this study were chosen either because 1) considerable differences in opinion exist concerning their positional behaviors or 2) they have the potential to aid in functional interpretations of other extinct primate sacra.

Oreopithecus bambolii is a large-bodied extinct hominoid from the late Miocene (Rook et al., 2000; Rook et al., 2011) of Tuscany and Sardinia, Italy. *Oreopithecus* shares with extant nonhuman hominoids an extensive list of postcranial synapomorphies, such as a mediolaterally wide trunk and shortened lumbar vertebral column, long fore-limbs relative to hind limbs, and mobile fore- and hind limb joints, suggesting that it probably relied on orthograde suspensory behaviors (Harrison, 1987, 1991; see also Wunderlich et al., 1999; Susman, 2004, 2005). Yet, some researchers contend that, superimposed on an orthograde bauplan, *Oreopithecus* exhibits several anatomical features of the postcranial axial locomotor skeleton that indicate it relied on habitual terrestrial bipedalism like that of modern humans, including dorsally wedged lumbar vertebrae and a caudally progressive increase in postzygapophyseal interfacet distance (e.g., Kohler and Moyà–Solà, 1997; Rook et al., 1999). These inferences are based on BA#72, which is an *Oreopithecus* specimen preserving three partial lower lumbar vertebrae and the first and second sacral vertebrae (Figure 2.2). Recently, Russo and Shapiro (2013) reevaluated the external morphology of this specimen and demonstrated that its lumbosacral morphology was unlike that of humans, with no evidence for lordosis in the lumbar region, and clear morphological affinities with nonhuman hominoids in the sacral region (e.g., mediolaterally narrow alae, small prezygapophyseal articular facets). This study will expand on their analysis by examining the trabecular morphology of the BA#72 sacral

specimen in order to further improve our understanding of the axial skeletal anatomy of *Oreopithecus* and to offer additional insight into debate concerning its positional behaviors.

Nacholapithecus kerioi is an extinct hominoid from the Middle Miocene. Generally, the vertebral morphology of *Nacholapithecus* is consistent with that of pronograde, quadrupedal mammals and most likely permitted sagittal plane flexibility (Slijper, 1946; Schultz, 1953, 1961; Benton, 1967; Ward, 1993). For example, like earlier hominoids (e.g., *Proconsul*), *Nacholapithecus* had a relatively long lumbar vertebral spine (comprised of 6 lumbar vertebrae) with craniocaudally elongated vertebral bodies bearing rudimentary accessory processes, ventral median keels, and transverse processes arising from the vertebral body or body-pedicle junction (Ward, 1997; Ishida et al., 2004; Nakatsukasa and Kunimatsu, 2009), and probably retained a sacrum with anthropoid-like numbers of sacral vertebrae (3-4 sacral vertebrae, Nakatsukasa and Kunimatsu, 2009). However, some derived modern ape-like features of the fore- and hind limbs suggest that *Nacholapithecus* may have also practiced orthograde positional behaviors to some extent as well. For example, the *Nacholapithecus* elbow joint has more pronounced mobility-enhancing features (e.g., more inflated capitulum) which, along with a long clavicle and large manual phalanges relative to pedal phalanges, have been used to infer that it probably relied more on forelimb-dominated activities (e.g., orthograde clambering, bridging) than earlier hominoids (Nakatsukasa and Kunimatsu, 2009). This study examines the first sacral vertebra belonging to *Nacholapithecus kerioi* (Figure 2.2; KNM-

BG 17822; Rose, 1996; Nakatsukasa and Kunimatsu, 2009) in order to assess, to what extent, this hominoid relied on nonstereotypical, orthograde postures and locomotion.

Although this study of positional behaviors chiefly concerns hominoid taxa, the inclusion of other groups of extinct primates expands the possibilities for postural and locomotor reconstructions in extinct hominoids beyond what is accounted for by extant primates alone. Additionally, unique aspects of positional behaviors found in extinct apes may have characterized other extinct primate taxa.

Epipliopithecus vindobonensis (Zapfe and Hürzeler, 1957; Zapfe, 1958; 1960) is a primitive catarrhine (Pliopithecidae) that has no living descendents and was once thought to be an ape (Begun, 2007). *Epipliopithecus* has an intermembral index of 94 (indicating that the hind limbs were slightly longer than the fore-limbs), long, curved manual and pedal phalanges, and a long lumbar vertebral column (comprised of ~7 lumbar vertebrae) (Zapfe, 1958; Begun, 2002). These features suggest that *Epipliopithecus* was an agile arboreal quadruped with some suspensory abilities, probably similar to *Lagothrix* (Zapfe, 1958; Rose, 1993). A recent investigation of the trabeculae in the *Epipliopithecus* os coxa suggests its locomotor mode may have more closely resembled that of *Hylobates* (Macchiarelli et al., 2001). O.E. 304-45 is complete sacral specimen from "Individual I" (Zapfe, 1958). A partial first sacral vertebra is also known from "Individual II." The complete sacrum from Individual I is comprised of three sacral vertebrae (Figure 2.2), and exhibits a distal end that suggests it possessed a reduced tail (Zapfe, 1958; Chapter 3). This study independently tests the inferred positional behaviors of *Epipliopithecus* by examining the trabecular architecture in S1 of O.E. 304-45 (Figure 2.2).

Subfossil Malagasy lemurs, an extinct radiation of Primates, are excellent subjects with which to compare the results of the extinct hominoid sample because they likely exhibited considerable diversity in their positional behaviors. Previous research has identified morphological parallels between some subfossil lemurs (e.g., *Palaeopropithecus*) and *Oreopithecus* with respect to postcranial anatomy that is suggestive of a highly arboreal and possibly sloth-like lifestyle (Wunderlich et al., 1999). Thus, the inclusion of subfossil lemurs in this study may further help elucidate the locomotor nature of extinct hominoids.

Megaladapis is a large-bodied lemur likened to living koalas based on its large body size, limb proportions, long digits, and curved phalanges (Jungers et al., 2002; Godfrey and Jungers, 2002), and can be probably best characterized as a deliberate arboreal climber with powerful grasping capabilities. *Megaladapis* also exhibited craniocaudally short lumbar vertebrae with reduced spinous processes (Shapiro et al., 2005). Craniocaudally short lumbar vertebrae are also characteristic of extant apes (when compared to the primitive catarrhine condition), and provide sagittal lumbar stability during orthograde, suspensory behaviors by reducing intervertebral bending movements (Cartmill and Milton, 1977; Ward, 1993). The presence of short lumbar vertebral bodies in *Megaladapis* (compared to some other subfossil lemurs, though notably most subfossil lemurs appear to have shorter lumbar vertebrae than living strepsirrhines) indicates it exhibited considerable spinal stability and may have employed some antipronograde activities (Jungers et al., 2002; Shapiro et al., 2005). The *Megaladapis* sacrum (DLC 7950; Figure 2.2) examined in this study consists of four sacral vertebrae and, like the

lumbar vertebrae, exhibits extremely reduced spinous processes. Its anatomy is unusual in that the distal end is noticeably transversely wider than the proximal end, with this expansion occurring just distal to the sacroiliac joint surface (Figure 2.2). The morphology of the distal sacrum suggests it possessed a shorter tail than *Archaeolemur* (Chapter 3). This study independently tests the inferred positional behaviors of *Megaladapis* by examining the trabecular architecture in S1 of DLC 7950.

Archaeolemur is a lemur whose postcranial anatomy is compatible with that of a terrestrial quadruped with some arboreal and climbing abilities (Jungers et al., 2002; Shapiro et al., 2005; Godfrey and Jungers, 2002). The *Archaeolemur* postcrania are robust, and it appears to have possessed craniocaudally short lumbar vertebral bodies, short limbs, and short digits (Jungers et al., 2002; Godfrey and Jungers, 2002). Several sacra are known for this taxon and have been discussed previously, primarily with respect to tail length (e.g., Godfrey et al., 2006). Generally, the sacra appear robust, particularly dorsoventrally, and most are comprised of two (e.g., DLC 11826) to three (e.g., DLC 11823, DLC 11835, DLC 9905, DLC 11836) vertebrae. The ventral faces of the sacra are squared, providing considerable surface area for the attachment of the anterior longitudinal ligament (Godfrey et al., 2006). The size of the caudal neural openings (relative to the cranial neural openings) of these sacra, and the presence of associated caudal vertebrae, suggest that *Archaeolemur* possessed a long tail (Godfrey et al., 2006; Chapter 3). This study independently tests the inferred positional behaviors of *Archaeolemur* by examining the trabecular architecture in S1 of DLC 9905, 11823, and 11835 (Figure 2.2).

Palaeopropithecus is a lemur that converges morphologically with living sloths with respect to some aspects of postcranial anatomy, including its short hind limbs relative to fore-limbs, highly curved manual and pedal phalanges, reduced pollex and hallux, and lumbar vertebrae having considerably reduced spinous processes, wide laminae and dorsally positioned transverse processes (Jungers et al., 2002; Shapiro et al., 2005; Godfrey and Jungers, 2002). Taken together, *Palaeopropithecus* postcranial morphology is like that of extant sloths and is consistent with inverted, under-branch suspensory locomotion. *Palaeopropithecus* sacra have been discussed elsewhere with respect to tail length (Huq and Jungers, 2009). The size of the distal sacral aperture is considerably smaller than the proximal sacral aperture, suggesting its tail was vestigial (Huq and Jungers, 2009; Chapter 3). DLC 24778 is a complete *Palaeopropithecus sp.* sacrum comprised of four vertebrae (Figure 2.2). In overall appearance, the sacrum is mediolaterally wide and dorsoventrally compressed, in striking contrast to the dorsoventrally deep and robust sacra of *Archaeolemur* (Figure 2.2). Like the lumbar vertebrae, the spinous processes are greatly reduced with little dorsal projection (Figure 2.2). This study independently tests the inferred positional behaviors of *Palaeopropithecus* by examining the trabecular architecture in S1 of DLC 24778 (Figure 2.2).

MATERIALS AND METHODS

Sample

Extant Primates

The extant primate sacral sample used in this study consists of 78 sacra belonging to adult individuals from 13 extant primate genera that vary in posture and locomotion (see Table 2.1 for classification of positional behaviors). Sacral specimens derive from the anthropology and mammalogy collections at the American Museum of Natural History (New York, NY, USA) and the National Museum of Natural History (Washington, D.C., USA). A power analysis (PS v3.0.43) indicated that six sacra per species affords the power to detect a 20% difference between taxon means ($p < 0.05$) in a subset of pilot data for two trabecular bone variables that arguably most influence trabecular bone strength (degree of anisotropy and bone volume fraction; Goldstein et al., 1993). Previous studies have demonstrated that statistically significant differences among trabecular variables are detectable with comparable numbers of individuals (e.g., MacLatchy and Müller, 2001, n=5/group; Ryan and Ketcham, 2005, n= 1 to 10/group). Therefore, this study aimed to examine at least six sacra per taxon. Nonetheless, sufficient museum material was not always available, and some sacra had to be excluded from analyses because test scans revealed internal bone damage.

Extinct Primates

The extinct primate sacral sample used in this study consists of 8 sacra from six genera of extinct primates, including three subfossil lemurs (*Archaeolemur*, *Megaladapis*, and *Palaeopropithecus*), one extinct pliopithecoid (*Epipliopithecus*), and two extinct hominoids (*Nacholapithecus* and *Oreopithecus*) (Figure 2.2). The subfossil lemur sacra are housed at the Duke University Primate Center Division of Fossils (Durham, NC, USA). The subfossil lemur specimens examined include *Archaeolemur* DLC 11823, DLC

11835, and DLC 9905, *Megaladapis* DLC 7950, and *Palaeopropithecus* DLC 24778. The *Epipliopithecus* (O.E. 304-45) and *Oreopithecus* (BA#72) sacra are housed at the Naturhistorisches Museum Basel (Basel, Switzerland). The *Nacholapithecus* sacral specimen is BG 17822, which is housed at the National Museums of Kenya (Nairobi, Kenya). All extinct primate sacra were scanned at either The University of Texas at Austin (Austin, TX) or in facilities located in or near the cities where they are housed (see below for details).

CT Data Collection

Extant Primates

All extant primate sacra were scanned at the High Resolution X-ray Computed Tomography Facility at The University of Texas at Austin, Department of Geological Sciences (UTCT) (see Ketcham and Carlson [2001] for details on the scanner). Similarly-sized extant primate sacra were scanned together to minimize scanning time and reduce calibration costs, resulting in CT image datasets containing as many as four sacra. Sacra were secured in the scanner using synthetic foam mold and mounted craniocaudally in order to collect transverse slices. All UTCT scans were collected using source energy settings of 200kV/0.2 mA and obtaining between 1600-1800 views with two samples per view. For each scan, 31 slices were collected per rotation. Images were reconstructed as unsigned 16-bit TIFF grayscale images with a 1024 x 1024 pixel matrix.

Serial cross-sectional scans were collected for the entire sacrum. As such, the highest spatial resolution depended on sacral element size. Because the study primates, and thus their sacra, varied considerably in size (Table 2.1), three scan protocols were

defined in order to best standardize resolutions across the sample. The "small" protocol (i.e., highest scan resolution) included the smallest-bodied taxa in the sample and used a 45.5 field of view (FOR), yielding an in-plane (x, y) resolution of 44µm and an out-of-plane (z [interslice]) resolution of 47µm. The "medium" protocol included primates with mid-range body sizes in the sample and used a FOR of 60.5, yielding an in-plane resolution of 59µm and an out-of-plane resolution of 63µm. The "large" protocol (i.e., lowest scan resolution) included the largest bodied-taxa in the sample and used a FOR of 76.5, yielding an in-plane resolution of 75µm and an out-of-plane resolution of 80µm. External measurements of sacral maximum dorsoventral and mediolateral dimensions, obtained during prior visits to the museums to hand-select specimens, were used to place sacra into the appropriate size category.

To facilitate data processing, individual sacra were segmented from datasets in Avizo 7.0 (Visualization Sciences Group, Inc., Burlington, MA, USA). Slice stacks were then imported into VGStudioMax (Volume Graphics Software, Heidelberg, Germany) where images were reduced from unsigned 16-bit to unsigned 8-bit format with no impact on resolution. Data were then down-sampled to the out-of-plane resolution, and image stacks were resliced so the cranial articular surface of the sacrum was flush with the transverse plane. Down-sampling the data produced final isotropic voxel sizes of 47µm for the "small" protocol sacra, 63µm for the "medium" protocol sacra and 80µm for the "large" protocol sacra. The resolution classes examined here are smaller than typical trabecular thickness (Kothari et al., 1998) and are near or within the range of resolution classes employed in previous trabecular bone studies (e.g., Gosman and

Ketcham, 2009; Cotter et al., 2011; Ryan and Shaw, 2012; Su et al., 2013), suggesting that they can be used to accurately quantify the study trabecular bone variables.

While scanning elements at different resolutions can be time intensive because it requires different protocols, it is desirable to obtain the best resolution per specimen given its geometric constraints (e.g., large size or irregular shape) (Kim et al., 2004). In order to evaluate the potential error introduced into the sample by comparing specimens scanned at different resolutions (see Gosman and Ketcham, 2009), the distal end of three sacra belonging to *Gorilla gorilla* were scanned using each size protocol and corresponding regions of trabeculae were analyzed (Tables 2.6 and 2.7). The distal end of the sacrum was chosen over the proximal end for its smaller dimensions, which afforded reduced scan time and cost for this investigation. Datasets were not resampled or resolution-reduced for analysis (following Gosman and Ketcham, 2009). Corresponding trabecular regions were identified using recognizable bony landmarks and features. Although this process results in regions that are not analogous, there is likely a substantial amount of spatial overlap (see also Gosman and Ketcham, 2009; but see Fajardo and Müller, 2001). Following Gosman and Ketcham (2009), percent differences between resolution classes were calculated for each trabecular bone variable. Correction factors were derived from these data and applied to the lower resolution data. The resolution-reduced (i.e., -corrected) dataset was evaluated against the original dataset by comparing the results for individual trabecular bone variables and using multivariate analyses.

Extinct Primates

The *Oreopithecus* (BA#72) and *Epipliopithecus* (O.E. 304-45) sacra were scanned by the Naturhistorisches Museum Basel at the Universitätsspital Basel on a GE Phoenix Nanotom m. Source energy settings were 180kV/0.35mA, yielding isotropic voxel sizes of 44µm and 30µm, respectively, for *Oreopithecus* and *Epipliopithecus*. However, the *Epipliopithecus* proximal sacrum had to be subsequently removed from the study because some of the CT slice files were corrupted that precluded the ability to analyze this specimen. The *Nacholapithecus* S1 vertebra (BG 17822) was scanned by M. Nakatsukasa on a Stratec pQCT research SA+ portable scanner at the Kenyan National Museum. The resulting isotropic voxel size was 50µm for the *Nacholapithecus* specimen.

The subfossil lemur specimens were hand-transported to the HRXCT Facility at UT Austin and scanned using settings similar to those employed for the extant primate sample. Subfossil sacra were all scanned at an energy source setting of 200 kV/0.24 mA, 1800 views with two samples per view, and 31 slices were collected per rotation. The HRXCT Facility staff completed ring-removal and beam-hardening processing. The *Archaeolemur* DLC 9905, 11823, and 11835 and *Palaeopropithecus* DLC 24778 sacra were scanned using the "medium" protocol defined for the extant taxa, yielding an in-plane (x, y) resolution of 59µm and an out-of-plane resolution of 63µm. The *Megaladapis* sacrum, which was considerably larger than the *Archaeolemur* and *Palaeopropithecus* sacra, was scanned at the "large" protocol, yielding an in-plane (x, y) resolution of 75µm and an out-of-plane resolution of 80µm.

CT Data Processing

Volumes of Interest and Trabecular Parameters

QUANT3D analysis software (developed at the HRXCT facility; Ryan and Ketcham 2002a, b; Ketcham and Ryan, 2004) was used to quantify trabecular structural parameters in a single three-dimensional spherical volume of interest (VOI). VOIs were positioned at midline subjacent to the lumbosacral joint in the S1 vertebral body (Figure 2.1). Following Fajardo et al. (2013), VOIs were adjusted to exclude end plate bone tissue by repositioning the sphere so that ten slices separated its outer boundary and any visible evidence of the cranial endplate. The limiting vertebral dimension for scaling the VOIs was the dorsoventral breadth because the sacral cranial articular surfaces of the specimens included in this sample are all narrower dorsoventrally than mediolaterally (i.e., dorsoventral/mediolateral ratio values were all less than 1; data not shown). VOI were scaled by 50% dorsoventral breadth of the sacrum's cranial articular surface in order to prevent over-sampling of trabeculae in taxa that varied in body size (see Fajardo and Müller, 2001 for discussion; see also Lazenby et al., 2011). All VOIs were visually inspected in views from three perpendicular planes to ensure that no cortical bone was contained within the boundary of the sphere and subsequently repositioned if necessary. VOIs in the smallest specimens were also inspected to ensure that a minimum of three to five trabecular lengths were included to satisfy the continuum assumption (Harrigan et al., 1988). Where certain taxa violated this assumption, they were removed from the sample. The VOIs ranged in size from approximately 1.2 to 9.4 mm in diameter.

Quantification of six trabecular structural variables was automated in QUANT3d using the star volume distribution (SVD) algorithm (Ketcham and Ryan, 2005) with the exception of trabecular number, which was calculated using the mean intercept length method. In the SVD algorithm, intercept lengths in the shape of cones are drawn outward from a number of points until encountering another trabecular strut (Ryan and Ketcham, 2002). Data are then compiled into a 3x3 weighted orientation matrix that derives a fabric tensor describing the distribution of bone in three dimensions (Ryan and Krovitz, 2006). The matrix contains eigenvectors (μ_1, μ_2, μ_3) and eigenvalues (τ_1, τ_2, τ_3,) that describe the primary, secondary and tertiary orientations and magnitude, respectively, of trabecular bone (Ryan and Krovitz, 2006; Maga et al., 2006; Ryan and Walker, 2010). Eigenvalues are used to calculate the degrees of anisotropy (DA), which reflect how strongly (i.e., magnitude) the trabeculae organize themselves in the three axes (Maga et al., 2006). The first DA is the primary axis (τ1) / the tertiary axis (τ3), the second DA is τ1/ the secondary axis (τ2), and the third DA is τ2/ τ3. A DA index value (dimensionless) of 1 indicates the structure is fully isotropic or randomly organized, while an increasing DA index (i.e., away from 1), is associated with increasing structural organization or anisotropy (Fajardo and Müller, 2001). Trabecular organization can also be described using the isotropy index (I [dimensionless]), which is the calculated as the inverse of DA (τ_3/τ_1). The trabecular elongation index (E [dimensionless]), calculated as 1-(τ2/ τ1), reveals the preferred orientations of trabeculae as defined by the first and second axes to describe trabecular shape. When the DA index value is greater than 1, corresponding E

values distinguish between rod-shaped (E values closer to 1) and plate-shaped trabeculae (E values closer to 0).

Bone volume fraction (BV/TV [dimensionless]) is defined as the total number of bone voxels to total voxels per unit volume and is generally accepted as a surrogate of the density of the trabecular network (Fajardo and Müller, 2001; Maga et al., 2006). Higher BV/TV values indicate greater bone density per unit volume, while lower values indicate lower bone density per unit volume. Trabecular thickness (Tb.Th [mm]) is the mean thickness of trabecular struts defined by placing non-overlapping spheres *within* the mid-axes of trabecular struts (centered mid-axis) and calculating the average diameter of all spheres in the volume of interest (Fajardo and Müller, 2001; see their Figure 2A). Trabecular number (Tb.N [mm^{-1}]) is calculated by placing spheres *between* the mid-axes of trabecular struts in the VOI and calculating the inverse of the average diameter of all spheres in the volume of interest (Fajardo and Müller, 2001; see their Figure 2C). The settings for the SVD analyses are 513 uniform orientations, with random rotations, and 1000 points.

Thresholds

The collection of trabecular morphometric data from the extant primate sample requires thresholding the CT images in order to determine exact boundaries between bone and air (background) interfaces. For all extant taxa, VOIs were processed using an adaptive, iterative threshold algorithm (Ridler and Calvard, 1978) that is frequently employed in trabecular bone studies (e.g., Maga et al., 2006; Fajardo et al., 2013) and is a standard function in QUANT3d. Identifying thresholds for the extinct primate sacra was

more complicated than that for extant primate sacra because matrix in-filled the trabecular network in S1 in all sampled sacra. Thus, determining a threshold required consideration of the matrix as a third material that may be more or less dense than the bone. In such instances, threshold values were determined using a modified version of the half-maximum height method (HMH) (Ulrich et al., 1980; Spoor et al., 1993). An HMH value is a determined grayscale value that is halfway between the highest and lowest grayscale value on either side of a tissue interface (e.g., bone – air) within a region of interest (Ulrich et al., 1980; Spoor et al., 1993). HMH was introduced to the paleoanthropology community by Spoor and colleagues (1993) for use with cortical bone data, and later modified by Fajardo et al. (2002) for use with trabecular bone data. Previous studies demonstrate that measurements obtained using HMH-determined thresholded scans perform considerably better than visually-determined thresholded scans when both are compared to measurements taken on actual dried specimens (Coleman and Colbert, 2007), and that the HMH thresholding method can accurately resolve trabecular mesh networking (Fajardo et al., 2002).

This study derived HMH values to determine the boundaries at three material interfaces: 1) matrix-bone, 2) matrix-air, and 3) bone-air (Figure 2.3). For specimens where matrix was denser (i.e., had a higher grayscale value; toward 255 in 8-bit images) than bone, the matrix-bone and matrix-air boundary HMH values were averaged to find a "high threshold", while the HMH values for the bone-air boundary was used as the "low threshold." Averaging the matrix-bone and matrix-air values was necessary because sole use of the matrix-air HMH value would overestimate the volume of bone, while sole use

of the bone-air boundary would likely underestimate the amount of bone. This method was employed for *Archaeolemur* DLC 11835 and 11823, and *Megaladapis* DLC 7950. The *Nacholapithecus* scan exhibited scatter, or dark and light streaks through the image. Scatter results from the detection of more photons than expected and consequently, the appearance of dark streaks along the axis of greatest attenuation. Filter detection of these dark streaks exaggerates the differences between elements and consequently produces bright streaks in the opposing direction. A binary threshold was applied to this scan using an HMH value from the bone-air boundary. The *Palaeopropithecus* sacrum contained two types of matrix: one that was denser than bone, and one that was less dense than bone. In this case, the "low threshold" (which cannot be air) was the matrix-air HMH value. The "high threshold" was the HMH value from matrix-bone and matrix-air. The *Oreopithecus* sacrum and one of the *Archaeolemur* sacra (DLC 9905) could not be evaluated because of similarities in the density of the matrix and bone, which produces a "solid block-like" appearance and precluded the ability to threshold the slice stack.

The modified HMH protocols for extinct primate sacra as defined above were carried out in ImageJ and then applied to CT image slice stacks in Avizo *Fire* (Visualization Sciences Group, Inc., Burlington, MA, USA). First, the cranial and caudal endplates of S1 were determined for each scanned sacrum. Then, 10 slices were counted inward (i.e., counting toward the center of the vertebra) starting from the last visible evidence of the cranial and caudal endplates. All other slices, including those of the other sacral vertebrae, were omitted from the CT stack. The slice stack was then imported into ImageJ and converted to an 8-bit image type. Fossil sacra were not subject to resampling

or resolution-reduction for analysis. Starting with the first (i.e., most proximal) slice, five-to-ten regions of interest within S1 were selected, and the HMH was determined for a row of pixels drawn across the boundary of interest (e.g., bone-air) (Figure 2.3). Sampling was restricted to the first sacral vertebral body where the VOI would be placed, and any trabeculae extending into the alae and/or bony struts that were near the ventral or dorsal body edges and questionably "cortical bone" were excluded. Regions of interest were selected from the dorsal, ventral, medial, lateral aspects and the center of S1 to ensure adequate sampling of the CT slice. All three phases (matrix-bone, matrix-air, bone-air) were obtained from the same slice number to determine the threshold needed. This process was repeated every 50-75 slices in the CT stack, depending on the number of slices, and the average was taken to identify the boundary of each material interface (following Coleman and Colbert, 2007). 8-bit TIFF slice stacks were then imported into Avizo *Fire* in order to apply the defined thresholds to the extinct primate sacra. Minimum and maximum thresholds were applied using the Interactive Thresholding function. An arithmetic function was then applied to extract only the thresholded data, which was consequently recognized as a separate material field. Slice stacks were then saved as 2d TIFFS for further analysis in QUANT3d.

Statistical Analysis

Data analysis began with Pearson's correlations (two-tailed) to determine the relationship, if any, between raw values for all trabecular variables and mediolateral width of the first sacral vertebra (MLW-S1). Previous studies show that least-squares slope for the mediolateral width of the S1 regressed on body mass is slightly negatively

allometric [i.e., allometry exponent <0.333], but not significantly different from isometry, in catarrhines (Russo and Shapiro, 2011; see also Jungers, 1991; Ward, 1991). This study includes a broader taxonomic sample than previous studies (with additional small- and large-bodied platyrrhines and strepsirrhines) but also found that the least-squares slope for MLW-S1 regressed on body mass is isometric (b =0.330, lower/upper 95% confidence intervals= 0.303/0.350). Body mass and MLW-S1 were also strongly correlated in this sample (Pearsons's r = 0.97, p<0.001). Therefore, in order to evaluate the relationship between body size and trabecular parameters, this study elected to use MLW-S1 measurements specific to museum specimens in the data set rather than published data on species means. Significant relationships ($p < 0.05$) between trabecular bone variables and MLW-S1 were further examined using reduced major axis (Type II) regressions (Fajardo et al., 2013; Ryan and Shaw, 2013). Following Ryan and Shaw (2013), regressions were performed using log-transformed trabecular bone variables and log-transformed MLW-S1.

It is worth noting that the studies by Ryan and Shaw (2013) and Fajardo et al. (2013) also employed phylogenetic generalized least-squares regressions to examine the influence of phylogeny on trabecular bone variables. Ryan and Shaw (2013) examined a sample with broader taxonomic range (34 species; strepsirrhines, platyrrhines, cercopithecoids, and hominoids [see the electronic supplement for taxa]) than Fajardo et al. (2013) (lumbar vertebral trabecular morphology in nine strepsirrhine species), and found the influence of phylogeny to be present but weak in their examination of primate humeri and femora (see also Doube et al., 2011). Moreover, conventional and

phylogenetic regressions produced very similar results in their study (Ryan and Shaw, 2013). As such, this study relied on conventional regression models.

Previous studies of trabecular scaling trends generally suggest that scaling patterns depend on factors such as the sampled taxa, anatomical region and bone geometry, and range of body masses. Both Swartz and colleagues (1998; 42 bat and non-volant mammal species) and Doube et al. (2011; 90 species of bird and mammals) found that Tb. Th in femora and humeri scaled negatively with body mass, with the exception of within Chiroptera for which Tb.Th scaled isometrically with body mass (Swartz et al. 1998). Within primates, Ryan and Shaw (2013) found that Tb.Th and Tb.N scaled negatively with increasing femoral head height in a large sample of primate femora and humeri from 34 species (235 individuals). Fajardo et al. (2013) found that Tb.Th scaled with isometry with body mass in the last lumbar vertebral body in a sample of nine strepsirrhine species (N=29). The values for expected isometric slopes (i.e., geometric similarity) depend on the variable of interest (see Fajardo et al., 2013 and Ryan and Shaw, 2013 for additional discussion). Shape variables, such as BV/TV, Tb.N, DA, I, and E, should be invariant with changes in body mass (approximated here as MLW-S1). Thus, the expected isometric slope for the relationship between these variables and MLW-S1 is 0 (Ryan and Shaw, 2013). Positive and negative slopes significantly different from 0 (defined here as slopes not encompassed within the upper and lower limits of 95% confidence intervals) are indicative of positive and negative allometry, respectively (Ryan and Shaw, 2013). The expected isometric slope for the relationship between Tb.Th and MLW-S1 is 1 because it is a linear variable (Ryan and Shaw, 2013). Reduced major

axis linear regressions were performed in PAST (PAleontological STatistics) (Hammer et al., 2001).

Only recently have studies of trabecular bone structure employed multivariate techniques such as discriminant function analysis (DFA) (Ryan and Shaw, 2012) and principal components analysis (PCA) (Scherf et al., 2013) to examine the relationship between suites of trabecular bone parameters and primate positional behaviors. DFA constructs a new variable as a function of the input variables (Sokal and Rohlf, 1995). In this method, categories (e.g., locomotor groups as in Ryan and Shaw, 2012) are assigned *a priori* and the discriminant function serves to maximize their separation (Sokal and Rohlf, 1995). While *a priori* classification of positional behaviors facilitates this type of data analysis and interpretation, it also likely obscures biologically meaningful variation in trunk posture and locomotion introduced by researcher biases. In other words, how to best classify primate positional behaviors, an issue already inherent to locomotor studies, has direct impact on DFA results. Moreover, the number of variables included in the model directly influences the predictive power of DFA. Specifically, as the number of variables of interest increases within a model, the greater the predictive power of that model is to assign taxa to locomotor categories. The present study employed principal components analysis (PCA), also known as factor analysis. In contrast to DFA, PCA reduces the number of input variables to form composite variables that maximize separation of the dataset as a whole without respect to categorical classifications (Sokal and Rohlf, 1995). In this way, the number of variables the PCA model considers can be lower than the number of input variables (Sokal and Rohlf, 1995). Thus, any potential

relationship between trabecular parameters and positional behaviors is identified *a posteriori*. This study used PCA to evaluate suites of trabecular bone variables among the major primate clade subsamples (hominoids, all catarrhines, platyrrhines). Strepsirrhines were excluded from the PCA and all subsequent analyses because there were fewer than three taxonomic groups.

Two principal components were extracted from the PCAs. Following extraction, one-way ANOVAs were used to compare PC1 and PC2 scores for each major primate clade subsample. ANOVAs were followed by Games-Howell post hoc pairwise comparisons, chosen because these data do not meet assumptions of homogeneity of variance or equal sample size (Games and Howell, 1976; Sokal and Rohlf, 1995). PCA and ANOVAS were performed in SPSS 16.0 (Chicago, IL, USA) with significance recognized at $p < 0.05$.

To be conservative in the interpretation of these data, results were considered first by taxon for all analyses. Postural and locomotor adaptations were secondarily considered as a means of offering functional perspective on the observed morphologies. For this study, postural and locomotor behavioral data were taken from field observations reported in the literature (see references in Table 2.1).

RESULTS

Correlations and Regressions

Results from Pearson's (two-tailed) correlation tests revealed that BV/TV (r= -0.075, p = 0.519), E (r= 0.087, p = 0.454), and I (r= -0.144, p = 0.210) were not significantly correlated with MLW-S1(r= 0.087, p = 0.454). Therefore, these variables

were not further examined in regression analyses. Raw values for Tb.N (r= -0.575, p < 0.000), DA (r= 0.261, p = 0.022), and Tb.Th (r= -0.800, p < 0.000) were significantly correlated with MLW-S1. Results of reduced major axis linear regression analyses of log-transformed Tb.N, DA, and Tb.Th on log-transformed MLW-S1 using the full dataset (i.e., individuals) are presented in Table 2.2. Degree of anisotropy and MLW-S1 scaled with positive allometry (i.e., 95% confidence intervals did not include 0, slope greater than 0) (Table 2.2; Figure 2.4D), indicating that larger-bodied primates have relatively more organized trabeculae than smaller-bodied primates. Trabecular thickness and MLW-S1 scaled with negative allometry (95% confidence intervals did not include 1; slope less than 1) (Table 2.2; Figure 2.8D), indicating that larger primates have thinner trabeculae per unit volume than do smaller primates. Trabecular number and MLW-S1 also scaled with negative allometry (95% confidence intervals did not include 0; slope less than 0), indicating that larger primates have a relatively fewer trabeculae per unit volume than do smaller primates (Table 2.2; Figure 2.9D).

Boxplots

Taxon means and standard deviations for trabecular variables are presented in Table 2.3. Data are depicted for each variable by taxon in Figures 2.4-2.9, with "A" figures depicting the results for the original dataset and "B" figures depicting results for the resolution-reduced dataset (discussed below). Data are additionally depicted for each positional behavior group in Figures 2.4-2.9 "C" figures. Asterisks indicate suspect outliers and circles indicate very suspect outliers (as determined by SPSS). Results are discussed with respect to positional behavior groups.

Consistent with predictions, DA values were highest in humans, followed by vertical clingers and leapers (Table 2.3; Figure 2.4C). This finding suggests that trabeculae are more organized (i.e., more anisotropic) in these positional behavior groups. Inconsistent with predictions, values were next highest in orthograde manual suspensors, followed by pronograde quadrupeds and orthograde-adapted quadrupeds (Figure 2.4C). Differences in DA values were not significant among any of the positional behavior groups (p>0.05Table 2.4).

Inconsistent with predictions, E values were highest in orthograde manual suspensors, followed by pronograde quadrupeds, humans, orthograde-adapted quadrupeds and then vertical clingers and leapers (Figure 2.5C). Differences in E values were not significant among any of the positional behavior groups (p>0.05; Table 2.4). This finding suggests that trabeculae are most rod-shaped in orthograde manual suspensors and more plate-shaped in vertical clingers and leapers.

The isotropy index is the inverse of DA. Therefore, consistent with what would be expected given the predictions for DA, values are highest in orthograde-adapted quadrupeds, followed by pronograde quadrupeds, then orthograde manual suspensors, vertical clingers and leapers and humans (Figure 2.6C). However, like DA, differences in I values were not significant among any of the positional behavior groups (Table 2.4).

Inconsistent with predictions, bone volume fraction was lowest in humans (Figure 2.7C). Differences between humans and all other groups were significant (p>0.05; Table 2.4). Bone volume fraction was highest in vertical clingers and leapers, followed by orthograde-adapted quadrupeds, orthograde manual suspensors and then pronograde

quadrupeds (Figure 2.7C). Orthograde manual suspensors and pronograde quadrupeds had significantly lower bone volume fraction values than orthograde-adapted quadrupeds and vertical clingers and leapers ($p<0.05$), but their values were not significantly different from each other ($p>0.05$Table 2.4).

Because trabecular thickness (the only linear variable examined in the study) was significantly correlated with body size (approximated here by MLW-S1), it was size-corrected by dividing thickness values by MLW-S1 for all remaining comparisons (boxplots and PCAs). Inconsistent with predictions, size-corrected trabecular thickness values were lowest in humans (Figure 2.8C). Vertical clingers and leapers had the thickest trabeculae, followed by orthograde manual suspensors, pronograde quadrupeds, and then orthograde-adapted quadrupeds. Differences between humans and orthograde manual suspensors and pronograde quadrupeds are significant ($p<0.05$; Table 2.4). Orthograde-adapted quadrupeds are significantly different from pronograde quadrupeds and manual suspensors ($p<0.05$; Table 2.4).

Inconsistent with predictions, humans had the fewest trabeculae (Figure 2.9C). Pronograde quadrupeds had the greatest number of trabeculae, followed vertical clingers and leapers, orthograde-adapted quadrupeds, and then manual suspensors. Differences were significant between pronograde quadrupeds and all other groups with the exception of vertical clingers and leapers (Table 2.4).

I and E are descriptors of trabecular fabric structure which can be visualized using ternary shape diagrams (Figure 2.10). Originally produced for particle-shape data (Sneed and Folk, 1958), these diagrams can be modified in order to evaluate other types of fabric

data such as trabecular networks (Benn, 1994; Graham and Midgley, 2000). In these shape diagrams, data toward the ternary's top apex indicate that trabecular are more isotropic and sphere-like, data toward the bottom left apex indicate that trabeculae are more anisotropic and plate-like, and data toward the bottom right apex indicate that trabeculae are more anisotropic and rod-like. To facilitate comparisons, the ternary diagrams are presented by the major primate clade subgroupings. Within hominoids, the distribution of values for modern humans is separated from that of *Pan*, with *Pan* exhibiting more isotropic trabeculae than modern humans in S1, which exhibit relatively more anisotropic trabeculae in (Figure 2.10). However, distributions for *Gorilla*, *Pongo* and *Hylobates* overlap those of both *Pan* and modern humans (Figure 2.10). The distribution of values for modern humans appears less circumscribed than that of the other hominoids. When other catarrhines are considered (*Macaca* sp. and *Mandrillus*), there is little to no separation between taxa, and distributions for all three *Macaca* species and *Mandrillus* overlap those for hominoid taxa considerably (Figure 2.10). Within platyrrhines, the distribution for *Ateles* is separated from that of *Sapajus*, and is positioned lower in the ternary diagram, indicating more anisotropic trabeculae in S1. The distribution for *Saimiri* is intermediate between, and overlaps with, those of *Ateles* and *Sapajus* (Figure 2.10). Few strepsirrhine individuals are considered in this study. However, the two *Varecia* individuals are positioned higher in the ternary diagram, and thus have more isotropic trabeculae in S1, in comparison to the two *Indri* individuals, which are positioned lower in the ternary diagram and thus have more anisotropic

trabeculae in S1. Because there is little inter-taxonomic separation in these diagrams, positional behaviors are not considered here.

Although I and E (and DA, the inverse of I) provide information about trabecular organization and shape, they are not indicators of trabecular *orientation*. Consideration of trabecular orientation is important as bone is strongest when loaded on-axis, and thus the principal axes of trabecular bone structure correspond closely to its primary elastic directions (Odgaard, 1997). Two individuals may exhibit similar levels of anisotropy, but very different primary orientations of trabecular struts as a result of different loading regimes. The principal axes of trabecular orientation can be visualized in three-dimensional space by plotting eigenvectors (μ_1, μ_2, μ_3) onto an equal-area stereoplot (Maga et al., 2006). Figure 2.11 shows the projection of the first eigenvector for all taxa in the sample. Polygons were not drawn around positional behaviors group distributions given the wide spread of data points in this analysis. Inconsistent with predictions, extant primates exhibit a variety of orientations in S1 and there does not appear to be any orientation that is positional behavior- specific within any of the major primate clade subgroupings.

Principal components analyses (PCAs)

Table 2.5 presents the results for PC1 and PC2 in analyses of all primates and the major primate clade subgroupings. The correlation between each of the trabecular variables and the first two principal components is presented in the component matrix. All trabecular variables examined were included in the PCA with the exception of I as it is the inverse of DA. Bivariate plots of PC1 (x-axis) and PC2 (y-axis) are depicted in

Figures 2.12-2.14. Table 2.6 presents the ANOVAs for PC1 and PC2 scores among taxon means and Games-Howell post-hoc pairwise comparisons.

Among all primates, PC1 and PC2 accounted for approximately 78% of the total variance in the entire dataset (Table 2.5). Of the total variance, PC1 accounted for 45% and PC2 accounted for 20%. The component matrix indicates that BV/TV and Tb.N are both negatively correlated with PC1, while DA, E, and Tb.Th are positively correlated with PC1. A bivariate plot and pairwise comparisons are not included for all primates given the large number of included taxa.

Among only hominoids, PC1 and PC2 accounted for approximately 69% of the total variance in the entire dataset. Of the total variance, PC1 accounted for 44% and PC2 accounted for 26% (Table 2.5, Figure 2.12). The component matrix indicates that BV/TV and Tb.N are both positively correlated with PC1, while DA, E, and Tb.Th are negatively correlated with PC1. Figure 2.12 depicts a bivariate plot of PC1 (x-axis) and PC2 (y-axis) scores among hominoid individuals with fitted polygons around the individuals of each taxon. Mean PC1 scores distinguish between modern humans and orthograde-adapted quadrupedal *Pan* ($p<0.05$), but not *Gorilla.* Humans exhibit primarily negative PC1 scores, which are associated with lower bone volume fraction and trabecular number, and higher degree of anisotropy, elongation index values and trabecular thickness, while *Pan* exhibits primarily negative PC1 scores, which are associated with higher bone volume fraction and trabecular numbers, and lower degree of anisotropy, elongation index values and trabecular thickness. PC1 does not distinguish among any other hominoid taxa (Table

2.5, Figure 2.12). However, mean PC2 scores distinguish between humans and the manual suspensor *Hylobates* ($p<0.05$), but not *Pongo* (Figure 2.12).

Among all catarrhines (i.e., hominoids + macaques and mandrills), PC1 and PC2 accounted for approximately 63% of the total variance in the entire dataset. Of the total variance, approximately 41% is accounted for by PC1, while 22% is accounted for by PC2 (Table 2.5). The component matrix indicates that BV/TV and Tb.N are both negatively correlated with PC1, while DA, E, while Tb.Th are positively correlated with PC1. BV/TV, Tb.N, Tb.Th, and E are all positively correlated with PC2. Figure 2.13 depicts a bivariate plot of PC1 (x-axis) and PC2 (y-axis) scores among all catarrhines in the sample with fitted polygons around the individuals of each taxon. Mean PC1 scores distinguished among no extant taxa. Mean PC2 scores distinguished between *Hylobates* and all other extant taxa, except *M.tonkeana* and *M. fascicularis* ($p>0.05$) (Table 2.5; Figure 2.13). Mean PC2 scores distinguished between humans and all macaques, but not between humans and *Mandrillus,* or between humans and the other hominoids (Table 2.5; Figure 2.13).

Among platyrrhines (i.e., *Ateles, Sapajus* and *Saimiri*), PC1 and PC2 accounted for approximately 76% of the total variance in the entire dataset. Of the total variance, approximately 54% is accounted for by PC1, while 22% is accounted for by PC2 (Table 2.5). The component matrix indicates that BV/TV and Tb.Th are both postively correlated with PC1, while DA, E, and Tb.N are negatively correlated with PC1. Figure 2.14 depicts a bivariate plot of PC1 (x-axis) and PC2 (y-axis) scores among platyrrhines in the sample with fitted polygons around the individuals of each taxon. Mean PC1 scores

do not distinguish among taxa (p>0.05). Along PC2, *Ateles* differs from *Saimiri* and *Sapajus*, but the latter do not differ from each other. All *Ateles* individuals exhibit positive PC2 scores, which are associated with lower bone volume fraction and values for the elongation index, and higher degree of anisotropy, trabecular number and trabecular thickness. All *Sapajus* and *Saimiri* individuals exhibit primarily negative PC2 scores (Figure 2.14).

Resolution effects

The resolution analysis data used to derive correction factors are presented in Table 2.6. Tb.Th was not size-corrected for these analyses. BV/TV and Tb.Th. showed consistently lower values in the higher-resolution data compared to the lower-resolution data across specimens. These parameters decreased by approximately 7% - 37% from the lower-resolution data to the higher-resolution data, with the highest percent reductions correlating with the lowest resolutions (Table 2.6). By contrast, Tb.N. showed consistently higher values in the higher-resolution data compared to the lower-resolution data. Values for this parameter increased by a smaller amount between approximately 3% and 8%. Values for the DA, E, and I indices showed less consistent trends, though generally these values also decreased from the lower-resolution data to the higher-resolution data (Table 2.6). The finding that, from the lower-resolution data to the higher-resolution data, values for BV/TV and Tb.Th. decreased while those for Tb.N. slightly increased, accords with the results for tests of resolution effects in previous studies (Gosman and Ketcham, 2009).

Despite these apparent resolution-dependent trends in the trabecular bone structural variables evaluated here, visual comparison of boxplots for individual resolution-reduced variables (Figures 2.4B-2.9B) reveals little overall change in the inter-taxonomic trends. This is quantitatively demonstrated by a comparison of PCA results and the results for ANOVA post-hoc pairwise comparisons of PC1 and PC2 scores of the resolution-reduced and original dataset among hominoids (Table 2.7). The PCs in the resolution-reduced dataset account for slightly less variance in the hominoid dataset than do the PCs in the original dataset (Table 2.7). When pairwise comparisons are considered, there are few differences between the results for the two datasets. The exceptions are the pairwise comparison between *Pan* and *Pongo*, which changes from non-significant to significant, and that for *Hylobates* and *Gorilla*, which changes from significant to non-significant (Table 2.7). It was for these few differences that the original dataset was retained for statistical analyses.

Extinct primates

The extant primate sample provides a somewhat functionally informative context for evaluating the trabecular bone parameters of the extinct primate sample. All values for the extinct primate sample are presented in Table 2.3 and alongside the extant sample by taxon in 2.15-2.17, and 2.18A and 2.19A. In 2.18B and 2.19B, results for the fossil sample are presented alongside the extant sample grouped by positional behavior for BV/TV and Tb.N, respectively. BV/TV and Tb.N were chosen for direct comparison because they were two variables for which significant differences were detected among positional behavior groups in the extant sample (Table 2.4). Tb.Th was not included

because MLW-S1 was not available for many of the extinct primate sample and thus size-corrected values could not be derived.

Values for the extinct primate sample fall among the ranges of values for a number of extant taxa for DA (Figure 2.15), E, (Figure 2.16), and I (Figure 2.17). *Palaeopropithecus* exhibits the highest BV/TV value, while *Nacholapithecus* exhibits the lowest BV/TV value (2.18A). Among extant taxa, the value for *Palaeopropithecus* falls above the range of any extant taxon, and the value for *Nacholapithecus* falls only within the range of humans (2.18A). The findings are similar for *Palaeopropithecus* and *Nacholapithecus* when compared to the extant taxa grouped by positional behavior (2.18B). Values for the *Archaeolemur* specimens and *Megaladapis* fall within the ranges for a number of extant taxa. When compared to extant taxa grouped by positional behavior, these taxa fall within the range of pronograde quadrupeds, but also that of manual suspensors (2.18B).

Megaladapis has the lowest value for trabecular number, while the two *Archaeolemur* specimens have the highest numbers among the subfossil lemurs (Figure 2.19A). Among extant taxa, the value for *Megaladapis* falls within the range of *Ateles*, but also that of humans, and the values for *Palaeopropithecus* and *Archaeolemur* fall among those of many taxa (Figure 2.19A). *Nacholapithecus* has an unusually high value for Tb.N that falls well above the range or individual values of any extant taxon (Figure 2.19A). When compared with extant taxa grouped by positional behavior, the Tb.N value for *Megaladapis* falls within the range of the manual suspensors but also that of humans (Figure 2.19B). The values for *Archaeolemur* and *Palaeopropithecus* fall within ranges

for a number of taxa (2.19B). The value for *Nacholapithecus* falls above the ranges of all positional behaviors (2.19B).

The elongation index values and isotropy index (inverse of DA) for the extant and extinct hominoids and strepsirrhines are plotted in Figure 2.20 to summarize trabecular fabric structure. *Nacholapithecus* falls near the center of the ternary diagram, indicative of neither fully isotropic nor fully anisotropic S1 trabeculae. *Megaladapis*, *Archaeolemur*, and *Palaeopropithecus* all fall toward the top of the ternary diagram, suggesting that their trabeculae in S1 are somewhat more isotropic. Figure 2.21 depicts the trabecular orientation data for the extant and extinct hominoids and strepsirrhines. Trabeculae in S1 of *Nacholapithecus* are oriented primarily mediolaterally. *Megaladapis* also exhibited trabeculae oriented primarily in a mediolateral direction. One *Archaeolemur* individual (DLC 11823) and *Palaeopropithecus* exhibited trabeculae oriented nearly craniocaudally. The other *Archaeolemur* individual (DLC 11835) exhibited trabeculae oriented nearly dorsoventrally.

DISCUSSION

This study is the first to apply high-resolution computed tomography to a comparative evaluation of the sacrum's internal bony morphology among a broad sample of living and extinct primates. This study tested the hypothesis that trabecular morphology in the first sacral vertebrae would differ among primates that vary in positional behaviors. Results suggest that some differences in positional behaviors may be detected from trabecular bone structure in the first sacral vertebra, though these findings were not always consistent with predictions.

Specifically, it was predicted that values for parameters related to trabecular bone strength (DA, BV/TV, Tb.N, Tb.Th) would be highest in habitually humans, followed by vertical clingers and leapers, then pronograde quadrupeds, orthograde-adapted quadrupeds and then manual suspensors. This prediction was received partial support from the data. Contrary to expectations, humans exhibited significantly lower bone volume fraction values than extant primates grouped by positional behavior, and had the lowest mean values among extant taxa (Table 2.3). This finding suggests that humans generally have lower bone density per unit volume than do most other primates in the sample. It was not expected that humans would exhibit the lowest bone volume density in the first sacral vertebra, given that trabecular bone strength generally increases with increasing bone density (Rice et al., 1988; Keaveny et al., 2001) and presumably human sacra must be structured to withstand the greatest loads among extant taxa given their unique reliance on habitual bipedalism, in which the hands are completely freed from a locomotor role. Yet, studies of trabecular bone in other regions of the human skeleton have also demonstrated low bone density in humans compared to other primates (e.g., calcaneus, Maga et al., 2006; metatarsals, Griffin et al., 2010; femoral head, Ryan and Shaw, 2012). At present, one potential explanation for this observation is the overall gracilization in the human skeleton (see Griffin et al., 2010 and citations therein). Although low bone volume fraction is suggestive of low bone tissue elasticity, it is possible that the specific orientation and placement of trabeculae could help alleviate stresses (Ryan and Shaw, 2012). However, it was also predicted that trabeculae would be primarily oriented in a mediolateral direction in all primates, but this prediction also did

not receive support. In fact, among the modern humans in this study sample, the observed orientations of trabeculae in S1 varied greatly. Of the eight human sacra examined, half of the individuals exhibited S1 trabeculae oriented mediolaterally, one individual exhibited S1 trabeculae oriented craniocaudally, two individuals exhibited S1 trabeculae oriented dorsoventrally, and one individual exhibited primarily off-orthogonal trabecular orientations. This finding is somewhat surprising as the clinical literature documents a fairly stereotypical pattern of trabeculae in the first sacral vertebral body that clearly accords with the pathway of stresses from the lumbosacral to sacroiliac joint (Pal 1989; Peretz et al. 1998; Ebraheim et al. 2000; Mahato, 2010). In S1 in humans, the trabeculae arise primarily from the dorsal and ventral cortices near the junction of the alae, and fan medially (toward the center of the vertebral body). There are also trabeculae secondarily coursing in a dorsoventral direction that interdigitate to create a cruciate pattern (Ebraheim et al., 2000). Distally, trabeculae become less predictable and more variably oriented in human sacra (Ebraheim et al., 2000). Findings from the clinical literature are largely based off of qualitative examination of 2D slices of the entire sacrum, while this study quantified trabecular morphology within a specific volume of interest scaled to body size. Therefore, methodological differences could explain why the findings from this study suggest a greater degree of intraspecific variation in trabecular morphology than has been previously considered. Overall, there was substantial intra-taxonomic variation with respect to trabecular bone orientation in S1 with no clear indicators of differences in loading patterns. Yet, this study considered only the primary eigenvectors, and did not quantitatively compare the secondary or tertiary eigenvectors. It is possible

that the secondary or tertiary eigenvectors may distinguish among the extant primates sampled here although the primary eigenvectors did not.

While orientations varied considerably among the extant taxa, DA values were highest in humans, followed by vertical clingers and leapers. This finding is consistent with predictions and suggests that humans and vertical clingers and leapers have the most organized trabeculae. Trabeculae tend to align themselves in the principal directions of stress (Wolff, 1892; Gibson, 1985; Goldstein et al., 1993) because bone is strongest (i.e., bending moments are reduced) when loaded on-axis (Wainwright et al., 1976; Currey, 1984; Gibson, 1985; Goldstein et al., 1991; Biewener et al. 1996; Ulrich et al., 1999; Huiskes et al., 2000; Keaveny et al., 2001). However, inconsistent with predictions, values were next highest in orthograde manual suspensors, followed by pronograde quadrupeds and orthograde-adapted quadrupeds.

Trabecular number and (size-corrected) trabecular thickness was also lowest in humans, contrary to expectations. And, like bone volume fraction, results for these variables among other taxa were also not always consistent with predictions, though differences among many of the positional behavior groups were significant. Vertical clingers and leapers (*Indri* and *Propithecus*) had dense, numerous, thick trabeculae that were highly organized. This finding is consistent with expectations that vertical clingers and leapers would have proximal sacral trabeculae structured to withstand high loads, presumably induced from more habitual orthograde posture, the fact that the fore-limbs are freed from substantial weight bearing during vertical clinging and leaping, and that

the hind limbs primarily support the body's weight and propel the animal during locomotion.

From a functional perspective, patterns in trabecular morphology specific to the other positional behaviors were less clear. Orthograde manual suspensors (*Ateles, Hylobates, Pongo*) had low bone density, and few, thick, but somewhat organized trabeculae; orthograde-adapted quadrupeds (*Pan* and *Gorilla*) had low bone density, and few, thin, unorganized trabeculae; and pronograde-adapted quadrupeds (*Mandrillus, Macaca, Sapajus, Saimiri, Varecia*) had low bone density, but the greatest number of trabeculae and intermediate (between positional behavior groups) trabecular thickness and organization.

Results describing trabecular shape are also unclear. Although, within hominoids, the distribution of values for modern humans is separated from that of *Pan*, with *Pan* exhibiting more isotropic trabeculae than modern humans in S1, distributions for *Gorilla*, *Pongo* and *Hylobates* overlap those of both *Pan* and modern humans. Further, when other catarrhines are considered (*Macaca* sp. and *Mandrillus*), there is little to no separation between taxa, and distributions for all three *Macaca* species and *Mandrillus* overlap those for hominoid taxa considerably. Within platyrrhines, the distribution for *Ateles* is separated from that of *Sapajus*, and is positioned lower in the ternary diagram, indicating more anisotropic trabeculae in S1. The distribution for *Saimiri* is intermediate between, and overlaps with, those of *Ateles*

Nonetheless, when multiple trabecular bone variables are considered together as a functional suite in multivariate principal component analyses, it is possible to distinguish

among some primate taxa. For example, highly suspensory *Hylobates* is distinguished from all other hominoid taxa along PC2 in the principal components analysis of all hominoids. Although the distribution for *Pongo*, the other highly suspensory ape in the sample, and that of *Hylobates* are separated from each other, this may result from the fact that postcranial morphology of *Hylobates* reflects adaptations to its specialized form of brachiation (Jungers, 1984). However, when all catarrhine taxa are considered, *Hylobates* falls above, but nearer to, the cercopithecoids than to the other hominoids. Thus, it is also possible that the separation of *Hylobates* from the great apes reflects its more cercopithecoid-like sacral morphology (e.g., transversely wide sacrum; Rosenman, 2008). Similarly, among hominoids, humans are distinct from *Pan* along PC1. However, humans are not distinguished from any other great apes.

Implications for the fossil record

The results from the current study, which sampled 78 sacra from extant primate, provided some functional information that could be used to reconstruct the positional behaviors of extinct primate taxa. Like its external morphology, the internal morphology of human sacra appears to distinguish humans from other hominoids with respect to some trabecular parameters. However, the goal of this study was to further elucidate the functional morphology of nonhuman primate sacra. Among nonhuman primates, functional signals in S1 were less clear than those observed for humans as the internal morphology of proximal sacra did not always distinguish among positional behavior groups in a manner consistent with functional expectations. These observations could be an artifact of how primates were categorized for analysis. Alternatively, results could

suggest that the sacrum is not an ideal element for examining trabecular morphology among primates that vary in positional behaviors, or, that another region of the sacrum (i.e., the alae, which articulate directly with the innominates) might be more functionally informative.

Moreover, though previous work on trabecular morphology emphasizes its utility in distinguishing among hominoid taxa for the purposes of reconstructing early hominin morphology (e.g., Griffin et al., 2010; Su et al., 2013), the results from this study suggest that any interpretation based on a limited number of sampled primate taxa may be premature. That is, though some taxonomic trends were present in the multivariate results of this study (e.g., humans are significantly different from *Pan* along PC1), the distributions of most hominoid taxa are indistinguishable from those of nonhominoid taxa that rely on fundamentally different postural and locomotor behaviors (e.g., *Macaca*) when the sample is broadened beyond hominoids.

Extinct primates were not included in the PCAs of extant primates for several reasons. First, *Nacholapithecus*, the extinct hominoid in the sample, exhibited unusual values for several of the trabecular parameters examined, including very low bone volume fraction values, a higher trabecular number value than was observed for any living primate, and a lower value for trabecular thickness than was observed for any living primate. It is possible that these unusual values could be attributed to the poor scan quality of the specimen, which required subsequent use of a binary threshold. When the *Nacholapithecus* specimen was included in the hominoid sample to investigate its morphology using multivariate analysis (not shown), it was strongly separated from all

other hominoids, which consequently grouped tightly together. The extant strepsirrhines sampled were vertical clingers and leapers (*Indri*, *Propithecus*), and one arboreal quadruped (*Varecia*). Without a larger strepsirrhine sample with which to contextualize the results for the subfossil lemur sample, particularly one that includes more suspensory-adapted and more quadrupedal taxa, any functional interpretation is limited. Further, the sample sizes here for the extant strepsirrhines was too small to include in the principal components analyses.

CONCLUSIONS

This study of comparative trabecular bone in the first sacral vertebra of extant primates identified some functional relationships between trabecular variables and differences in positional behaviors. Bone volume fraction was lowest in humans, a finding that accords with previous studies of trabecular bone in other regions of the skeleton. When small taxonomic groups are considered in multivariate principal components analyses some locomotor-specific trends could be argued for. However, the inclusion of a greater number of taxa reveals substantial overlap in the distributions of primates that rely on disparate forms of locomotion. This finding, in turn, suggests that studies considering the trabecular morphology of hominoid taxa only, for the purposes of reconstructing the postcranial functional anatomy and positional behaviors of extinct primates, should do so with caution.

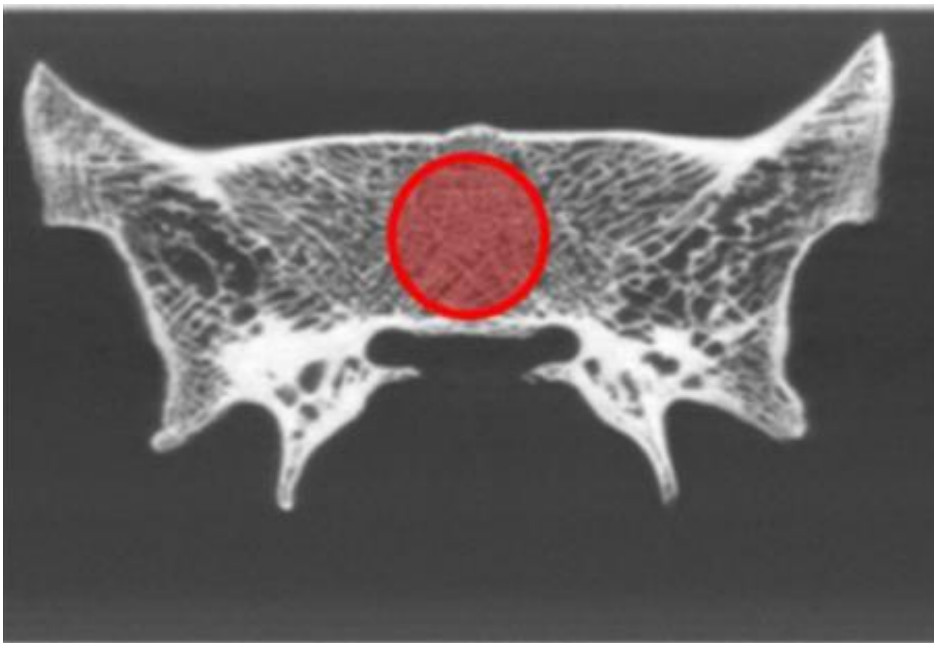

Figure 2.1 Example of VOI positioned in the first sacral vertebra. CT slice through the coronal plane. View is cranial.

Figure 2.2 Extinct primate sacral specimens. Top row (left to right): *Megaladapis* (DLC 7950), *Archaeolemur* (DLC 11823, DLC 11835, DLC 9905); Bottom row: *Palaeopropithecus* (DLC 24778), *Epipliopithecus* (O.E. 304-45), *Oreopithecus* (BA#72), *Nacholapithecus* (BG 17822). All views ventral, except *Nacholapithecus* for which view is dorsal. White scale bars = 1cm.

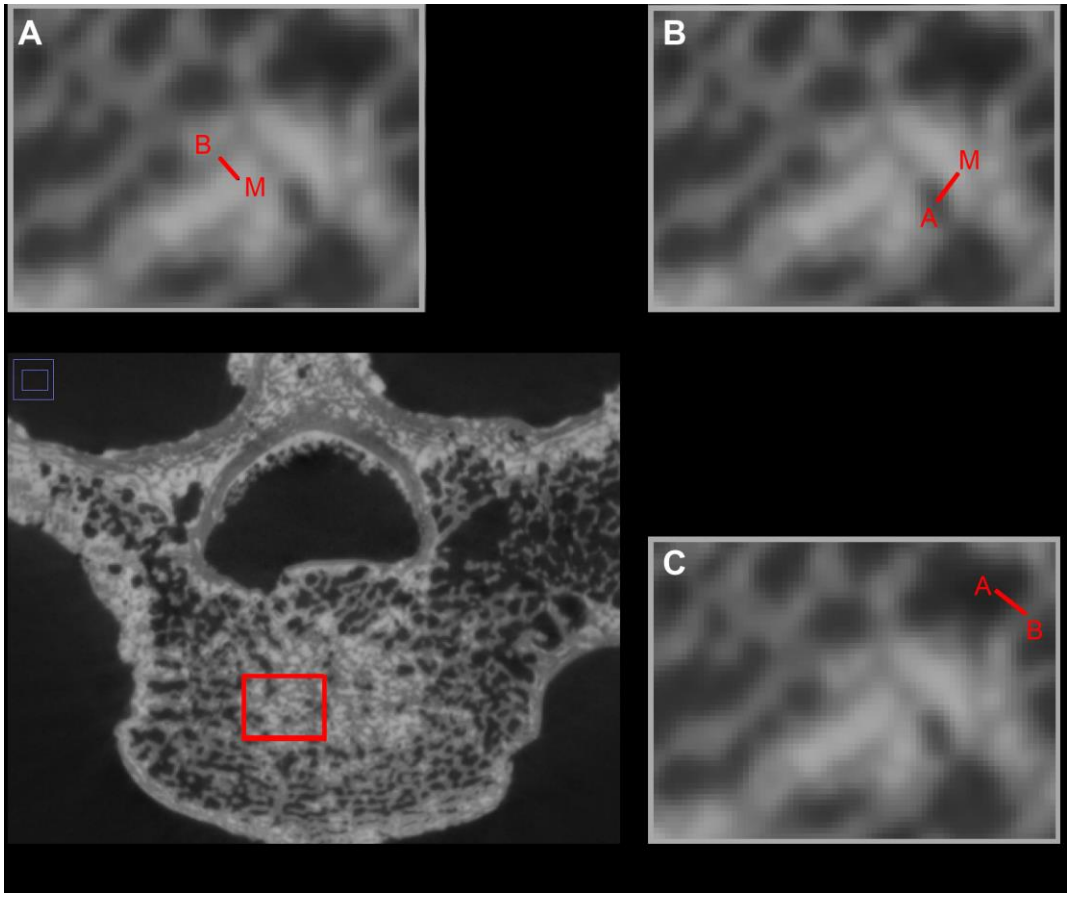

Figure 2.3 Modified half-maximum height method for thresholding extinct primate sacra that exhibit matrix infilling the trabecular network. The sacrum shown (bottom left) belongs to *Megaladapis* (DLC 7950; View is cranial, dorsal is up). Inset box A shows a sampling of grayscale values across the boundary of a bone (B) – matrix (M) interface; Inset box B shows a sampling of grayscale values across the boundary of an air (A) – matrix interface; and Inset box C shows a sampling of grayscale values across the boundary of an air-bone interface. For this specimen, the matrix in-filling the trabecular network is denser than the trabecular bone itself. The matrix-bone and matrix-air boundary HMH values were averaged to find a "high threshold" and the HMH values for the bone-air boundary was used as the "low threshold." See text for more detail.

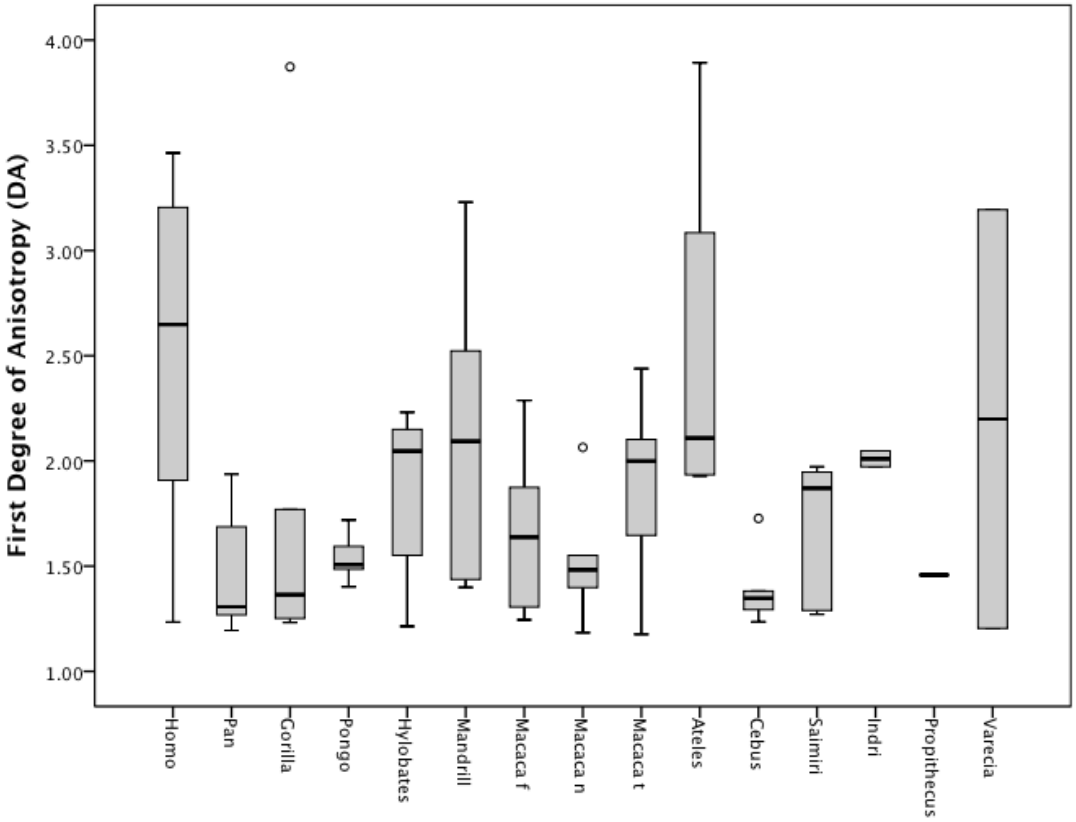

Figure 2.4A Boxplots of values for the first degree of anisotropy across all taxa.

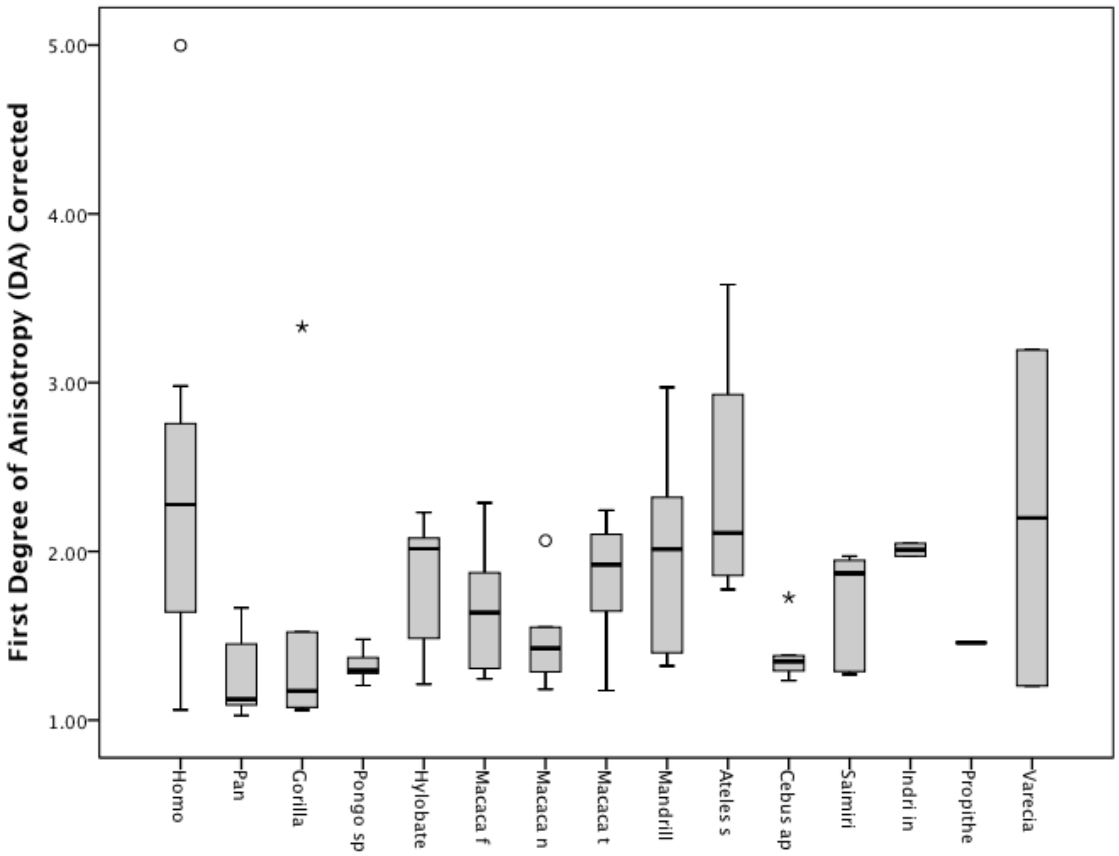

Figure 2.4B Boxplots of resolution-corrected values for the first degree of anisotropy across all taxa.

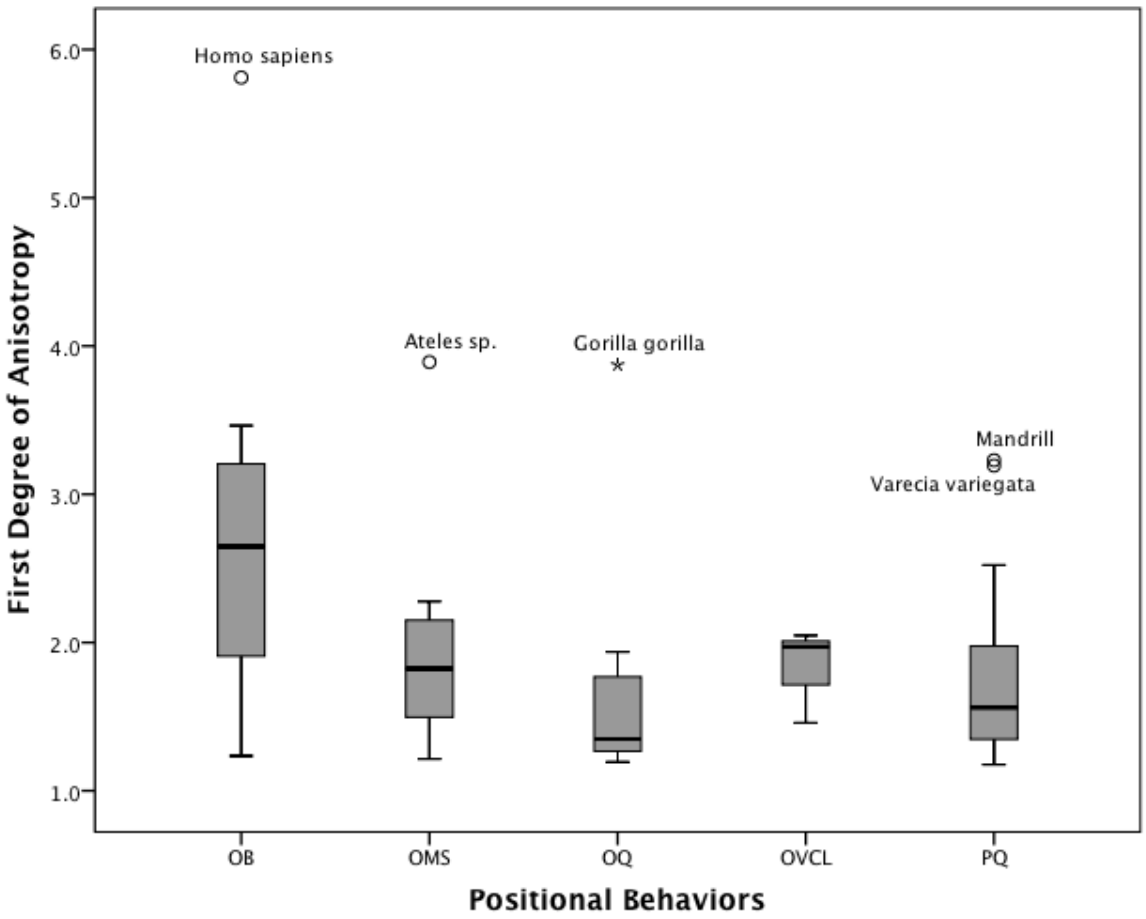

Figure 2.4C Boxplots of values for the first degree of anisotropy for taxa grouped by positional behavior. OB = Orthograde Biped; OMS = Orthograde Manual Suspensor; OQ = Orthograde-adapted Quadruped; OVCL= Orthograde Vertical Clinger and Leaper; PQ = Pronograde Quadruped.

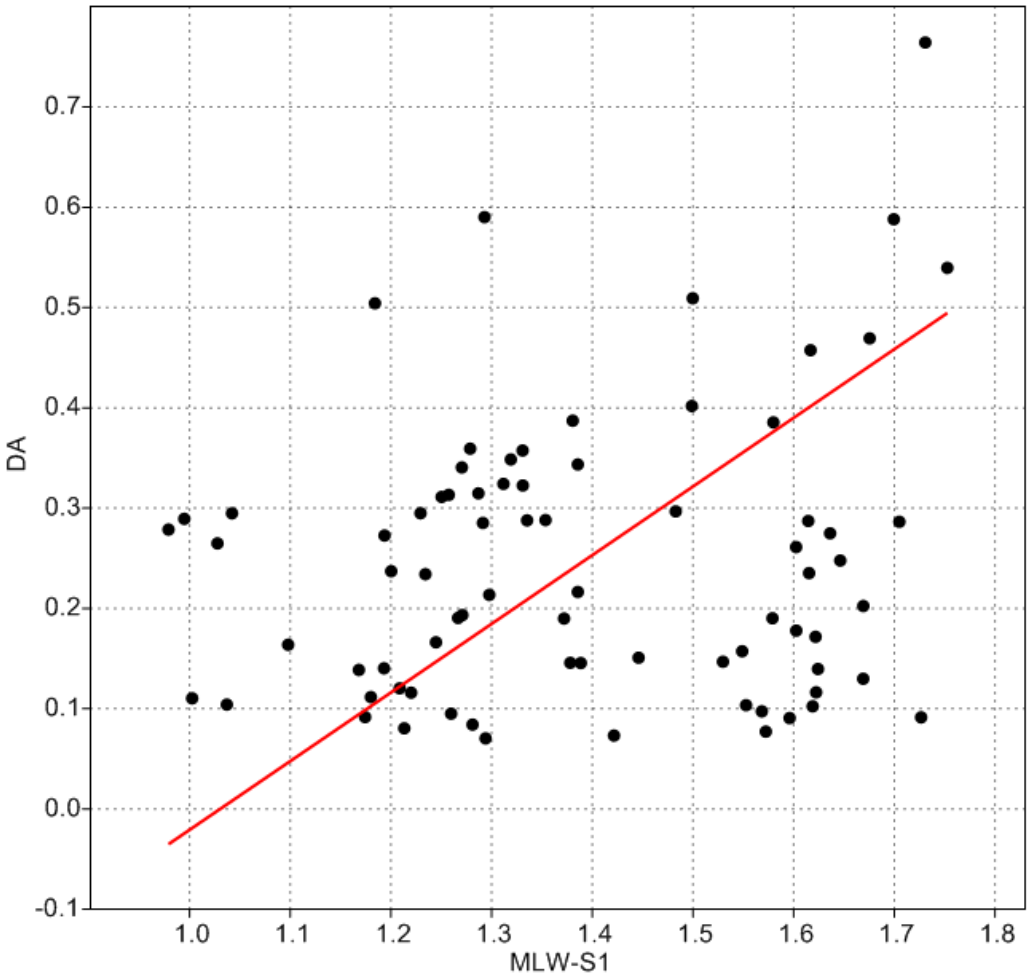

Figure 2.4D Log-transformed degree of anisotropy (values for individuals) plotted against log-transformed MLW-S1. Degree of anisotropy scales positively. See text for details.

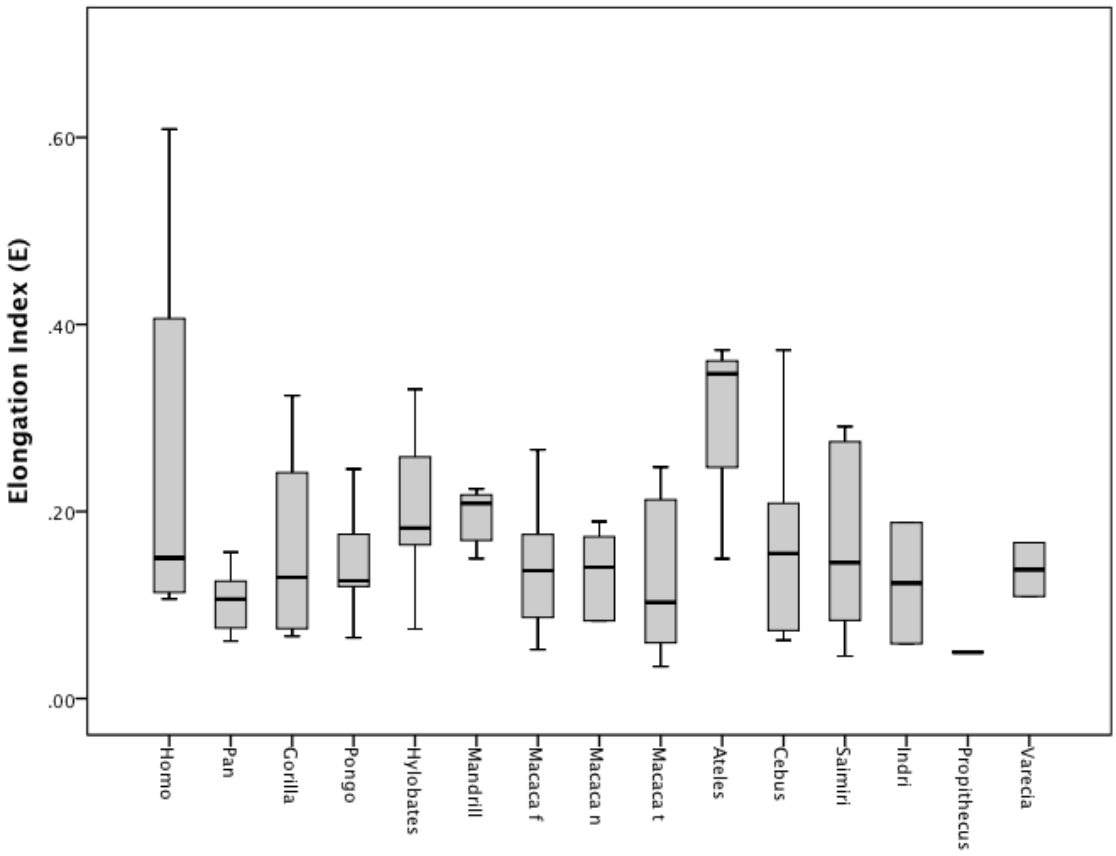

Figure 2.5A Boxplots of values for elongation index across all taxa.

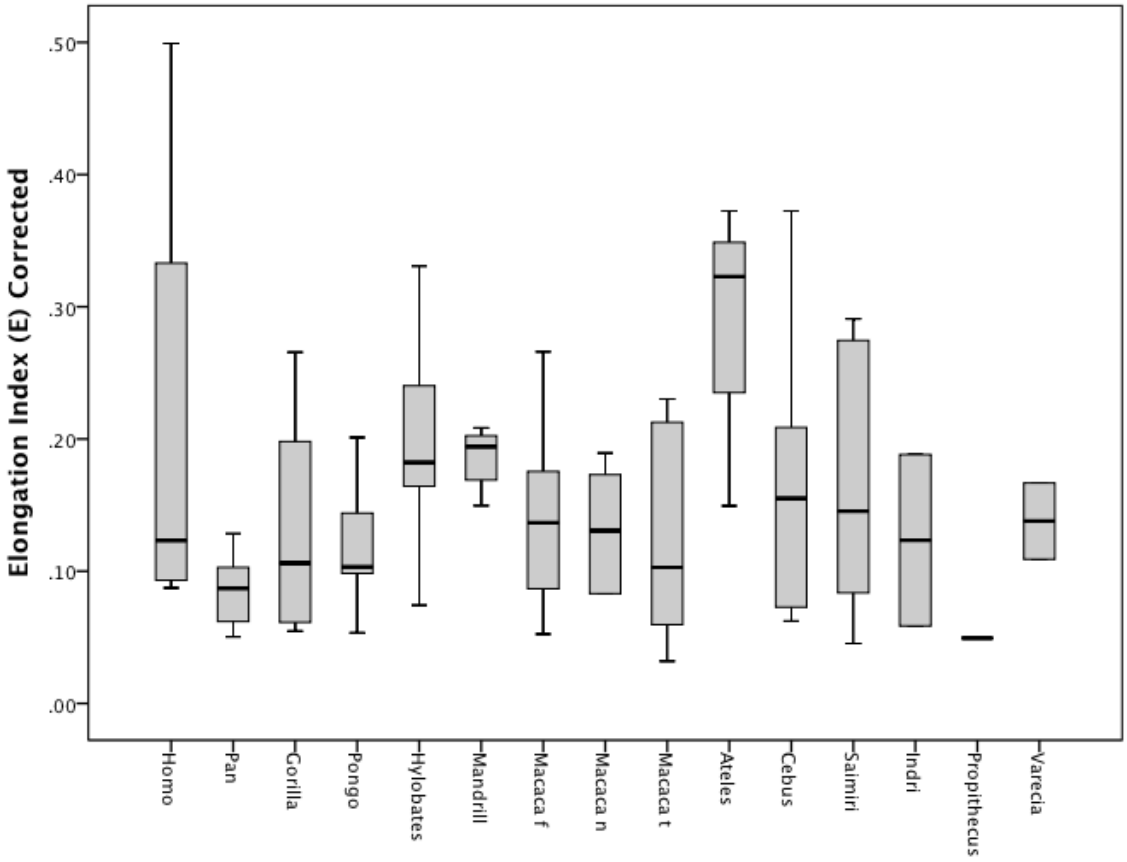

Figure 2.5B. Boxplots of resolution-corrected values for elongation index across all taxa.

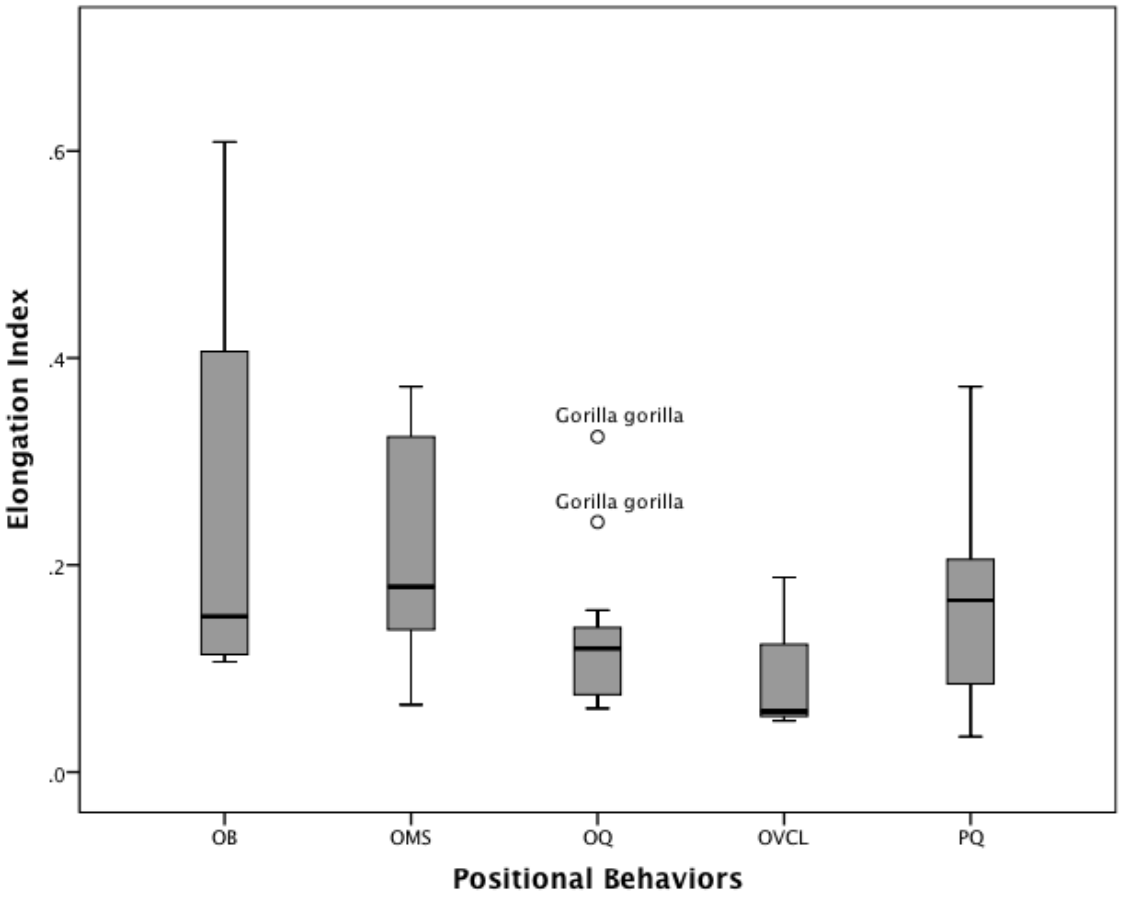

Figure 2.5C Boxplots of values for elongation index for taxa grouped by positional behavior. OB = Orthograde Biped; OMS = Orthograde Manual Suspensor; OQ = Orthograde-adapted Quadruped; OVCL= Orthograde Vertical Clinger and Leaper; PQ = Pronograde Quadruped.

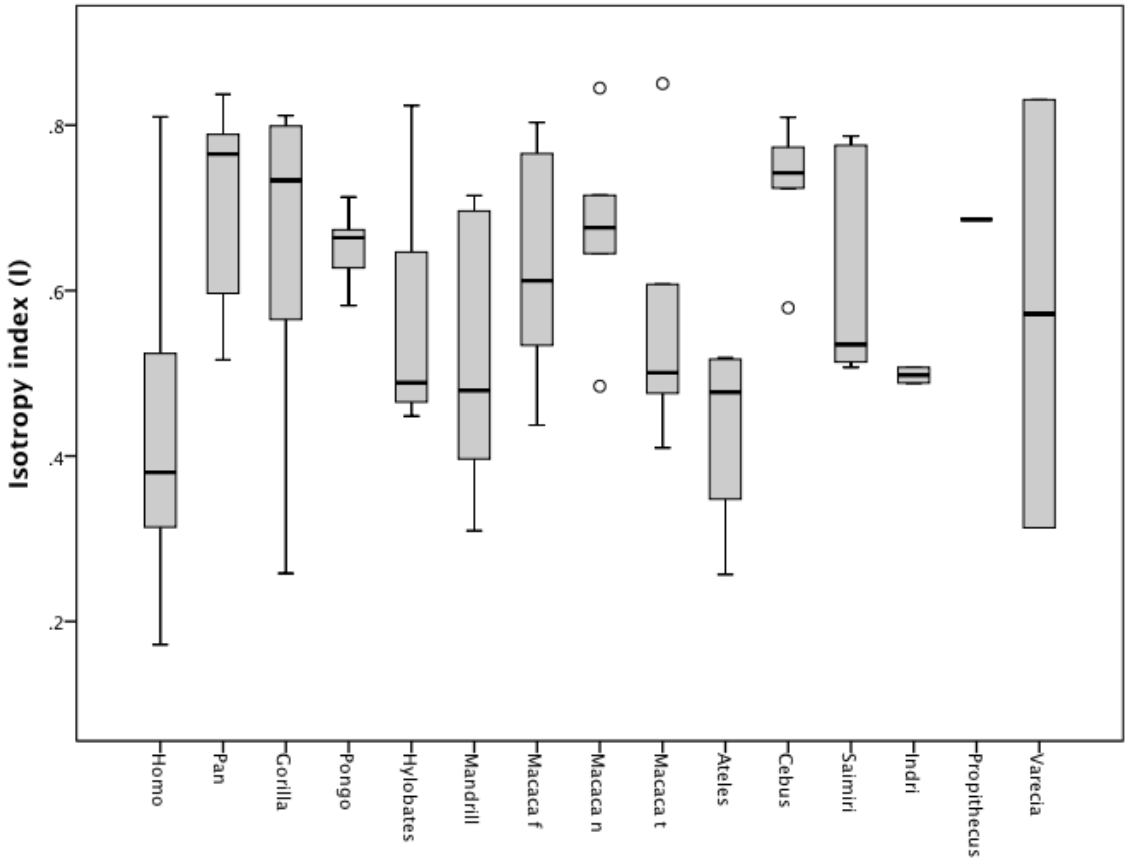

Figure 2.6A. Boxplots of values for isotropy index across all taxa.

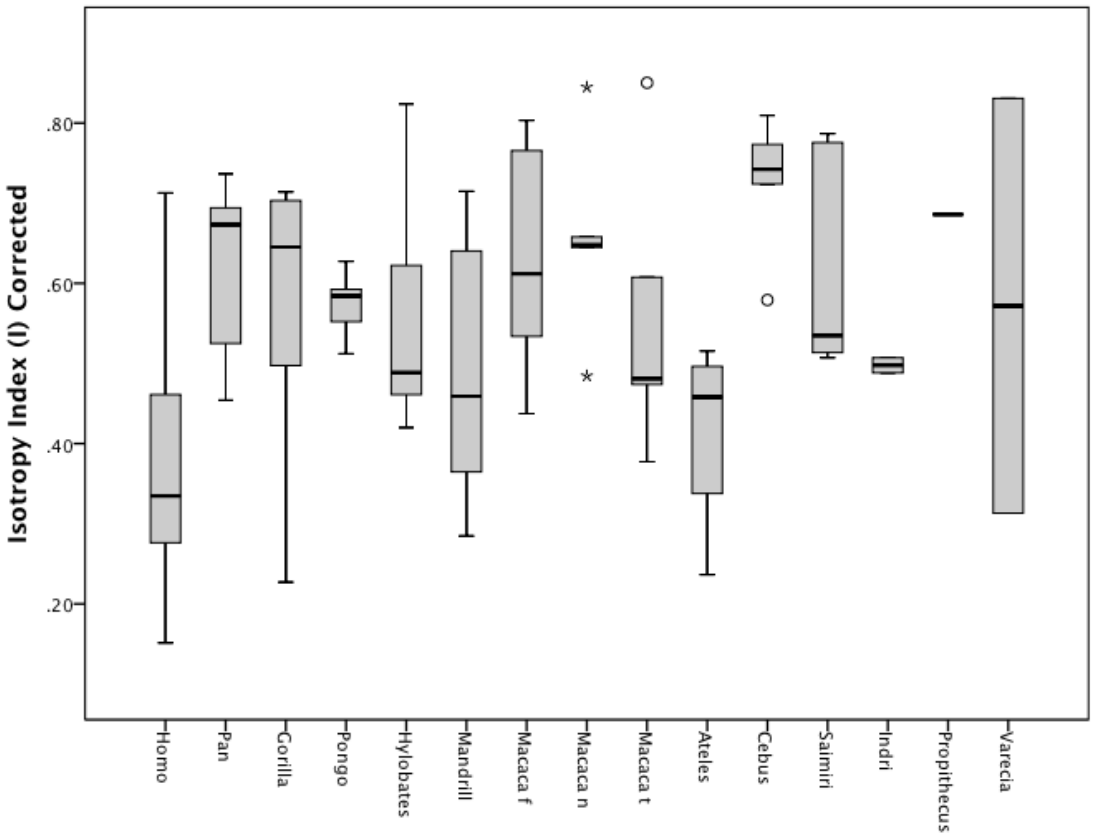

Figure 2.6B. Boxplots of resolution-corrected values for isotropy index across all taxa.

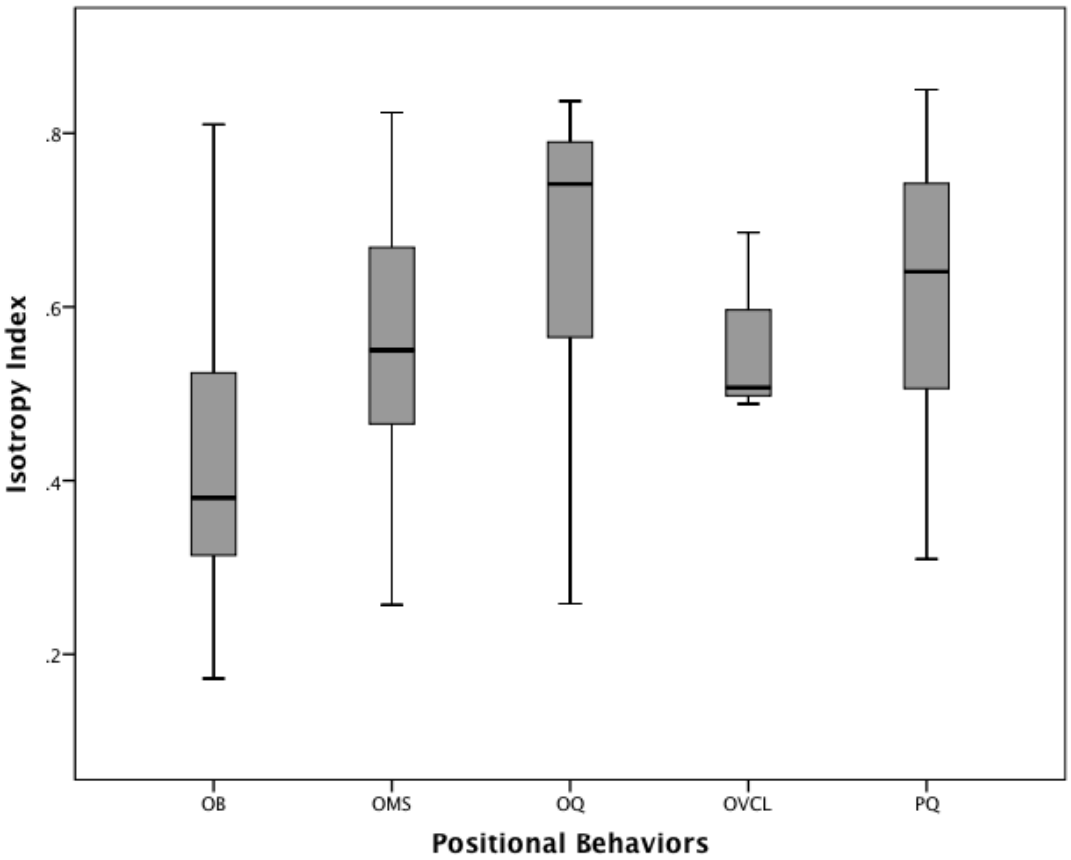

Figure 2.6C Boxplots of values for isotropy index for taxa grouped by positional behavior. OB = Orthograde Biped; OMS = Orthograde Manual Suspensor; OQ = Orthograde-adapted Quadruped; OVCL= Orthograde Vertical Clinger and Leaper; PQ = Pronograde Quadruped.

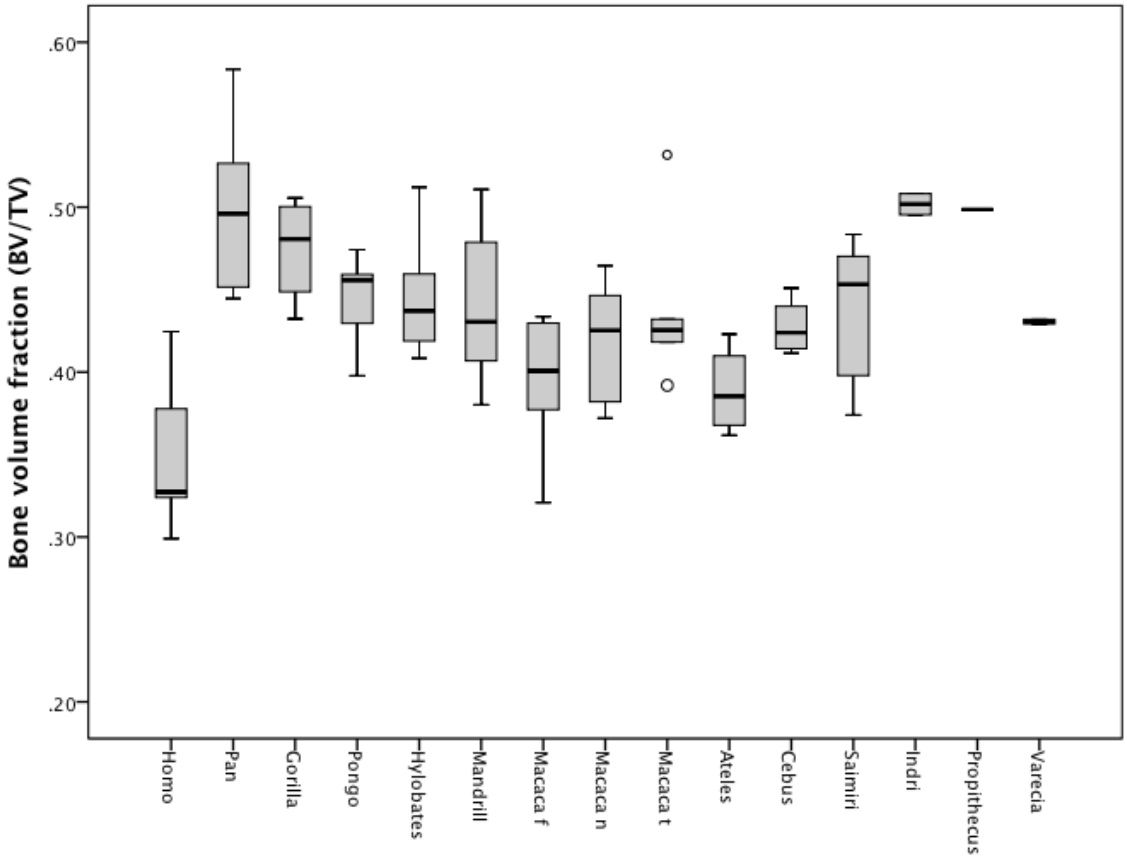

Figure 2.7A. Boxplots of values for bone volume fraction across all taxa.

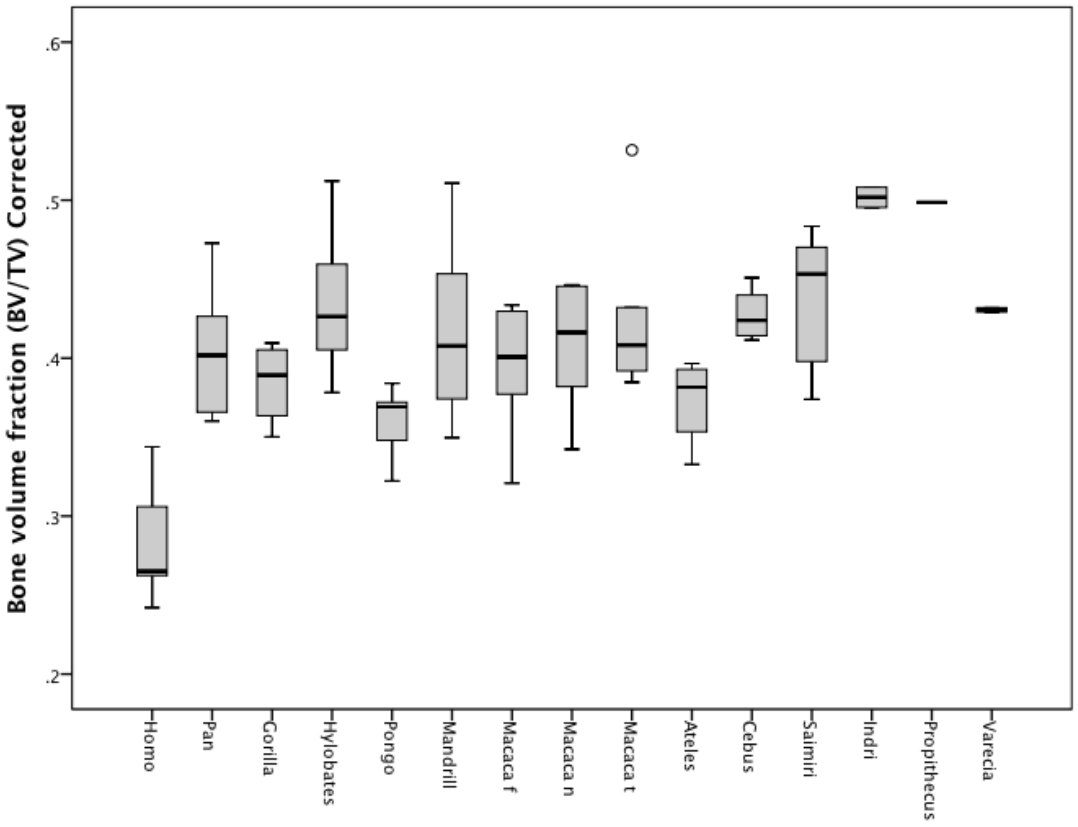

Figure 2.7B. Boxplots of resolution-corrected values for bone volume fraction across all taxa.

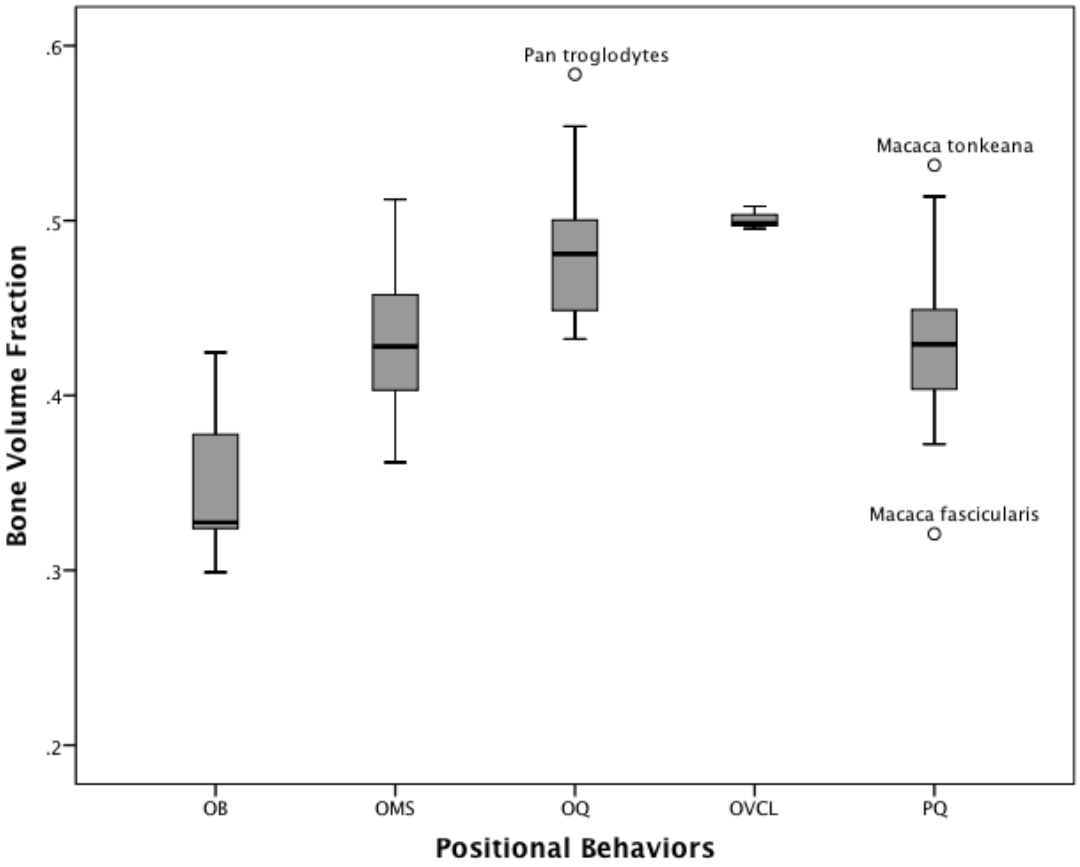

Figure 2.7C Boxplots of values for bone volume fraction for taxa grouped by positional behavior. OB = Orthograde Biped; OMS = Orthograde Manual Suspensor; OQ = Orthograde-adapted Quadruped; OVCL= Orthograde Vertical Clinger and Leaper; PQ = Pronograde Quadruped.

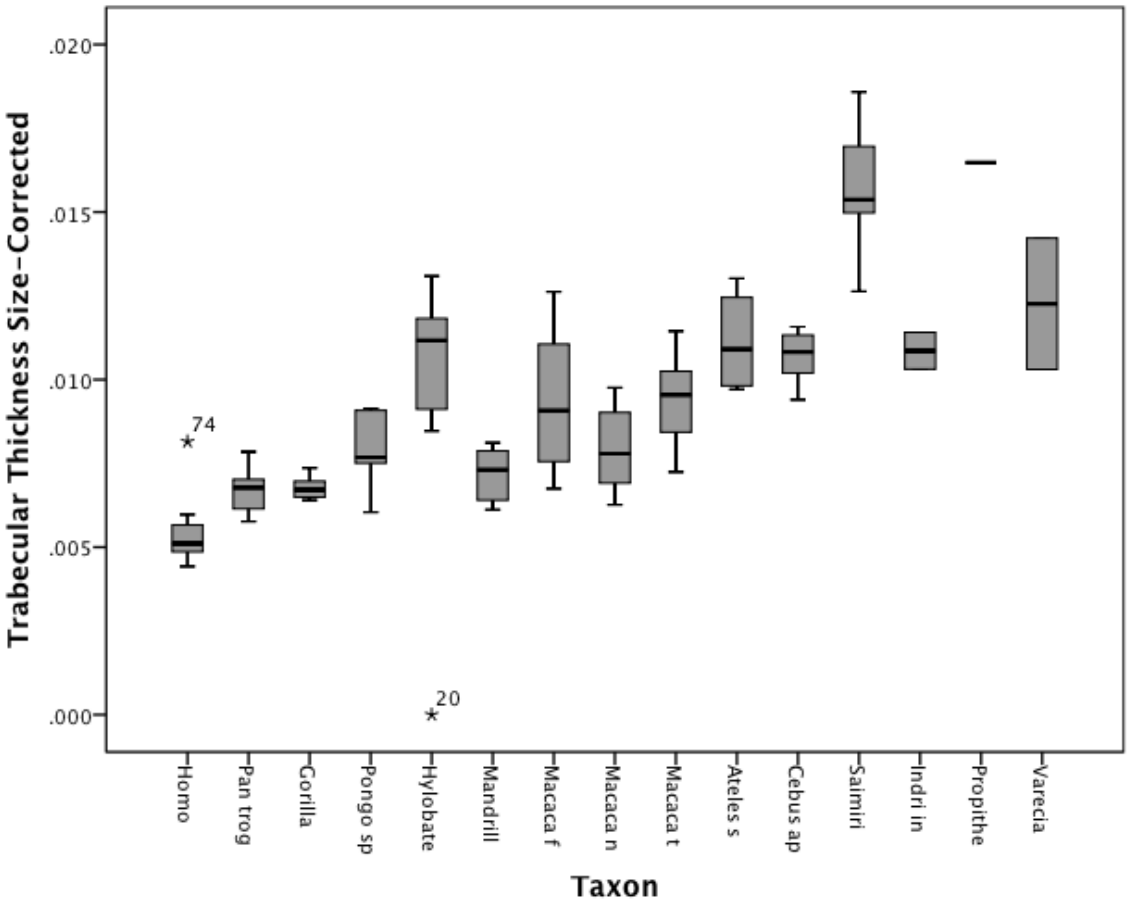

Figure 2.8A Boxplots of size-corrected values for trabecular thickness across all taxa.

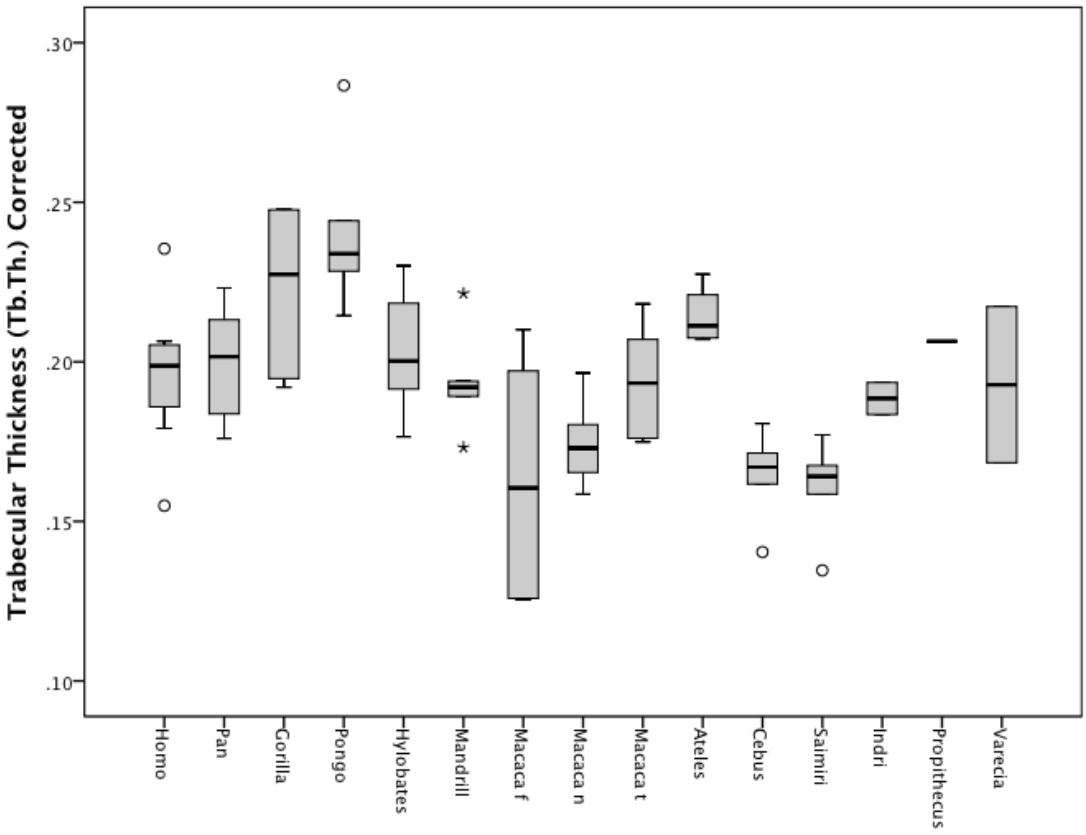

Figure 2.8B Boxplots of resolution-corrected raw values for trabecular thickness across all taxa.

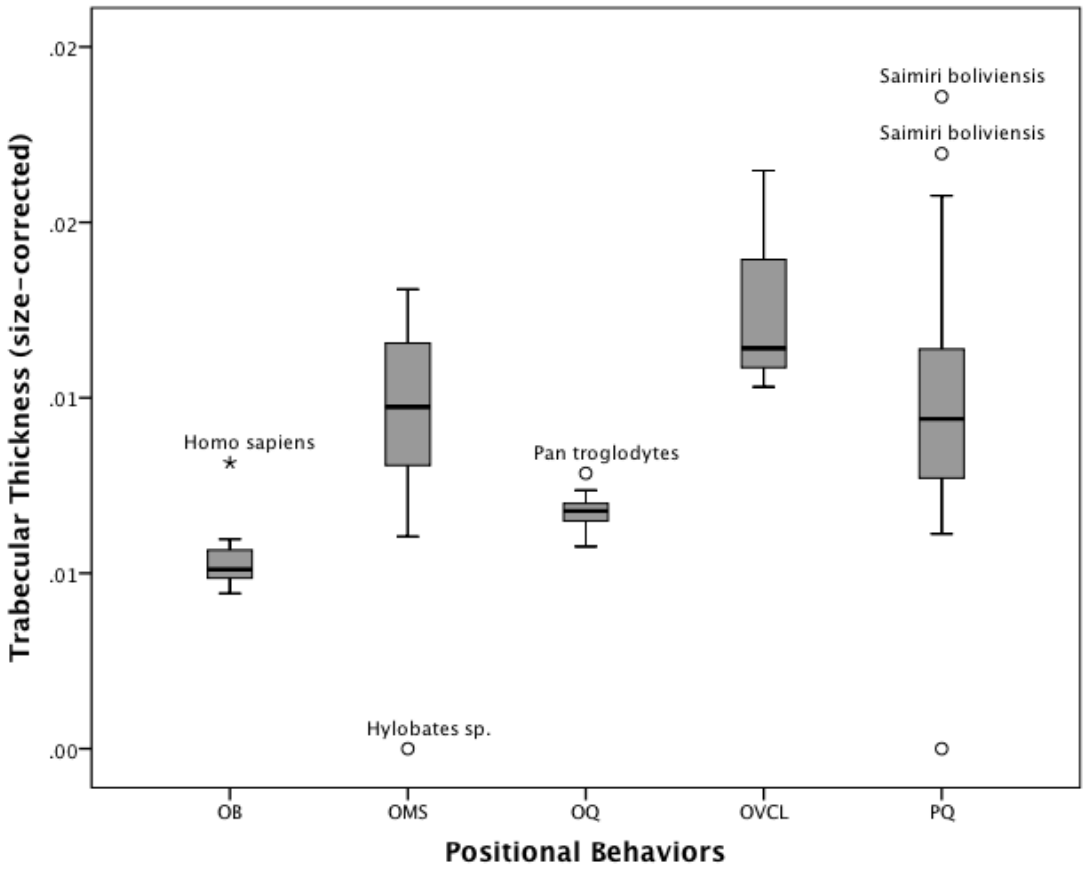

Figure 2.8C Boxplots of values for trabecular thickness for taxa grouped by positional behavior. OB = Orthograde Biped; OMS = Orthograde Manual Suspensor; OQ = Orthograde-adapted Quadruped; OVCL= Orthograde Vertical Clinger and Leaper; PQ = Pronograde Quadruped.

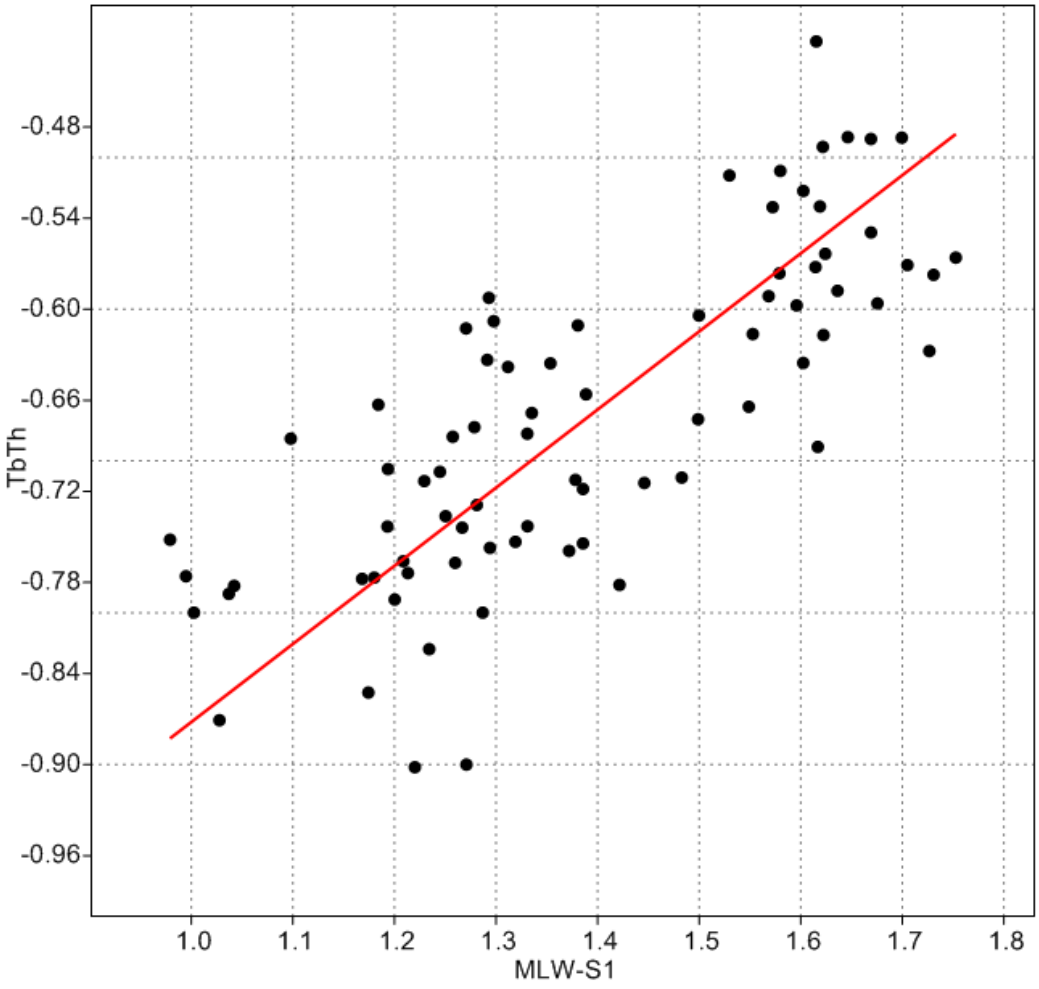

Figure 2.8D Log-transformed trabecular thickness (raw values for individuals) plotted against log-transformed MLW-S1. Trabecular thickness scales negatively. See text for details.

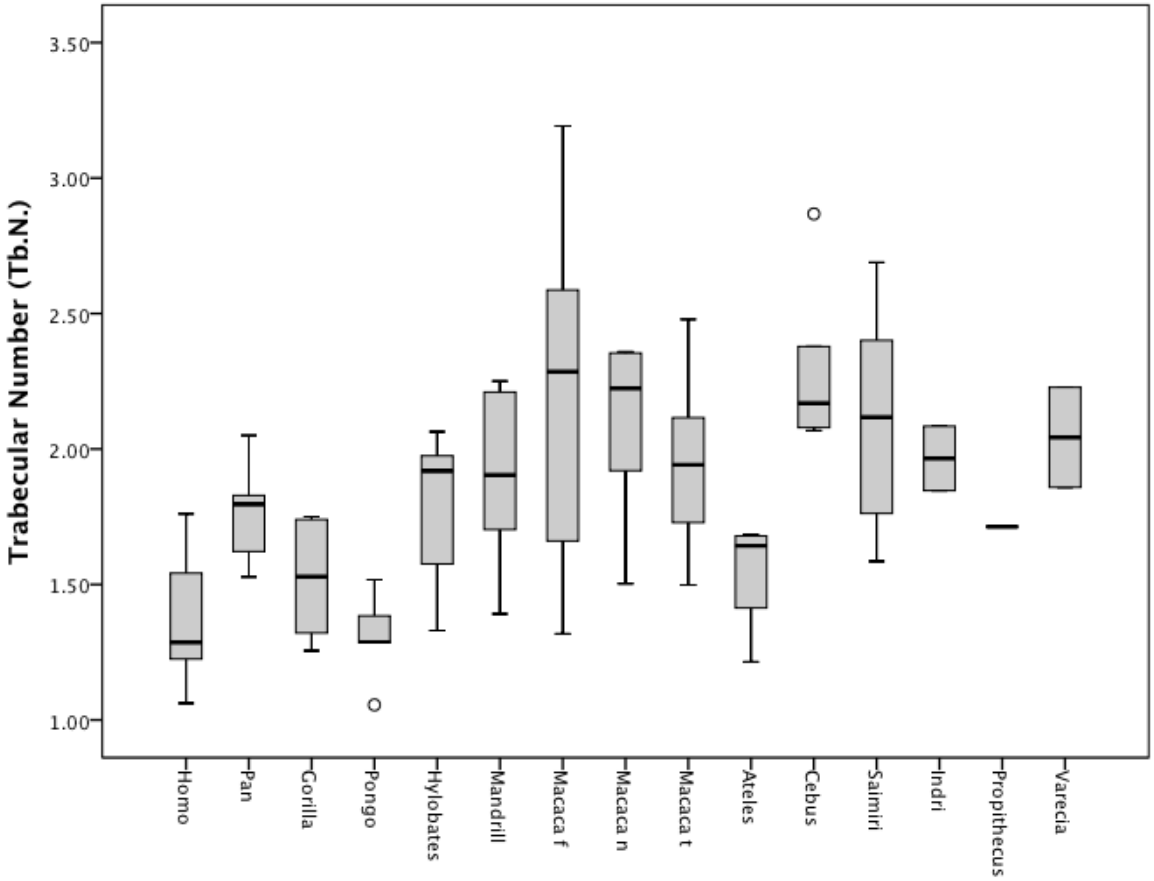

Figure 2.9A Boxplots of values for trabecular number across all taxa.

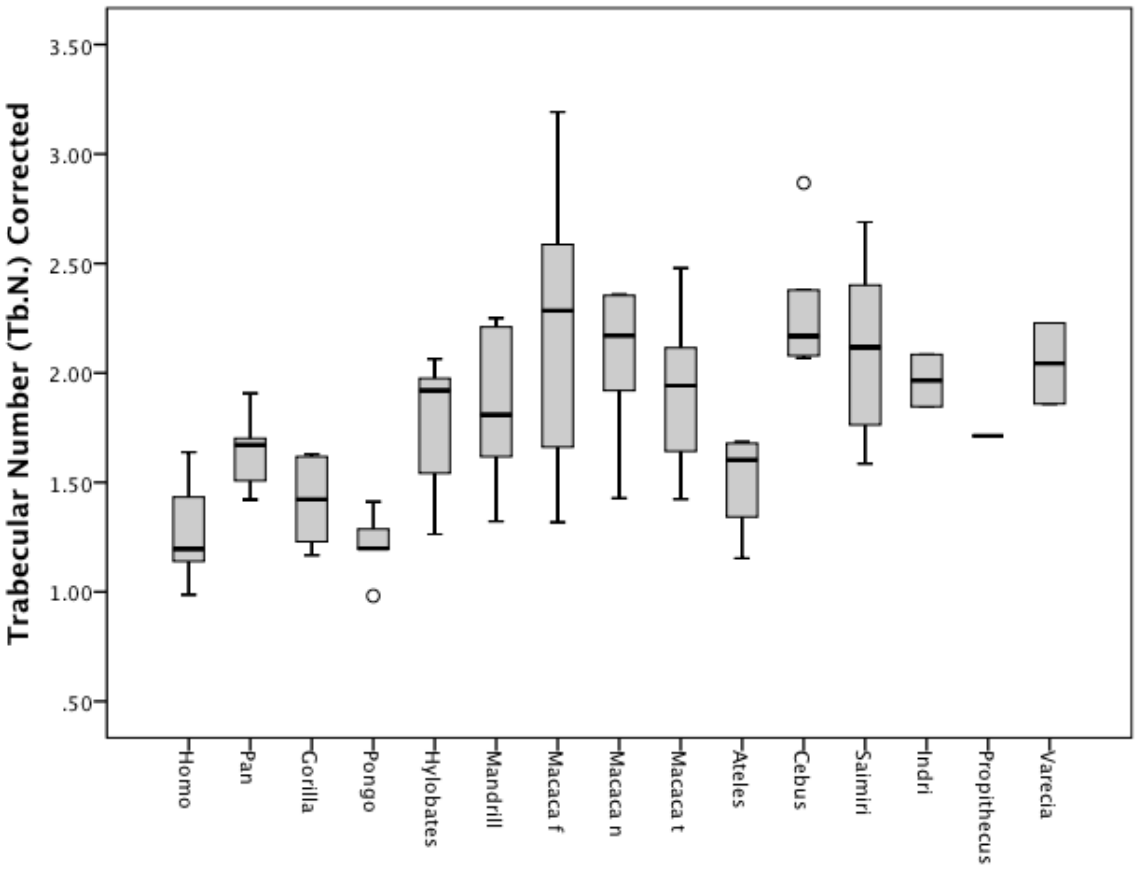

Figure 2.9B Boxplots of resolution-corrected values for trabecular number across all taxa.

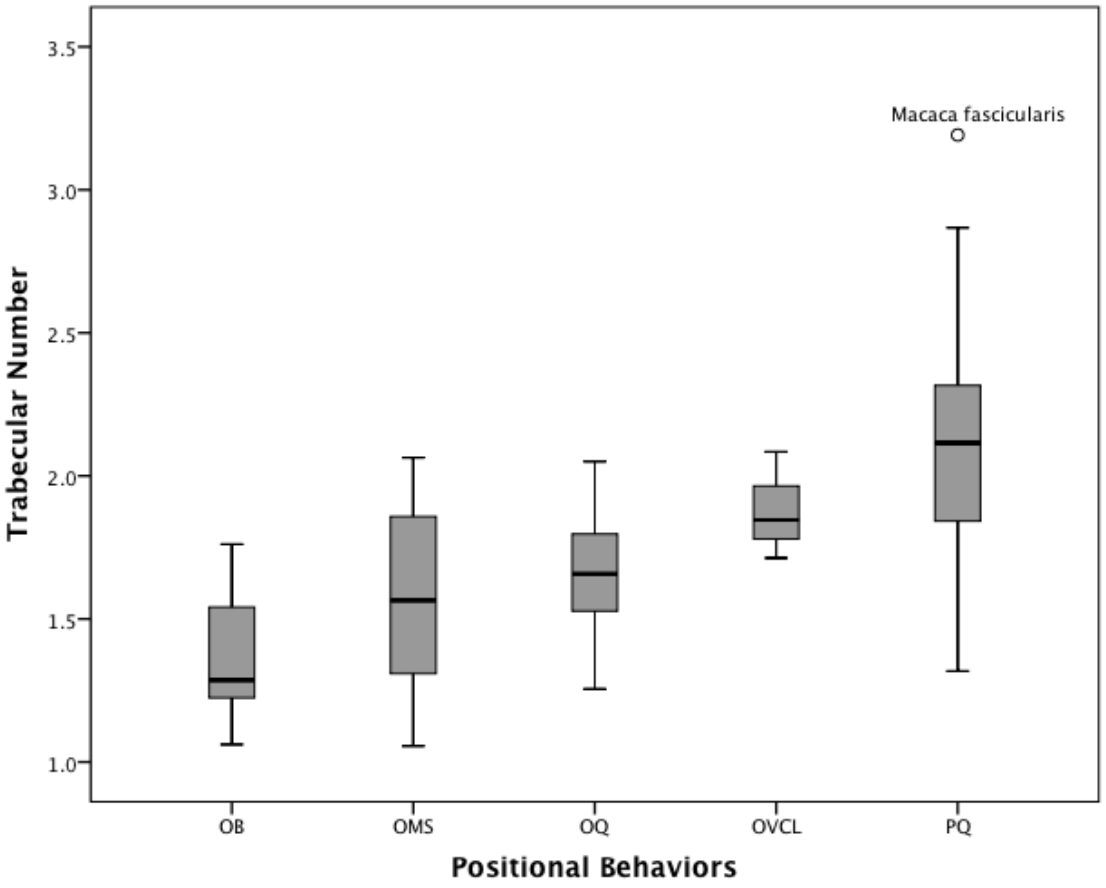

Figure 2.9C Boxplots of values for trabecular number for taxa grouped by positional behavior. OB = Orthograde Biped; OMS = Orthograde Manual Suspensor; OQ = Orthograde-adapted Quadruped; OVCL= Orthograde Vertical Clinger and Leaper; PQ = Pronograde Quadruped.

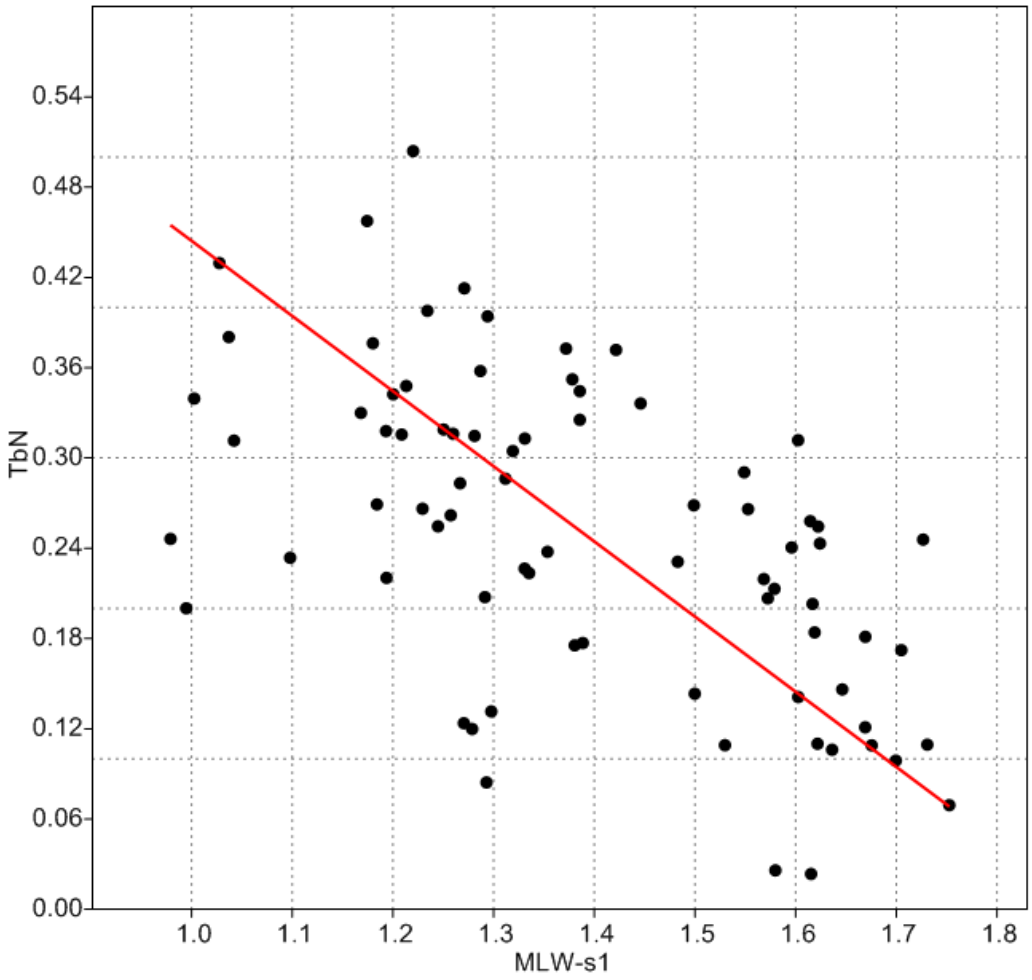

Figure 2.9D Log-transformed trabecular number (values for individuals) plotted against log-transformed MLW-S1. Trabecular number scales negatively. See text for details.

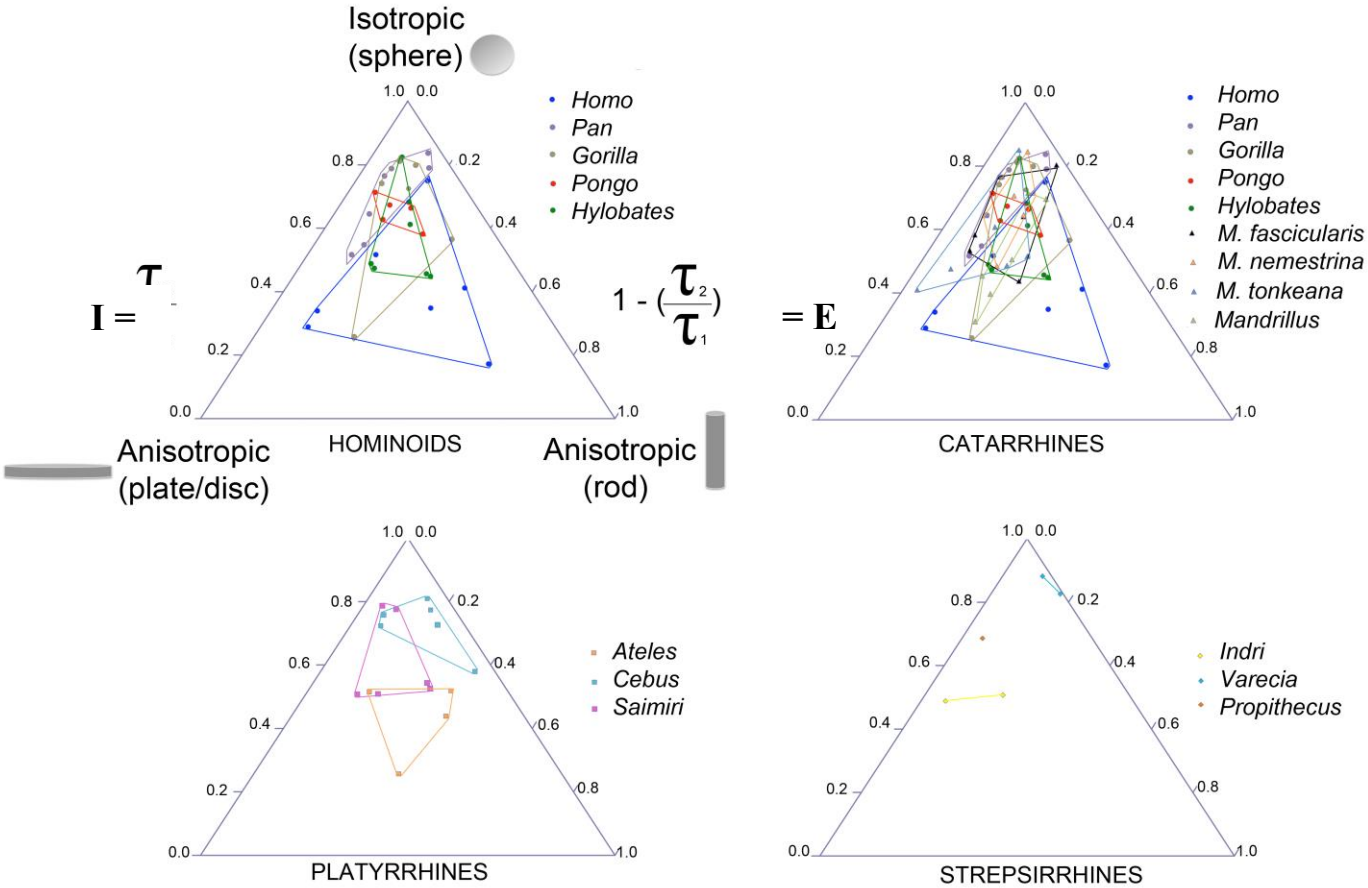

Figure 2.10 Ternary shape diagrams, formed by values for the elongation index (=1-[τ_2/τ_1]) and the isotropy index (=[τ_3/τ_1]) illustrating the bone fabric structure in the first sacral vertebra in extant primates. Polygons enclose the individuals for each taxon to facilitate visual comparison. Data toward the ternary's top apex indicate that trabecular are more isotropic and sphere-like, data toward the bottom left apex indicate trabeculae are more anisotropic and plate-like, and data toward the bottom right apex indicate that trabeculae are more anisotropic and rod-like. From top left to bottom right ternary diagrams depict results for hominoids, catarrhines, platyrrhines, and strepsirrhines.

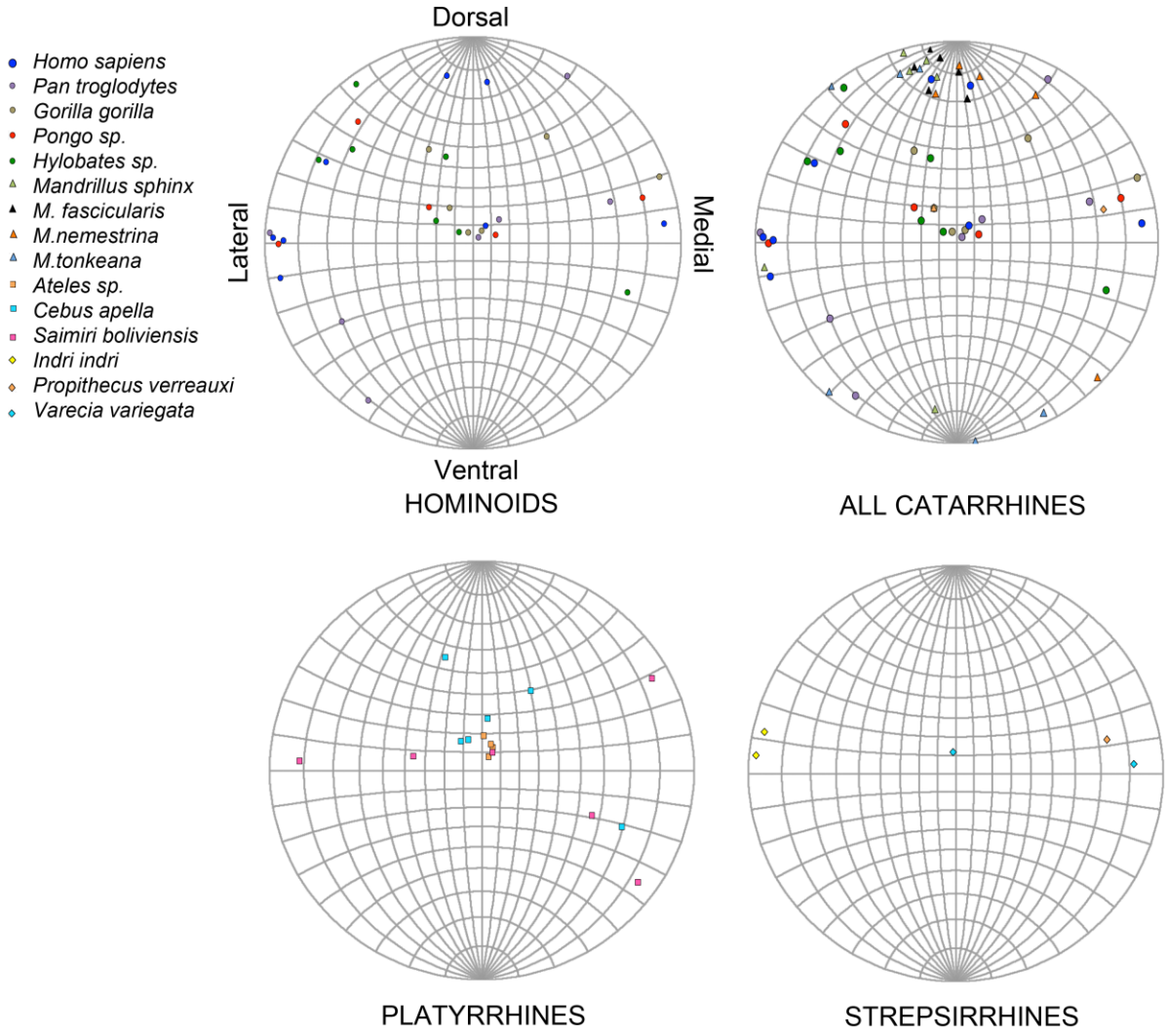

Figure 2.11 Equal-area stereographic projections illustrating the estimates of the primary (i.e., first eigenvector [μ1]) of the trabecular fabric in extant primates. Data toward the top and bottom of the sphere are indicative of more dorsoventral orientations, data toward the left and right of the sphere are indicative of more medio-lateral orientations, and data toward the middle of the sphere (i.e., into the plot) are indicative of more craniocaudal orientations. From top left to bottom right stereoplots depict results for hominoids, catarrhines, platyrrhines, and strepsirrhines.

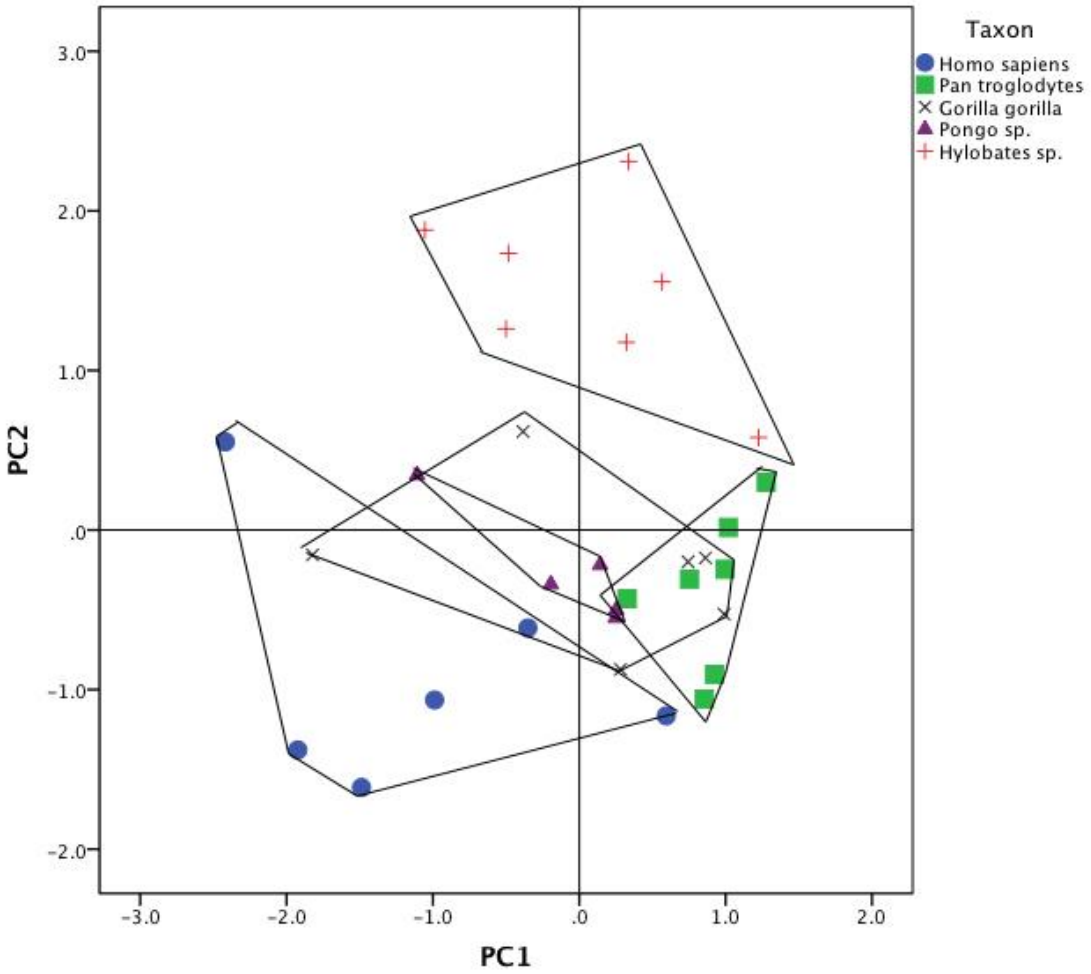

Figure 2.12 Bivariate plot of PC1 and PC2 scores for hominoids. Legend in figure.

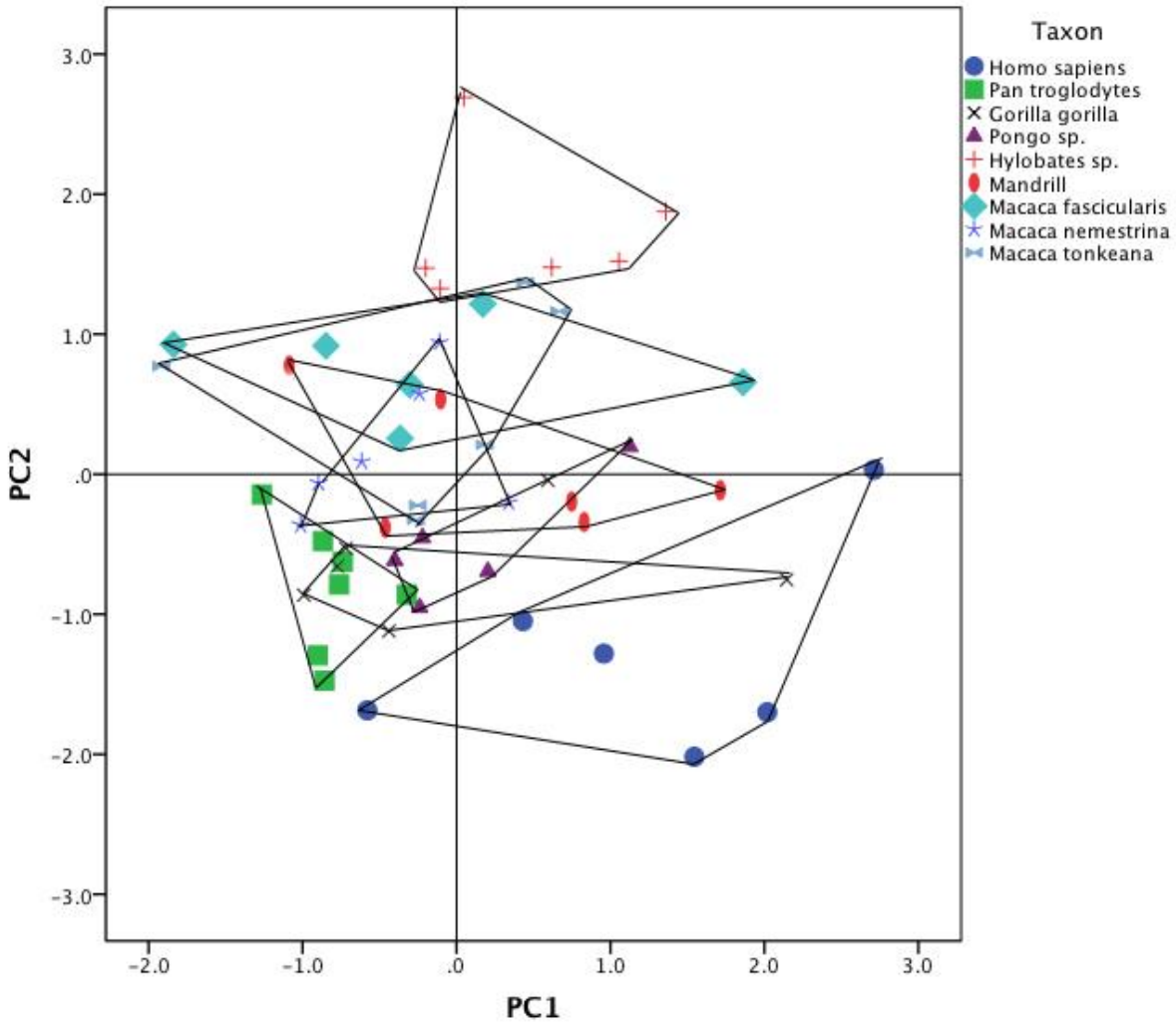

Figure 2.13 Bivariate plot of PC1 and PC2 scores for catarrhines. Legend in figure.

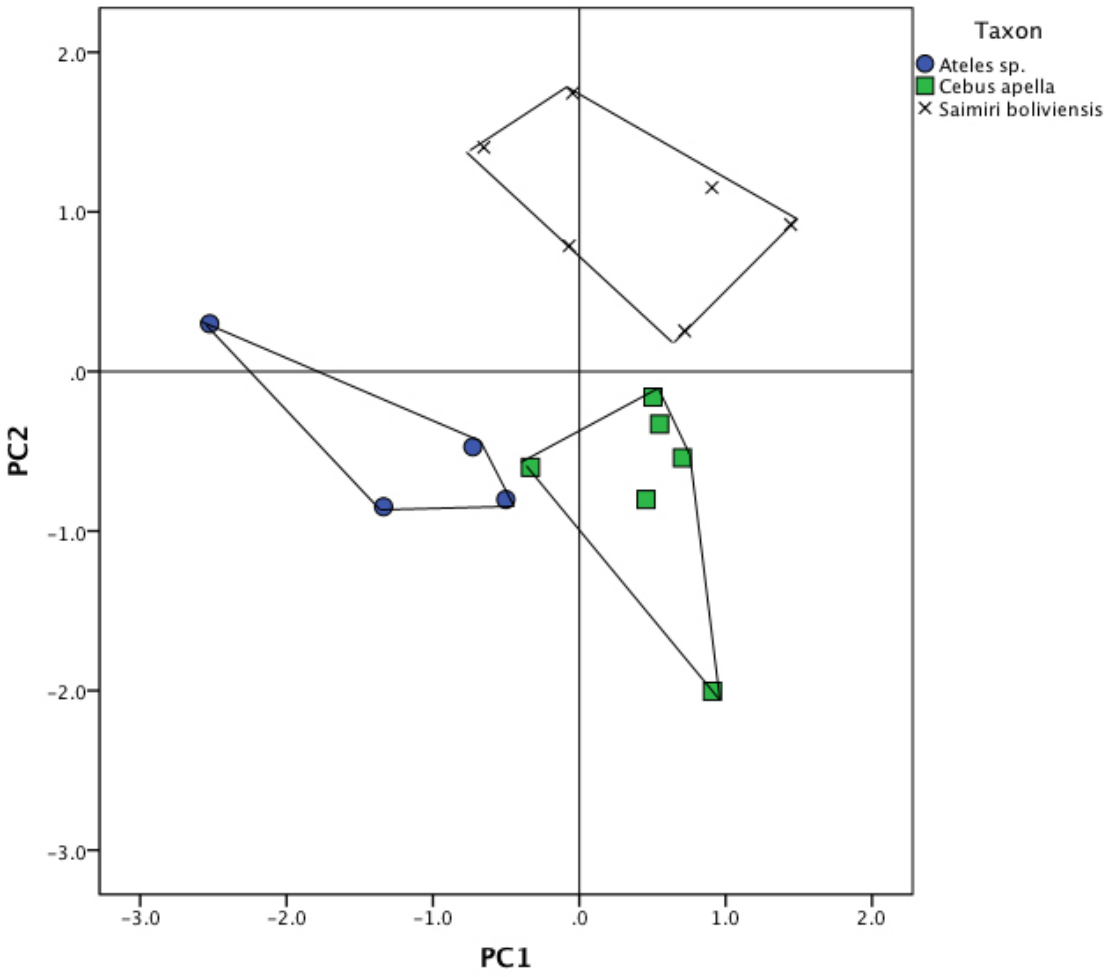

Figure 2.14 Bivariate plot of PC1 and PC2 scores for platyrrhines. Legend in figure.

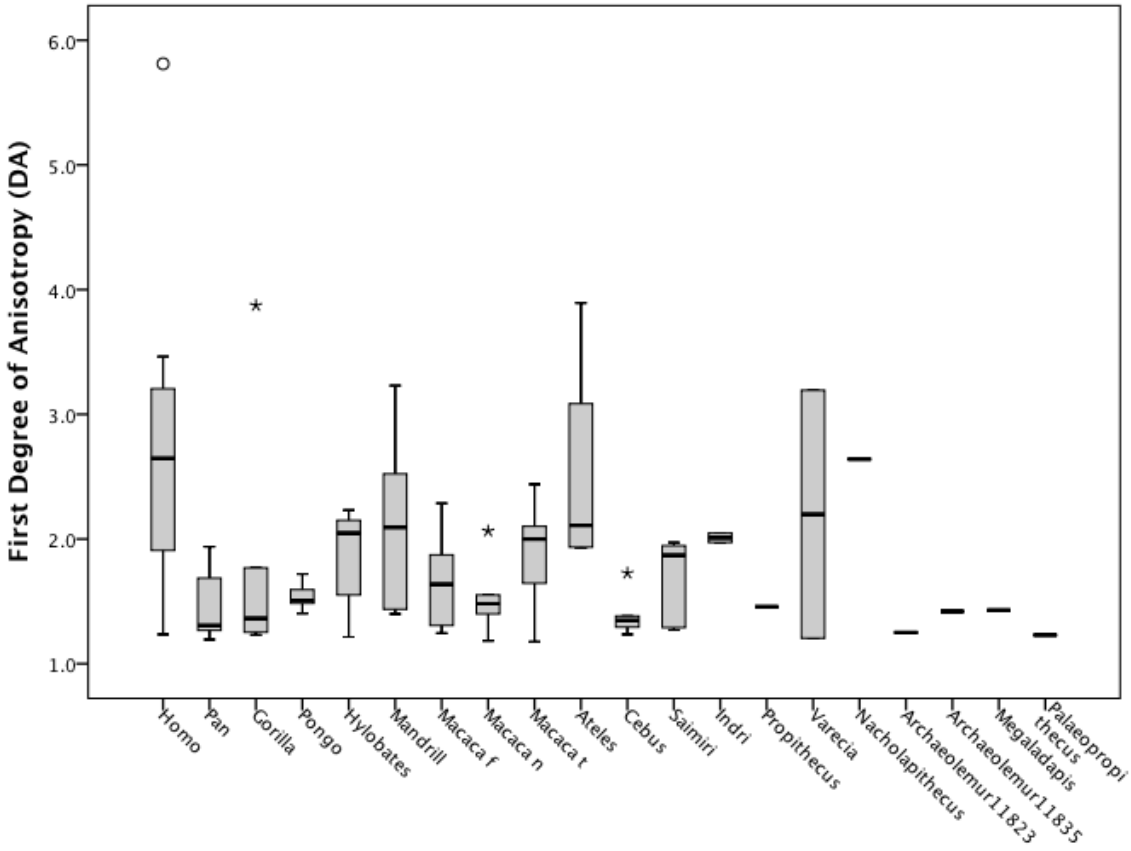

Figure 2.15 First degree of anisotropy in the extant and extinct primates sampled.

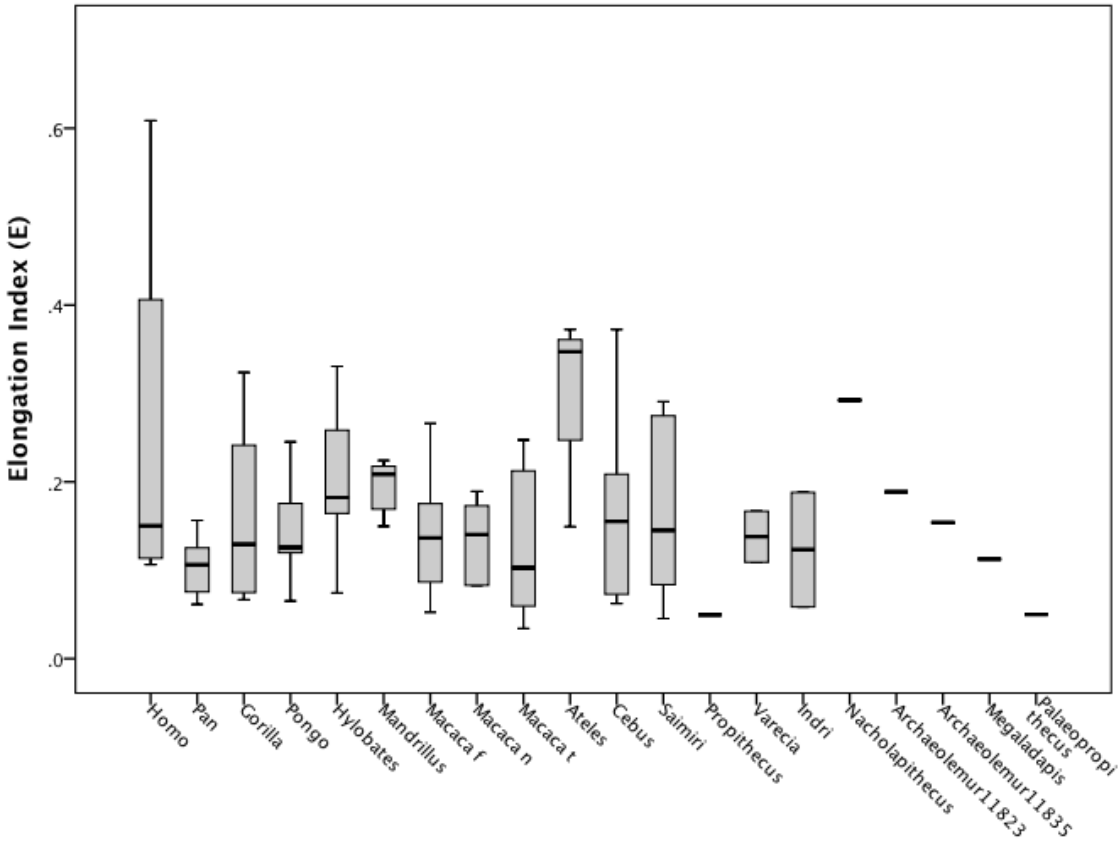

Figure 2.16 Elongation index in the extant and extinct primates sampled.

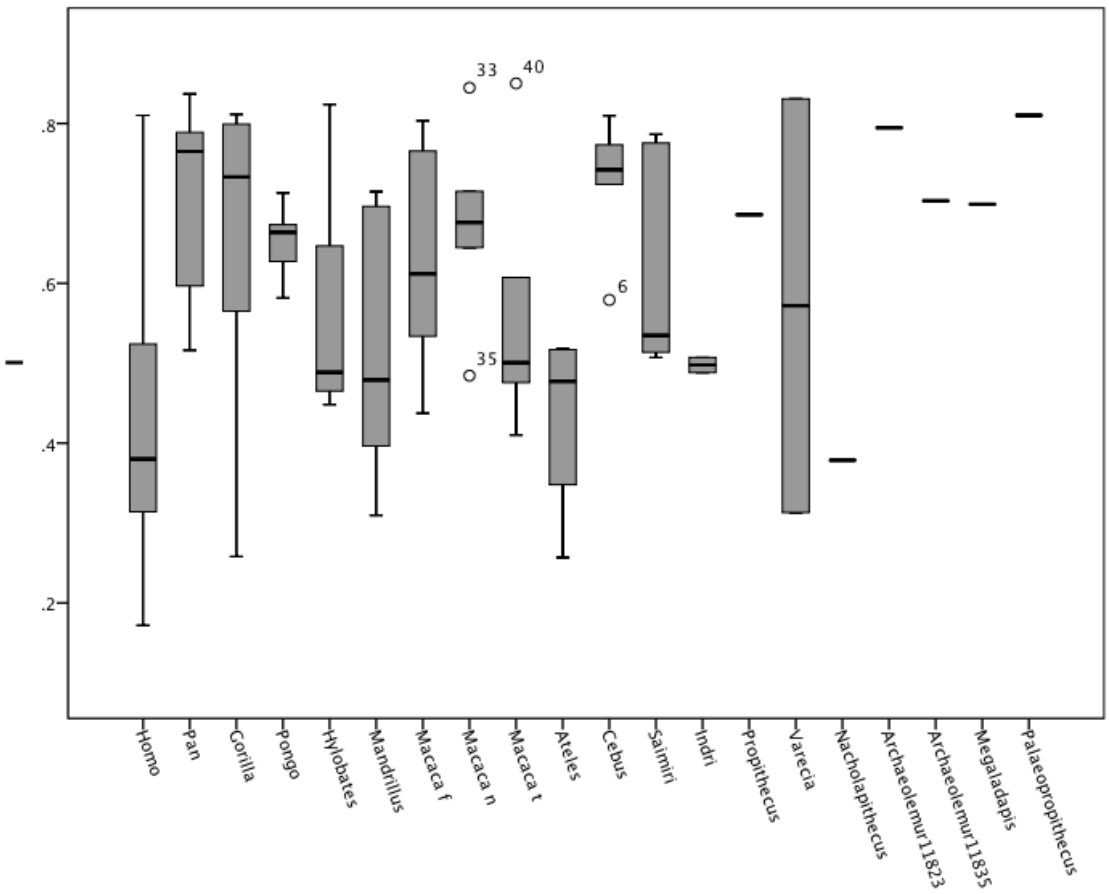

Figure 2.17 Isotropy index in the extant and extinct primates sampled.

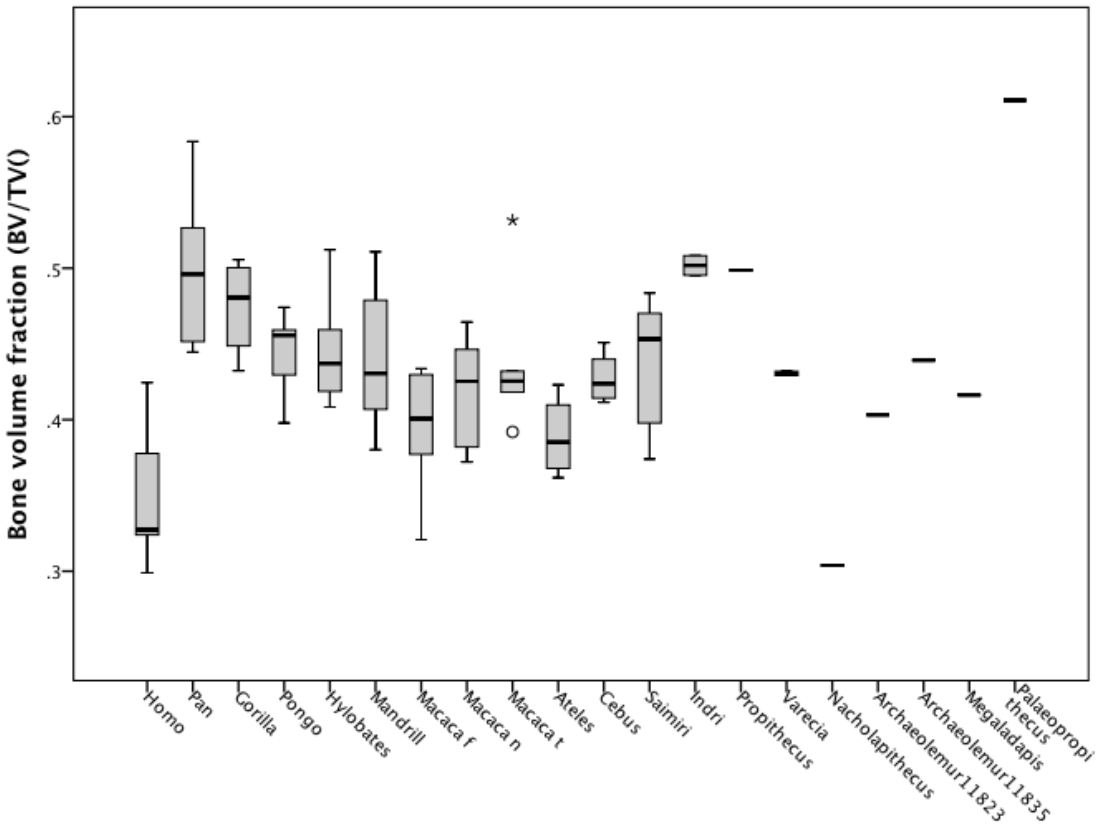

Figure 2.18A Bone volume fraction in the extant and extinct primates sampled.

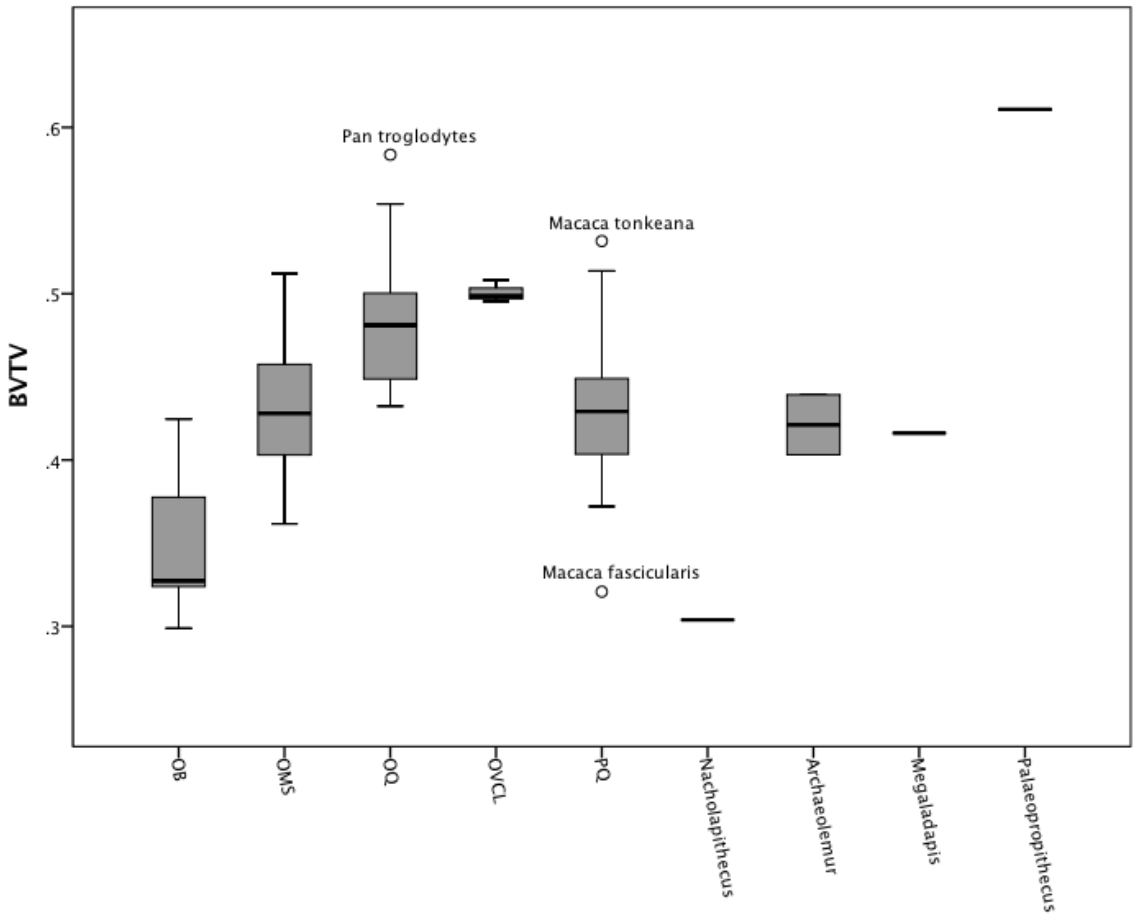

Figure 2.18B Bone volume fraction in the extant and extinct primates sampled with extant taxa grouped by positional behavior.

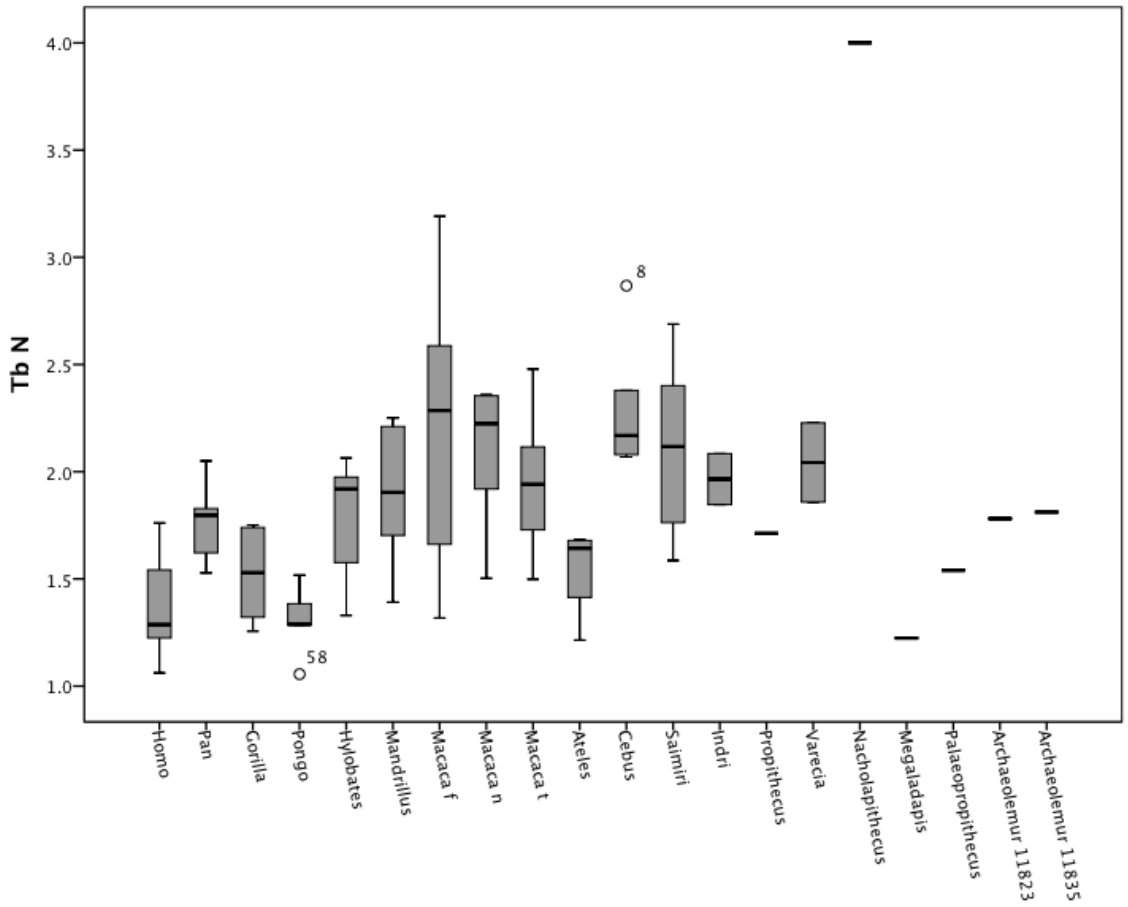

Figure 2.19A Trabecular number in the extant and extinct primates sampled.

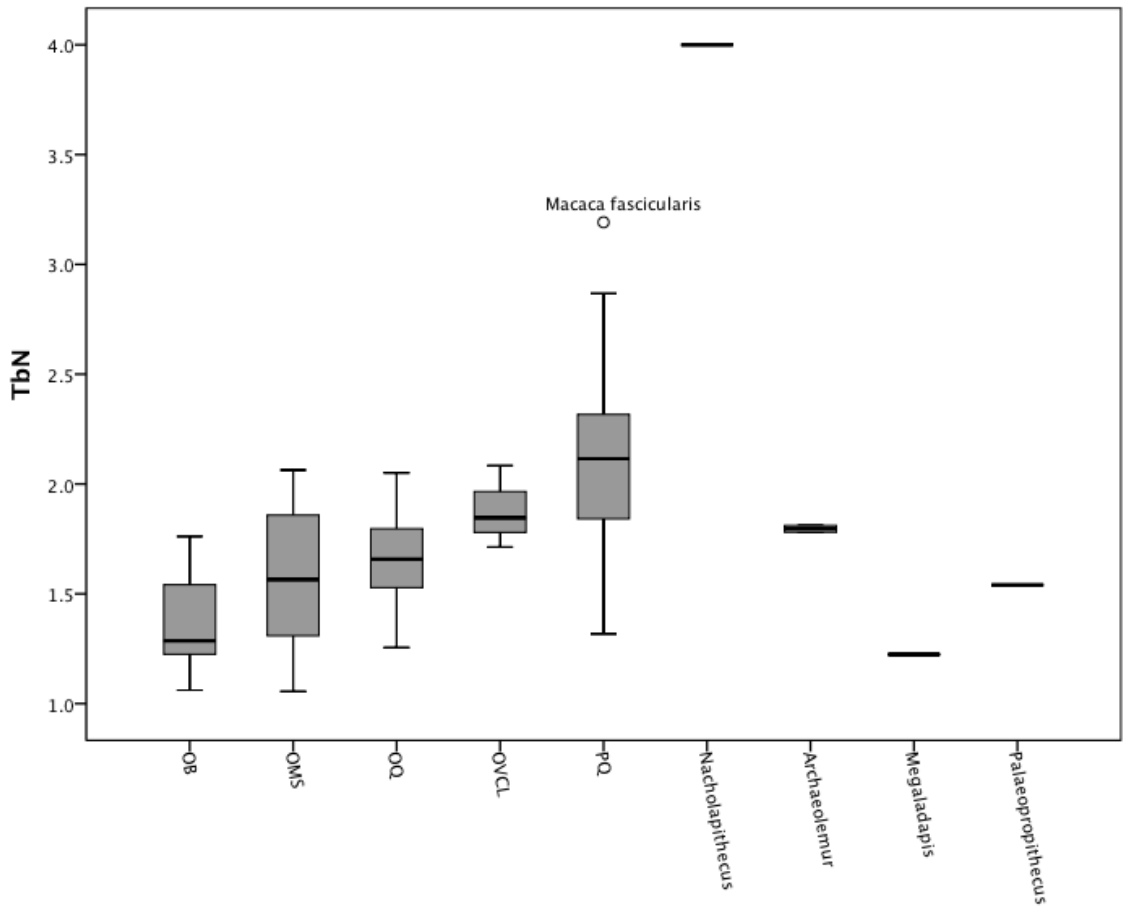

Figure 2.19B Trabecular number in the extant and extinct primates sampled with extant taxa grouped by positional behavior.

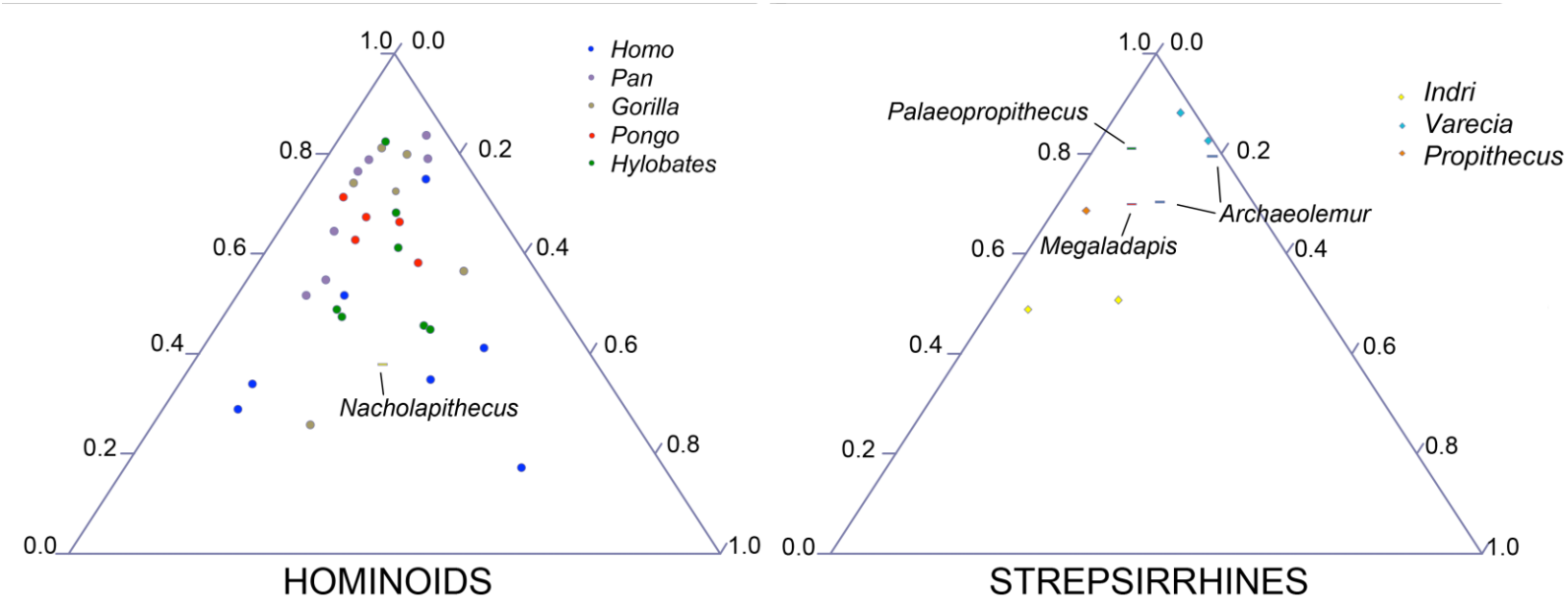

Figure 2.20 Ternary shape diagrams, formed by values for the elongation index [=1-(τ_2/τ_1)] and the isotropy index (=τ_3/τ_1)], illustrating the bone fabric structure in the first sacral vertebra in extant and extinct primates. Polygons enclose the individuals for each taxon to facilitate visual comparison. Data toward the ternary's top apex indicate that trabecular are more isotropic and sphere-like, data toward the bottom left apex indicate trabeculae are more anisotropic and plate-like, and data toward the bottom right apex indicate that trabeculae are more anisotropic and rod-like. See Figure 10 for more detail. Hominoids are shown left, strepsirrhines are shown right.

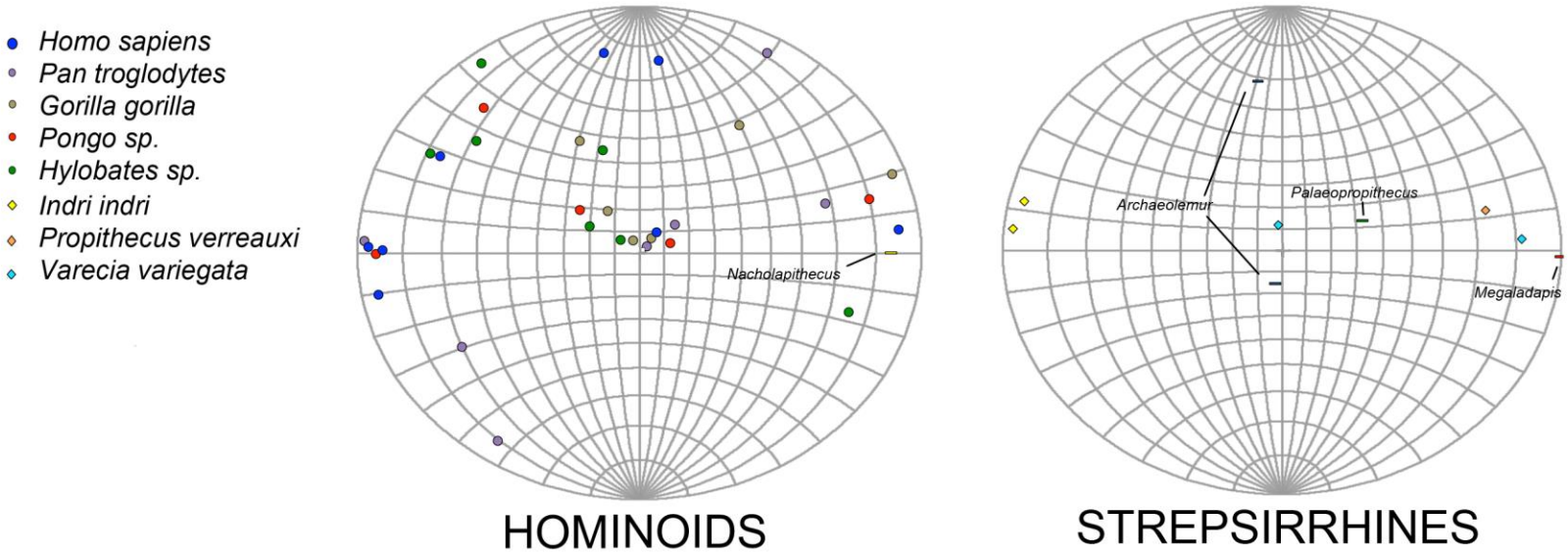

Figure 2.21 Equal-area stereographic projections illustrating the estimates of the primary (i.e., first eigenvector [μ1]) of the trabecular fabric in extant and extinct. Data toward the top and bottom of the sphere are indicative of more dorsoventral orientations, data toward the left and right of the sphere are indicative of more mediolateral orientations, and data toward the middle of the sphere (i.e., into the plot) are indicative of more craniocaudal orientations. Hominoids left, Strepsirrhines right. Each point represents an individual.

Table 2.1. Extant primate sample and positional behaviors. Abbreviations in parentheses are category labels used in analyses.

Taxon	*N*	Positional behaviors	Body mass (kg)
Homo sapiens	8	Orthograde-adapted Biped (OB)	M: 64.24; F: 56.17
Pan troglodytes	7	Orthograde-adapted Quadruped (OQ)	M: 59.7; F: 42.7
Gorilla gorilla	6	Orthograde-adapted Quadruped	M: 170.4; F: 71.5
Pongo sp.	5	Orthograde-adapted Manual Suspensor (OMS)	M: 77.9 – 78.5; F: 35.8
Hylobates sp.	7	Orthograde-adapted Manual Suspensor	M: 5.88 - 6.87; F: 5.34 – 5.82
Mandrillus sphinx	6	Pronograde Quadruped (PQ)	M: 31.6; F: 12.9
Macaca fascicularis	6	Pronograde Quadruped	M: 5.36; F: 3.59
Macaca nemestrina	6	Pronograde Quadruped	M: 9.45; F:4.9
Macaca tonkeana	6	Pronograde Quadruped	M: 14.9; F: 9.0
Ateles sp.	4	Orthograde-adapted Manual Suspensor	F: 7.85; U: 9.025
Sapajus apella	6	Pronograde Quadruped	M: 3.65
Saimiri boliviensis	6	Pronograde Quadruped	M: 0.911
Indri indri	2	Orthograde-adapted Vertical Clinger and Leaper (OVCL)	F: 6.84; U: 6.34
Propithecus verrauxi	1	Orthograde-adapted Vertical Clinger and Leaper	M: 3.25
Varecia variegata	2	Pronograde Quadruped	F: 3.52
Total N	78		

References: Substrate use and locomotor descriptors primarily from Schmitt, 2010; see also Fleagle, 1976; Rodman, 1979; Tuttle and Watts, 1985; Cant, 1987; Meldrum, 1998; Doran, 1989; Hunt, 1989, 1991; Sueur et al., 2011. Body mass data from Smith and Jungers, 1997.

Table 2.2. Results of RMA linear regressions of log-transformed trabecular bone variables on log-transformed mediolateral width of the first sacral vertebra in all primate individuals.

Variable	Geometric Similarity	slope	CL -	CL +	y-int	r^2	result
DA	0	0.685	0.536	2.029	-0.705	0.030	**(+)**
Tb.Th	1	0.515	0.429	0.590	-1.387	0.598	**(-)**
Tb.N	0	-0.500	-0.580	-0.408	0.944	0.322	**(-)**

CL - = lower 95% confidence limit on slope, CL+ = 95% upper confidence limit on slope, y-int = y-intercept. For the results column, X = not different from expected slope, (+) = scales positively, (-) = scales negatively. BV/TV, E, and I were excluded from regressions because they were not significantly correlated with mediolateral width of the first sacral vertebra. See text for details.

Table 2.3 Taxon means and standard deviations (in parentheses) of raw values for trabecular bone variables.

	Trabecular bone variables					
Taxon	DA	E	I	BV/TV	Tb.Th*	Tb.N
Homo sapiens	2.82 (1.40)	0.26 (0.20)	0.43 (0.19)	0.35 (0.05)	0.26 (0.03)	1.37 (0.23)
Pan troglodytes	1.48 (0.30)	0.10 (0.03)	0.70 (0.13)	0.50 (0.05)	0.26 (0.03)	1.75 (0.17)
Gorilla gorilla	1.81 (1.02)	0.16 (0.10)	0.65 (0.21)	0.47 (0.03)	0.29 (0.04)	1.52 (0.22)
Pongo sp.	1.54 (0.12)	0.15 (0.07)	0.65 (0.05)	0.44 (0.03)	0.32 (0.03)	1.31 (0.17)
Hylobates sp.	1.84 (0.40)	0.20 (0.09)	0.57 (0.14)	0.44 (0.04)	0.21 (0.03)	1.77 (0.30)
Mandrillus sphinx	2.13 (0.70)	0.20 (0.03)	0.51 (0.16)	0.44 (0.05)	0.21 (0.02)	1.89 (0.32)
Macaca fascicularis	1.66 (0.40)	0.14 (0.08)	0.63 (0.14)	0.39 (0.04)	0.16 (0.04)	2.22 (0.70)
Macaca nemestrina	1.53 (0.30)	0.13 (0.04)	0.67 (0.18)	0.42 (0.04)	0.18 (0.02)	2.10 (0.33)
Macaca tonkeana	1.89 (0.43)	0.13 (0.09)	0.56 (0.16)	0.44 (0.04)	0.20 (0.03)	1.95 (0.34)
Ateles sp.	2.51 (0.93)	0.30 (0.10)	0.43 (0.12)	0.39 (0.03)	0.23 (0.02)	1.55 (0.22)
Sapajus apella	1.39 (0.17)	0.17 (0.11)	0.73 (0.08)	0.43 (0.02)	0.16 (0.01)	2.29 (0.31)
Saimiri boliviensis	1.70 (0.33)	0.16 (0.10)	0.61 (0.13)	0.44 (0.04)	0.16 (0.01)	2.11 (0.41)
Indri indri	2.01 (0.05)	0.12 (0.10)	0.50 (0.01)	0.50 (0.01)	0.19 (0.01)	1.97 (0.17)
Propithecus verreauxi	1.46 (NA)	0.05 (NA)	0.21 (NA)	0.50 (NA)	0.21 (NA)	1.71 (NA)
Varecia variegata	2.20 (1.41)	0.14 (0.04)	0.57 (0.37)	0.43 (0.01)	0.19 (0.03)	2.04 (0.26)
Archaeolemur (DLC11823)	1.25	0.19	0.79	0.40	0.20	1.78
Archaeolemur (DLC11835)	1.42	0.15	0.70	0.44	0.21	1.81
Megaladapis	1.43	0.11	0.70	0.42	0.30	1.22
Palaeopropithecus	1.23	0.05	0.81	0.61	0.31	1.54
Nacholapithecus	2.64	0.29	0.38	0.30	0.07	4.00

*Values for Tb.Th are not size-corrected

Table 2.4 ANOVA results with Games-Howell post hoc pairwise comparisons among positional behavior groups. Boldface indicates significant result.

DA

F= 4.521		Orthograde Biped	Orthograde Manual Suspensor	Orthograde-adapted Quadruped	Orthograde VCL	Pronograde Quadrupedalism
p=**0.003**	Orthograde Biped	X	0.458	0.248	0.392	0.287
	Orthograde Manual Suspensor	X	X	0.793	0.995	0.838
	Orthograde-adapted Quadruped	X	X	X	0.946	0.988
	Orthograde VCL	X	X	X	X	0.987
	Pronograde Quadrupedalism	X	X	X	X	X

Elongation Index

F=3.416		Orthograde Biped	Orthograde Manual Suspensor	Orthograde-adapted Quadruped	Orthograde VCL	Pronograde Quadrupedalism
p=**0.013**	Orthograde Biped	X	0.966	0.438	0.362	0.604
	Orthograde Manual Suspensor	X	X	0.132	0.355	0.308
	Orthograde-adapted Quadruped	X	X	X	0.959	0.836
	Orthograde VCL	X	X	X	X	0.752
	Pronograde Quadrupedalism	X	X	X	X	X

Isotropy Index

F=3.684		Orthograde Biped	Orthograde Manual Suspensor	Orthograde-adapted Quadruped	Orthograde VCL	Pronograde Quadrupedalism
p=**0.009**	Orthograde Biped	X	0.453	0.063	0.631	0.148
	Orthograde Manual Suspensor	X	X	0.294	1.000	0.655
	Orthograde-adapted Quadruped	X	X	X	0.614	0.799
	Orthograde VCL	X	X	X	X	0.894
	Pronograde Quadrupedalism	X	X	X	X	X

Table 2.4 continued…

BVTV

F= 15.893		Orthograde Biped	Orthograde Manual Suspensor	Orthograde-adapted Quadruped	Orthograde VCL	Pronograde Quadrupedalism
p=**0.000**	Orthograde Biped	X	**0.007**	**0.000**	**0.000**	**0.008**
	Orthograde Manual Suspensor	X	X	**0.011**	**0.000**	1.000
	Orthograde-adapted Quadruped	X	X	X	0.812	**0.004**
	Orthograde VCL	X	X	X	X	**0.000**
	Pronograde Quadrupedalism	X	X	X	X	X

Trabecular Thickness (size-corrected)

F=6.842		Orthograde Biped	Orthograde Manual Suspensor	Orthograde-adapted Quadruped	Orthograde VCL	Pronograde Quadrupedalism
p=**0.000**	Orthograde Biped	X	**0.003**	0.113	0.172	**0.000**
	Orthograde Manual Suspensor	X	X	**0.036**	0.575	0.985
	Orthograde-adapted Quadruped	X	X	X	0.246	**0.000**
	Orthograde VCL	X	X	X	X	0.661
	Pronograde Quadrupedalism	X	X	X	X	X

Tb.N

F= 12.836		Orthograde Biped	Orthograde Manual Suspensor	Orthograde-adapted Quadruped	Orthograde VCL	Pronograde Quadrupedalism
p=**0.000**	Orthograde Biped	X	0.398	0.098	0.071	**0.000**
	Orthograde Manual Suspensor	X	X	0.941	0.287	**0.000**
	Orthograde-adapted Quadruped	X	X	X	0.459	**0.000**
	Orthograde VCL	X	X	X	X	**0.536**
	Pronograde Quadrupedalism	X	X	X	X	X

Table 2.5 PCA results for all primates and the major primate clade subgroupings.

All Primates	*Variance explained*		*Component matrix*				
	% variance	Eigenvalue	BV/TV	Tb.N	DA	E	Tb.Th
PC1	45.424	2.271	-0.648	-0.828	0.811	0.645	0.305
PC2	20.339	1.017	0.244	-0.148	-0.007	-0.359	0.898
	78.266						

Hominoids							
	% variance	Eigenvalue	BV/TV	Tb.N	DA	E	Tb.Th
PC1	43.83	2.192	0.783	0.755	-0.775	-0.639	-0.016
PC2	25.72	1.286	0.247	0.270	0.020	0.575	0.906
	69.55						

Catarrhines							
	% variance	Eigenvalue	BV/TV	Tb.N	DA	E	Tb.Th
PC1	40.583	2.029	-0.666	-0.673	0.793	0.705	0.073
PC2	22.258	1.113	0.097	0.336	-0.017	0.334	0.937
	62.841						

Platyrrhines							
	% variance	Eigenvalue	BV/TV	Tb.N	DA	E	Tb.Th
PC1	54.018	2.701	0.847	-0.896	-0.908	-0.688	0.149
PC2	22.268	1.113	-0.290	0.242	0.157	-0.089	0.973
	76.286						

* PCA could not be performed for strepsirrhines because there are fewer than three groups

Table 2.6 ANOVA results for taxon PC1/PC2 scores with Games-Howell post hoc pairwise comparisons. Boldface indicates significant result.

Hominoids		*Pan troglodytes*	*Gorilla gorilla*	*Pongo sp.*	*Hylobates sp.*
F = 4.832 / 17.836	*Homo sapiens*	**0.032** / 0.655	0.363 / 0.452	0.404 / 0.456	0.277 / **0.001**
Model p = **0.005 / 0.000**	*Pan troglodytes*	xxx	0.500 / 0.591	0.066 / 0.985	0.160 / **0.000**
	Gorilla gorilla	xxx	xxx	0.987 / 1.000	1.000 / **0.001**
	Pongo sp.	xxx	xxx	xxx	0.987 / **0.000**

Catarrhines		*Pan troglodytes*	*Gorilla gorilla*	*Pongo sp.*	*Hylobates sp.*	*Mandrillus sphinx*	*Macaca fascicularis*	*Macaca nemestrina*	*Macaca tonkeana*
F = 2.321 / 17.834	*Homo sapiens*	0.083 / 0.880	0.701 / 0.647	0.598 / 0.479	0.768 / **0.000**	0.861 / 0.072	0.562/ **0.006**	0.195 / **0.047**	0.448 / **0.028**
Model p = **0.035** / **0.000**	*Pan troglodytes*	xxx	0.795 / 0.999	0.227 / 0.944	0.154 / **0.000**	0.362 / 0.119	0.937 / **0.000**	0.746 / 0.067	0.780 / 0.065
	Gorilla gorilla	xxx	xxx	1.000 / 0.998	1.000 / **0.000**	1.000 / 0.217	1.000/ **0.001**	0.996 / 0.124	1.000 / 0.107
	Pongo sp.	xxx	xxx	xxx	1.000 / **0.001**	1.000 / 0.583	0.999 / 0.012	0.835 / 0.338	0.999 / 0.226
	Hylobates sp.	xxx	xxx	xxx	xxx	1.000 / **0.008**	0.994 / 0.184	0.695 / **0.016**	0.989 / 0.204
	Mandrillus sphinx	xxx	xxx	xxx	xxx	xxx	0.996 / 0.181	0.829 / 1.000	0.993 / 0.917
	Macaca fascicularis	xxx	xxx	xxx	xxx	xxx	xxx	1.000 / 0.350	1.000 / 0.990
	Macaca nemestrina	xxx	xxx	xxx	xxx	xxx	xxx	xxx	1.000 / 0.984

Platyrrhines		*Sapajus apella*	*Saimiri boliviensis*
F = 8.878 / 15.943	*Ateles sp.*	0.051 / 0.741	0.056 / **0.009**
Model p = **0.004 / 0.000**	*Sapajus apella*	xxx	0.972 / **0.001**

Table 2.7 Resolution analysis data for three *Gorilla gorilla* individuals. VOI was positioned in distal sacrum, see text for discussion.

		AMNH 90290	AMNH 167335	AMNH 167340
DA				
Resolution (μ)	80	1.769	1.934	2.238
	63	1.735	2.506	1.993
	48	2.002	2.470	2.178
% Reduction / Increase	80-48	+13.13	+27.71	-2.66
	63-48	+13.30	+1.46	+9.32
E				
Resolution (μ)	80	0.324	0.409	0.416
	63	0.375	0.563	0.354
	48	0.365	0.495	0.329
% Reduction / Increase	80-48	+11.31	+17.29	-26.70
	63-48	+2.49	-12.14	-7.29
I				
Resolution (μ)	80	0.565	0.517	0.447
	63	0.576	0.399	0.502
	48	0.500	0.405	0.459
% Reduction / Increase	80-48	-11.60	-21.70	+2.73
	63-48	-13.30	-1.46	-8.52
BV/TV				
Resolution (μ)	80	0.500	0.346	0.457
	63	0.425	0.306	0.426
	48	0.385	0.279	0.395
% Reduction / Increase	80-48	-22.98	-19.32	-13.44
	63-48	-9.41	-8.86	-7.17
Tb.Th*				
Resolution (μ)	80	0.326	0.206	0.236
	63	0.230	0.182	0.228
	48	0.205	0.157	0.208
% Reduction / Increase	80-48	-37.00	-24.13	-12.01
	63-48	-10.66	-13.83	-8.96
Tb.N				
Resolution (μ)	80	1.400	1.442	1.512
	63	1.467	1.438	1.545
	48	1.516	1.567	1.591
% Reduction / Increase	80-48	+7.65	+7.94	+5.00
	63-48	+3.33	+8.98	+2.99

*Tb.Th was not size-corrected in these analyses

Table 2.8 Comparisons between the original hominoid dataset and the resolution-corrected hominoid dataset of results for PCA and taxon pairwise comparisons of PC1/PC2 scores. Boldface indicates significant result.

PCA Original Dataset

	Variance explained		*Component matrix*				
	% variance	Eigenvalue	BV/ TV	Tb.N	DA	E	Tb.Th
PC1	51.551	2.578	-0.783	-0.757	0.823	0.772	0.342
PC2	29.997	1.5	-0.279	0.602	0.356	0.331	-0.908
Total	81.548						

PCA Resolution -corrected dataset

	Variance explained		*Component matrix*				
	% variance	Eigenvalue	BV/ TV	Tb.N	DA	E	Tb.Th
PC1	47.456	2.373	-0.785	-0.773	0.763	0.696	0.306
PC2	28.254	2.413	-0.031	0.579	0.489	0.428	-0.809
Total	75.71						

ANOVA Original dataset

		Pan troglodytes	*Gorilla gorilla*	*Pongo sp.*	*Hylobates sp.*
F = 6.097 / 9.400	*Homo sapiens*	**0.014** / 0.639	0.232 / 0.114	0.385 / **0.011**	0.069 / 0.063
Model p = **0.001** / **0.000**	*Pan troglodytes*	xxx	0.419 / 0.591	0.059 / 0.063	0.516 / 0.064
	Gorilla gorilla	xxx	xxx	0.946 / 0.424	0.976 / **0.007**
	Pongo sp.	xxx	xxx	xxx	0.536 / **0.001**

ANOVA Resolution-corrected dataset

		Pan troglodytes	*Gorilla gorilla*	*Pongo sp.*	*Hylobates sp.*
F = 5.085 / 5.786	*Homo sapiens*	**0.016** / 0.285	0.288 / 0.238	0.475 / **0.020**	0.054 / 0.999
Model p = **0.002** / **0.000**	*Pan troglodytes*	xxx	0.418 / 0.577	0.058 / **0.047**	0.910 / 0.582
	Gorilla gorilla	xxx	xxx	0.944 / 0.352	0.870/ 0.104
	Pongo sp.	xxx	xxx	xxx	0.343/ **0.009**

REFERENCES

Abitbol, M. 1987a. Evolution of the lumbosacral angle. Am. J. Phys. Anthropol. 72, 361–72.

Abitbol, M. 1987b. Evolution of the sacrum in hominoids. Am. J. Phys. Anthropol. 74, 65–81.

Abitbol, M. 1989. Sacral curvature and supine posture. Am. J. Phys. Anthropol. 80, 379–89.

Alba, D.M., Almécija, S., and Moyà-Solà, S. 2010. Locomotor inferences in *Pierolapithecus* and *Hispanopithecus*: Reply to Deane and Begun (2008). J. Hum. Evol. 59:143–149.

Arsuaga, J.L., Lorenzo, C., Carretero, J.M., Gracia, A., Martínez, I., García, N., de Castro, J.M.B., and Carbonell, E. 1999. A complete human pelvis from the Middle Pleistocene of Spain. Nature 399, 255–258.

Ashton-Miller, J.A., and McGlashen, K.M. 1989. Analysis of loads on the canine lumbar spine: an experimental and theoretical study. 13th Annual Meeting of the American Society of Biomechanics August 23-25, 258–259.

Begun, D.R. 2002. European hominoids. In: Hartwig, W. (Ed.) Cambridge Studies in Biological and Evolutionary Anthropology. Cambridge University Press. pp 339–368.

Benefit, B.R., and McCrossin, M.L. 1995. Miocene Hominoids and Hominid Origins. Ann. Rev. Anthropol. 24, 237–256.

Benn, D.I., 1994. Fabric shape and the interpretation of sedimentary fabric data. J. Sediment. Res. A 64, 910-915.

Benton R. 1967. Morphological evidence for adaptations within the epaxial region of the primates. In: Vagtborg, H (Ed.) The Baboon in Medical Research. pp 201–216.

Biewener, A., Fazzalari, N., Konieczynski, D., and Baudinette, R. 1996. Adaptive changes in trabecular architecture in relation to functional strain patterns and disuse. Bone 19, 1–8.

Burr, D.B., Robling, A.G., C.H. Turner. 2002. Effects of Biomechanical Stress on Bones in Animals. Bone 30(5): 781-786.

Cant, J.G. 1987. Positional behavior of female Bornean orangutans (*Pongo pygmaeus*). Am. J. Primatol. 12, 71–90.

Carter, D.R., Fyhrie, D.P., and Whalen, R.T. 1987. Trabecular bone density and loading history: regulation of connective tissue biology by mechanical energy. J. Biomech. 20, 785-794.

Cartmill, M., and Milton, K. 1977. The lorisiform wrist joint and the evolution of "'brachiating'"adaptations in the Hominoidea. Am. J. Phys. Anthropol. 47, 249–272.

Coleman MN, and Colbert MW. 2007. Technical note: CT thresholding protocols for taking measurements on three-dimensional models. Am J Phys Anthropol 133:723–725.

Cotter, M.M., Simpson, S.W., Latimer, B.M., and Hernandez, C.J. 2009. Trabecular microarchitecture of hominoid thoracic vertebrae. Anat. Rec. 292, 1098–1106.

Cotter, M.M., Loomis, D.A., Simpson, S.W., Latimer, B.,Hernandez, C.J. 2011. Human evolution and osteoporosis-related spinal fractures. PLoS ONE 6, e26658.

Currey, J.D. 1975. The effects of strain rate, reconstruction and mineral content on some mechanical properties of bovine bone. J.Biomech. 8, 81–86.

Currey, J.D. 1984. The mechanical adaptations of bones. Princeton University Press Princeton, NJ.

Deane, A.S., and Begun, D.R. 2010. *Pierolapithecus* locomotor adaptations: a reply to Alba et al.'s comment on Deane and Begun (2008). J. Hum. Evol. 59, 150–154.

Ding, M., and Hvid, I. 2000. Quantification of age-related changes in the structure model type and trabecular thickness of human tibial cancellous bone. Bone 26, 291–295.

Doran, D. 1989. Chimpanzee and pygmy chimpanzee positional behavior: the influence of environment, body size, morphology and ontogeny on locomotion and posture, Ph.D. dissertation, The State University of New York, Stony Brook, NY..

Doube, M., Klosowski, M.M., Wiktorowicz-Conroy, A.M.,Hutchinson, J.R., Shefelbine S.J. 2011 Trabecular bone scales allometrically in mammals and birds. Proc. R. Soc.B 278, 3067–3073.

Ebraheim, N., Sabry, F.F., Nadim, Y., Xu, R., and Yeasting, R.A. 2000. Internal architecture of the sacrum in the elderly: an anatomic and radiographic study. Spine 25, 292.

Fajardo, R.J., and Müller, R. 2001. Three dimensional analysis of nonhuman primate trabecular architecture using micro computed tomography. Am. J. Phys. Anthropol. 115, 327–336.

Fajardo, R.J., Ryan, T.M., and Kappelman, J. 2002. Assessing the accuracy of high-resolution X-ray computed tomography of primate trabecular bone by comparisons with histological sections. Am. J. Phys. Anthropol. 118:1–10.

Fajardo, R.J., Müller, R., Ketcham, R.A., and Colbert, M. 2007. Nonhuman anthropoid primate femoral neck trabecular architecture and its relationship to locomotor mode. Anat. Rec. 290, 422–436.

Fajardo, R.J., De Silva, J., and MacLatchy, L. 2010. Does the amount of bone dictate the trabecular bone structure in strepsirhine lumbar vertebrae? Am. J. Phys. Anthropol. S50:102.

Fajardo, R.J., Desilva, J.M., Manoharan, R.K., Schmitz, J.E., Maclatchy, L.M., and Bouxsein M.L. 2013. Lumbar Vertebral Body Bone Microstructural Scaling in Small to Medium-Sized Strepsirhines. Anat. Rec. 296,210–226.

Fyhrie, D.P., and Schaffler, M.B. 1995. The adaptation of bone apparent density to applied load. J. Biomech. 28:135–146.

Fleagle J. 1976. Locomotion and posture of the Malayan siamang and implications for hominoid evolution. Folia Primatol (Basel) 26:245–269.

Games, P., and Howell, J. 1976. Pairwise Multiple Comparison Procedures with Unequal N's and/or Variances: A Monte Carlo Study. J. Ed. Behav. Stat. 1, 113.

Gibson, L.J. 1985. The mechanical behaviour of cancellous bone. J. Biomech. 18,317.

Godfrey, L.R., and Jungers, W.L. 2002. Quaternary Fossil Lemurs. In The Primate Fossil Record. W. Hartwig (Ed.). Cambridge: Cambridge University Press, pp. 97-121.

Godfrey, L.R., Jungers, W.L., Burney, D.A., Vasey, N., Wheeler, W., Lemelin, P., Shapiro, L.J., Schwartz, G.T., King, S.J, et al. 2006. New discoveries of skeletal elements of *Hadropithecus stenognathus* from Andrahomana Cave, southeastern Madagascar. J. Hum. Evol. 51,395–410.

Goldstein, S.A., Goulet, R., and McCubbrey, D. 1993. Measurement and significance of three-dimensional architecture to the mechanical integrity of trabecular bone. Calc. Tiss. Intl. 53, S127–S133.

Gosman, J.H., and Ketcham, R.A. 2009. Patterns in ontogeny of human trabecular bone from SunWatch Village in the prehistoric Ohio Valley: general features of microarchitectural change. Am. J. Phys. Anthropol. 138, 318–332.

Graham, D.J., Midgley, N.G., 2000. Graphical representation of particle shape using triangular diagrams: an excel spreadsheet method. Earth Surf. Proc. Landf. 25, 1473-1477.

Granhed H, Jonson R, and Hansson T. 1987. The loads on the lumbar spine during extreme weight lifting. Spine 12,146–149.

Gregory, W.K. 1928. The upright posture of man: A review of its origin and evolution. Proc. Am. Phil. Soc. 67, 339–377.

Hammer, Ø., Harper, D.A.T., Ryan, P.D. 2001. PAST: Paleontological statistics software package for education and data analysis. Palaeontologia Electronica 4(1), 9pp.

Harrigan, T.P., Jasty, M., Mann ,R.W., and Harris, W.H. 1988. Limitations of the continuum assumption in cancellous bone. J. Biomech. 21:269–275.

Harrison, T. 1987. A reassessment of the phylogenetic relationships of *Oreopithecus bambolii* Gervais 1872. J. Hum. Evol. 15, 541–583.

Harrison, T. 1991. The implications of *Oreopithecus bambolii* for the origins of bipedalism. In: Coppens, Y., Senut, B. (Eds.), Origine (s) de la bipédie chez les hominidés, Cahiers de Paléoanthropologie. Paris: Editions du CNRS. pp. 235–244.

Harrison T, and Rook L. 1997. Enigmatic anthropoid or misunderstood ape? The phylogenetic status of Oreopithecus bambolii reconsidered. Function, Phylogeny, and Fossils: Miocene Hominoid Evolution and Adaptations:327–362.

Hunt, K. 1989. Positional behavior in Pan troglodytes at the Mahale Mountains and the Gombe stream national parks, Tanzania, Ph.D. dissertation, University of Michigan, Ann Arbor, Michigan.

Hunt, K. 1991. Positional behavior in the Hominoidea. Int. J. Primatol. 12, 95–118.

Hürzeler, J. 1958. *Oreopithecus bambolii* Gervais: A preliminary report. Verh. naturf. Ges. Basel. 69, 1-48.

Huq, E. and Jungers, W.L. 2009. Tail length and the sacral index in living and subfossil Malagasy prosimians. Am. J. Phys. Anthropol. 138, 231 (abstract).

Ishida, H., Kunimatsu, Y., Takano, T., Nakano Y, and Nakatsukasa, M. 2004. *Nacholapithecus* skeleton from the Middle Miocene of Kenya. J. Hum. Evol. 46,69–103.

Johanson, D.C., Lovejoy, C.O., Kimbel, W.H., White, T.D., Ward, S.C., Bush, M.E., Latimer, B.M., Coppens, Y. 1982. Morphology of the Pliocene partial hominid skeleton (AL 288–1) from the Hadar formation, Ethiopia. Am. J. Phys. Anthropol. 57, 403–451.

Johanson, D.C., Lovejoy, C.O., Kimbel, W.H., White, T.D., Ward, S.C., Bush, M.E., Latimer, B.M., Coppens, Y. 1982. Morphology of the Pliocene partial hominid skeleton (AL 288-1) from the Hadar formation, Ethiopia. Am. J. Phys. Anthropol. 57, 403–451.

Johnson S, and Shapiro L. 1998. Positional behavior and vertebral morphology in atelines and cebines. Am. J. Phys. Anthropol. 105, 333–354.

Jungers, W.L. 1988. Relative joint size and hominoid locomotor adaptations with implications for the evolution of hominid bipedalism. J. Hum. Evol. 17, 247–265.

Jungers, W.L., 1991. Scaling of postcranial joint size in hominoid primates. J. Hum. Evol. 6, 391-399.

Jungers, W.L., Godfrey LR, Simons EL, Wunderlich RE, Richmond BG, Chatrath PS, Plavcan JM, Kay RF, Jungers WL, et al. 2002. Ecomorphology and behavior of giant extinct lemurs from Madagascar. In: Plavcan, J.M. (Ed.) Reconstructing behavior in the primate fossil record. Plenum Press: New York. pp. 371–411.

Keaveny, T.M., Morgan, E.F., Niebur, G.L., and Yeh, O.C. 2001. Biomechanics of trabecular bone. Ann. Rev. Bio. Eng. 3, 307–333.

Ketcham, R.A., and Carlson, W.D. 2001. Acquisition, optimization and interpretation of X-ray computed tomographic imagery: applications to the geosciences. Computers & Geosciences 27, 381–400.

Ketcham, R.A., and Ryan, T. 2004. Quantification and visualization of anisotropy in trabecular bone. J. Microscop. 213, 158–171.

Kim, D. G., Christopherson, G. T., Dong, X. N., Fyhrie, D. P., & Yeni, Y. N. (2004). The effect of microcomputed tomography scanning and reconstruction voxel size on the accuracy of stereological measurements in human cancellous bone. Bone, *35*(6), 1375-1382.

Kirk E.C., and Gosselin-Ildari A.D. 2009. Cochlear labyrinth volume and hearing abilities in primates. Anat. Rec. 292, 765–776.

Köhler, M., and Moyà-Solà, S. 1997. Ape-like or hominid-like? The positional behavior of *Oreopithecus bambolii* reconsidered. Proc. Natl. Acad. Sci. 94, 11747-11750.

Kothari, M., Keaveny, T.M., Lin, J.C., Newitt, D.C., Genant, H.K., Majumdar, S. Impact of spatial resolution on the prediction of trabecular architecture parameters. Bone. 22(5), 437-443.

Larson, S. 1998. Parallel evolution in the hominoid trunk and forelimb. Evol. Anthropol. 6, 87–99.

Lazenby, R.A., Skinner, M.M., Kivell TL, and Hublin, J.J. 2011. Scaling VOI size in 3D CT studies of trabecular bone: A test of the over sampling hypothesis. Am. J. Phys. Anthropol. 144, 196-203.

Leutenegger, W. 1977. A functional interpretation of the sacrum of *Australopithecus africanus*. S. Afr. J. Sci. 73, 308–10.

Lieberman, D.E., Devlin, M.J., and Pearson, O.M. 2001. Articular area responses to mechanical loading: effects of exercise, age and skeletal location. Am. J. Phys. Anthropol. 116, 266-277.

Lieberman, D.E., Polk, J.D., and Demes B. 2004. Predicting long bone loading from cross-sectional geometry. Am. J. Phys. Anthropol. 123, 156-171.

Lovejoy, C.O. 1988. Evolution of human walking. Sci. Am. 259, 82–89.

Lovejoy, C.O., McCollum, M.A., Reno, P.L., and Rosenman, B.A. 2003. Developmental biology and human evolution. Ann. Rev. Anthropol. 32, 85–109.

Macchiarelli, R., Rook, L., Bondioli, L. 2001. Comparative analysis of the iliac trabecular architecture in extant and fossil primates by means of digital image processing techniques: implications for the reconstruction of fossil locomotor behaviours. In: Agusti, J., Rook, L., Andrews, P. (Eds.), Hominoid Evolution and Climatic Change in Europe. Cambridge University Press, U.K. pp 60–101.

Machida, A., and Inoue, T. 1994. The effect of weight-bearing on the bone tissue of bipedal rats. J. Bone Min. Met. 12, 15–29.

MacLatchy, L., Gebo, D., Kityo, R., and Pilbeam, D. 2000. Postcranial functional morphology of *Morotopithecus bishopi*, with implications for the evolution of modern ape locomotion. J. Hum. Evol. 39, 159–183.

MacLatchy, L., Müller, R. 2002. A comparison of the femoral head and neck trabecular architecture of *Galago* and *Perodicticus* using micro-computed tomography (mCT). J. Hum. Evol. 43, 89–105.

Maga, M., Kappelman, J., Ryan, T.M., and Ketcham. R.A. 2006. Preliminary Observations on the Calcaneal Trabecular Microarchitecture of Extant Large-Bodied Hominoids. Am. J. Phys. Anthropol. 129, 410–417.

Mahato, N.K. 2010. Trabecular architecture in human sacra: patterns observed in complete sacralisation and accessory articulation with the fifth lumbar vertebrae. J. Morphol. 27, 19–22.

Moyà Solà, S., and Kohler, M. 1996. A *Dryopithecus* skeleton and the origins of great-ape locomotion. Nature 379, 156–159.

Moyà Solà, S., Köhler, M., Alba, D.M., Casanovas-Vilar, I., Galindo, J., 2004. *Pierolapithecus catalaunicus*, a new Middle Miocene great ape from Spain. Science 306, 1339-1344.

Mullender, M.G., Huiskes, R., Versleyen, H., Burma, P.1996. Osteocyte density and histomorphometric parameters in cancellous bone of the proximal femur in five mammalian species. J. Orthop. Res. 14, 972–979.

Nakatsukasa, M., and Kunimatsu, Y. 2009. *Nacholapithecus* and its importance for understanding hominoid evolution. Evol. Anthropol. 18, 103–119.

Odgaard A. 1997. Three-dimensional methods for quantification of cancellous bone architecture. Bone. 20, 315–328.

Oxnard CE, and Yang HCL. 1981. Beyond biometrics: studies of complex biological patterns. Symp. Zool. Soc. Lond. 46, 127–167.

Pearson, O.M., Lieberman, D.E. 2004. The aging of Wolff's "law": ontogeny and responses to mechanical loading in cortical bone. Am. J. Phys. Anthropol. 125, 63-99.

Peretz, A.M., Hipp, J.A., and Heggeness, M.H. 1998. The internal bony architecture of the sacrum. Spine 23, 971-974.

Pilbeam, D., and Young, N. 2004. Hominoid evolution: synthesizing disparate data. Comptes. Rendus. Palevol. 3, 305–321.

Rafferty, K.L. 1998. Structural design of the femoral neck in primates. J. Hum. Evol. 34, 361–383.

Rafferty, K.L., and Ruff, C. 1994. Articular structure and function in *Hylobates, Colobus*, and *Papio*. Am. J. Phys. Anthropol. 94, 395–408.

Rice, J.C., Cowin, S.C., and Bowman, J.A. 1988. On the dependence of the elasticity and strength of cancellous bone on apparent density. J. Biomech. 21, 155-168.

Ridler, T. W., and Calvard, S. 1978. Picture thresholding using an iterative selection method. IEEE transactions on Systems, Man and Cybernetics, 8(8), 630-632.

Robinson, J.T. 1972. Early hominid posture and locomotion. University of Chicago Press, Chicago.

Robson-Brown, K., Katharine, A., Davies, E.N., and McNally, D.S. 2002. The angular distribution of vertebral trabeculae in modern humans, chimpanzees and the Kebara 2 Neanderthal. J. Hum. Evol.43:189–205.

Rook, L., Bondioli, L., Köhler, M., Moyà-Solà, S., and Macchiarelli, R. 1999. *Oreopithecus* was a bipedal ape after all: evidence from the iliac cancellous architecture. Proc. Natl. Acad. Sci. 96, 8795-8799.

Rook, L., Oms, O., Benvenuti, M.G., Papini, M. 2011. Magnetostratigraphy of the Late Miocene Baccinello–Cinigiano basin (Tuscany, Italy) and the age of *Oreopithecus bambolii* faunal assemblages. Palaeogeogr. Palaeoclimatol. Palaeoecol. 305, 286–294.

Rook, L., Renne, P., Benvenuti, M., Papini, M. 2000. News and Views Geochronology of *Oreopithecus*-bearing succession at Baccinello (Italy) and the extinction pattern of European Miocene hominoids. J. Hum. Evol. 39, 577–582.

Rose, M.D., 1993. Locomotor anatomy of Miocene hominoids. In: Gebo, D. (Ed.), Postcranial Adaptation in Nonhuman Primates. Northern Illinois University Press, DeKalb, pp. 252-272.

Rose, M.D., 1997. Functional and phylogenetic features of the forelimb in Miocene hominoids. In: Begun, D.R., Ward, C.V., Rose, M.D. (Eds.), Function, Phylogeny, and Fossils: Miocene Hominoid Evolution and Adaptations. Plenum Press, New York, pp. 79-100.

Rose, M.D., Nakano, Y., and Ishida, H. 1996. *Kenyapithecus* postcranial specimens from Nachola, Kenya. Afr. Stud. Monogr. 24, 3–56.

Rosenman, B. 2008. Triangulating the evolution of the vertebral column in the last common ancestor: thoracolumbar transverse process homology in the Hominoidea. Ph.D. Dissertation. Kent State University, Kent, Ohio.

Rubin, C.T., and Lanyon, L.E. 1985. Regulation of bone mass by mechanical strain magnitude. Calc. Tiss. Intl. 37, 411–417.

Ruff, C.B. 1999. Skeletal structure and behavioral patterns of prehistoric Great Basin populations. In: Hemphill, B.E., Larsen, C.S. (Eds.) Prehistoric Lifeways in the Great Basin Wetlands: Bioarchaeological Reconstruction and Interpretation. Salt Lake city: University Utah Press. pp. 290-320.

Ruff, C. B. 2008. Biomechanical analyses of archaeological human skeletons. In: Katzenberg, M.A. and S.R. Saunders (Eds). Biological Anthropology of the Human Skeleton, Second Edition. John Wiley & Sons, Inc. pp 183-206.

Ruff, C., Holt, B., & Trinkaus, E. 2006. Who's afraid of the big bad Wolff?:"Wolff's law" and bone functional adaptation. Am. J. Phys. Anthropol. 129, 484-498.

Russo, G.A., Shapiro, L.J. 2011. Morphological correlates of tail length in the catarrhine sacrum. J. Hum. Evol. 30, 223–232.

Russo, G.A., Shapiro, L.J. 2013. Reevaluation of the lumbosacral region of *Oreopithecus bambolii.* J. Hum. Evol. (doi: 10.1016/j.jhevol.2013.05.004)

Ryan, T.M., and Ketcham, R.A. 2002a. The three-dimensional structure of trabecular bone in the femoral head of strepsirrhine primates. J. Hum. Evol. 43,1–26.

Ryan, T.M., and Ketcham, R.A. 2002b. Femoral head trabecular bone structure in two omomyid primates. J. Hum. Evol. 43,241–263.

Ryan, T.M., and Ketcham R.A. 2005. Angular Orientation of Trabecular Bone in the Femoral Head and Its Relationship to Hip Joint Loads in Leaping Primates. J. Morpol. 265:249.

Ryan, T.M., Krovitz, G.E. 2006. Trabecular bone ontogeny in the human proximal femur. J. Hum. Evol. 51, 591–602.

Ryan, T.M., and Shaw, C.N. 2012 Unique suites of trabecular bone features characterize locomotor behavior in human and non-human anthropoid primates. PLoS ONE 7, e41037.

Ryan TM, Shaw CN. 2013. Trabecular bone microstructure scales allometrically in the primate humerus and femur. Proceedings of the Royal Society B: Biological Sciences 280.

Ryan, T.M., and Ketcham R.A. 2005. Angular Orientation of Trabecular Bone in the Femoral Head and Its Relationship to Hip Joint Loads in Leaping Primates. J. Morpol. 265, 249-263.

Ryan, T.M., and Walker, A. 2010 Trabecular bone structure in the humeral and femoral heads of anthropoid primates. Anat. Rec. 293, 719–729.

Scherf, H., Harvati, K., and Hublin, J.J. 2013. A comparison of proximal humeral cancellous bone of great apes and humans. J. Hum. Evol. 65: 29-38.

Schmidt-Nielsen, K. 1984. Scaling: why is animal size so important? Cambridge: Cambridge University Press.

Schmitt, D. 2010. Primate locomotor evolution: Biomechanical studies of primate locomotion and their implications for understanding primate neuroethology. In: Platt, M.L. and Ghazanfar, A.A. (Eds.) Primate neuroethology. pp 31-63.

Schultz, A. 1930. The skeleton of the trunk and limbs of higher primates. Wayne State University Press.

Schultz, A.H. 1960. Einige Beobachtungen und Maße am Skelett von *Oreopithecus*: im Vergleich mit anderen catarrhinen Primaten. Z. Morph. Anthropol. 50, 136–149.

Shapiro, L.J., Seiffert, C., Godfrey, L., Jungers, W.L., Simons, E., Randria, G. 2005. Morphometric analysis of lumbar vertebrae in extinct Malagasy strepsirrhines. Am. J. Phys. Anthropol. 128, 823-839.

Shaw, C.N., Ryan, T.M. 2012 Does skeletal anatomy reflect adaptation to locomotor patterns? Cortical and trabecular architecture in human and nonhuman anthropoids. Am. J. Phys. Anthropol. 147, 187–200.

Simpson, S.W., Quade, J. Levin, N.E., Butler, R. et al. 2008. A female *Homo erectus* Pelvis from Gona, Ethiopia. Science 322, 1089-1092.

Slijper, E. 1946. Comparative biologic-anatomical investigations on the vertebral column and spinal musculature of mammals. Verh. K. Ned. Akad. Wet. Afd. Natuurkd. Tweede Reeks 42,1–128

Smit, T.H. 2002. The use of a quadruped as an in vivo model for the study of the spine-biomechanical considerations. European Spine Journal 11, 137–144.

Smit, T.H., Odgaard, A., and Schneider, E. 1997. Structure and function of vertebral trabecular bone. Spine 22, 2823-2833.

Sneed, E.D., and Folk, R.L. 1958. Pebbles in the lower Colorado River, Texas, a study in particle morphogenesis. J. Geol. 66, 114-150.

Sokal R, Rohlf S. 1995. Biometry. New York: WH Freeman.

Sode, M., Burghardt, A. J., Nissenson, R. A., & Majumdar, S. 2008. Resolution dependence of the non-metric trabecular structure indices. Bone. 42, 728-736.

Sokal. R., Rohlf, S. 1995. Biometry. New York: WH Freeman.

Spoor, C.F., Zonneveld, F.W., and Macho, G.A. 1993. Linear measurements of cortical bone and dental enamel by computed tomography: applications and problems. Am. J. Phys. Anthropol. 91, 469–484.

Stern, Jr., J.T., and Susman, R. 1983. The locomotor anatomy of *Australopithecus afarensis*. Am. J. Phys. Anthropol. 60, 279–317.

Straus, W.L. 1963. The classification of *Oreopithecus*. In: Washburn, S.L. (Ed.), Classification and Human Evolution. Aldine Pub. Co., Chicago. pp, 146–177.

Su, A., Wallace, I.J., Nakatsukasa, M. Trabecular anisotropy and orientation in an Early Pleistocene hominin talus from East Turkana, Kenya. J. Hum. Evol. 64, 667-677.

Sueur, C., Salze, P., Weber, C., and Petit, O. 2011. Land use in semi-free ranging Tonkean macaques *Macaca tonkeana* depends on environmental conditions: A geographical information system approach. Zool. 57, 1.

Susman, R.L. 2004. *Oreopithecus bambolii*: an unlikely case of hominid like grip capability in a Miocene ape. J. Hum. Evol. 46, 105–117.

Susman, R.L. 2005. *Oreopithecus*: still apelike after all these years. J. Hum. Evol. 49, 405–411.

Swartz, S.M., Parker, A., Huo, C. 1998 Theoretical and empirical scaling patterns and topological homology in bone trabeculae. J. Exp. Biol. 201, 573–590.

Thompson, D.W. 1919. On Growth and Form. University Press, Cambridge.

Turner, C.H. 1992. On Wolff's law of trabecular architecture. J. Biomech. 25,1–9.

Turner, C.H. 1992. Functional determinants of bone structure: beyond Wolff's law of bone transformation. Bone 13,403.

Tuttle, R.H., Watts, D.P. 1985. The positional behavior and adaptive complexes of *Pan gorilla*. In: Kondo S, editor. Primate morphophysiology, locomotor analyses, and human bipedalism. p.261–288.

Ulrich, D., van Rietbergen, B., Laib, A., Ruegsegger, P. 1999. The ability of three-dimensional structural indices to reflect mechanical aspects of trabecular bone. Bone 25,55–60.

Ulrich, C.G., Binet, M.G., Sanecki, M.G, Kieffer SA. 1980. Quantitative assessment of the lumbar spinal canal by computed tomography. Radiology 134,137–143.

Wallace, I.J., Tommasini, S.M., Judex, S., Garland Jr., T., Demes, B., 2012. Genetic variations and physical activity as determinants of limb bone morphology: an experimental approach using a mouse model. Am. J. Phys. Anthropol. 148, 24-35.

Wainwright, S. A., W. D. Biggs, J, D. Currey, and J. M. Gosline. 1976. Mechanical Design in Organisms. Princeton University Press, Princeton, NJ.

Walker, A.C., and Pickford, M. 1983. New postcranial fossils of *Proconsul africanus* and *Proconsul nyanzae*. New interpretations of ape and human ancestry:325–351.

Walker, A., and Leakey, R. 1993. The postcranial bones. In: Walker, A. and Leakey, R. (Eds.) The Nariokotome *Homo erectus* Skeleton. Harvard University Press, Cambridge. pp, 95–160.

Ward, C.V. 1991. Functional anatomy of the lower back and pelvis of the Miocene hominoid Proconsul nyanzae from Mfangano Island, Kenya. Ph.D. Dissertation. Johns Hopkins University, Baltimore, MD.

Ward, C.V. 1993. Torso morphology and locomotion in *Proconsul nyanzae*. Am. J. Phys. Anthropol. 92,291–328.

Ward, C., Walker, A., Teaford, M., and Odhiambo, I. 1993. Partial skeleton of *Proconsul nyanzae* from Mfangano Island, Kenya. Am. J. Phys. Anthropol. 90,77–111.

Ward, C.V. 1997. Functional anatomy and phyletic implications of the hominoid trunk and hindlimb. In: Begun. D., Ward, C., Rose, M. (eds.). Function, Phylogeny, and Fossils: Miocene Hominoid Evolution and Adaptations. New York, Plenum. pp 101–130.

Weidenreich, F. 1913. Uber das Huftbein und das Becken der Primaten und ihre Umformung durch den aufrechten Gang. Anat. Anz. 44,497–513.

Weisl, H. 1954. The ligaments of sacroiliac joint examined with their particular reference to function. Acta. Anat. 20, 201–213.

Welch, J., Turner, C., Devareddy, L., Arjmandi, B., and Weaver, C. 2008. High impact exercise is more beneficial than dietary calcium for building bone strength in the growing rat skeleton. Bone 42,660–668.

Whitcome, K. 2006. Obstetric load and the evolution of human lumbopelvic sexual dimorphism. Ph.D. Dissertation. The University of Texas at Austin, Austin, TX.

Wilke, H.J, Kettler, A., and Claes, L.E. 1997. Are sheep spines a valid biomechanical model for human spines? Spine 22,2365.

Wolff, J. 1892. The law of bone transformation. Berlin: Hirschwald.

Wunderlich, R..E., Walker, A., Jungers, W.L. 1999. Rethinking the positional repertoire of *Oreopithecus*. Am. J. Phys. Anthropol. 108, 528.

Young, N.M. 2003. A reassessment of living hominoid postcranial variability: implications for ape evolution. J. Hum. Evol. 45,441–464.

Zapfe, H. 1958. The skeleton of *Pliopithecus* (*Epipliopithecus*) *vindobonensis* (Zapfe and Hürzeler). Am. J. Phys. Anthropol. 16,441–457.

Zapfe, H. 1960. A new fossil anthropoid from the Miocene of Austria. Current Anthropology 1,428–429.

Chapter 3: External and internal bony morphology of the sacrum and its relationship to relative tail length

ABSTRACT

An understanding of the anatomy linked with tail length among living primates has the potential to inform our understanding of postcranial adaptations and phylogenetic affiliations among extinct primates. Yet, tail length is difficult to determine from the fossil record because complete caudal vertebral sequences are rarely found and little is known about nonprehensile-tailed caudal vertebral structure. This study enhances our understanding of the anatomy associated with tail length reduction by examining the external and internal morphology of the sacrum - the tail's bony link to the body – in a broad comparative sample of mammals that differ in tail length. Results support previously defined functional links between relative tail length and Ankel's (1965) sacral index, Ward and colleagues' (1991) measure of degree of tapering, and Russo and Shapiro's (2011) caudal articular surface shape index and measure of transverse process breadth. Results from analysis of new metrics further demonstrate that the last sacral vertebra's spinous process length and caudal articular surface area are also associated with relative tail length. The relationship between trabecular bone structure in the sacrum's distal end and relative tail length is less convincing than that between external sacral morphology and relative tail length. Using the extant primate data, tail length reconstructions in this study support previous interpretations that *Proconsul* was tailless, *Archaeolemur* possessed a long tail, and *Palaeopropithecus* possessed a short tail. Results also demonstrate that *Megaladapis* and *Epipliopithecus* had short tails. The

findings presented here support the utility of these data and methodologies for tail length reconstructions of other extinct primates.

INTRODUCTION

Variation in tail morphology among living primates is functionally and phylogenetically significant. For example, prehensile tails, which are capable of providing sole support of an animal's body weight, characterize just six primate genera from two platyrrhine clades (*Alouatta, Ateles*, *Brachyteles, Lagothrix* [Atelidae] and *Cebus* and *Sapajus* [Cebinae]; Groves, 2001, 2005; Ryland and Mittermeier, 2009; see also Rosenberger and Matthews, 2008). Functionally, prehensile tails assist in travel and foraging activities by allowing animals to distribute their weight over a greater number of supports and access food resources located in terminal branch settings (Emmons and Gentry, 1983; Gebo, 1992; Garber and Rehg, 1999; Bezanson, 2004, 2005, 2006, 2009). By contrast, the majority of living primates possess nonprehensile tails. However, a number of primates are characterized by very short tails (e.g., some macaques) or the complete absence of a tail (e.g., hominoids). Functionally, nonprehensile tails may be laterally abducted during arboreal quadrupedal progression to create oppositely-directed angular momentum to stabilize the body during moments of imbalance (Horner, 1954; Wada et al., 1993; Larson and Stern, 2006), or, dorsally extended during walking, bounding, or leaping between discontinuous substrates to reorient the body to prepare for landing (Bernstein et al., 1978; Emerson, 1985; Demes et al., 1996; Essner, 2002). Accordingly, research has shown that arboreal animals with shortened or reduced tails cannot attain the same level of locomotor competence as their counterparts with longer

tails (e.g., rodents, Buck et al., 1925; Horner, 1954; Siegel, 1970; primates, Igarashi and Levy, 1981).

An understanding of the anatomy linked with tail features, such as external length, among living primates thus has the potential to inform our understanding of postcranial adaptations and phylogenetic affiliations among extinct primates. Yet, tail length is difficult to determine from the fossil record because complete caudal vertebral sequences are rarely found. Further, little is known about how caudal vertebral anatomy varies among living primates that differ in tail length, and so the ability to make inferences about the tail lengths of extinct primates represented by only one, or few, caudal vertebral elements is limited (but see Chapter 4). Moreover, absence of evidence cannot be taken as evidence of absence, and so extinct primates cannot necessarily be considered "tailless" in fossil sample cases where no caudal vertebrae are preserved. As such, researchers must look to other skeletal elements for establishing anatomical correlates of tail length and presence (Ankel, 1965, 1972; Ward et al., 1991; 1999; McCrossin and Benefit, 1992; McCrossin, 1994; Rose et al., 1996; Nakatsukasa et al., 2004; Schmitt et al., 2005). The sacrum is the sole bony link between the tail and the rest of the body, and a vertebral element preserved in many extinct primates (e.g., subfossil lemurs: *Hadropithecus* [e.g., Godfrey et al., 2006], *Megaladapis* [e.g., DPC 7950], *Palaeopropithecus* [e.g., DPC 24778], and *Archaeolemur* [e.g., BMNH M7909, Godfrey et al., 2006; DPC 11823, DPC 11835, DPC 9905]; early catarrhines and hominoids: *Epipliopithecus* [O.E. 304-45 Zapfe, 1958, 1960], *Proconsul* [e.g., KNM-KPS V42, KNM-MV 13142M, Walker et al., 1983; Ward et al., 1993], *Nacholapithecus* [e.g.,

KNM-BG17822, Rose et al., 1996; Ishida et al., 2004], *Oreopithecus* [e.g., BA#50, BA#72, Hürzeler, 1958; Straus, 1963]; and hominins: *Australopithecus* [Sts 14, Robinson, 1972; A.L.288-1, Johanson et al., 1982], *Homo* [KNM-WT 15000, Walker and Leakey, 1993; Pelvis 1 Atapuerca, Arsuaga et al., 1999; BSN49/P27, Simpson et al., 2008]). Therefore, the sacrum has been the subject of much attention for those interested in identifying correlates of tail morphology (Ankel, 1965, 1972; Ward et al., 1991, 1999; Rose, 1993; Rose et al., 1996; Nakatsukasa et al., 2004; Schmitt et al., 2005).

Previous studies of sacrocaudal functional links have focused primarily on identifying differences between prehensile- and nonprehensile-tailed primates (e.g., Ankel, 1965, 1972; Leutenegger, 1970), among prehensile-tailed primates (e.g., Schmitt et al., 2005), and between tailless hominoids and tail-bearing primates (e.g., Ward et al., 1991). Leutenegger (1970) demonstrated that prehensile-tailed primates have more craniocaudally expanded sacroiliac joints in comparison to nonprehensile-tailed primates, presumably in order to better withstand stresses encountered during tail-only suspension. Ankel (1965, 1972) demonstrated that hominoid sacra exhibit relatively smaller caudal neural openings compared to cranial neural openings, reflecting decreased innervation and vascularization to a reduced caudal region (Ankel, 1965, her Figure 5, see also Ankel, 1972). By contrast, the sacra of long nonprehensile- or prehensile-tailed primate taxa exhibit similarly-sized or relatively larger caudal neural openings compared to the cranial neural openings, reflecting an increase in the accommodation of innervation and vascularization to a well-developed caudal region (Ankel, 1965, her Figure 5, see also Ankel, 1972). This functional interpretation is supported by studies of the neurovascular

systems of the lower spine in primates. For example, the *filum terminale* of the spinal cord is positioned near the upper lumbar vertebral region in humans, whereas it is positioned near the eighth caudal vertebra in *Ateles* (Chang and Ruch, 1947).

Ward and colleagues (1991) found that the mediolateral width of the last sacral vertebra's caudal end tapers relative to that of the cranial end in hominoids, reflecting the fact that the distal sacrum articulates with a vestigial caudal (coccygeal) vertebra. By contrast, the mediolateral width of the last sacral vertebra's caudal end remains nearly as wide or is wider than that of the cranial end in tail-bearing primates, reflecting the fact that the distal sacrum articulates with a more robust first caudal vertebra (Ward et al., 1991).

More recently, Russo and Shapiro (2011) showed that catarrhines with reduced tail lengths exhibit more elliptically-shaped sacral caudal articular surfaces (CAS) compared to catarrhines with longer tails, which exhibit sacral CAS that are more circularly-shaped. Clinical work has suggested that an elliptically-shaped CAS restricts the range of motion at the sacrococcygeal joint (Kapandji, 2008), while a more circularly-shaped CAS should permit a greater range of motion in multiple directions. Russo and Shapiro (2011) also demonstrated that catarrhines with reduced tail lengths exhibit less expanded transverse processes and more obtuse sacrocaudal articulation angles (i.e., the sacrum's caudal articular surface tilts less dorsally; Schmitt et al., 2005) compared to longer-tailed catarrhines, suggesting that the former group has relatively reduced mechanical advantage for tail lateral abductors and a decreased ability to dorsally extend the tail.

Additional sacrocaudal functional links may include, in some cases, the absence of postzygapophyseal joints at the sacrocaudal junction (Nakatsukasa et al., 2004), and/or increased numbers of sacral vertebrae (Ankel, 1972) in primates with no tails or reduced tail lengths. The absence of postzygapophyseal joints at the sacro- caudal/coccygeal junction reflects the sacrum's articulation with coccygeal vertebrae, which are distinct from caudal vertebrae in that they lack neural arches and thus zygapophyseal articulating facet joints, and instead possess vestigial cornuae (but see below). Therefore, the sacrococcygeal articulation occurs primarily via the vertebral bodies. Further, in some primates with reduced tail lengths, such as lorises, reduction in the number of caudal vertebrae appears to occur via "sacralization" of the vertebral bodies (i.e., they become incorporated into the sacrum), resulting in an increased number of sacral vertebrae (but see below).

Objectives

This study has three main goals. The first goal of this study is to reevaluate previously defined aspects of sacral morphology that have been linked to variation in tail length/function among a taxonomically and morphologically diverse sample of extant mammals. The aforementioned studies by Ankel (1965; 1972), Ward et al. (1991) and Russo and Shapiro (2011) examine only primate taxa. Russo and Shapiro's (2011) study sought to look for instances of morphological divergence in a broad sample (21 species) of closely-related taxa (catarrhines) (N=110). Ward and colleagues (1991) examined a sample of eight catarrhine and one platyrrhine species (N=85) in order to provide context for the evaluation of the last sacral vertebra belonging to the fossil catarrhine *Proconsul*

(KNM-KPS V42). Ankel's (1965) study of the sacral index included the taxonomically broadest sample, and included 13 catarrhine, five platyrrhine, and four strepsirrhine taxa. This study evaluates Ankel's (1965) sacral index, Ward and colleagues' (1991) degree of tapering of the last sacral vertebra, and Russo and Shapiro's (2011) measures for sacral CAS shape and lateral expansion of the transverse processes in a sample of 96 mammalian species spanning six Orders. Taxa for the extant comparative mammalian sample were chosen based on evolutionary relatedness and diversity in tail length and/or function (Table 3.1). A taxonomically diverse sample permits the verification of functional hypotheses by identifying instances of morphological convergence among mammals possessing reduced tail lengths.

Along with tail length differences, the mammals sampled also differ in their trunk posture, locomotor mode, and body size, offering an opportunity to tease apart the factors that contribute to sacral morphology and identify specific morphological correlates of tail length. Isolating morphological correlates of tail length is important because, for example, features characteristic of modern ape torso morphology (e.g., lumbar reduction and orthogrady) do not appear frequently in the hominoid fossil record until the Mid to Late Miocene (Moyà Solà and Köhler, 1996; Moyà Solà et al., 2004; Ward, 2007; but see MacLatchy, 2004). Definitively tailless early hominoids, such as *Nacholapithecus kerioi* (Nakatsukasa et al., 2004), possessed cercopithecoid-like numbers of lumbar (six to seven) and sacral (three to four) vertebrae and emphasized pronograde posture (Ward, 1993; Ishida et al., 2004; Nakatsukasa and Kunimatsu, 2009). It is thus problematic to assume that tail loss in hominoids originated in conjunction with the sacral anatomy

characteristic of modern apes. The combination of tail loss with cercopithecoid-like axial morphology and pronograde posture in some extinct hominoids makes it unclear to what extent the sacral morphology of living hominoids is functionally associated with tail loss, lumbar reduction, orthograde posture, or a combination of all three factors. A prerequisite to more properly reconstructing tail length in the catarrhine fossil record is thus a better understanding of its morphological correlates in the context of pronograde posture and morphologically and taxonomically diverse sacral form (Russo and Shapiro, 2011).

Sacral counts, presence/absence of postzygapophyses, and the sacrocaudal articulation angle are not considered in this study. With respect to sacral number, it has already been demonstrated that counts of sacral vertebrae are not reliable indicators of tail length because, as mentioned above, primates can have the same number of sacral vertebrae but very different tail lengths (Ankel, 1972; Russo and Shapiro, 2011; see also Table 3.1). Moreover, increased numbers of sacral vertebrae in hominoids occurs via sacralization of the lower lumbar vertebrae, as opposed to of the caudal vertebrae as in some primates (Russo and Shapiro, 2011). Additionally, the presence of postzygapophyseal facets on the distal sacrum is variable, and among nonprimate mammalian taxa, instances of absent sacral postzygapophyses/ present first postsacral prezygapophyses or present sacral postzygapophyses/ absent first postsacral prezygapophyses are common (Chapter 4). The sacrocaudal articulation angle was not calculated for the mammals in the sample because a number of mammalian taxa exhibit moderate degrees of sacral curvature that could influence angular measurements (e.g., hominoids, sloths, koalas).

The second goal of this study is to build upon our body of knowledge about the anatomy associated with tail loss/length reduction by quantifying two previously unexamined aspects of external sacral morphology (caudal articular surface area and spinous process length) and, by evaluating the internal bony morphology (i.e., trabecular bone) of the sacrum at its distal end where caudal or coccygeal vertebrae articulate. A preliminary examination of the internal bone structure of the last sacral vertebra among a small sample of macaques (N<10) provided preliminary evidence that the distal sacrum of long-tailed taxa may be structured to resist higher loads than the distal sacrum of short-tailed taxa (Russo et al., 2012). This finding suggests that trabecular bone parameters may provide another avenue by which to identify morphological correlates of tail length. An investigation of the sacrum's internal bone structure is of particular importance given that external vertebral features, such as projecting transverse processes and ring-like neural arches, are often broken postmortem and thus typically poorly preserved in the fossil record. For example, as described by Ward et al. (1991), although the last sacral vertebra of *Proconsul heseloni* preserves most of the vertebral body, the left aspect of the vertebra is damaged and both laminae are crushed into the neural canal. This study will quantify a suite of functionally informative trabecular bone variables in the last sacral vertebral body in a subsample of primates (Table 3.1, asterisked taxa). The use of a subsample from the larger mammal sample was necessary because the collection of CT data is costly and time intensive.

The third goal of this study is to apply the results of the extant sample to an evaluation of the external and internal sacral anatomy of sacra belonging to extinct

primates, including *Archaeolemur, Megaladapis, Palaeopropithecus, Epipliopithecus* and *Proconsul*. Specifically, external and internal morphological variables will be evaluated together in multivariate analyses in order to reconstruct the tail lengths of these extinct taxa.

Significance

Because all living hominoids lack an external tail, it is assumed that extinct hominoids lacked tails as well. The implications of tail loss for our understanding of the evolutionary relationships (Harrison, 1987, 1993, 2002; Ward et al., 1991, 1999; Andrews, 1992; Begun et al., 1997; Rose, 1997; Ward, 1997; Nakatsukasa et al., 2003, 2004) and positional behaviors (Rose, 1993; Begun et al., 1994; Kelley, 1997; Ward, 1997, 2007) of extinct catarrhines have been discussed extensively. Current evidence suggests that tail loss is one of few modern ape-like traits that can be identified in the postcranial axial skeleton of extinct early hominoids. Thus, the ability to confidently identify taillessness in the catarrhine fossil record has importance for identifying some of the earliest members of the hominoid clade (if it is assumed that tail loss evolves once). *Proconsul* is an early Miocene catarrhine that has been alternately classified as a hominoid (Ward et al., 1991; Andrews, 1992; Rose, 1997; Begun et al., 1997; Rae, 1999), a stem hominid (Walker and Teaford, 1989; Walker, 1997), a stem catarrhine (Harrison, 1987, 1988, 1993, 2002; Harrison and Rook, 1997; Harrison and Gu, 1999), and placed in its own superfamily Proconsuloidea (Harrison, 2009; Gebo et al., 2009). Conflicting opinions about its phylogenetic affinities result in part from debate concerning a last sacral vertebral specimen (KNM-KPS V42; Walker et al., 1983) central to determining

tail length/presence in this taxon. Ward and colleagues (1991) reported that the degree of tapering of the caudal end of V42 falls within the range of that for extant apes, indicating that the distal sacrum articulated with a coccygeal vertebra. Their result thus suggests that *Proconsul* lacked an external tail and supports the placement of *Proconsul* within the Hominoidea. However, Harrison (1998) argued that the specimen is better identified as a caudal vertebra because the shape of its cranial articular surface resembles that of Old World monkey proximal caudal vertebrae. Harrison (1998) maintained that not only did *Proconsul* probably have a tail, but it may have been long. Nakatsukasa and colleagues (2004) reevaluated the specimen, and agreed with Ward and colleagues (1991) that it was a sacral vertebra that probably articulated with a coccyx**.** However, they were only able to reexamine V42 qualitatively (Nakatsukasa et al., 2003). This study will examine the morphology of the last sacral vertebra central to this controversy in order to lend some resolve to the debate concerning the phylogenetic placement of *Proconsul*. This study will also examine the sacral morphology of an extinct pliopithecoid (*Epipliopithecus vindobonensis*) for which past inferences about its tail length have been contradictory (*Epipliopithecus*: tailless, Zapfe, 1960; long tail, Ankel, 1972). *Epipliopithecus* (Zapfe and Hürzeler, 1957; Zapfe, 1958; 1960) is a primitive catarrhine (Pliopithecidae) that has no living descendants and was once thought to be an ape (Begun, 2002). The inclusion of *Epipliopithecus* is important because if it is determined that this taxon lacks a tail, then it is possible that tail loss may be subject to considerable homoplasy in catarrhine evolution.

Extinct Malagasy lemurs are an excellent comparative study group for testing

sacrocaudal form-function links because previous research has hypothesized that they exhibited considerable diversity in tail length, ranging from long-tailed (e.g., *Archaeolemur* and *Hadropithecus*, Godfrey et al., 2006) to vestigial-tailed (e.g., *Palaeopropithecus* and *Babakotia,* Godfrey and Jungers, 2003; Huq and Jungers, 2009). This study will examine the sacra of three extinct Malagasy lemurs (*Archaeolemur, Palaeopropithecus* and *Megaladapis*). By independently testing functional hypotheses concerning tail length in distantly-related extinct primates, this study has significance our understanding of the postcranial anatomy and evolution of both subfossil lemurs and hominoids.

Predictions

The following sections provide predictions for the previously described quantitative methods (i.e., sacral index, degree of tapering, transverse process breadth and caudal articular surface shape), and functional background and predictions for the new study variables (caudal articular surface area and spinous process length of the last sacral vertebra).

***Sacral Index* (Ankel, 1965)**

The sacral index quantifies the size of the sacrum's caudal neural opening relative to its cranial neural opening. The functional significance of this feature was described above. Following Ankel (1965), the sacral index is calculated as (Figure 3.1):

$$\frac{\text{Mediolateral breadth (Msmt. 3) x dorsoventral breadth (Msmt. 4) of the sacrum's caudal neural opening}}{\text{Mediolateral breadth (Msmt. 1) x dorsoventral breadth (Msmt. 2) of the sacrum's cranial neural opening}} \text{ x100}$$

Sacral indices close to 100 or greater than 100 indicate that the sacrum's caudal neural opening is similarly sized or larger than the cranial neural opening, respectively. Sacral indices less than 100 indicate that the sacrum's caudal neural opening is smaller than the cranial neural opening. Based on Ankel's (1965, 1972) findings, this study predicts that the sacral index will increase as tail length increases, with longer-tailed mammals having indices close to or greater than 100, and mammals with reduced tail lengths having indices less than 100.

Degree of Tapering of the Last Sacral Vertebra **(Ward et al., 1991)**

The degree of tapering measures the mediolateral narrowing of the last sacral vertebra's caudal end relative to its cranial end. The functional significance of this feature was described above. Following Ward and colleagues (1991; see also Digiovanni et al., 1989), the degree of tapering of the last sacral vertebra is calculated as:

Tapering = 2 arctan (Y/X),

where Y = (mediolateral width of the cranial articular surface [Msmt. 5] – mediolateral width of the caudal articular surface [Msmt. 6] /2), and X = craniocaudal vertebral body length (Msmt. 7) (Figure 3.1). Positive values for the degree of tapering indicate that the mediolateral width of the last sacral vertebra tapers caudally (i.e., the mediolateral width of the caudal articular surface is narrower than that of the cranial articular surface), while negative values for the degree of tapering indicate that the mediolateral width of the last sacral vertebra expands caudally (i.e., the mediolateral width of the caudal articular surface is wider than that of the cranial articular surface) (Ward et al., 1991). Based on

the findings of Ward and colleagues (1991), this study predicts that the degree of tapering will decrease as tail length increases.

***Sacrum's Caudal Articular Surface (CAS) Shape Index* (Russo and Shapiro, 2011)**

Following Russo and Shapiro (2011), the shape of the sacrum's CAS is quantified as a ratio of its mediolateral width (Msmt. 6) divided by its dorsoventral breadth (Msmt. 8) (Figure 3.1). The functional significance of this feature was described above. CAS shape indices greater than 1 indicate that the sacrum's CAS is mediolaterally wider than it is dorsoventrally, and is thus more elliptically shaped (long axis in the mediolateral plane); CAS indices closer to 1 indicate that the sacrum's CAS possesses more equal mediolateral and dorsoventral dimensions and is thus more circularly shaped; and CAS indices less than 1 indicate that the sacrum's CAS is dorsoventrally wider than it is mediolaterally, and thus is also more elliptically shaped (long axis in the dorsoventral plane). Following Russo and Shapiro (2011), it is predicted that as tail length increases the CAS shape index will also decrease, with longer-tailed mammals having indices close to 1, and mammals with reduced tail lengths having indices greater than 1.

***Lateral Expansion of the Transverse Processes of the Last Sacral Vertebra* (Russo and Shapiro, 2011)**

The *abductor caudae medialis* mm. and *abductor caudae lateralis* mm. are primary abductors (i.e., lateral flexor) of the proximal tail (Lemelin, 1995). The *abductor caudae medialis* mm. take origin on the dorsolateral surfaces of the last sacral vertebral (and first proximal caudal) vertebra and insert via wide, flat tendons onto the dorsolateral surfaces of the transverse processes of the subjacent proximal caudal vertebrae (typically

first through third, though they may extend to the fourth caudal vertebra in prehensile-tailed primates) (Lemelin, 1995). The *abductor caudae lateralis* mm. are positioned ventrally to the *abductor caudae medialis* mm. and have a more caudal extension (from the fourth through seventh caudal vertebrae) (Lemelin, 1995). In atelines, the *abductor caudae lateralis* mm. also take origin on the last sacral vertebra's transverse processes, but a sacral origin has not yet been observed in other primate taxa (Lemelin, 1995). The potential leverage of (or area of attachment for) these muscles, particularly *abductor caudae medialis* mm., that laterally flex the tail at its base is determined by the lateral expansion of the transverse processes. Notably, other primary tail abductors include the *ilio-*, *ischio-* and *pubo- caudalis* mm., however these muscles originate on the innominate bones (ilium, ischium, and pubis, respectively). Primates have been observed to use lateral tail movements during arboreal quadrupedalism, presumably to create oppositely directed angular momentum to help stabilize the body during moments of imbalance (Larson and Stern, 2006). Functionally, more laterally expanded transverse processes of the last sacral vertebra would presumably provide greater surface area of attachment for, and/or increase the mechanical advantage of, these tail abductors, thereby improving the ability of the tail to stabilize the body on arboreal substrates (Russo and Shapiro, 2011). Russo and Shapiro (2011) demonstrated that long-tailed cercopithecoids have more laterally expanded transverse processes of the last sacral vertebra and exhibit high values for this measure compared to hominoids and other shorter-tailed primates, which have less expanded last sacral vertebral transverse processes and exhibit low values for this measure. In the latter, reduced transverse process expansion is likely related to an overall

reduction (and reorganization in hominoids) of basal tail musculature (Elftman, 1932). Lateral expansion of the transverse processes is measured as the distance between the apices of the left and right transverse processes of the last sacral vertebra (Msmt. 10, Figure 3.1; see also Russo and Shapiro, 2011). Following Russo and Shapiro (2011), it is predicted that lateral expansion of the transverse processes (size-corrected by dividing by body mass$^{1/3}$) of the last sacral vertebra will increase as tail length increases.

CAS Area

Tail length is likely proportional to tail mass (Organ, 2007). Grand (1977) showed that the tail of *M. fascicularis* (RTL =108) comprises 3.6% of total body weight, while the tail of *M.nemestrina* (RTL = 37) comprises only 0.2% of total body weight. As such, the sacrocaudal joint should be subject to greater loads in primates with long tails compared to primates with reduced tail lengths. Relatively large vertebral articular surface dimensions serve to distribute high loads over a wider area, thereby reducing forces (Schultz, 1930; Jungers, 1988; Kapandji, 2008). Articular surface area is calculated using the formula for an ellipse, where area = π * ½ articular surface dorsoventral breadth (Msmt. 8) * ½ articular surface mediolateral breadth (Msmt. 6), and size-corrected by body mass$^{2/3}$ (Figure 3.1). A higher value indicates a relatively larger articular surface area than a lower value, which indicates a smaller surface area. It is predicted that, relative to body mass$^{2/3}$, the sacrum's CAS area will increase as tail length increases.

Spinous Process Length of the Last Sacral Vertebra

Behavioral research demonstrates that arboreal primates hold their tails in dorsally extended positions during quadrupedal walking, running and bounding (Bernstein et al., 1978; Stevens et al., 2008). Moreover, dorsal extension of the tail functions to reorient the body during leaping by counteracting angular momentum produced by pelvic rotation during takeoff (Emerson, 1985; Günther et al., 1991; Essner, 2002). Russo and Shapiro (2011) demonstrated that longer-tailed cercopithecoids exhibited sacrocaudal articulation angles (i.e., the angle at which the first caudal vertebra articulates with the distal sacrum), which would permit greater tail extension than shorter-tailed primates. They suggested that dorsal tail extension at the sacrocaudal joint may be advantageous for longer-tailed arboreal cercopithecoids that use their tails to assist in moving along and leaping between discontinuous substrates. The ability to dorsally extend the tail may also be influenced by the length of the spinous processes of the distal sacrum and proximal caudal vertebrae. The *extensor caudae medialis* mm. are the caudal extension of the lumbar spine's *multifidus lumborum* mm. (Hartman and Strauss, 1933; Lemelin, 1995). These muscles are bilaterally present and originate on the lateral and caudal surfaces of the sacral spinous processes and insert on the prezygapophyses of proximal caudal vertebrae 4 to 6 levels caudad (Lemelin, 1995). Along with the *interspinales* mm., which originate on the spinous process of the last sacral vertebra and insert on the spinous process of the subjacent caudal vertebra (Lemelin, 1995), the *extensor caudae medialis* mm. serve to dorsally extend the tail. The *extensor caudae lateralis* mm., which partially attach to the median sacral crest, are also primary tail extensors (Lemelin, 1995). Therefore, the

leverages of the *extensor caudae medialis* mm. and the *interspinales* mm. depend on the length of the sacral spinous processes. Sacral spinous process length is measured as the maximum distance from the dorsalmost aspect of the caudal neural opening to the apex of the spinous process (Msmt. 9; Figure 3.1). This study predicts that the length of the last sacral spinous process (size-corrected by dividing by body mass$^{1/3}$) will increase as tail length increases.

Internal Sacral Morphology

If tail length is proportional to tail mass (Organ, 2007), the proximal tail region should be subject to greater loads in primates with long tails compared to primates with reduced tail lengths. Preliminary data from trabecular and cortical bone analyses of the last sacral vertebra (near the sacro- caudal/coccygeal joint) generally support this idea (Russo et al., 2012). For example, the distal sacrum of primates with longer tails may exhibit features associated with increased bone strength, such as thicker cortical bone and more numerous trabeculae, compared to primates with shorter tails (Russo et al., 2012). This study examines the trabecular bone architecture in a volume of interest near the sacro- caudal/coccygeal joint in the last sacral vertebral body. It is predicted that measures of trabecular bone strength (specifically, bone volume fraction, trabecular number, and the degree of anisotropy) will increase as tail length increases.

MATERIALS AND METHODS

Extant Mammal Sample

External sacral measurements were collected for 472 individuals from 96 species spanning six mammalian Orders, including Primates, Carnivora, Diprotodonia, Rodentia, Pilosa and Scandentia (Table 3.1). The sample comes from osteological collections at the American Museum of Natural History (New York, NY, USA), the Natural Museum of Natural History (Washington, D.C., USA), and the Field Museum of Natural History (Chicago, IL, USA). The comparative sample includes 329 primates (59 species), 28 carnivores (10 species), 40 diprotodonts (11 species), 31 pilosans (six species), 37 rodents (seven species) and seven tree shrews (three species) (Table 3.1). Six to ten specimens were examined per species where sufficient material was available and time permitted. In this study, species' sample sizes that are less than six-to-ten individuals reflect either the poor preservation of sacral elements in museum collections (i.e., completely articulated pelves and/or vertebral columns) or limited availability of skeletal material for examination. Species for which sample sizes are greater than six-to-ten derive from the large samples obtained for previous studies on primate sacral vertebrae (Russo and Shapiro, 2011, 2013).

As mentioned above, the acquisition of high-resolution computed tomography scans is costly and time intensive. As such, evaluation of the sacrum's trabecular bone was restricted to a subsample of primates (asterisked taxa in Table 3.1). A power analysis (PS v3.0.43) indicated that six sacra per species affords the power to detect a 20% difference between taxon means ($p < 0.05$) in a subset of pilot data for two trabecular

bone variables that greatly influence trabecular bone strength (degree of anisotropy and bone volume fraction; Currey, 1984; Gibson, 1985; Goldstein et al., 1991, 1993). Previous studies have demonstrated that statistically significant differences among trabecular variables are detectable with comparable numbers of individuals (e.g., MacLatchy and Müller, 2001, n=5/per group; Ryan and Ketcham, 2005, n= 1 to 10/per group). Therefore, this study endeavored to examine at least six sacra per taxon. Nonetheless, sufficient museum material was not always available and some sacra had to be excluded from analyses because test scans revealed internal bone damage (e.g., one *Pongo* sacrum). All examined individuals were wild-captured and classified as adult based on long bone epiphyseal fusion and/or dental eruption. Sacral specimens were excluded from the study if they exhibited substantial damage or markers indicating bone disorders (e.g., osteophytes).

Taxa for the extant comparative mammalian sample were chosen based on evolutionary relatedness and diversity in tail length and/or function (Table 3.1) In addition to nonprehensile-tailed taxa, which make up the majority of the mammalian sample, prehensile-tailed taxa were also included because, for some clades, these taxa possess the longest tails (e.g., Primates: *Ateles*, Table 3.1). *Indri*, lorises, some macaques (e.g., *Macaca tonkeana*), a colobine (*Nasalis concolor*), and hominoids are all primate taxa exhibiting reduced tail lengths. *Macaca* is a particularly useful taxonomic group for studies of tail functional morphology as tail length reduction occurs within several species groups (e.g., *sinica* species group, Fooden, 1988; Deinard and Smith, 2001). Carnivores, diprotodonts, rodents, pilosans, and tree shrews were chosen for comparison

because these clades also contain species characterized by reduced tail lengths (Table 3.1). The carnivores sampled include short-tailed felids (e.g., *Lynx*) and mustelids (e.g., *Gulo*), and long nonprehensile- (e.g., *Genetta*) or prehensile- tailed (e.g., *Arctictis*) viverrids. The diprotodonts sampled include short-tailed vombatiformes (*Phascolarctos* and *Vombatus*), and long-tailed macropodiformes (e.g., *Dendrolagus*) and phalangeriformes (e.g., *Trichosurus*). Pilosans sampled include modern two- (*Choloepus*) and three- (*Bradypus*) toed sloths, which have likely independently evolved tail loss as these living taxa are distantly related and all known fossil genera have long tails (Tito, 2008). Other modern representatives of Pilosa sampled include anteaters, some of which have long nonprehensile (e.g., *Myrmecophaga*) or long partially prehensile (e.g., *Tamandua*) tails. The rodents sampled include tailless caviids (e.g., *Hydrochaeris* and *Cavia*), short-tailed North American beavers (*Castor*) and common porcupines (*Erethizon*), and long-tailed heteromyids (e.g., *Dipodomys*).

Extant species were assigned a relative tail length index (RTL; Fooden, 1997) defined as:

(tail length / [head + trunk length]) x 100,

and calculated using morphometric data collected from the literature (Table 3.1). Use of this index (and the literature cited for its calculation) for approximating tail length is well established in the literature (e.g., Youlatos, 2003; Russo and Shapiro, 2011; Hamada et al., 2012). Further, while tail and body length measurements may vary between sexes of a single species, corresponding tail length indices typically do not (e.g., macaques, Fooden, 1997; see also Fooden and Albrecht, 1999). Hominoid primates were assigned a RTL of 0

because they lack an external tail. Nonprimate mammalian taxa described in the literature as "vestigial-tailed" or as possessing "diminutive tails", and thus without associated published tail length measurements, were also assigned a RTL of 0 (Table 3.1).

Extinct Primate Sample

The extinct primate sample includes sacra from *Proconsul heseloni*, *Epipliopithecus vindobonensis*, *Archaeolemur edwardsi, Palaeopropithecus kelyus* and *Megaladapis grandidieri* (Figure 3.2). The *Proconsul heseloni* specimen is a last sacral vertebra (KNM-KPS V42) housed at the National Museums of Kenya. The anatomy of V42 has been described in full detail elsewhere as this specimen is central to debate concerning the tail length of *Proconsul* (Ward et al., 1991; Harrison, 1998; Ward et al., 1999). The *Epipliopithecus* specimen is a complete sacrum exhibiting three sacral vertebra from Individual I (O.E. 304-45) (Zapfe, 1958) that is housed at the Naturhistorisches Museum Basel (Switzerland). The extinct subfossil lemur sacra belonging to *Archaeolemur* (DPC 9905, 11823, 11835), *Palaeopropithecus* (DPC 24778), and *Megaladapis* (DPC 7950) are housed at the Duke University Primate Center Division of Fossil Primates (Durham, NC, USA). The *Archaeolemur* sacral specimens (DPC 9905, 11823 and 11835) are nearly complete, but DPC 11823 and 11835 are ensconced in cave deposits. These sacra are from Anjohi ny Olona and are attributed to *Archaeolemur edwardsi*, a locality previously affiliated with *A. edwardsi* vertebral specimens (Shapiro et al., 2005). The *Palaeopropithecus* specimen (DPC 24778) is a complete sacrum comprised of four sacral vertebrae and attributed to the *Palaeopropithecus kelyus* (Gommery et al., 2009). The *Megaladapis* specimen (DPC

7950) is a complete sacrum comprised of four sacral vertebrae and attributed to *Megaladpis grandidieri* because it is from Antsiroandoha, a cave deposit locality at Ankarana with which only this *Megaladapis* species has been affiliated (Godfrey et al., 1999; their Table 8).

Numbers of Sacral Vertebrae

Data for the number of sacral vertebrae recorded for each extant taxon are presented in Table 3.1. The number of sacral vertebrae equals ½ the total number of sacral foramina (left and right side of the specimen) plus one (Schultz and Straus, 1945). Asymmetrical formation can result in the incomplete fusion of sacral foramina on either the proximal or the distal end of the sacrum (Schultz and Straus, 1945). In these cases, sacral number was rounded upward (e.g., 3) instead of being recorded as a half segment (e.g., 2 ½) in order to facilitate data collection and analysis.

External Sacral Morphology

Ten measurements (Figure 3.1) were obtained to calculate the external sacral study variables defined above. Sliding digital calipers (with measurements recorded to the nearest 0.01mm) were used to take the following measurements on the last sacral vertebra: mediolateral breadth of the cranial and caudal articular surfaces (Measurements 5 and 6), dorsoventral breadth of the caudal articular surface (Measurement 8), craniocaudal length of the vertebral body (Measurement 7), and lateral expansion of the transverse processes (Measurement 10). These measurements were used to calculate the degree of tapering, caudal articular surface shape and area, and lateral expansion of the transverse processes. If one transverse process was broken or damaged, a reasonable

estimate of total breadth was obtained by multiplying the measure of the lateral projection of the intact transverse process from the midline by two. Measures of craniocaudal vertebral body height and mediolateral breadth of the cranial articular surface were taken on the ventral surface and were primarily obtained on sacra with fused vertebral epiphyses (see also Ward et al., 1991). Because sacral morphology varied greatly across the study's broad taxonomic sample, influencing the ability to fit calipers into and around the neural canal, greater confidence was placed in collecting measurements 1-4 (needed to calculate the sacral index and spinous process length) from digital photographs rather than from digital calipers. A Panasonic Lumix DMC-G2 12.1 MP (SLR) digital camera was used to photograph sacral specimens in cranial and caudal views (e.g., Figure 3.1). A 1cm scale and a dry erase marker board denoting species, museum identification number, and sex were placed in the camera's viewfinder. To ensure consistent orientation, in cranial view, the camera was positioned so the light path was orthogonal to the cranial articular surface of the first sacral vertebra, while in caudal view, the camera was positioned so the light path was orthogonal to the caudal articular surface of the last sacral vertebra. Photographs were then imported into ImageJ v1.42j software (http://rsbweb.nih.gov/ij/) where the "line tool" was used to measure mediolateral and dorsoventral dimensions of the cranial and caudal neural openings, and spinous process length (Measurements 1, 2, 3, 4 and 9; Figure 3.1). Although area measurements of the cranial and caudal neural openings could have been obtained using the "polygon tool" in ImageJ, the use of linear measurements was retained in order to calculate the sacral index as defined by Ankel (1965).

Sacra belonging to *Epipliopithecus, Palaeopropithecus,* and *Megaladapis* are well preserved (Figure 3.2), and as such every external measure could be obtained for these sacra. Because the only data for the *Proconsul* last sacral vertebra available to the author at this time is a microCT scan (provided by M. Nakatsukasa), most measurements were obtained from an isosurface of the *Proconsul* last sacral specimen in Avizo *Fire* 7.1. A second-check of the external caudal vertebral measures was performed by using measurements taken on the images in Ward and colleagues (1991), which were imported into ImageJ (the authors' [Ward et al. 1991] provided a scale bar). The value of 29.3 for the degree of tapering of the *Proconsul* V42 specimen provided by Ward and colleagues (1991) was used in this study. The caudal vertebral surface of V42 appears incomplete on the left side (see also Ward et al., 1991). As such, an estimate of the mediolateral breadth of the sacrum's caudal articular surface was obtained by measuring from the outline of the more complete right side to the midline and multiplying by two. Dorsoventral breadth of the caudal articular surface was also obtained, though the measurement had to be taken slightly to the left of midline. The caudal articular surface shape ratio obtained from the microCT scan (2.14) was slightly less, but comparable to, the measurement obtained from the Ward and colleagues (1991) paper (2.6).

Because matrix ensconced two of the *Archaeolemur* specimens (DPC 11823 and 11835), external measurements for these sacra were obtained from CT scans in Avizo *Fire* 7.1. These measurements include lateral expansion of the transverse processes, mediolateral width of the last sacral vertebra's cranial and caudal articular surfaces, dorsoventral breadth of the last sacral vertebra's caudal articular surface, and

mediolateral and dorsoventral breadths of the cranial and caudal neural openings. Moving caudally in the slice stack, mediolateral and dorsoventral breadths for the cranial neural opening were measured on slices documenting the first appearance of a fully formed neural arch of the first sacral vertebra. Likewise, moving cranially in the slice stacks, mediolateral and dorsoventral breadths for the cranial neural opening were measured on slices documenting the first appearance of a fully formed neural arch of the last sacral vertebra. For the *Archaeolemur* DPC 11835 sacrum, craniocaudal length of the last sacral vertebra could not be confidently obtained from the scan, and so this measure was excluded. Because of damage to the caudal end of the specimen, spinous process length was also excluded from measurements obtained on this specimen. All measures with the exception of transverse process breadth could be obtained for *Archaeolemur* DPC 9905. The left last sacral vertebral transverse process is missing entirely, and the right one is incomplete. All measures were obtained for *Archaeolemur* DPC 11823. Values for each of the calculated variables for extinct primate sacra are presented in Table 3.2.

Datasets

Because of the large sample size, collection of photographic measurements for calculating the sacral index and spinous process length was limited to a subset of the sample (boldfaced taxa in Table 3.1) to facilitate data collection. Therefore, the sample was partitioned into two main datasets. Dataset #1 is comprised of all mammals in the sample (i.e., all taxa listed in Table 3.1). For Dataset #1, four variables were calculated: degree of tapering, CAS shape and area, and transverse process breadth of the last sacral vertebra. These variables were chosen for Dataset#1 for three reasons. First, these

variables derive from features on the vertebral body, and so they may be more likely to be preserved in the fossil record than variables that derive from the neural arch (e.g., spinous process length and sacral index). Second, these variables can all be calculated from the last sacral vertebra, which articulates directly with the first coccygeal/caudal vertebra. Though the sacral index has been shown to distinguish among primates of different tail lengths (Ankel, 1965, 1972), its calculation requires a complete sacrum, or at least one with mostly intact proximal and distal ends. As such, the applicability of the sacral index to fragmentary fossil sacra (e.g., *Proconsul,* KNM-KPS V42, see Ward et al., 1991) is limited. Finally, the measurements needed to calculate these variables can be easily obtained using standard digital calipers. Because, for example, the sacrum's last sacral vertebral spinous process may vary in craniocaudal orientation, this measure is difficult to quantify using calipers. In these ways, Dataset #1 may be more readily applicable to studies of fossil sacra. Dataset #2 contains a subset of the total mammal sample (boldfaced taxa in Table 3.1). For Dataset #2, the sacral index and spinous process length were included as additional variables.

Size Adjustments

Body mass, an appropriate proxy of body size (Fleagle, 1984; Schmidt-Nielsen, 1984), varies greatly across the taxa in this study. Therefore, variables need to be size-adjusted prior to comparative analyses. Previous studies of vertebral morphology often standardize measurements by the geometric mean of (nonangular) variables (e.g., Shapiro, 2007). However, sacra in museum collections are often partially/fully articulated with the lumbar or caudal vertebral sequence (or the innominates), often hindering the

ability to obtain all measurements/photographs for each individual. To exclude such cases from the analysis would have drastically reduced the study's sample size. Therefore, body mass data from museum records and the literature were used to make size-adjustments so that partial datasets could be retained for analyses. Body mass data were available for some individual specimens from museum documents and applied where possible. However, this information was absent for the majority of specimens, and so body masses were obtained from the literature (primates: Smith and Jungers, 1997; nonprimate mammals: Silva and Downing, 1995; Nowak, 1991) and applied on a by-species (or subspecies when possible) and by-sex basis. In cases where sex was unknown, the average of male and female body mass values was used. Linear measurements (mm) were standardized (i.e., divided by) by body mass$^{1/3}$; area measurements (mm^2) were standardized by body mass $^{2/3}$; angular measurements (°) were not subject to standardization.

Body mass data for the extinct primate species were taken from the literature. The estimated body size of *Epipliopithecus vindobonensis* is 7kg (Fleagle, 2013). The estimated *Proconsul heseloni* body mass is 17kg (Fleagle, 2013). For the subfossil lemurs, the *Palaeopropithecus kelyus* estimated body mass is 35kg (Ramanivosoa and Gommery, 2011), the *Megaladpis grandidieri* estimated body mass is 63kg, and the *Archaeolemur edwardsi* estimated body mass is 25kg (Jungers et al. 2002).

Internal Sacral Morphology

Extant Primate Data Collection

Primate sacra were hand-selected for CT scanning during visits to the American Museum of Natural History (New York, New York, USA) and National Museum of Natural History (Washington, D.C., USA). All extant primate sacra were scanned at the High Resolution X-ray Computed Tomography scanner at The University of Texas (HRXCT) at Austin (Austin, TX, USA) (see Ketcham and Carlson [2001] for details on the scanner). Similarly-sized extant primate sacra were scanned together to minimize scanning time and reduce calibration costs, resulting in CT image datasets containing as many as four sacra. Sacra were secured in the scanner using synthetic foam mold and mounted craniocaudally in order to collect transverse slices. All HRXCT scans were collected using source energy settings of 200kV/0.2 mA and obtaining between 1600-1800 views with two samples per view. For each scan, 31 slices were collected per rotation. Images were reconstructed as unsigned 16-bit TIFF grayscale images with a 1024 x 1024 pixel matrix.

Serial cross-sectional scans were collected for the entire sacrum. As such, the highest spatial resolution depended on sacral element size. Because the study primates, and thus their sacra, varied considerably in body size, three scan protocols were defined in order to best standardize resolutions across the sample. The "small" protocol (i.e., highest scan resolution) included the smallest-bodied taxa in the sample and used a 45.5 field of view (FOR), yielding an in-plane (x, y) resolution of 44μm and an out-of-plane (z [interslice]) resolution of 47μm. The "medium" protocol included primates with mid-

range body sizes in the sample and used a FOR of 60.5, yielding an in-plane resolution of 59µm and an out-of-plane resolution of 63µm. The "large" protocol (i.e., lowest scan resolution) included the largest bodied-taxa in the sample and used a FOR of 76.5, yielding an in-plane resolution of 75µm and an out-of-plane resolution of 80µm. External measurements of sacral maximum dorsoventral and mediolateral dimensions were obtained during prior visits to the museums in order to hand-select specimens and used to place sacra into the appropriate size category.

To facilitate data processing, individual sacra were segmented from datasets in Avizo 7.0 (Visualization Sciences Group, Inc., Burlington, MA, USA). Slice stacks were then imported into VGStudioMax (Volume Graphics Software, Heidelberg, Germany) where images were reduced from unsigned 16-bit to unsigned 8-bit format with no impact on resolution. Data were then down-sampled to the out-of-plane resolution, and image stacks were resliced so the cranial articular surface of the sacrum was flush with the transverse plane. Down-sampling the data produced final isotropic voxel sizes of 47µm for the "small" protocol sacra, 63µm for the "medium" protocol sacra and 80µm for the "large" protocol sacra. The resolution classes examined here are smaller than typical trabecular thickness (Kothari et al., 1998) and are near or within the range of resolution classes employed in previous trabecular bone studies (e.g., Gosman and Ketcham, 2009; Cotter et al., 2011; Ryan and Shaw, 2012; Su et al., 2013), suggesting that they can be used to accurately quantify the study trabecular bone variables.

While scanning elements at different resolutions can be time intensive because it requires different protocols, it is desirable to obtain the best resolution per specimen

given its geometric constraints (e.g., large size or irregular shape) (Kim et al., 2004). In order to evaluate the potential error introduced into the sample by comparing specimens scanned at different resolutions (see Gosman and Ketcham, 2009), the distal end of three sacra belonging to *Gorilla gorilla* were scanned using each size protocol and corresponding regions of trabeculae were analyzed. Datasets were not resampled or resolution-reduced for analysis (following Gosman and Ketcham, 2009). Corresponding trabecular regions were identified using recognizable bony landmarks and features. Though this process results in regions that are not \analogous, there is likely a substantial amount of spatial overlap (see also Gosman and Ketcham, 2009; but see Fajardo and Müller, 2001). Following Gosman and Ketcham (2009), percent differences between resolution classes were calculated for each trabecular bone variable. Correction factors were derived from these data and applied to the lower resolution data. Both of these datasets, and the evaluation of the resolution-corrected dataset against the original dataset, are presented in Chapter 2. Briefly, comparison of these two datasets revealed little overall change in the inter-taxonomic trends after adjusting for resolution-dependent differences in trabecular variables. As such, it was deemed unnecessary to apply correction factors to the trabecular data presented here.

Extinct Primate Data Collection

The *Epipliopithecus* (O.E. 304-45) sacrum was scanned by the Naturhistorisches Museum Basel at the Universitätsspital Basel on a GE Phoenix Nanotom m. Source energy settings were 180kV/0.35mA, yielding an isotropic voxel size 30μm. The *Proconsul* last sacral vertebra (KNM-KPS V42) was scanned by M. Nakatsukasa on a

Stratec pQCT research SA+ portable scanner at the Kenyan National Museum. The resulting isotropic voxel size was 50μm for this specimen. The subfossil lemur specimens were hand-transported to the UTCT facility and scanned using settings similar to those employed for the extant primate sample. Subfossil sacra were all scanned at an energy source setting of 200 kV/0.24 mA, 1800 views with two samples per view, and 31 slices were collected per rotation. The UTCT staff completed ring-removal and beam-hardening processing. The *Archaeolemur* (DPC 9905, 11823 and 11835) and *Palaeopropithecus* (DPC 24778) sacra were scanned using the "medium" protocol defined for the extant taxa, yielding an in-plane (x, y) resolution of 59μm and an out-of-plane resolution of 63μm. The *Megaladapis* sacrum (DPC 7950), which was considerably larger than the *Archaeolemur* and *Palaeopropithecus* sacra, was scanned at the "large" protocol, yielding an in-plane (x, y) resolution of 75μm and an out-of-plane resolution of 80μm.

Volumes of Interest and Trabecular Parameters

QUANT3D analysis software (developed at the HRXCT; Ryan and Ketcham 2002a,b; Ketcham and Ryan, 2004) was used to quantify trabecular structural parameters in a single three-dimensional spherical volume of interest (VOI). The VOI was positioned at midline in the lower half of the last sacral vertebral body. Following Fajardo et al. (2013), VOIs were adjusted to exclude end plate bone tissue by repositioning the sphere so that ten slices separated its outer boundary and any visible evidence of the cranial endplate. The limiting vertebral dimension for scaling the VOIs was the dorsoventral breadth because the sacral cranial articular surfaces of the specimens included in this

sample are all narrower dorsoventrally than mediolaterally (i.e., mediolateral/dorsoventral ratio values are greater than 1; see Figure 3.5). As such, VOI were scaled by 50% dorsoventral breadth of the sacrum's caudal articular surface in order to prevent over-sampling of trabeculae in taxa that varied in body size (see Fajardo and Müller, 2001 for discussion; see also Lazenby et al., 2011). All VOIs were visually inspected in views from three perpendicular planes to ensure that no cortical bone was contained within the boundary of the sphere and subsequently repositioned if necessary. VOIs in the smallest specimens were also inspected to ensure that a minimum of three to five trabecular lengths were included to satisfy the continuum assumption (Harrigan et al., 1988). Where certain taxa violated this assumption, they were removed from the sample. Two hominoid individuals (*Hylobates* and *Pan*) were removed from the scan sample because the last sacral vertebral bodies were dorsoventrally compressed to the extent that dorsal and ventral cortical bone edges were in contact. The VOIs ranged in size from approximately 0.9 to 2.6 mm in diameter in the final sample.

Quantification of five trabecular structural variables was automated in QUANT3d using the star volume distribution (SVD) algorithm (Ketcham and Ryan, 2005) with the exception of trabecular number, which was calculated using the mean intercept length method. In the SVD algorithm, intercept lengths in the shape of cones are drawn outward from a number of points until encountering another trabecular strut (Ryan and Ketcham, 2002). Data are then compiled into a 3x3 weighted orientation matrix that derives a fabric tensor describing the distribution of bone in three dimensions (Ryan and Krovitz, 2006). The matrix contains eigenvectors ($\mu1$, $\mu2$, $\mu3$) and eigenvalues ($\tau1$, $\tau2$, $\tau3$,) that describe

the primary, secondary and tertiary orientations and magnitude, respectively, of trabecular bone in three dimensions (Ryan and Krovitz, 2006; Maga et al., 2006; Ryan and Walker, 2010). Eigenvalues are used to calculate the degrees of anisotropy (DA [dimensionless]), which reflect how strongly (i.e., magnitude) the trabeculae organize themselves in the three axes (Maga et al., 2006). The first DA is the primary axis ($\tau 1$) / the tertiary axis ($\tau 3$), the second DA is $\tau 1$/ the secondary axis ($\tau 2$), and the third DA is $\tau 2$/ $\tau 3$. A DA index value (dimensionless) of 1 indicates the structure is fully isotropic or randomly organized, while an increasing DA index (i.e., away from 1), is associated with increasing structural organization or anisotropy (Fajardo and Müller, 2001). The trabecular elongation index (E [dimensionless]), calculated as $1-(\tau 2/ \tau 1)$, reveals the preferred orientations of trabeculae as defined by the first and second axes to describe trabecular shape. When the DA index value is greater than 1, corresponding E values distinguish between rod-shaped (E values closer to 1) and plate-shaped trabeculae (E values closer to 0).

Bone volume fraction (BV/TV [dimensionless]) is defined as the total number of bone voxels to total voxels per unit volume and is generally accepted as a surrogate of the density of the trabecular network (Fajardo and Müller, 2001; Maga et al., 2006). Higher BV/TV values indicate greater bone density per unit volume, while lower values indicate lower bone density per unit volume. Trabecular thickness (Tb.Th [mm]) is the mean thickness of trabecular struts defined by placing non-overlapping spheres *within* the mid-axes of trabecular struts (centered mid-axis) and calculating the average diameter of all spheres in the volume of interest (Fajardo and Müller, 2001; see their Figure 2A).

Trabecular number (Tb.N [mm-1]) is calculated by placing spheres *between* the mid-axes of trabecular struts in the VOI and calculating the inverse of the average diameter of all spheres in the volume of interest (Fajardo and Müller, 2001; see their Figure 2C). The settings for the SVD analyses are 513 uniform orientations, with random rotations, and 1000 points.

Because BV/TV, Tb.N, DA, and E, are shape variables, they should be invariant with changes in body mass. However, Tb.Th is a linear variable, and Pearson's two-tailed correlation tests reveal that it is significantly correlated (r=0.669, p<0.000) with mediolateral width of the first sacral vertebra (a body size proxy available for the trabecular data subset in this study). Therefore, trabecular thickness was size-corrected prior to analyses by dividing trabecular thickness (mm) values by mediolateral width of the first sacral vertebra (mm) for each individual.

Thresholding

The collection of trabecular morphometric data from the extant primate sample requires thresholding of the CT images in order to determine the exact boundaries between bone and air (background) interfaces. For all extant taxa, VOIs were processed using an adaptive, iterative threshold algorithm (Ridler and Calvard, 1978) that is frequently employed in trabecular bone studies (e.g., Maga et al., 2006; Fajardo et al., 2013) and is a standard function in QUANT3d. Identifying thresholds for the extinct primate sacra was more complicated than that for extant primate sacra because matrix in-filled the trabecular network in the last sacral vertebral body in many of sacra that were sampled. Thus, determining a threshold required consideration of the matrix as a third

material that may be more or less dense than the bone. In such instances, threshold values were determined using a modified version of the half-maximum height method (HMH) (Ulrich et al., 1980; Spoor et al., 1993) (Figure 2.3). An HMH value is a determined grayscale value that is halfway (between the highest and lowest grayscale value on either side of a tissue interface (e.g., bone – air) within a region of interest (Ulrich et al., 1980; Spoor et al., 1993). HMH was introduced to the paleoanthropology community by Spoor and colleagues (1993) for use with cortical bone data, and later modified by Fajardo et al. (2002) for use with trabecular bone data. Previous studies demonstrate that measurements obtained using HMH-determined thresholded scans perform considerably better than visually-determined thresholded scans when both are compared to measurements taken on actual dried specimens (Coleman and Colbert, 2007), and that the HMH thresholding method can accurately resolve trabecular mesh networking (Fajardo et al., 2002).

This study derived HMH values to determine the boundaries at three material interfaces: 1) matrix-bone, 2) matrix-air, and 3) bone-air (see Figure 2.3). For specimens where matrix was denser (i.e., had a higher grayscale value; toward 255 in 8-bit images) than bone, the matrix-bone and matrix-air boundary HMH values were averaged to find a "high threshold", while the HMH values for the bone-air boundary was used as the "low threshold." Averaging the matrix-bone and matrix-air values was necessary because sole use of the matrix-air HMH value would overestimate the volume of bone, while sole use of the bone-air boundary would likely underestimate the amount of bone. This method was employed for *Archaeolemur* DPC 11835 and 11823, and *Megaladapis* DPC 7950. By contrast, the matrix appeared less dense (i.e., had a lower grayscale value; toward 0 in

8-bit images) than bone in the *Epipliopithecus* specimen. Therefore, for the *Epipliopithecus* scan, the bone-matrix boundary became the "low threshold." The *Palaeopropithecus* sacrum contained two types of matrix: one that was denser than bone, and one that was less dense than bone. In this case, the "low threshold" (which cannot be air) was the matrix-air HMH value. The "high threshold" was the HMH value from matrix-bone and matrix-air. One of the *Archaeolemur* sacra (DPC 9905) could not be evaluated because of similarities in the density of the matrix and bone, which produces a "solid block-like" appearance and precluded the ability to threshold the slice stack. Additionally, the energy source of the microCT scanner used to collect slices for the *Proconsul* specimen was not powerful enough to penetrate the dense fossil material. Accordingly, the *Proconsul* last sacral vertebral CT scans were also unable to be analyzed.

The modified HMH protocols for extinct primate sacra as defined above were carried out in ImageJ and then applied to CT image slice stacks in AVIZO *Fire* (Visualization Sciences Group, Inc., Burlington, MA, USA). First, the cranial and caudal endplates of the last sacral vertebra were determined for each scanned sacrum. Then, 10 slices were counted inward (i.e., counting toward the center of the vertebra) starting from the last visible evidence of the cranial and caudal endplates. All other slices, including those of the proximal sacral vertebrae, were omitted from the CT stack. The 16-bit TIFF slice stack was then imported into ImageJ and converted to an 8-bit image type. Fossil sacra were not subject to resampling or resolution-reduction for analysis. Starting with the first (i.e., most proximal) slice, five-to-ten regions of interest within the last sacral

vertebra were selected, and the HMH was determined for a row of pixels drawn across the boundary of interest (e.g., bone-air) (Figure 2.3). Regions of interest were selected from the dorsal, ventral, medial, lateral aspects and the center of the last sacral vertebra to ensure adequate sampling of the CT slice. All three phases (matrix-bone, matrix-air, bone-air) were obtained from the same slice number to determine the threshold needed. This process was repeated every 50-75 slices in the CT stack, depending on the number of slices, and the average was taken to identify the boundary of each material interface (following Coleman and Colbert, 2007). 8-bit TIFF slice stacks were then imported into Avizo *Fire* in order to apply the defined thresholds to the extinct primate sacra. Minimum and maximum thresholds were applied using the Interactive Thresholding function. An arithmetic function was then applied to extract only the thresholded data, which was subsequently recognized as a separate material field. Slice stacks were then saved as 2d TIFFS for further analysis in QUANT3d.

Statistical Analyses

Data were analyzed using species means for all sacral variables. Analyses were performed for all mammals and for all primates. Additionally, the data were analyzed for nonprehensile-tailed primate taxa only. This study elected to examine nonprehensile-tailed taxa independently because the primate sample in its entirety includes hominoid and prehensile-tailed taxa. Both of these latter groups may be considered to possess "specialized" pelvi-caudal anatomy that could arguably impact results. For example, in hominoids, tail musculature is reduced and reorganized to support the abdominal and pelvic viscera (Elftman, 1932; and see below). Moreover, prehensile-tailed primates

exhibit a number of sacral and caudal anatomical (bony and soft) features that are associated with their specialized tail function and distinguish them from nonprehensile-tailed taxa (see German, 1982; Lemelin, 1995; Schmitt et al., 2005; Organ, 2010; Organ et al, 2009, 2011).

The relationship between each trait and RTL was evaluated using a phylogenetic generalized least-squares (PGLS) regression technique. The PGLS method is generalized least-squares regression model that incorporates an error term in order to consider covariation among taxa on the basis of phylogenetic similarity (Martins and Hansen, 1997). Using a measure of phylogenetic correlation, λ (Pagel 1999; see also Freckleton et al. 2002), the covariance matrix accounts for the degree to which trait evolution deviates from the Brownian motion model of evolution. The Brownian motion model of evolution predicts that λ =1, assuming closely-related species (using the inferred phylogeny) are anatomically similar and thus traits are proportional to phylogenetic relatedness. In other words, variation in a trait is a sole function of evolutionary distance among taxa. Models that assume phylogenetic independence predict that λ=0, indicating the absence of a relationship between the trait and phylogenetic relatedness. In other words, variation in a trait is independent of evolutionary distance among taxa. For this study, mammalian phylogenetic information and branch lengths were taken from Bininda-Emonds et al. (2007). Branch length data were not available for *Papio cynocephalus* (n = 6) or *Gulo luscus* (n=1). Therefore, *Papio cynocephalus* and *Gulo luscus* were reclassified as *P. hamadryas* and *Gulo gulo,* taxa for which branch length data were available. The impact of this adjustment is likely negligible as the taxa in question are more closely related to

their alternative taxonomic classifications than to any other taxon in the sample. Although previous studies have found the influence of phylogeny on trabecular bone structure to be present but weak (Ryan and Shaw, 2013; Doube et al., 2011), this study elected to use PGLS for regression analyses to maintain consistency in data analysis. Moreover, where $\lambda=0$, PGLS produces results comparable to those of ordinary least squares regressions.

Because linear and area measurements were size-standardized prior to analysis (i.e., were divided by body mass$^{1/3}$ and body mass$^{2/3}$ respectively, thus rendered "dimensionless"), the relationship between body mass and each variable should be nonsignificant unless allometric effects remain. Multiple regression PGLS was employed to test for allometry, wherein each vertebral variable was evaluated as a function of both log-transformed RTL and log-transformed body mass. Where the influence of body mass on the variable was nonsignificant, body mass was removed from the PGLS regression model and the model was reevaluated with RTL as the only predictive factor (Table 3.3). All PGLS analyses were conducted in the R Statistical Package (Ihaka and Gentleman, 1996) using Analysis of Phylogenetics and Evolution (APE) package (Paradis et al., 2004) and nlme, with code provided by W.A. Barr.

Where RTL significantly predicted a given variable (Tables 3.3 and 3.4), the variable was subsequently included in principal components analyses (PCAs) conducted in SPSS. For the external sacral morphology variables, PCAs were conducted for all mammalian taxa and for only primate taxa. PCA that included trabecular bone variables

were restricted to the primate taxa in the trabecular bone study sample (Table 3.1, starred taxa).

PC1 scores were then extracted from the PCA models and used to predict RTL for the extinct primate taxa using the regression equation model:

$$Y = mX + b,$$

where *Y* represents the predicted RTL, m is the slope, X is the extracted PC1 score, and b is the constant or *Y*-intercept.

The standard error of the estimate (SEE), calculated as:

$$SEE = sdY\sqrt{1-r^2},$$

where sd*Y* is the standard deviation of the *Y*-variable and r is the correlation between the X and *Y* variables, was used to provide 95% confidence limits (i.e., +/- 2 SEE) for the predictions. All PCAs were conducted in SPSS (IBM, Chicago, IL). For PGLS and PCA analyses, significance was recognized at $p<0.05$.

RESULTS

Sacral Numbers

Schultz and Straus (1945) state that the number of sacra in the primitive primate condition was likely 3. In their extensive study of vertebral numbers in primates, they found that numbers for sacra vary between two and eight (but see Schultz, 1961 for sacral counts up to nine), and three is the modal number in the majority of primates (Schultz and Straus, 1945; see their Table 5). The number of sacra varied between 2 and 8 among mammals in this study. Two was a common sacral vertebral number among mammals (e.g., *Dendrolagus lumholtzi*), and was also exhibited by some primates (e.g., *Macaca*

fascicularis), though no primate species exhibited two sacral vertebrae on average. The taxa possessing eight sacral vertebrae were *Choloepus didactylus* and *Nycticebus coucang*. Consistent with findings by Schultz and Straus (1945), three is the modal number of sacral vertebrae in the primates sampled here.

PGLS

Figures 3.3-3.13 depict the external and internal morphometric variables regressed on RTL for the model that includes all mammalian taxa. Results for all mammals, for only primate taxa, and for only nonprehensile-tailed primate taxa (i.e., excluding hominoids and prehensile-tailed taxa) are provided in Tables 3.3 (external morphometrics) and 3.4 (internal morphometrics). Below, the PGLS results are discussed for each of the vertebral variables examined.

Sacral Index **(Ankel, 1965)**

Consistent with predictions, values for the sacral index increased as relative tail length increased (Figure 3.3, Table 3.3). This finding indicates that the size of the caudal neural opening approached the size of the cranial neural opening as tail length increased. RTL was a significant predictor of the sacral index ($p<0.05$) among all mammals and among only primates, but not among only nonprehensile-tailed primate taxa ($p=0.199$) (Table 3). Among all mammalian taxa, RTL accounted for 52% of variation in the sacral index. Among only primate taxa, RTL accounted for 60% of variation in the sacral index. Among only nonprehensile-tailed primate taxa, RTL accounted for 4% of variation in the sacral index.

Body mass was a nonsignificant predictor of the sacral index among all mammals, among only primates, and among nonprehensile-tailed primate taxa ($p>0.05$). A phylogenetic signal was absent ($\lambda = 0.00$) for the sacral index among all mammals, among only primates, and among nonprehensile-tailed primate taxa.

Degree of Tapering of the Last Sacral Vertebra **(Ward et al., 1991)**

Consistent with predictions, values for the degree of tapering for the last sacral vertebra decreased as relative tail length increased (Figure 3.4, Table 3.3). This finding indicates that the mediolateral width of the last sacral vertebra's caudal articular surface increased relative to the mediolateral width of the last sacral vertebra's cranial articular surface as tail length increased. RTL was a significant predictor of the degree of tapering ($p<0.05$) among all mammals and among only primates, but not among only nonprehensile-tailed primate taxa ($p=0.083$) (Table 3.3). Among all mammalian taxa, RTL accounted for 27% of variation in the degree of tapering of the last sacral vertebra. Among only primate taxa, RTL accounted for 32% of variation in the degree of tapering of the last sacral vertebra. Among only nonprehensile-tailed primate taxa, RTL accounted for 15% of variation in the degree of tapering of the last sacral vertebra.

Body mass was a nonsignificant predictor of the degree of tapering of the last sacral vertebra among all mammals, among only primates, and among nonprehensile-tailed primate taxa ($p>0.05$). A phylogenetic signal was present for this variable among all mammals ($\lambda = 0.328$) and among only primates ($\lambda = 0.173$), and was absent among nonprehensile-tailed primate taxa ($\lambda = 0.00$).

***Sacrum's Caudal Articular Surface (CAS) Shape Index* (Russo and Shapiro, 2011)**

Consistent with predictions, values for the CAS shape index generally decreased (i.e., it approached 1) as relative tail length increased (Figure 3.5, Table 3.3). This finding indicates that the mediolateral width of the last sacral vertebra's CAS relative to its dorsoventral breadth decreased as tail length increased, indicating an increasing circular CAS shape. RTL was a significant predictor of the CAS shape index ($p<0.05$) among all mammals and among only primates, but not among only nonprehensile-tailed primate taxa ($p=0.135$) (Table 3.3). Among all mammalian taxa, RTL accounted for 28% of variation in the CAS shape index. Among only primate taxa, RTL accounted for 22% of variation in the CAS shape index. Among only nonprehensile-tailed primate taxa, RTL accounted for 8.5% of variation in the CAS shape index.

Body mass was a nonsignificant predictor of CAS shape index among all mammals, among only primates, and among nonprehensile-tailed primate taxa ($p>0.05$). A phylogenetic signal was present for this variable among all mammals ($\lambda = 0.685$), among only primates ($\lambda = 0.685$), and among nonprehensile-tailed primate taxa ($\lambda = 0.871$).

***Lateral Expansion of the Transverse Processes of the Last Sacral Vertebra* (Russo and Shapiro, 2011)**

Consistent with predictions, transverse process breadth (size-corrected) of the last sacral vertebra increased as relative tail length increased (Figure 3.7, Table 3.3). RTL was a significant predictor of transverse process breadth among all mammals, among only primates, and among only nonprehensile-tailed primate taxa ($p<0.05$) (Table 3.3).

Among all mammalian taxa, RTL accounted for 31% of variation in transverse process breadth. Among only primate taxa, RTL accounted for 34% of variation in transverse process breadth. Among only nonprehensile-tailed primate taxa, RTL accounted for 50% of variation in transverse process breadth.

Body mass was also a significant predictor of size-corrected transverse process breadth among all mammals, among only primates, and among nonprehensile-tailed primate taxa ($p<0.05$), indicating allometric effects remained after size-adjustments. A strong phylogenetic signal was detected for this variable among all mammals ($\lambda = 0.973$), among only primates ($\lambda = 0.943$), and among only nonprehensile-tailed primate taxa ($\lambda = 0.908$).

CAS Area

Consistent with predictions, values for CAS area (size-corrected) of the last sacral vertebra increased as relative tail length increased (Figure 3.6, Table 3.3). RTL was a significant predictor of CAS area among all mammals, among only primates, and among only nonprehensile-tailed primate taxa ($p<0.05$) (Table 3.3). Among all mammalian taxa, RTL accounted for 30% of variation in CAS area of the last sacral vertebra. Among only primate taxa, RTL accounted for 33% of variation in CAS area of the last sacral vertebra. Among only nonprehensile-tailed primate taxa, RTL accounted for 38% of variation in CAS area of the last sacral vertebra.

Body mass was a nonsignificant predictor of CAS area among all mammals and among only primates ($p>0.05$), but was a significant predictor of CAS area among nonprehensile-tailed primate taxa ($p=0.024$). A strong phylogenetic signal was detected

for this variable among all mammals ($\lambda = 0.926$), among only primates ($\lambda = 0.903$), and among nonprehensile-tailed primate taxa ($\lambda = 0.715$).

Spinous Process Length of the Last Sacral Vertebra

Consistent with predictions, size-corrected spinous process length of the last sacral vertebra increased as relative tail length increased (Figure 3.8, Table 3.3). RTL was a significant predictor of spinous process length among all mammals, among only primates, and among only nonprehensile-tailed primate taxa ($p<0.05$) (Table 3.3). Among all mammalian taxa, RTL accounted for 56% of variation in spinous process length. Among only primate taxa, RTL accounted for 54% of variation in spinous process length. Among only nonprehensile-tailed primate taxa, RTL accounted for 62% of variation in spinous process length.

Body mass was a nonsignificant predictor of size-corrected spinous process length among all mammals and among only primates ($p>0.05$), but was a significant predictor of size-corrected spinous process length among nonprehensile-tailed primate taxa ($p<0.05$). A strong phylogenetic signal was detected for this variable among all mammals ($\lambda = 0.854$), among only primates ($\lambda = 0.884$), and among nonprehensile-tailed primate taxa ($\lambda = 1.000$).

Internal sacral morphology

Bone volume fraction

RTL was a significant predictor of bone volume fraction among only nonprehensile-tailed primate taxa ($p<0.05$), but not among any other groups (Figure 3.9, Table 3.4). Among only nonprehensile-tailed primate taxa, trabecular bone volume

fraction increased as relative tail length increased (Table 3.4) and RTL accounted for 45% of variation in this variable.

Body mass was a nonsignificant predictor of bone volume among all primates and among only nonprehensile-tailed primate taxa ($p>0.05$). A moderate phylogenetic signal was detected for this variable among all primates ($\lambda = 0.663$), and a strong phylogenetic signal was detected among only nonprehensile-tailed primate taxa ($\lambda = 1.000$).

Trabecular number

RTL was a nonsignificant predictor among all primates and among only nonprehensile-tailed primate taxa ($p>0.05$) (Figure 3.10; Table 3.4). Body mass was a significant predictor of trabecular number among all primates ($p<0.05$), but was a nonsignificant predictor of trabecular number among only nonprehensile-tailed primate taxa ($p>0.05$). A phylogenetic signal was absent for this variable among all primates ($\lambda = 0.000$), however, a moderate phylogenetic signal was detected among only nonprehensile-tailed primate taxa ($\lambda = 0.477$).

Degree of anisotropy

RTL was a nonsignificant predictor of the degree of anisotropy among all primates and among only nonprehensile-tailed primate taxa ($p>0.05$) (Figure 3.11; Table 3.4). Body mass was a nonsignificant predictor degree of anisotropy was nonsignificant among all primates and only nonprehensile-tailed primate taxa ($p>0.05$). A phylogenetic signal was absent for this variable among all primates and among only nonprehensile-tailed primate taxa ($\lambda = 0.000$).

Elongation index

RTL was a nonsignificant predictor of the elongation index among all primates and among only nonprehensile-tailed primate taxa ($p>0.05$) (Figure 3.12; Table 3.4), suggesting little change in trabecular shape in the last sacral vertebra in relation to tail length. Body mass was a nonsignificant predictor of the elongation index among all primates and only nonprehensile-tailed primate taxa ($p>0.05$). A phylogenetic signal was absent for this variable among all primates and among only nonprehensile-tailed primate taxa ($\lambda = 0.000$).

Trabecular thickness

Trabecular thickness (size-corrected) in the VOI in the last sacral vertebra slightly increased as relative tail length increased in all primates and among nonprehensile-tailed primate taxa (Figure 3.13, Table 3.4). RTL was a significant predictor of trabecular thickness among all primates ($p<0.05$), but was nonsignificant among only nonprehensile-tailed primate taxa ($p>0.05$) (Table 3.4). Among all primate taxa, RTL accounted for approximately 29% of variation in trabecular thickness. Body mass was a significant predictor of trabecular thickness among all primates and only nonprehensile-tailed primate taxa ($p<0.05$). A phylogenetic signal was absent for this variable among all primates and among only nonprehensile-tailed primate taxa ($\lambda = 0.000$).

Trabecular orientation

The principal axes of trabecular orientation can be visualized in three-dimensional space by plotting eigenvectors ($\mu1$, $\mu2$, $\mu3$) onto an equal-area stereoplot (Maga et al., 2006). Figure 3.14A shows the projection of the first eigenvector for all taxa in the

trabecular bone study sample. Extant primates exhibit a variety of orientations in the last sacral vertebra, though notably many individuals appear to exhibit craniocaudally-oriented trabeculae. Though there did not appear to be any patterns with respect to trabecular orientation in the extant taxonomic sample, both *Archaeolemur* specimens and *Epipliopithecus* exhibited trabeculae strongly oriented primarily in the craniocaudal direction in the last sacral vertebra, while *Palaeopropithecus* and *Megaladapis* exhibited primary trabecular orientations in off-orthogonal directions (Figure 3.14B).

Figure 3.15 plots the coefficient of variation for trabecular orientation, calculated from the first eigenvector, in extant primates. The blue line shows the trend among all primates, which appears to be driven largely by nonprehensile-tailed taxa, the trend for which is shown as the green line. Among nonprehensile-tailed taxa, there is a slight trend for the coefficient of variation to decrease as tail length increases, suggesting that as tail length increases, primates may exhibit greater consistency in the orientation of trabecular in the last sacral vertebra.

Principal components analyses

The variables included in the PCA are listed in Tables 3.3 and 3.4. Internal sacral morphometric variables were evaluated with the external sacral morphometric variables only if RTL was a significant predictor of the variable. The PCA results are presented in Table 3.5. As with the PGLS analyses, the PCAs were conducted among all mammals, among only primates, and among only nonprehensile-tailed primate taxa for the external morphometric variables. Only primates were examined in the trabecular bone study, and

as such, the analyses with external and internal sacral variables were restricted to primates.

RTL was a significant predictor of all external sacral variables in Dataset #1 (caudal articular surface shape index and area, the degree of tapering, and transverse process breadth) (Table 3.3) for all mammals and for only primates. Among all mammals in Dataset #1, PC1 accounted for approximately 62% of the variance, while among only primates in Dataset #1, PC1 accounted for 65% of the variance (Table 3.5). RTL was a significant predictor of only caudal articular surface area and transverse process breadth among nonprehensile-tailed primates in Dataset #1 (Table 3.3), for which PC1 accounted for approximately 92% of the variance (Table 3.5).

RTL was also a significant predictor of the sacral index and spinous process breadth among all mammals and among all primates (Table 3.3). As such, RTL was a significant predictor of all external sacral variables in Dataset #2 among all mammals and among all primates (sacral index, degree of tapering, caudal articular surface shape index and area, transverse process breadth, and spinous process breadth). Among all mammals and among only primates, PC1 accounted for approximately 71% of the variance (Table 5). Among nonprehensile-tailed primates, RTL was also a significant predictor of spinous process length in Dataset #2, and so RTL was a significant predictor of three external sacral variables only among nonprehensile-tailed primates (caudal articular surface area, transverse process breadth, and spinous process breadth). PC1 accounted for approximately 88% of variation among nonprehensile-tailed primate taxa (Table 3.5).

When considering internal sacral variables, the PCA among all primates included all six external sacral variables and trabecular thickness (Tables 3.3 and 3.4). PC1 accounted for approximately 69% of variation among all primates (Table 3.5). The PCA among all nonprehensile-tailed taxa included three external sacral variables (caudal articular surface area, transverse process breadth, and spinous process breadth) and bone volume fraction (Tables 3.3 and 3.4). PC1 accounted for approximately 74% of variation among all primates (Table 3.5).

RTL on PC1 scores

Figures 3.16 -3.18 depict bivariate plots of RTL on PC1 species mean scores for all mammals, only primates, and nonprehensile-tailed primates for both external morphometric datasets (Figures 3.16 and 3.17) and for the datasets that include external and internal sacral variables (Figure 3.18). Regression equation coefficients and model summaries are provided in Table 3.6. Figures 3.16A and 3.16B show RTL on species mean PC1 scores for all mammals and only primates in Dataset #1. For all mammals in Dataset #1, 66% of the variation in RTL is accounted for by species mean PC1 scores (Figure 3.16A). For only primates in Dataset #1, 86% of the variation in RTL is accounted for by species mean PC1 scores (Figure 3.16B). Figure 3.16C shows RTL on species mean PC1 scores for only nonprehensile-tailed primate taxa in Dataset #1. Less variation (75%) in RTL is accounted for by species mean PC1 scores for this taxonomic group than in the analysis of all primates. Thus, the model that includes all primates was used to predict the relative tail lengths of the extinct taxa because this model had the

higher R-squared value. Additionally, this model includes the probable taxonomic affiliation for *Proconsul.*

The PC1 scores for the extinct primate sacra predict RTLs of 27 (95% confidence limits: -17 to 71) for *Palaeopropithecus*, 59 (95% confidence limits: 15 to 103) for *Megaladapis,* 36 for *Epipliopithecus* (95% confidence limits: -8 to 80), 148 (95% confidence limits: -104 to 192) for *Archaeolemur* (DPC 11823), and -38 (95% confidence limits: -82 to 6) for *Proconsul* (1xSEE [68% confidence]= +/- 22; 2xSEE [95% confidence] =+/- 44). Since RTL cannot be negative, it may be assumed that *Proconsul* is predicted as tailless (see also discussion). Because the degree of tapering and transverse process breadth could not be obtained for *Archaeolemur* DPC 11835 and 9905, respectively, the PCA includes only *Archaeolemur* 11823. Regardless, values for the all other measures for DPC 11835 and 9905 are provided in Table 3.2 for comparison.

Figures 3.17A and 3.17B show RTL on species mean PC1 scores for all mammals and only primates in Dataset # 2. For all mammals in Dataset #2, 82% of the variation in RTL is accounted for by species mean PC1 scores (Figure 3.17A). For only primates in Dataset #2, 87% of the variation in RTL is accounted for by species mean PC1 scores (Figure 3.17B). Figure 3.17C shows RTL on species mean PC1 scores for only nonprehensile-tailed primate taxa in Dataset #2. 54% of the variation in RTL is accounted for by species mean PC1 scores. As with Dataset #1, the model that includes all primates had a higher R-squared value than the model that includes only nonprehensile-tailed primate taxa. The PC1 scores for the extinct primate sacra using this model predict RTLs of 18 (95% confidence limits: -22 to 58) for *Palaeopropithecus*, 38 (95% confidence

limits: -2 to 78) for *Megaladapis,* 36 (95% confidence limits: -4 to 76) for *Epipliopithecus*, and 126 (95% confidence limits: 86 to 166) for *Archaeolemur* (1xSEE [68% confidence]= +/- 20; 2xSEE [95% confidence] =+/- 40). *Proconsul* is excluded from this analysis because some variables (i.e., sacral index) could not be calculated for this specimen as it preserves only the last sacral vertebra.

Figures 3.18A and 3.18B show RTL on species mean PC1 scores for all primates and for nonprehensile-tailed primate taxa for the datasets that include external and internal sacral variables. For all primates, 94% of the variation in RTL is accounted for by species mean PC1 scores (Figure 3.18A). The PC1 scores for the extinct primate sacra using this model predict RTLs of 31 (95% confidence limits: -1 to 63) for *Palaeopropithecus*, 52 (95% confidence limits: 20 to 82) for *Megaladapis* and 29 (95% confidence limits: -3 to 61) for *Epipliopithecus* (1xSEE [68% confidence]= +/- 18; 2xSEE [95% confidence] =+/- 36). *Archaeolemur* could not be included in this analysis because the mediolateral width of the first sacral vertebra to size-correct trabecular thickness. For nonprehensile-tailed primate taxa, 87% of the variation in RTL is accounted for by species mean PC1 scores (Figure 3.18B). The PC1 scores for the extinct primate sacra using this model predict RTLs of 42 (95% confidence limits: -2 to 86) for *Palaeopropithecus*, 68 (95% confidence limits: 24 to 112) for *Megaladapis,* 58 (95% confidence limits: 14 to 102) for *Epipliopithecus*, and 143 (95% confidence limits: 99 to 187) for *Archaeolemur* (1xSEE [68% confidence]= +/- 22; 2xSEE [95% confidence] =+/- 44).

DISCUSSION

The first objective of this study was to examine aspects of sacral morphology previously related to variation in tail length/function among a taxonomically and morphologically diverse sample of extant mammals in order to verify purported sacral form-tail function links. The results of this study generally support the functional associations of the sacral index (Ankel, 1965, 1972), the degree of tapering (Ward et al., 1991), and the CAS shape index and lateral expansion of the transverse processes (Russo and Shapiro, 2011), with relative tail length. Consistent with predictions, values for the sacral index and lateral expansion of the transverse processes generally increased as tail length increased in the analysis of all mammals, all primates and nonprehensile-tailed taxa only. These findings indicate that the size of the sacrum's caudal neural opening increased relative to its cranial neural opening, and transverse processes became more laterally expanded, as tail length increases in the study sample (Ankel, 1965; 1972; Russo and Shapiro, 2011). Also consistent with predictions, values for the degree of tapering and the CAS shape index decreased as tail length increased in the sample. These findings indicate that the last sacral vertebra expands in mediolateral width caudally (relative to the cranial end), and that its CAS becomes more circularly shaped (i.e., more equal mediolateral and dorsoventral dimensions) as tail length increases (Ward et al., 1991; Russo and Shapiro, 2011).

RTL was significant predictor of these variables in the taxonomic analysis of all mammals and among all primates, however, among only nonprehensile-tailed primates, only transverse process breadth remained statistically significant. In general, this

observation could suggest that the relationship between the sacral index, the degree of tapering, and the CAS shape index, and RTL, might be largely driven by the specialized sacral function of the tail morphology extremes (e.g., tailless hominoids and prehensile-tailed platyrrhines). For instance, this explanation may account for the results for the caudal articular surface shape index, in which the negative relationship between mediolateral/dorsoventral caudal articular surface dimensions and relative tail length seems particularly influenced by the high values obtained for the hominoid taxa (see Figure 3.5). In fact, the one cercopithecoid species with an assigned RTL of 0 is *Macaca sylvanus* and, though only two individuals were examined for this taxon, its caudal articular surface shape index mean value is 1.67. This value is comparable to that of other cercopithecoids (e.g., *Cercopithecus ascanius* and *C. mitis*) that possess relative tail lengths of over 135. Functionally, that hominoids, but not necessarily other extant taxa considered tailless or having extremely reduced tail lengths, have dorsoventrally compressed distal sacral ends might reflect pelvi-caudal muscular reorganization rather than loss of the tail, per se. That is, though hominoids lack much of the musculature associated with the tail (e.g., *abductor caudae lateralis* mm., *interspinalis caudae* mm.), the basal tail musculature becomes reorganized. Specifically, in hominoids, homologs (e.g., *ilio-* and *pubo- coccygeas* mm.) of basal tail muscles that act chiefly as abductor-flexors in tailed primates (e.g., *ilio-*, *ischio-* and *pubo- caudalis,* Hartmann and Straus, 1933) are reorganized on each side of the pelvic floor to make up the *levator ani* mm. (along with the *puborectalis* mm). The *levator ani* mm. attach to the ventral and lateral surfaces of the coccyx (Gray, 1977). The *ischiococcygeus* mm. attach to the lateral

aspects of the last sacral vertebra and the coccygeal vertebrae (Gray, 1977). Right and left sides taken together, the *levator ani* mm. and the *ischiococcygeus* mm. form a hammock-like pelvic diaphragm, which supports the abdominal and pelvic viscera (Elftman, 1932; Wood, 1985; Woon and Stringer, 2012). Because the *levator ani* mm., as well as the sacro- tuberous and spinous ligaments (Kapandji, 2008), course anteroposteriorly, a relatively mediolaterally broad distal sacrum and coccygeal vertebrae might provide greater surface area for their attachment at these respective bony sites.

At the same time, two other factors must be considered when exploring the trends observed here for the sacrum's CAS shape. The first is that a similar trend of increasing dorsoventral compression with increasing tail length is observed for the cranial articular surface of caudal vertebrae at levels of the tail sequence not present in hominoids (Chapter 4). For example, at the level of the mid-proximal and transition caudal vertebrae among nonhominoid primates, relative tail length is a significant predictor of cranial articular surface shape, defined in the same manner as sacral caudal articular surface shape (Chapter 4). Because hominoids do not possess mid-proximal or transition vertebra, analysis at these vertebral levels are restricted to tail-bearing primates. Though arguably less convincing, another factor to consider is that the CAS shape indices for the extinct primate taxa align with expectations based on previous inferences concerning their tail lengths. For example, the *Archaeolemur* specimens, DPC 9950, DPC 11823 and DPC 11835, exhibit caudal articular surface shape indices of 1.31, 1.35 and 1.20, respectively. These indices are within the range of those observed for extant long-tailed primates and indicate that the *Archaeolemur* distal sacra are nearly circular in outline

with approximately equal mediolateral and dorsoventral dimensions (see also Figure 3.2). Additionally, the caudal articular surface shape index obtained for *Proconsul* is 2.14, a value that falls at the lower end of values obtained for hominoids, and indicates that the *Proconsul* distal sacrum is nearly elliptical in outline and twice as wide mediolaterally as it is broad dorsoventrally. Thus, at the time, it is not entirely clear how to account for the relationship between relative tail length and caudal articular surface shape.

With respect to the sacral index (Ankel, 1965; 1972), results are more taxonomically restricted than for the other variables because calculation of this variable was limited to taxa in Dataset #2, which is comprised mainly of primates. Compared to the values obtained for the sacral index by Ankel (1965, 1972), the values obtained in this study appear consistently lower. For example, this study obtained a mean sacral index value of 65 for *Ateles fusciceps* (N=6), with a range from 38-107, while Ankel (1965) obtained a mean sacral index value of 121 for *Ateles* (species unidentified, N=7). Thus, the range for *Ateles* sacral indices obtained here does not contain the mean value obtained by Ankel (1965). This discrepancy might be due to methodological differences, as Ankel (1965) obtained her measurements using calipers, whereas linear measures to calculate the index in this study were obtained from photographs. Nonetheless, since sacral indices for all taxa in this sample (including the extinct primate taxa) were obtained in this way, relative changes in this index can still be evaluated against tail length. The mean degree of tapering values obtained in this study are generally comparable to those obtained by Ward and colleagues (1991; their Table 1). For example, the mean degree of tapering value for *Gorilla gorilla* is 18.7 (versus 15.7), with a minimum of 4.1 (versus 10.2) and a

maximum of 32 (versus 25.5) (values for comparison from Ward et al., 1991). The consistency between the values for the degree of tapering found here and those attained by Ward and colleagues (measurements in both studies were collected using calipers) is important as the value used for *Proconsul* derives from their study.

The second objective of this study was to build upon our body of knowledge about the anatomy associated with tail loss/length reduction by quantifying two previously unexamined aspects of external sacral morphology (caudal articular surface area and spinous process length) and, by evaluating the internal bony morphology (i.e., trabecular bone) of the sacrum at its distal end where caudal or coccygeal vertebrae articulate. Consistent with predictions, results demonstrate that caudal articular surface area and spinous process length increase as tail length increases. Tail length is likely proportional to tail mass (Organ, 2007), and so presumably the forces generated at the sacro-caudal/coccygeal joint by shorter tails are smaller than those generated by long tails. Additionally, more restricted movements of the coccyx, resulting from more elliptically-shaped CASs, should result in smaller functional loads (Nakatsukasa et al., 2003), whereas the presumably greater loads in tail-bearing mammals should require greater articular surface areas. Thus, functionally, relatively smaller joint surfaces suggest a reduced ability to distribute high loads over a wider area, suggesting lower force magnitudes may transmitted across the caudal/coccygeal joint surfaces of shorter-tailed primates. An increase in the length of the last sacral spinous process increases the surface area for attachment, and increases the mechanical advantage, of the *extensor caudae medialis* mm. and *interspinales caudae* mm, two of the tail's (dorsal) extensors.

Increased spinous process length in conjunction with increased tail length could be functionally interpreted to reflect that long tailed primates might require enhanced ability to dorsally extend the tail to control body movements during bouts of leaping (Emerson, 1985; Günther et al., 1991; Essner, 2002). At the same time, it is also possible that a longer spinous process is simply needed to carry a longer, heavier tail to keep it from dragging along the locomotor substrate, as behavioral research demonstrates that arboreal primates hold their tails in dorsally extended positions during quadrupedal walking, running and bounding (Bernstein et al., 1978; Stevens et al., 2008).

The ways in which the trabecular bone structure in the last sacral vertebra relates to relative tail length in living primates are less clear than those for the external morphology of the sacrum. Generally, this study predicted that as relative tail length increases, measures of bone volume fraction, trabecular number, and the degree of anisotropy would increase. The results of this study partially support the study predictions. For example, RTL was a significant predictor of trabecular bone volume fraction in the last sacral vertebra (which increased as relative tail length increased) among only nonprehensile-tailed taxa, but not among all primates. Trabecular thickness slightly increased as relative tail length increased in both the analysis of all primates and among nonprehensile-tailed primate taxa. Among all primates, RTL was a significant predictor of trabecular thickness. These features are associated with increased bone strength (Currey, 1984; Gibson, 1985; Goldstein et al., 1991, 1993) and could suggest that the sacrocaudal joints of longer-tailed primates are structured to withstand greater loads than those of shorter-tailed primates. However, there is substantial amount of

scatter in the data, and several other trabecular variables associated with bone strength are not significantly predicted by RTL, which, together suggest that this functional explanation is not well supported. Nevertheless, there are a few interesting trends with respect to the trabecular data that are worth noting. For example, prehensile-tailed taxa appear to have somewhat thick trabeculae that are less organized (low values for degree of anisotropy) and more plate-like (low elongation index values), compared to other taxa in the sample. A trabecular network comprised of unorganized, thick, plate-like trabeculae could reflect a more varied loading regime at the sacrocaudal joint that results from use of the tail as a fifth appendage during suspensory locomotion.

The third goal of this study was to apply the results of the extant mammal sample to an evaluation of the external and internal sacral anatomy of sacra belonging to extinct primates, including *Archaeolemur, Megaladapis, Palaeopropithecus, Epipliopithecus* and *Proconsul,* in order to reconstruct their tail lengths. Below, the estimated relative tail lengths of the extinct primates calculated using the extant primate sacrum data are discussed with respect to previous inferences concerning their tail lengths.

In Zapfe's (1958) original description of the *Epipliopithecus* Individual I sacrum, he asserted that *Epipliopithecus* was "tailless" and that just "three [total] caudal vertebrae may be assumed" (447:1958). Presumably, with respect to this latter inference, Zapfe (1958) was suggesting that *Epipliopithecus* possessed coccygeal, and not caudal, vertebrae. His interpretation contrasts with Ankel's later interpretation of the *Epipliopithecus* tail as "pendant" based only on the specimen's sacral index of 63.2 (Ankel, 1965), which "falls within the range of long-tailed monkeys" (1972:236),

indicating that it, too, "must have had a long tail with at least ten to fifteen [total] caudal vertebrae" (1965:275). Indeed, her value of 63.2 is similar to that of extant long-tailed primates included in her sample, including *Cercopithecus sp.* (RTL = 119 -145), *Papio papio* (*P. cynocephalus* RTL =84), and *Macaca fascicularis* (RTL = 107). Though this study obtained a sacral index value of 55 for *Epipliopithecus,* as mentioned earlier, the sacral indices obtained in this study cannot be directly compared to those obtained by Ankel (1965) likely due to methodological differences. Yet, when this sacral index value is considered in conjunction with other functionally important variables in the PCA, the results of this study predicted the *Epipliopithecus* relative tail length as between 29 and 58. Some living primates possessing relative tail lengths within the range of that predicted for *Epipliopithecus* include *M. assamensis* (RTL=36)*, Macaca nemestrina* (RTL=37), and *M. mulatta* (RTL =47) (Table 3.1). Compared to *Archaeolemur*, the one extinct primate taxon included in the sample that was predicted to have the longest tail, and *Palaeopropithecus,* the extinct primate taxon predicted to have the shortest tail, the sacral features exhibited by *Epipliopithecus* that contribute to its more intermediate predicted tail lengths include an intermediate degree of tapering and moderate reduction in the length of spinous process of the last sacral vertebra (Figure 3.2 and Table 3.2). That *Epipliopithecus* likely possessed a relatively short tail suggests that tail length reduction may be subject to considerable homoplasy in catarrhine evolution. That tail length reduction might characterize extinct primates from multiple lineages throughout the course of catarrhine evolution should perhaps not be surprising as a number of extant

catarrhines from multiple lineages also possess shortened tails (e.g., *Mandrillus sphinx, Macaca tonkeana, Nasalis concolor*).

Results from this study support Ward and colleagues' (1991) previous interpretation that *Proconsul* was tailless. The extant primate sacrum dataset (#1) predicts the *Proconsul* relative tail length as -38. Though the PC score for *Proconsul* (-1.72) predicts a negative RTL, its PC score is well within the range of PC scores exhibited by extant hominoids. For example, the PC1 score range for *Pan troglodytes* is -1.82 to -0.36, the range for *Gorilla gorilla* is -1.64 to -0.95, the range for *Pongo pygmaeus* is -1.98 to -0.67, and the range for *Hylobates* is -2.33 to -0.67. Though, admittedly, the PC1 score ranges for extant hominoids and some very-short tailed cercopithecoids overlap, the *Proconsul* PC1 score value is outside of the range of values exhibited by the latter group. For example, *Macaca arctoides* (RTL = 6) exhibits a PC1 score range of -0.90 to -0.58; *M. tonkeana* (RTL =8) exhibits a PC1 score range of -.49 to -1.22; and the one nonhominoid taxon with an RTL of 0, *M. sylvanus*, exhibits a PC1 score of -0.31 (n =1 for the PCA). Because the *Proconsul heseloni* sacral specimen examined here preserves only the last sacral vertebra, it was not possible to calculate the sacral index (see also Ward et al., 1991), and thus it was excluded from Dataset #2 which would have provided a second relative tail length prediction. Notwithstanding, overall, Dataset#2 generally predicts shorter relative tail lengths for all extinct taxa than Dataset #1. This observation suggests that even if *Proconsul* could be included in Dataset #2, it is unlikely that it would be predicted to have a tail. Moreover, the relative tail length predicted for *Proconsul* is the shortest in the extinct primate sample examined here, even compared to

Palaeopropithecus, a subfossil lemur taxon thought to have possessed a vestigial tail (Godfrey and Jungers, 2003). With respect to tail presence/absence and its utility in determining the phylogenetic affinities of extinct catarrhines, the findings presented here parsimoniously support the inclusion of *Proconsul* in the Hominoidea on the basis of tail absence (Ward et al., 1991). Moreover, the results do not provide support for the interpretation that *Proconsul* possessed a long tail (Harrison, 1998). Compared to *Archaeolemur*, the only extinct primate taxon included in the sample that was predicted to have a long tail, the sacral features exhibited by *Proconsul* support the conclusion that it possessed no tail include a more elliptically-shaped caudal articular surface with relatively reduced articular surface area, a higher degree of caudal tapering, and less expanded last sacral vertebral transverse processes (Figure 3.2 and Table 3.2).

The relative tail lengths predicted for the subfossil lemur taxa included in the sample using the extant primate data are also generally consistent with previous inferences concerning their tail lengths. For example, the models examined here predict relative tail lengths for *Archaeolemur* as between 126 and 148. Since both of these estimated relative tail lengths are greater than 100, they indicate that *Archaeolemur* possessed a tail longer than the total length of its head and body. This generally accords with previous interpretations that *Archaeolemur* possessed a "long" tail (e.g., Godfrey et al., 2006). The living primates with the relative tail lengths closest to those predicted for *Archaeolemur* include, but are not limited to, *Saguinus sp.* (RTL=142), *Cercopithecus sp.* (*C. ascanius*, RTL=139; *C.mitis*, RTL=139), *Trachypithecus obscurus* (RTL=144), *Galago senegalensis* (RTL =130) and *Otolemur crassicaudatus* (RTL=122). Compared

to *Palaeopropithecus*, an extinct subfossil lemur predicted to have a short tail, the sacral features exhibited by *Archaeolemur* that contribute to the prediction that it possessed a long tail include a more circularly-shaped caudal articular surface with increased articular surface area, a low degree of tapering, and an elongated last sacral vertebral spinous process (Figure 3.2 and Table 3.2).

The models examined here predict relative tail lengths for *Palaeopropithecus* as between 18 and 42. These predicted relative tail lengths indicate that *Palaeopropithecus* possessed a tail shorter than even half its total head and body length, and one that may have been only 18% of its total head and body length. Thus, the estimated relative tail lengths for *Palaeopropithecus* obtained in this study support previous inferences that this taxon had a "short" tail (e.g., Godfrey and Jungers, 2003; Godfrey et al., 2006). The living primates with the relative tail lengths closest to those predicted for *Palaeopropithecus* include, but are not limited to, *M. assamensis* (RTL=36), *M. fuscata* (RTL=15), and *Mandrillus sphinx* (RTL=10). Compared to an extinct primate taxon included in the sample that was predicted to have a long tail (e.g., *Archaeolemur*), the sacral features exhibited by *Palaeopropithecus* that contribute to short predicted tail lengths include a more elliptically-shaped caudal articular surface with reduced articular surface area, a lower sacral index, a higher degree of tapering, and relatively extreme reduction in the length of spinous process of the last sacral vertebra (Figure 3.2 and Table 3.2). An additional feature may be the possession of four sacral vertebrae, as opposed to three, which is the modal number in the extant primate sample (Ankel, 1972; but see above). The extreme reduction of the distal (and presumably proximal; Figure 3.2) sacral

spinous process is consistent with observations in the lumbar vertebral region of this taxon and both indicate a resemblance to the lumbosacral morphology of extant sloths (Figure 3.19; Godfrey and Jungers, 2003; Shapiro et al., 2005).

The models examined here predict relative tail lengths for *Megaladapis* as between 38 and 68. These predicted relative tail lengths indicate that *Megaladapis* possessed a tail that was about a quarter to almost three-quarters of its and its total head and body length. Thus, the estimated relative tail lengths for *Megaladapis* obtained in this study generally suggest that this taxon had a relatively short tail (e.g., compared to *Archaeolemur*). Compared to an extinct primate taxon included in the sample that was predicted to have a long tail (e.g., *Archaeolemur*), the sacral features exhibited by *Megaladapis* that contribute to short predicted tail lengths include a more elliptically-shaped caudal articular surface with reduced articular surface area, a lower sacral index, a higher degree of tapering, and relatively extreme reduction in the length of spinous process of the last sacral vertebra (Figure 3.2 and Table 3.2). Like *Palaeopropithecus,* an additional feature may be the possession of four sacral vertebrae, as opposed to three, which is the modal number in the extant primate sample. As with the lumbar vertebrae (Shapiro et al., 2005), the sacrum of *Megaladapis* resembles that of *Palaeopropithecus* in that it also possessed reduced spinous process length of the sacral vertebra (Figure 3.2).

CONCLUSIONS

This study examined external and internal aspects of sacral morphology in relation to tail length. It sought to validate previously defined sacral form – tail function links put forth by Ankel (1965, 1972), Ward and colleagues (1991), and Russo and Shapiro (2011). The study also offered new functional insight into the anatomy associated with tail length reduction by examining previously unexamined aspects of external sacral morphology and the structure of trabeculae in the last sacral vertebra. Finally, using results from the extant primate sample, the tail lengths of a number of extinct primates are reconstructed.

Results support the functional link between Ankel's (1965) sacral index, Ward and colleagues' (1991) measure of degree of tapering, and Russo and Shapiro's (2011) caudal articular surface shape index and measure of transverse process breadth, and relative tail length among primates. Results further demonstrate that the length of the last sacral vertebra's spinous process and surface area of the sacrum's caudal articular surface are also associated with relative tail length. As tail length decreases, the area of the sacrum's caudal neural opening (relative to the cranial neural opening) decreases, the caudal end of the last sacral vertebra (relative to its cranial end) narrows mediolaterally, the caudal articular surface decreases in surface area and becomes more elliptically-shaped in a mediolateral direction, and the length of bony levers, including the spinous process and transverse process, decreases. In the analysis of nonprehensile-tailed taxa only, however, relative tail length had a significant effect on only transverse process breath, caudal articular surface area, and spinous process length. Taken together, these

features suggest that, compared to primates longer tail lengths, primates with reduced tail lengths exhibit a decrease in the innervation provided to the caudal region, more restricted movements at the sacro -caudal/-coccygeal joint that are likely subject to reduced forces, and decreased ability to extend and laterally abduct the tail. The relationship between trabecular bone structure and relative tail length was less convincing than that between the external morphology of the sacrum and relative tail length. In some cases, features indicative of trabecular bone strength appeared to decrease as tail length decreased, however the relationships between these variables and tail length were weak.

Using the extant primate data, the results of this study are consistent with previous interpretations that *Proconsul* was tailless, that *Archaeolemur* possessed a long tail, and that *Palaeopropithecus* possessed a short tail. Results also demonstrated that *Megaladapis* and *Epipliopithecus* had short tails. These findings support the utility of the data and methodologies employed in this study for tail length reconstructions of other extinct primates.

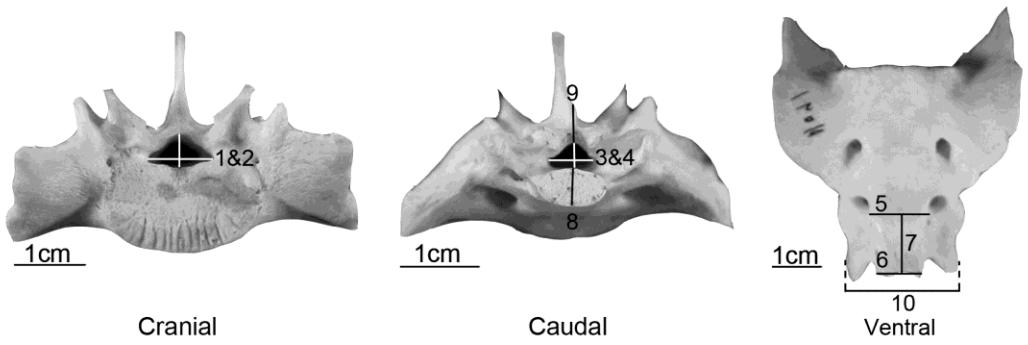

Figure 3.1 Sacral measurements obtained for the study. Sacrum from *Macaca nemestrina* shown in (from left to right) cranial, caudal, and ventral views. For cranial and caudal views, dorsal is up. For ventral view, cranial is up. 1) Maximum mediolateral breadth of the cranial neural opening; 2) Maximum dorsoventral breadth of the cranial neural opening; 3) Maximum mediolateral breadth of the caudal neural opening; 4) Maximum dorsoventral breadth of the caudal neural opening; 5) Maximum mediolateral breadth of the cranial articular surface of the last sacral vertebra; 6) Maximum mediolateral breadth of the caudal articular surface of the last sacral vertebra; 7) Craniocaudal length of the last sacral vertebra at midline of the ventral surface; 8) Maximum dorsoventral breadth of the caudal articular surface of the last sacral vertebra; 9) Spinous process length of the last sacral vertebra, measured from dorsalmost aspect of the caudal neural opening to the apex of the spinous process; 10) Maximum lateral expansion of the transverse processes of the last sacral vertebra measured as the transverse distance from the apex of the left transverse process to the right transverse process.

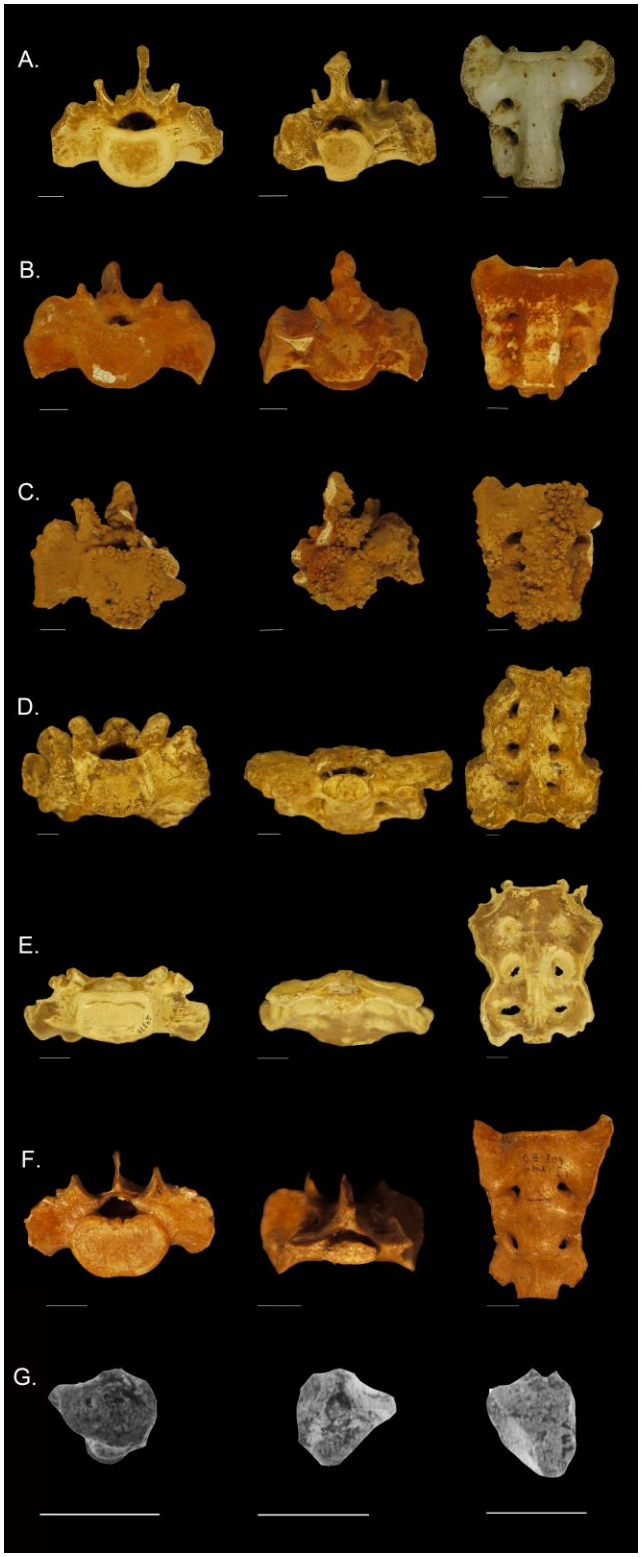

Figure 3.2 Sacra included in the extinct primate sample. A) *Archaeolemur edwardsi* DPC 9905; B) *Archaeolemur edwardsi* DPC 11823; C) *Archaeolemur edwardsi* DPC 11835; D) *Megaladapis grandidieri* DPC 7950; E). *Palaeopropithecus sp. nov.* DPC 24778; F) *Epipliopithecus vindobonensis* O.E. 304-45 sacrum from Individual I G) *Proconsul heseloni* KNM-KPS V42 (Images taken from Ward et al., 1991). Views are (from left to right) cranial, caudal and ventral. For cranial and caudal views, dorsal is up. For ventral view, cranial is up. All sacra are complete with the exception of the *Proconsul* specimen for which only the last sacral vertebra is preserved. White scale bars = approximately 1cm.

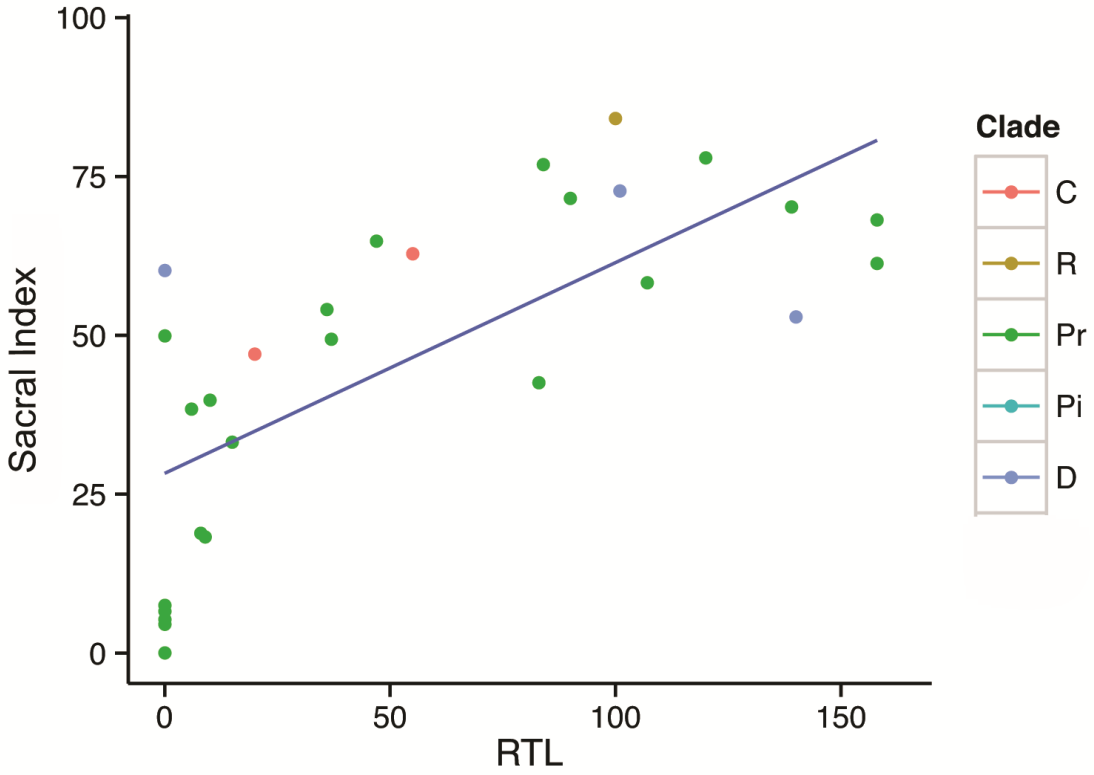

Figure 3.3 Sacral Index on RTL in the extant mammal sample. Key to right of figure: C= Carnivora, R= Rodentia; Pr = Primates, Pi= Pilosa; D= Diprotodontia.

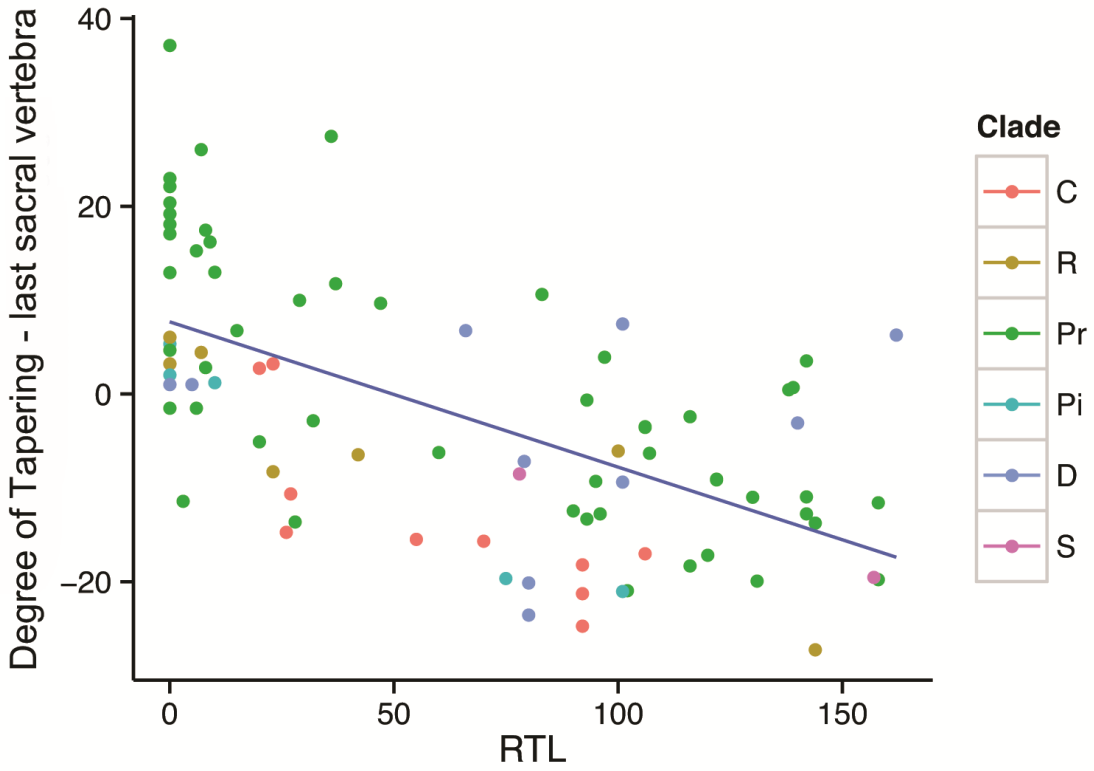

Figure 3.4 Degree of tapering of the last sacral vertebra on RTL in the extant mammal sample. Key to right of figure: C= Carnivora, R= Rodentia; Pr = Primates, Pi= Pilosa; D= Diprotodontia; S=Scandentia.

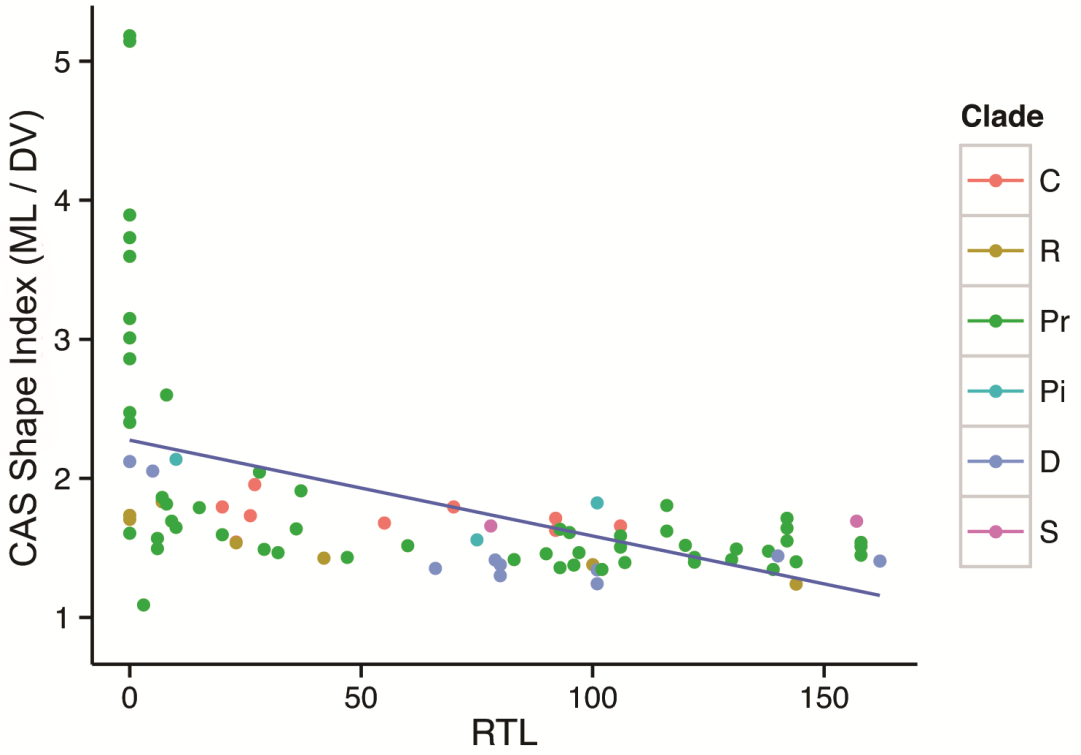

Figure 3.5 Caudal articular surface shape index (mediolateral / dorsoventral dimensions) on RTL in the extant mammal sample. Key to right of figure: C= Carnivora, R= Rodentia; Pr = Primates, Pi= Pilosa; D= Diprotodontia; S=Scandentia.

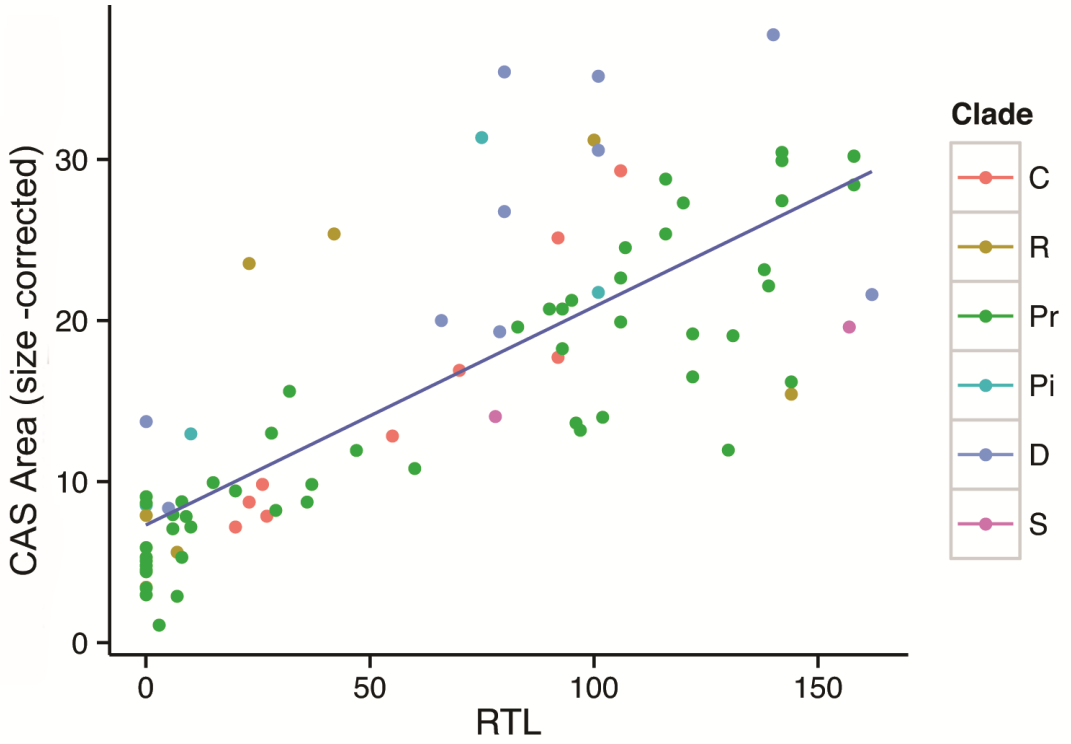

Figure 3.6 Caudal articular surface area (size-corrected) on RTL in the extant mammal sample. Key to right of figure: C= Carnivora, R= Rodentia; Pr = Primates, Pi= Pilosa; D= Diprotodontia; S=Scandentia.

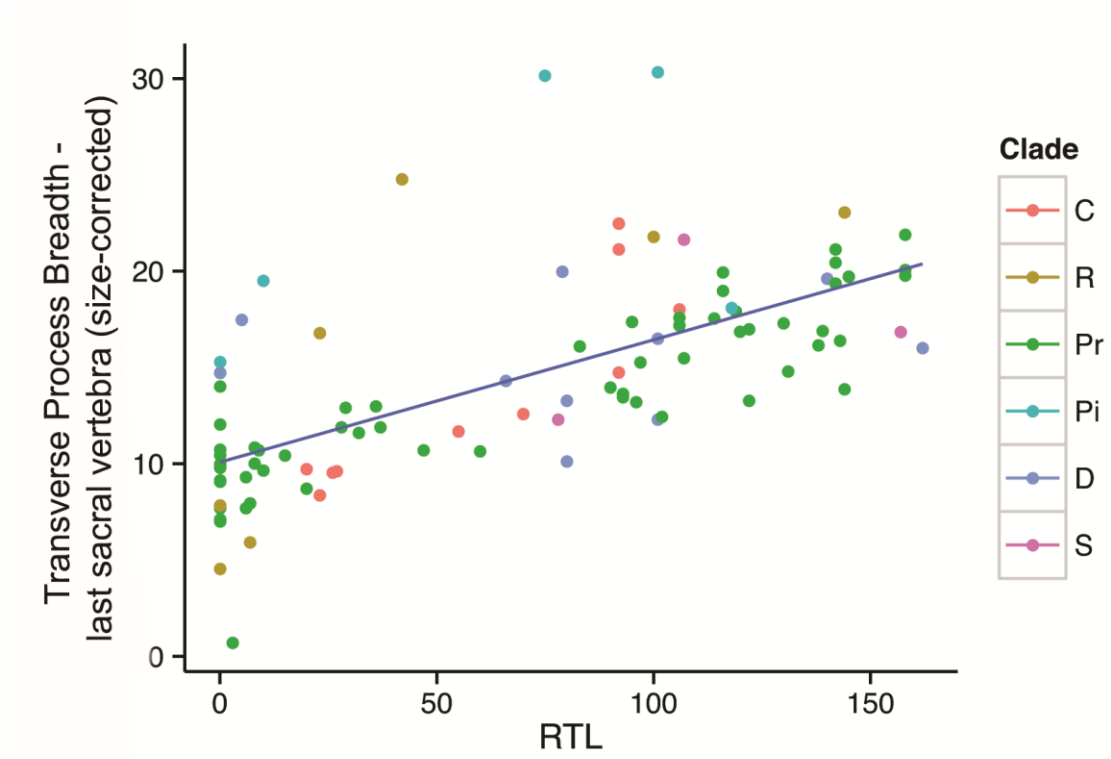

Figure 3.7 Transverse process breadth (size-corrected) of the last sacral vertebra on RTL in the extant mammal sample. Key to right of figure: C= Carnivora, R= Rodentia; Pr = Primates, Pi= Pilosa; D= Diprotodontia; S=Scandentia.

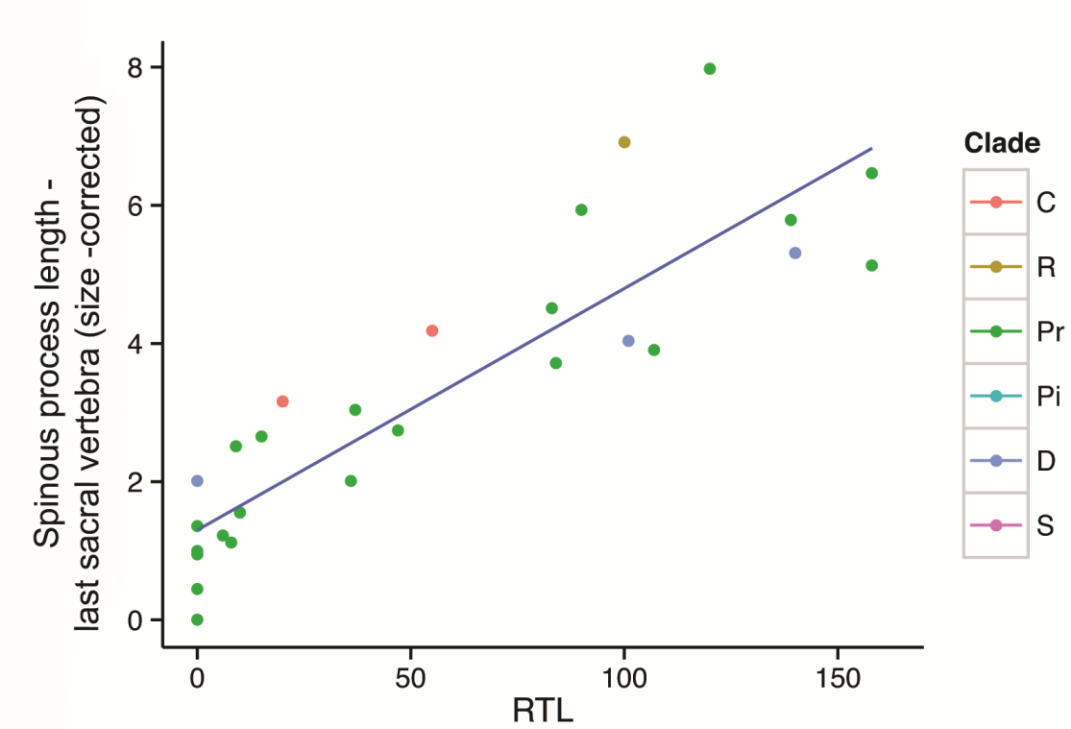

Figure 3.8 Spinous process length (size-corrected) of the last sacral vertebra on RTL in the extant mammal sample. Key to right of figure: C= Carnivora, R= Rodentia; Pr = Primates, Pi= Pilosa; D= Diprotodontia; S=Scandentia..

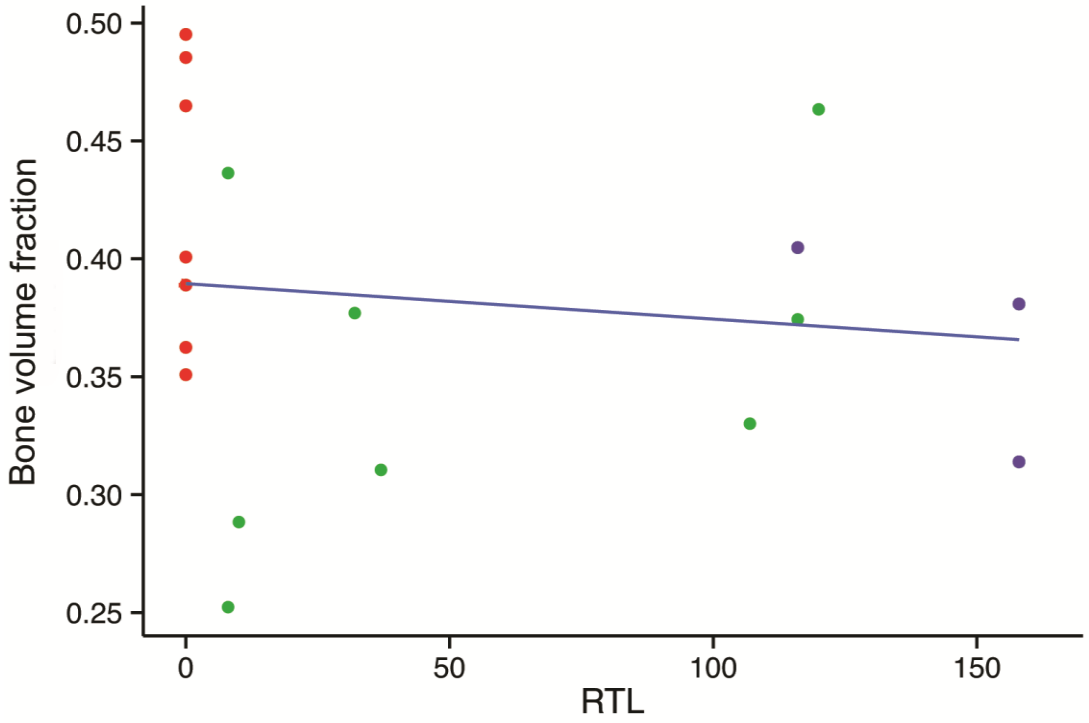

Figure 3.9 Bone volume fraction in the last sacral vertebra among extant primates. Red data points = hominoids, green data points = nonprehensile-tailed taxa, purple data points = prehensile-tailed taxa.

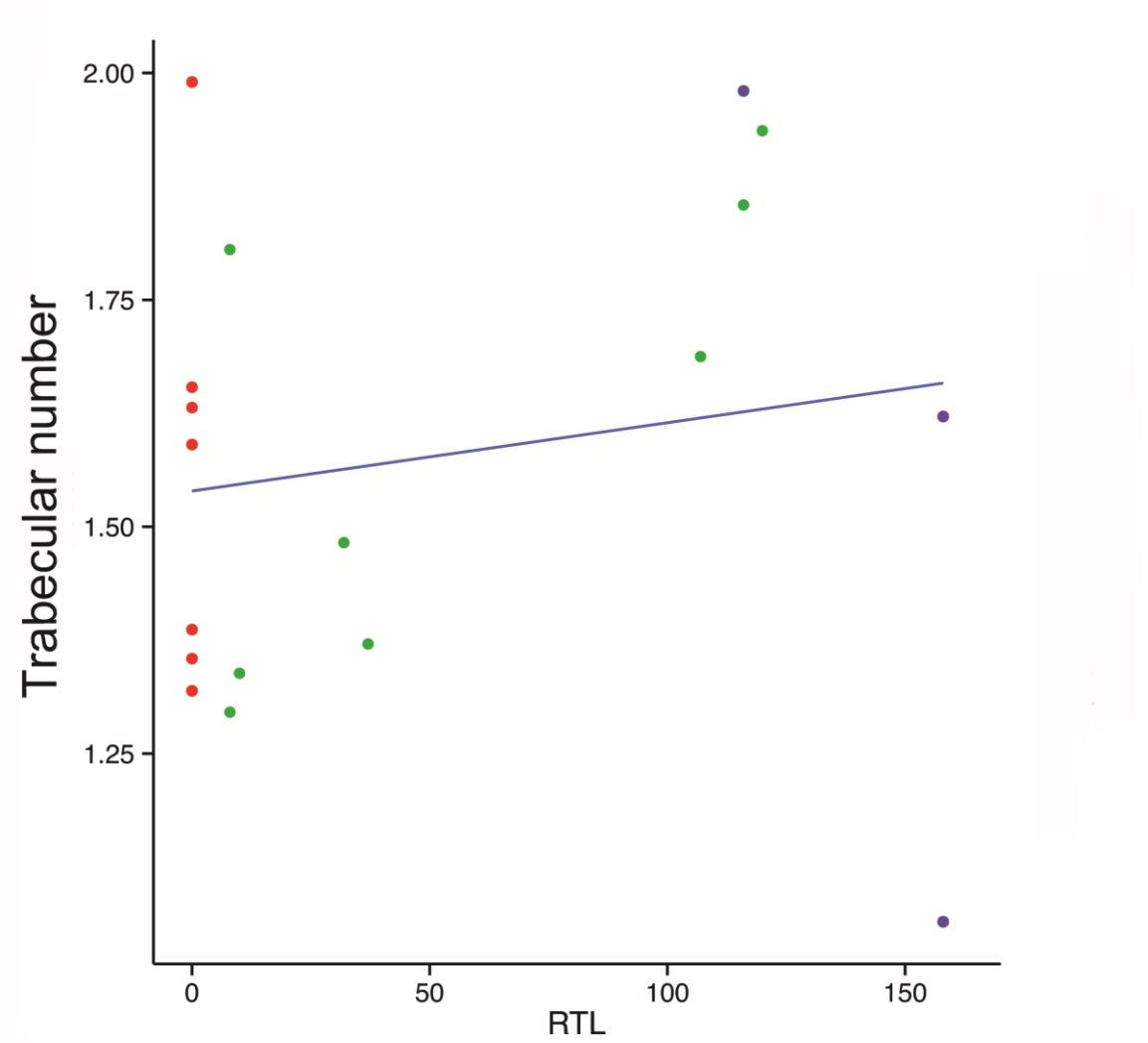

Figure 3.10 Trabecular number in the last sacral vertebra among extant primates. Red data points = hominoids, green data points = nonprehensile-tailed taxa, purple data points = prehensile-tailed taxa. Line fit to all data points.

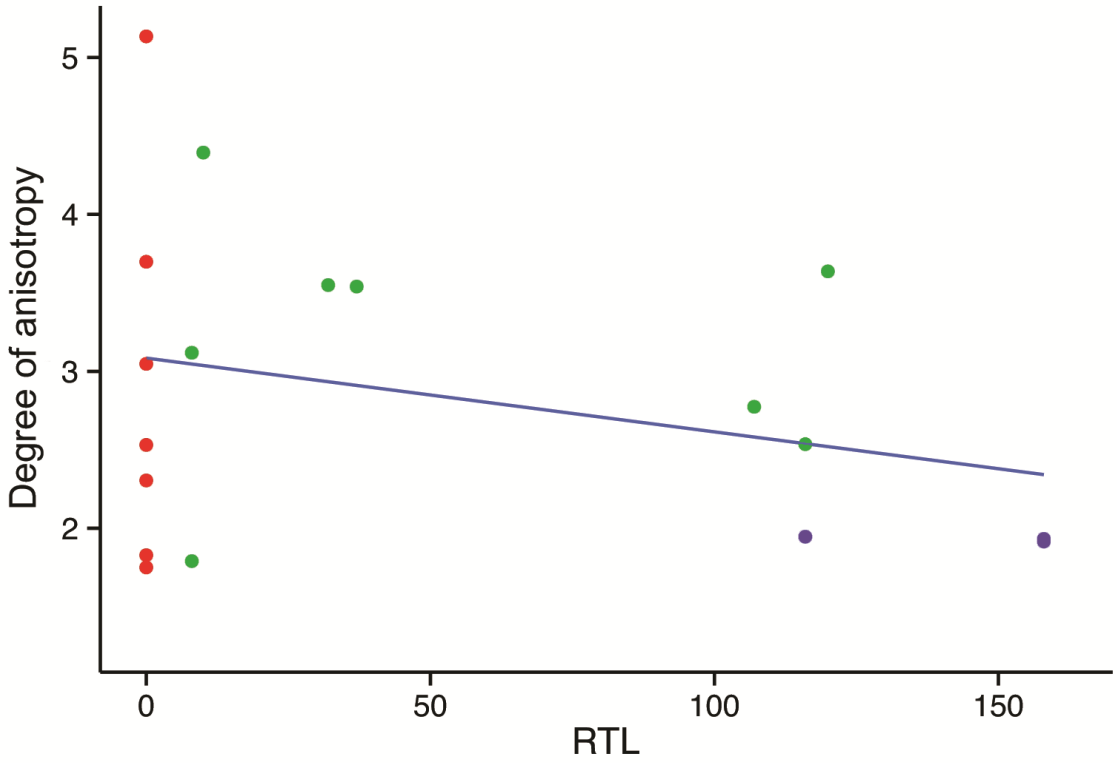

Figure 3.11 Degree of anisotropy in the last sacral vertebra in extant primates. Red data points = hominoids, green data points = nonprehensile-tailed taxa, purple data points = prehensile-tailed taxa.

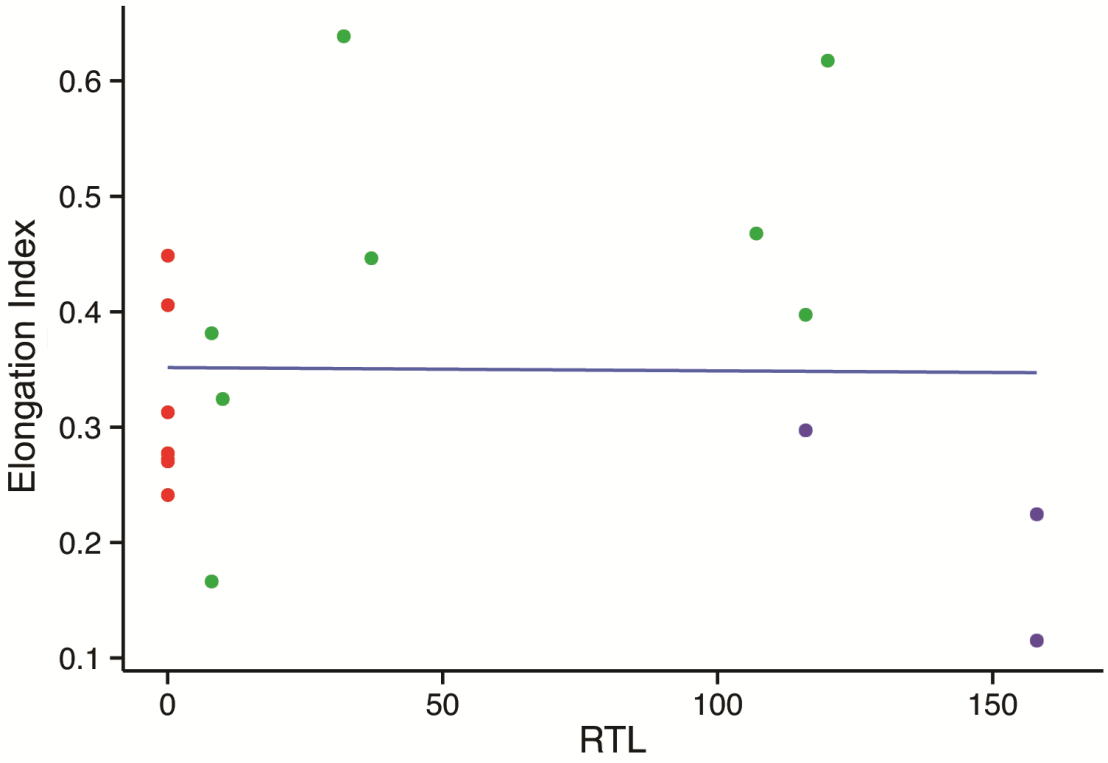

Figure 3.12 Elongation Index in the last sacral vertebra in extant primates. Red data points = hominoids, green data points = nonprehensile-tailed taxa, purple data points = prehensile-tailed taxa.

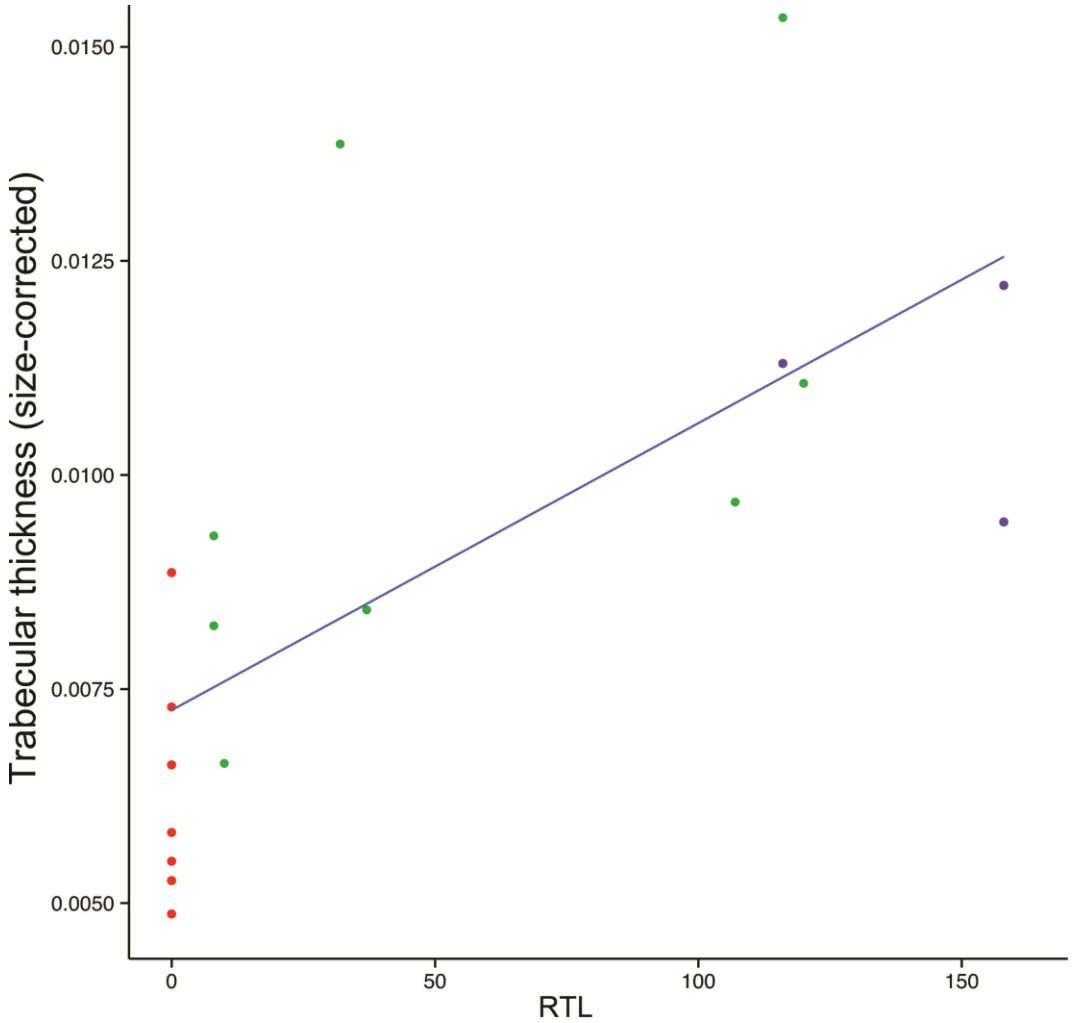

Figure 3.13 Trabecular thickness (size-corrected) in the last sacral vertebra in extant primates. Red datapoints = hominoids, green datapoints = nonprehensile-tailed taxa, purple datapoints = prehensile-tailed taxa.

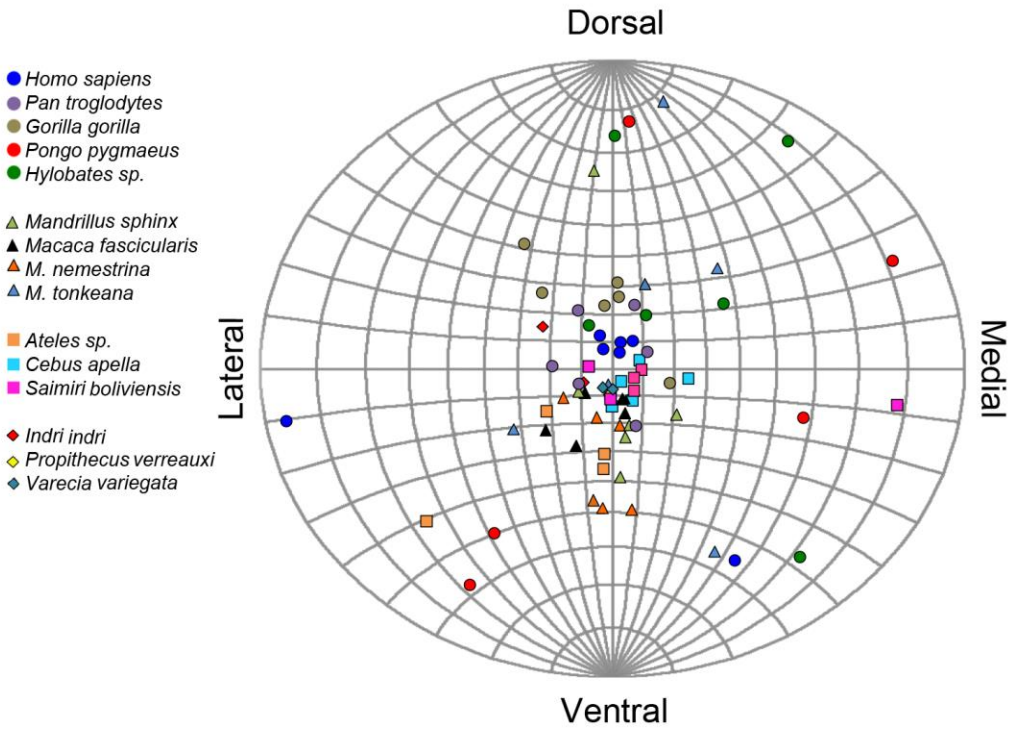

Figure 3.14A Equal-area stereographic projections illustrating the estimates of the primary (i.e., first) eigenvector [µ1] of the trabecular fabric in extant primates. Data toward the top and bottom of the sphere are indicative of more dorsoventral orientations, data toward the left and right of the sphere are indicative of more mediolateral orientations, and data toward the middle of the sphere (i.e., into the plot) are indicative of more craniocaudal orientations. Each point represents an individual.

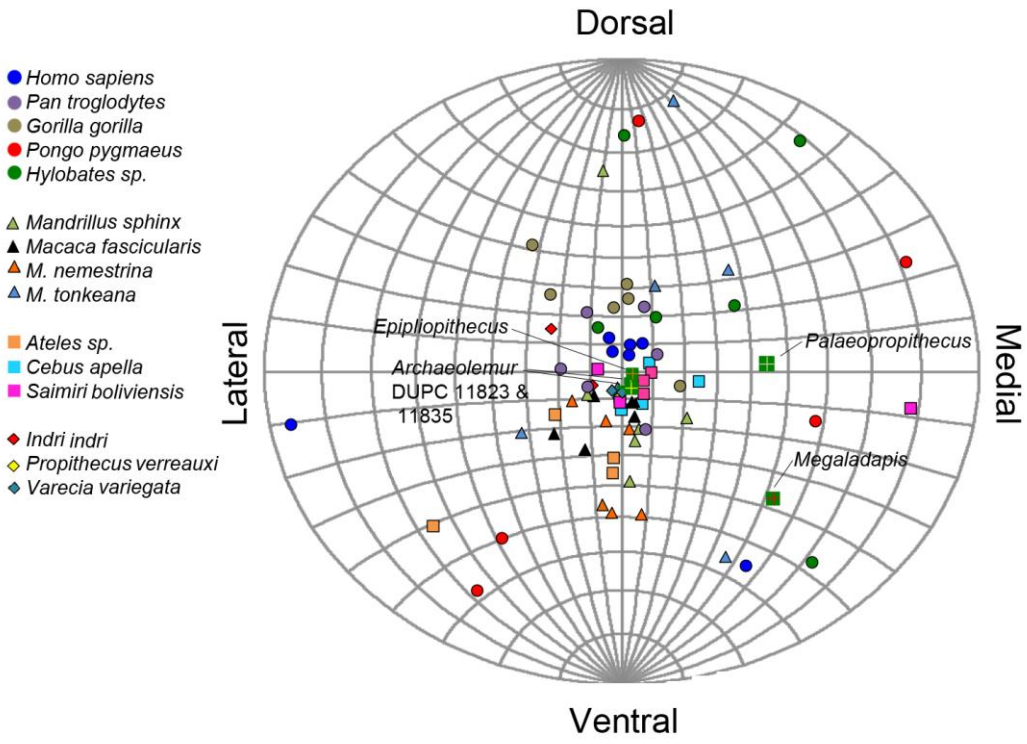

Figure 3.14B Equal-area stereographic projections illustrating the estimates of the primary (i.e., first) eigenvector [μ1] of the trabecular fabric in extant and extinct primates. Data toward the top and bottom of the sphere are indicative of more dorsoventral orientations, data toward the left and right of the sphere are indicative of more mediolateral orientations, and data toward the middle of the sphere (i.e., into the plot) are indicative of more craniocaudal orientations. Each point represents an individual.

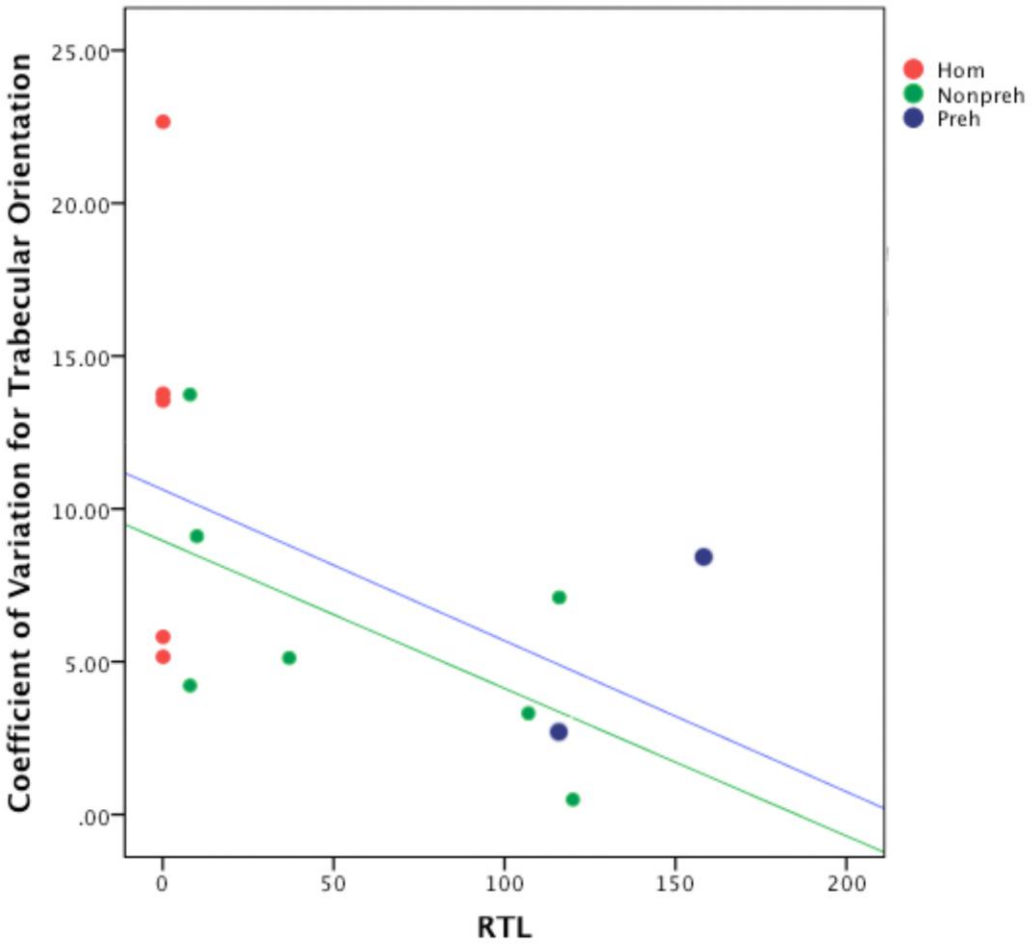

Figure 3.15 Bivariate plot of coefficient of variation for the first eigenvector of trabecular fabric structure on RTL in the last sacral vertebra. Red datapoints = hominoids, green datapoints = nonprehensile-tailed taxa, purple datapoints = prehensile-tailed taxa. Blue line represents trend among all taxa, and green line represents trend among nonprehensile-tailed taxa only.

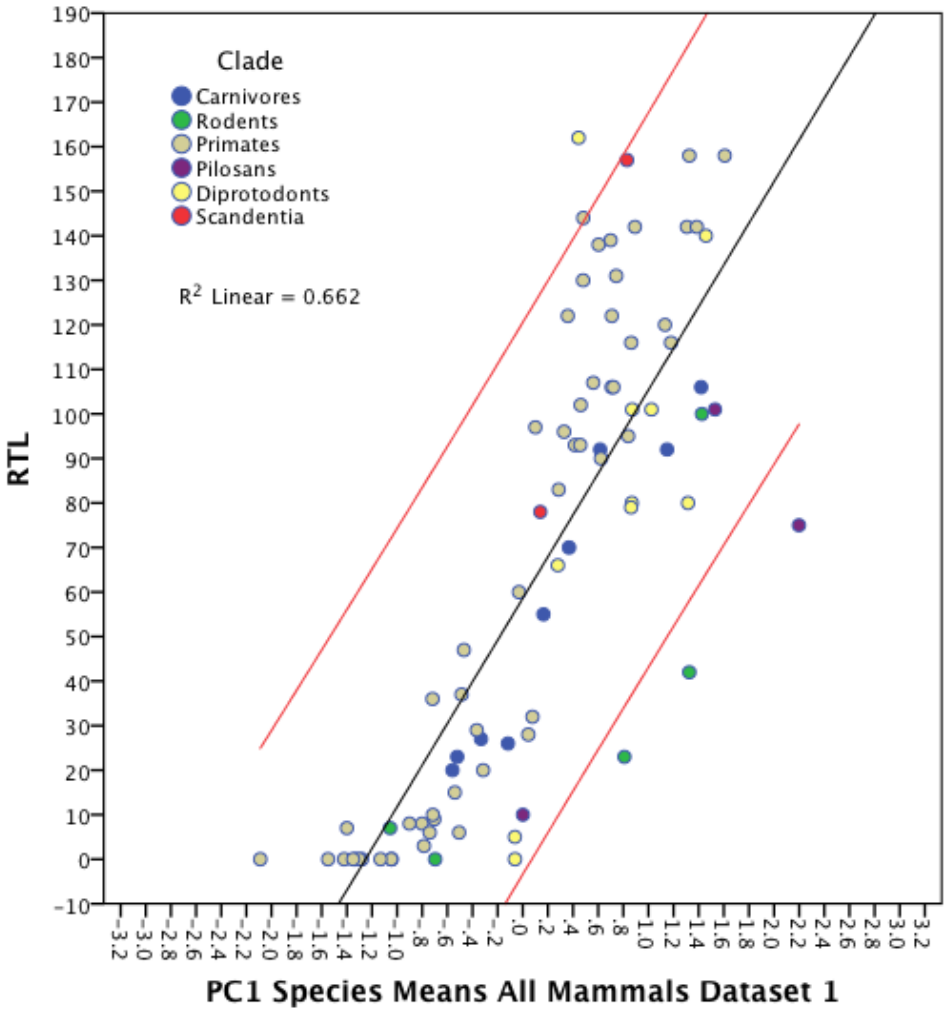

Figure 3.16A PC1 species mean scores for variables describing external sacral morphology (see Table 3.2) among all extant mammals in Dataset 1. 95% confidence intervals shown as red lines. $R^2 = 0.66$.

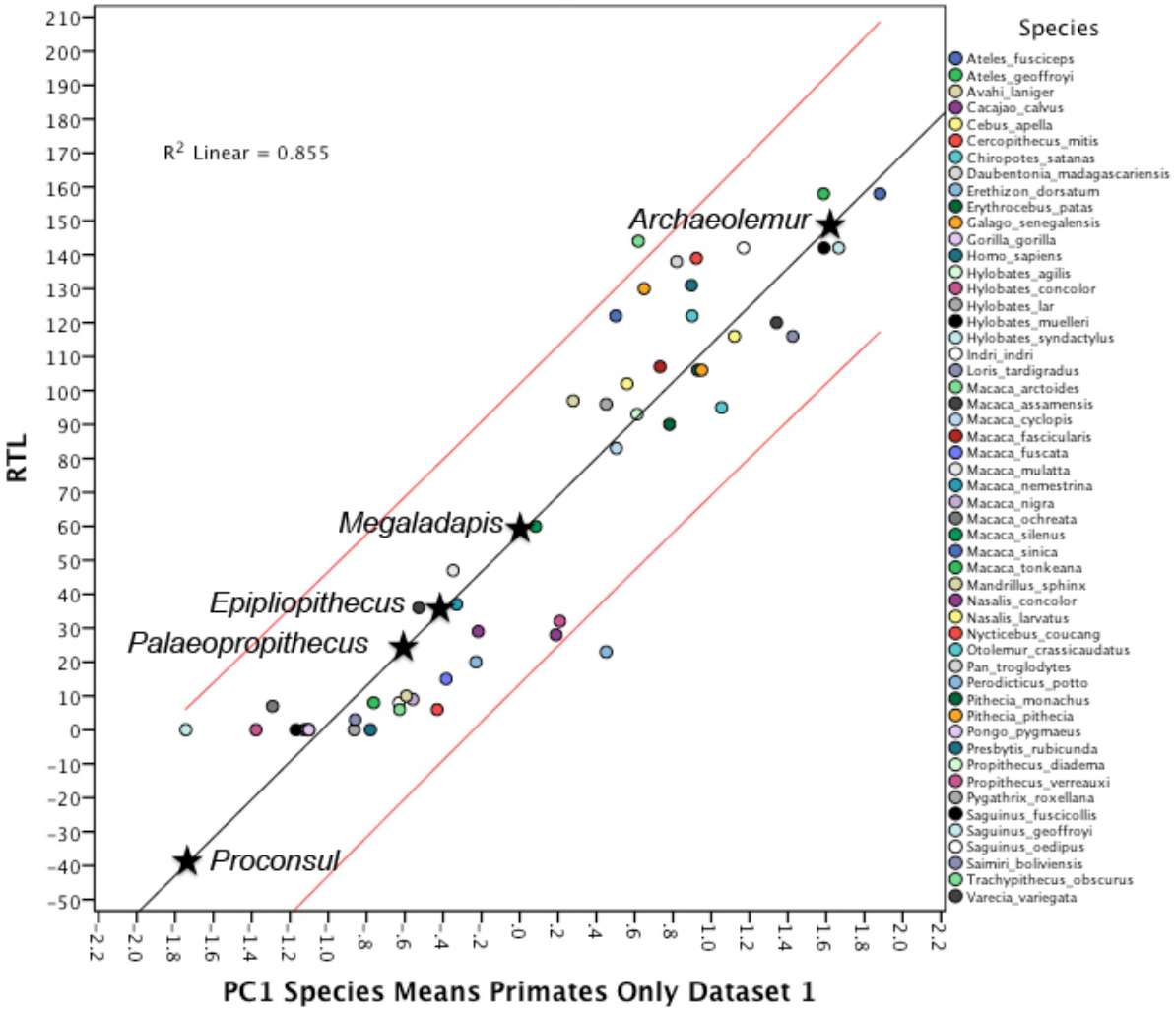

Figure 3.16B PC1 species mean scores for variables describing external sacral morphology (see Table 3.2) among all extant and extinct primates in Dataset 1. 95% confidence intervals shown as red lines. $R^2 = 0.86$.

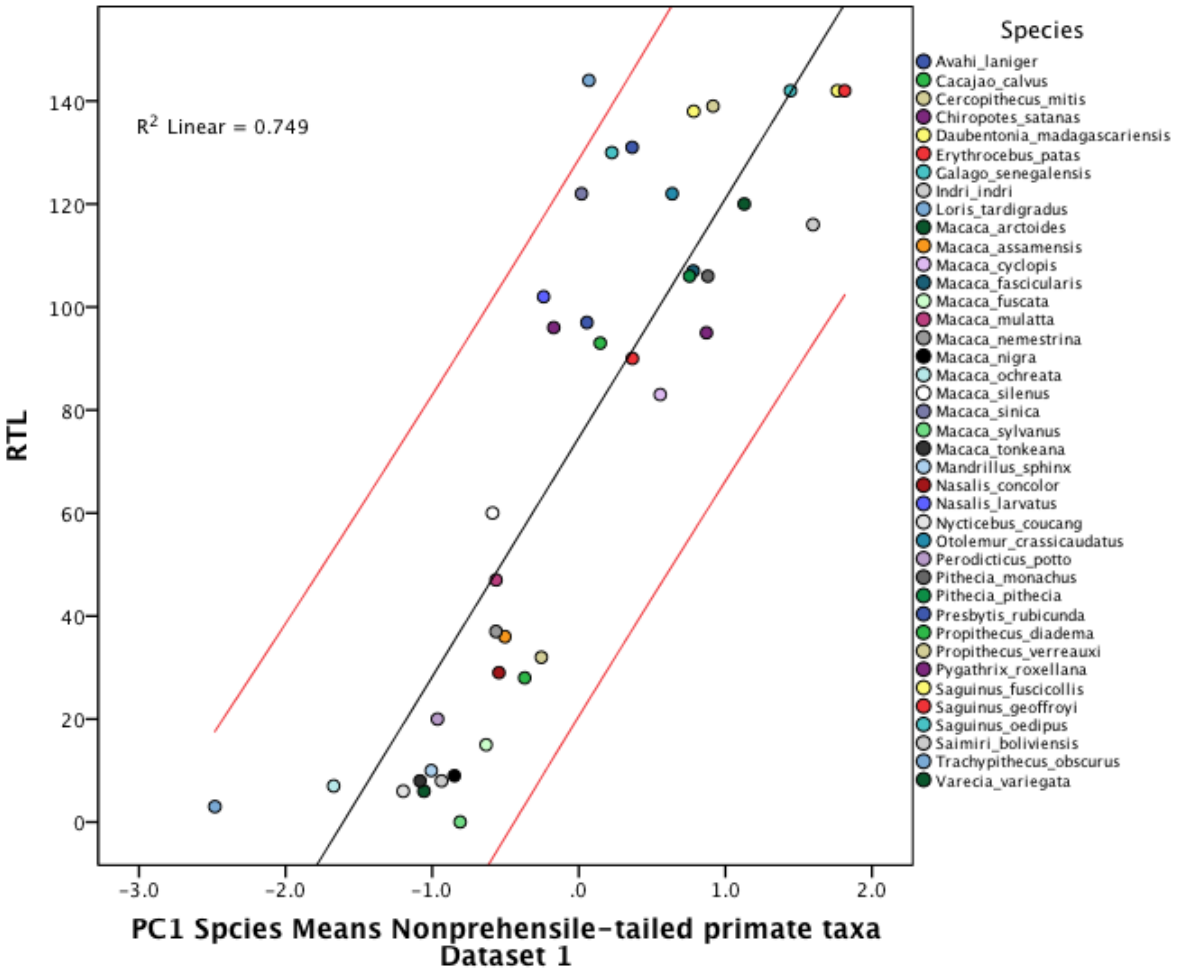

Figure 3.16C PC1 species mean scores for variables describing external sacral morphology (see Table 3.2) among extant nonprehensile-tailed primate taxa only in Dataset 1. 95% confidence intervals shown as red lines. $R^2 = 0.75$.

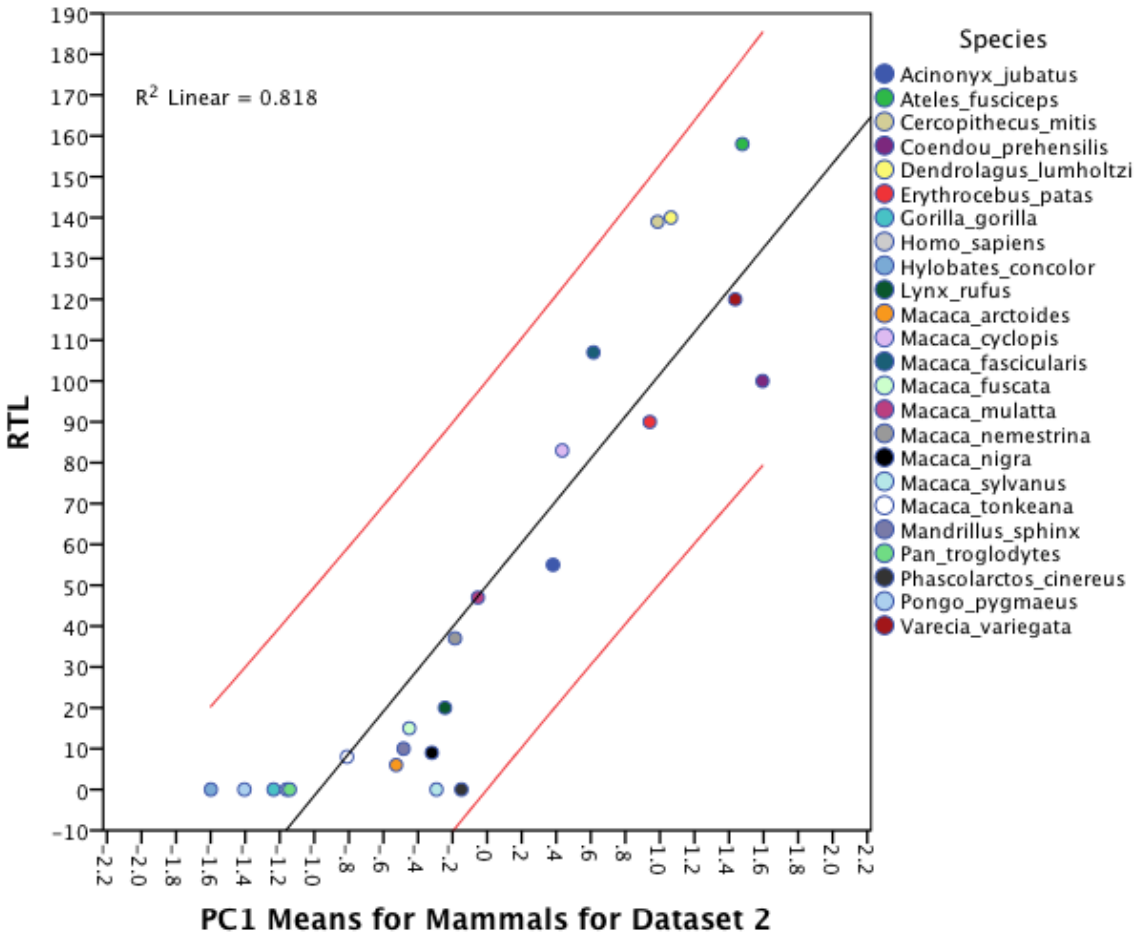

Figure 3.17A PC1 species mean scores for variables describing external sacral morphology (see Table 3.2) among all extant mammals in Dataset 2. 95% confidence intervals shown as red lines. $R^2 = 0.82$.

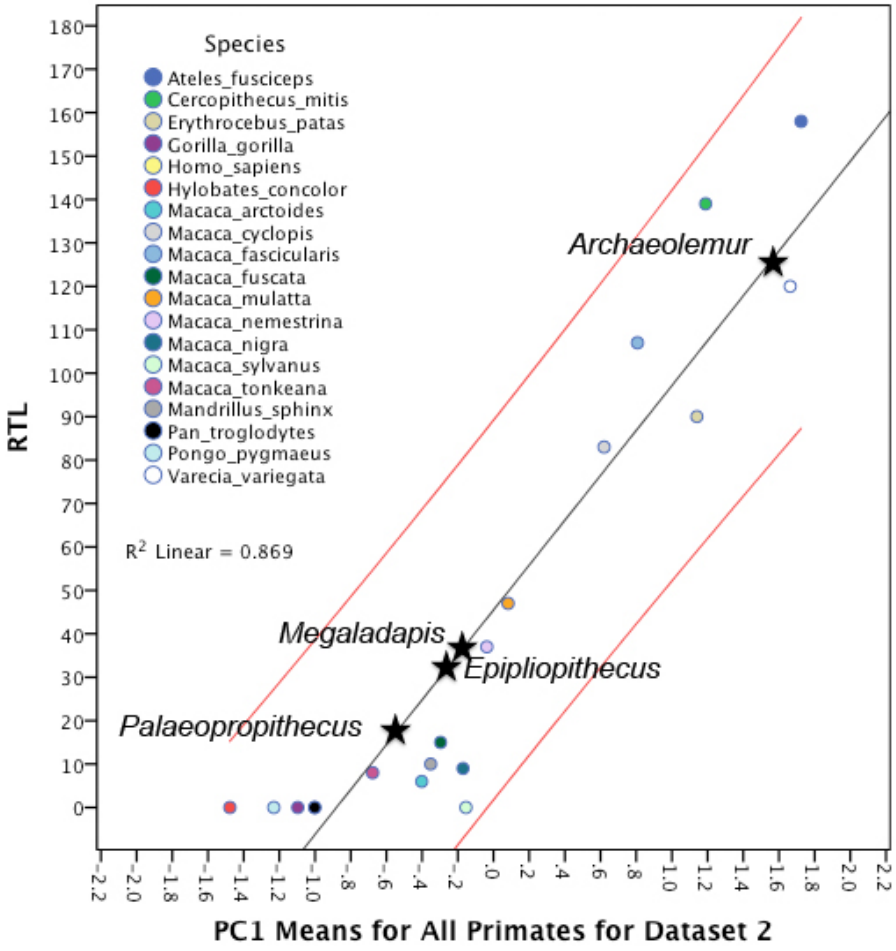

Figure 3.17B PC1 species mean scores for variables describing external sacral morphology (see Table 3.2) among all extant and extinct primates in Dataset 2. 95% confidence intervals shown as red lines. $R^2 = 0.87$.

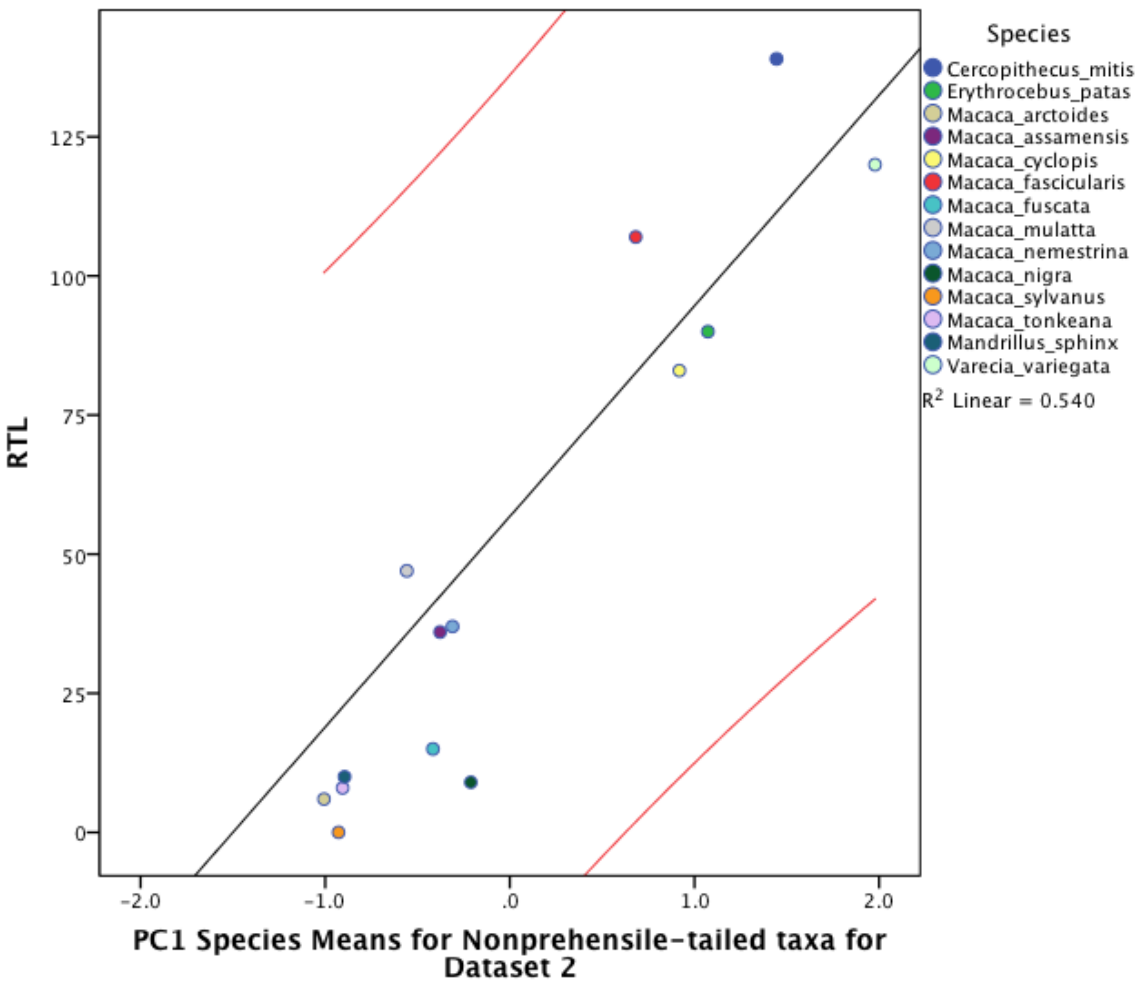

Figure 3.17C PC1 species mean scores for variables describing external sacral morphology (see Table 3.2) among extant nonprehensile-tailed primate taxa only in Dataset 2. 95% confidence intervals shown as red lines. $R^2 = 0.54$.

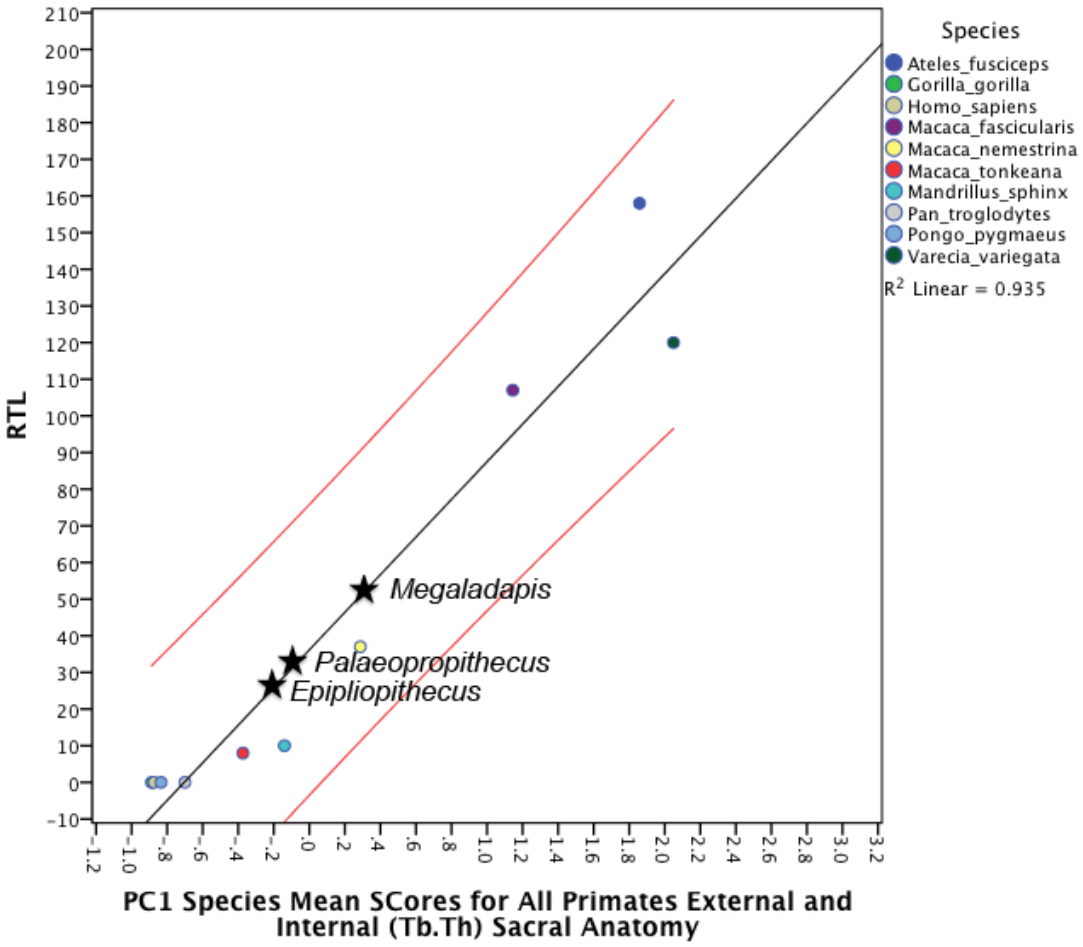

Figure 3.18A PC1 species mean scores for variables describing external and internal sacral morphology (see Table 3.2) among all extant and extinct primates. 95% confidence intervals shown as red lines. $R^2 = 0.94$.

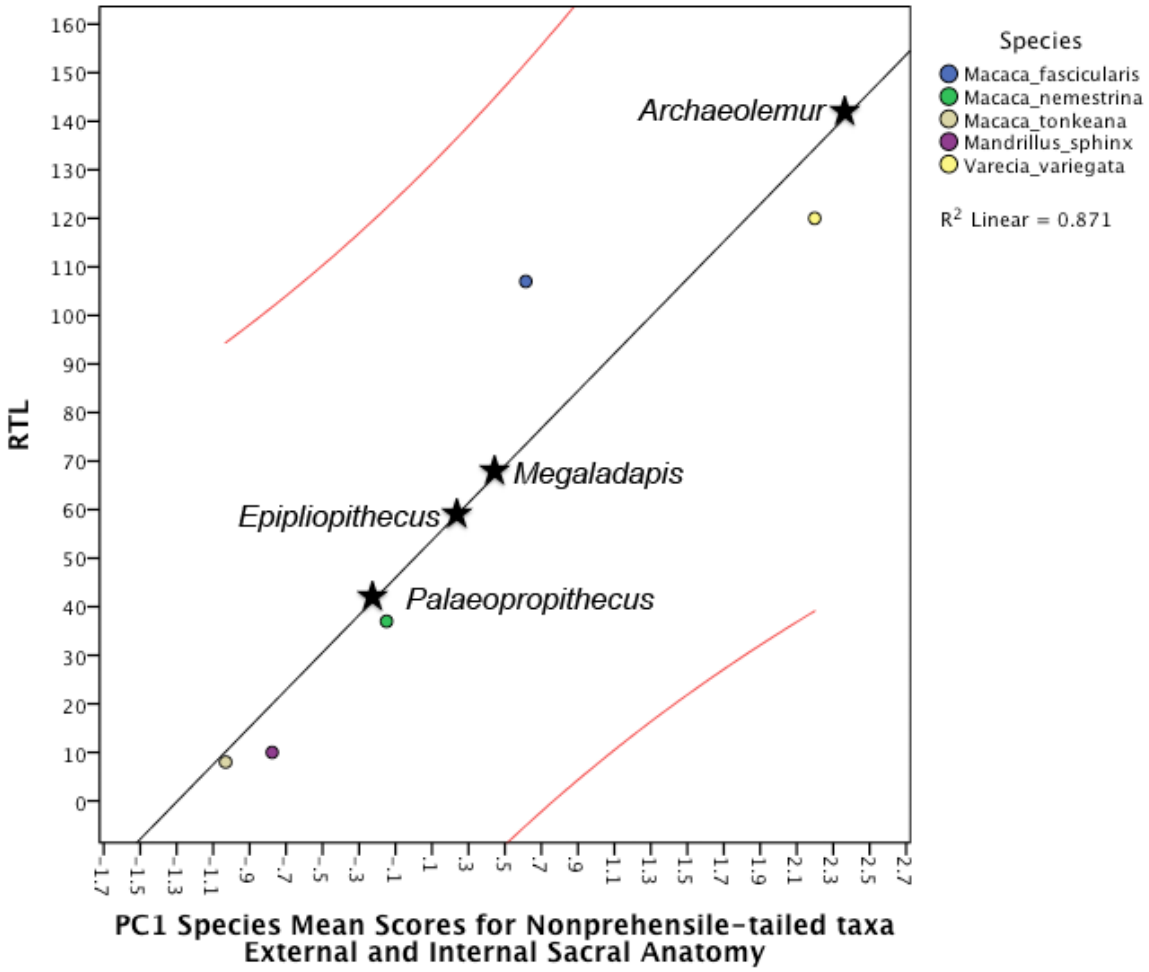

Figure 3.18B PC1 species mean scores for variables describing external and internal sacral morphology (see Table 3.2) among extant and extinct nonprehensile-tailed primate taxa only. 95% confidence intervals shown as red lines. $R^2 = 0.87$.

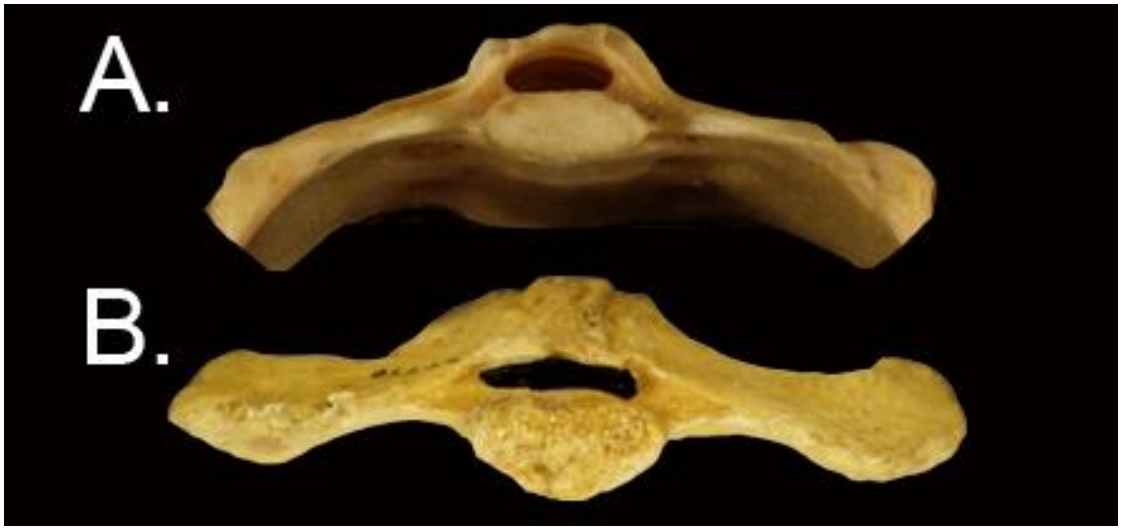

Figure 3.19 Comparison of distal sacral morphology between A) a living three-toed sloth (*Bradypus tridactylus*) and B) *Palaeopropithecus kelyus.* Images not to scale. Neural canal of *Palaeopropithecus* sacrum is filled-in black to facilitate comparison. Note the following shared anatomical features: dorsoventral compression of the caudal neural opening, and the extreme reduction of the spinous process. See text for description.

Table 3.1 Extant mammal sample for the study. In alphabetical order by Order, then Family, then Species.

Order	Family	Species[a]	N[b]	Mean (Range) no. sacral vertebrae	RTL[c]
Carnivora	Felidae	***Acinonyx jubatus***	6	3 (3)	55
		Lynx rufus	8	3 (3)	20
	Hyaenidae	*Crocuta crocuta*	2	4 (4)	27
	Viverridae	*Arctictis binturong*	3	3 (3)	92&
		Genetta servalina	2	3 (3)	92
		Genetta victoriae	1	3	92
		Nandinia binotata	2	3 (3)	106
		Arctonyx collaris	1	4	23
	Mustelidae	*Eira barbara*	2	3 (3)	70
		Gulo luscus	1	3	26
Diprotodontia	Macropodidae	*Dendrolagus goodfellowi*	1	3	101
		Dendrolagus lumholtzi	4	2 (2)	140
		Dendrolagus matschiei	4	2 (2)	101
		Macropus giganteus	3	2 (2)	80
		Macropus robustus	2	2 (2)	80
	Phascolarctidae	***Phascolarctos cinereus***	11	3 (3-4)	3 or 0
	Phalangeridae	*Caluromys lanatus*	2	2 (2)	162&
		Spilocuscus maculatus	3	2 (2-3)	93
		Trichosurus vulpecula	4	2 (2)	66&
	Potoroidae	*Potorous tridactylus*	1	3	79
	Vombatiidae	*Vombatus ursinus*	5	5 (4-5)	5
Pilosa		*Bradypus tridactylus*	10	6 (4-7)	10
		Choloepus didactylus	5	7 (6-7)	0
		Choloepus hoffmanni	2	7 (6-7)	0
		Cyclopes didactylus	3	4 (4-5)	118~&
		Myrmecophaga tridactyla	4	5 (5-6)	75
		Tamandua mexicana	7	5 (4-5)	101&
Primates	Atelidae	*Ateles belzebuth**	2 (2)	3 (3)	
		Ateles fusciceps*	6 (2)	3 (3-4)	158&
		Ateles geoffroyi	2	3 (3)	158&
	Callitrichidae	*Saguinus fuscicollis*	2	3 (3)	142

Table 3.1 continued....

	Saguinus geoffroyi	3	3 (3)	142
	Saguinus oedipus	1	3	142
Cebidae	***Sapajus apella****	8 (6)	3 (3)	107&
	Saimiri boliviensis*	11 (6)	3 (3)	116
Cercopithecidae	*Cercopithecus ascanius*	3	3 (2-3)	145
	Cercopithecus mitis	13	3 (2-3)	139
	Cercopithecus neglectus	2	3 (3)	119
	Chlorocebus aethiops	12	3 (2-3)	114
	Erythrocebus patas	4	3 (3-4)	90
	Lophocebus albigena	4	3 (3)	143
	Macaca arctoides	7	4 (3-4)	6
	Macaca assamensis	1	3	36
	Macaca cyclopis	1	3	83
	Macaca fascicularis*	24 (6)	3 (2-3)	107
	Macaca fuscata	5	3 (3-4)	15
	Macaca mulatta	11	3 (2-3)	47
	Macaca nemestrina*	14 (6)	3 (3)	37
	Macaca nigra	8	4 (3-4)	9
	Macaca ochreata	2	4 (3-4)	7
	Macaca silenus	3	3 (3)	60
	Macaca sinica	3	3 (3)	122
	Macaca sylvanus	2	3 (3)	0
	Macaca tonkeana*	9 (6)	3 (3-4)	8
	Mandrillus sphinx*	6 (6)	3 (3)	10
	Nasalis larvatus	5	3 (3)	102
	Nasalis (Simias) concolor	1	3	29
	Papio cynocephalus	6	3 (3)	84
	Presbytis rubicunda	2	3 (3)	131
	Pygathrix roxellana	3	4 (3)	96
	Trachypithecus obscurus	2	3 (3)	144
Daubentoniidae	*Daubentonia madagascariensis*	1	3	138
Galagidae	*Galago senegalensis*	7	3 (3)	130
	Otolemur crassicaudatus	6	3 (3)	122
Hominidae	***Gorilla gorilla****	14 (6)	6 (5-7)	0
	Homo sapiens*	7 (7)	5 (5-6)	0
	*Hylobates agilis****	2 (2)	5 (4-5)	0
	Hylobates concolor	4	5 (4-6)	0
	*Hylobates hoolock****	3 (2)	5 (4-5)	0
	*Hylobates lar****	4 (2)	4 (3-4)	0

Table 3.1 continued....

		Hylobates muelleri	3	4 (3-5)	0
		Hylobates syndactylus	5	4 (4-5)	0
		Pan troglodytes*	27 (6)	6 (5-7)	0
		Pongo pygmaeus*	13 (5)	5 (4-6)	0
	Indriidae	***Indri indri****	2 (2)	4 (3-4)	8
		Propithecus diadema	1	3	93
		Propithecus verreauxi*	6 (1)	3 (3-4)	32
	Lemuridae	*Avahi laniger*	1	3	96
		Varecia variegata*	2 (2)	3 (2-3)	120
	Lorisidae	*Loris tardigradus*	2	5 (4-6)	3
		Nycticebus coucang	10	6 (5-8)	6
		Perodicticus potto	7	5 (4-6)	20
	Pitheciidae	*Cacajao calvus*	2	5 (4-5)	28
		Chiropotes satanas	5	3(3)	95
		Pithecia monachus	3	3 (3)	106
		Pithecia pithecia	4	3 (3)	106
Rodentia	Castoridae	*Castor canadensis*	7	4 (3-5)	42
		Aplodontia rufa	4	5 (5)	7
	Caviidae	*Cavia porcellus*	5	4 (3-4)	0
		Hydrochaeris hydrochaeris	6	4 (3-4)	0
	Erethizontidae	***Coendou prehensilis***	6	3 (3-4)	91&
		Erethizon dorsatum	3	3 (3)	23
	Heteromyidae	*Dipodomys merriami*	6	5 (4-5)	144
Scandentia		*Tupaia glis*	1	3	157
		Tupaia gracilis	1	3	107
		Tupaia tana	5	3 (2-3)	78
		Total	**472 (75)**		

[a] boldface indicates that species is part of Dataset#2; asterisks indicates that species is part of trabecular bone study
[b] Number in parentheses denotes the trabecular bone study sample size for this species
[c] Data compiled from: Miller, 1900; Martin, 1968; Fooden, 2006, 2007; Wilson, 1972; Napier, 1981; Fa, 1985, 1989; Procter Gray and Ganslosser, 1986; Fooden and Albrecht, 1999; Jenkins, 1990; Parker, 1990; Nowak, 1991; Rowe, 1996; Francis, 2008
N = maximum number of individuals sampled per taxon
& = prehensile tail

Table 3.2 Values for variables and predicted RTLs for extinct primates. s-c = size-corrected.

Taxon	Sacral Index	Degree of Tapering	CAS shape index	CAS area (s-c)	Transverse Process breadth (s-c)	Spinous process length (s-c)	Trab-ecular thickness (raw)	BV/ TV	Predicted RTL range[1]
***Archaeolemur* (DPC 9905)**	61	-45.00	1.31	36.83	NA	7.48	NA	NA	NA
***Archaeolemur* (DPC 11823)**	59	-23.00	1.35	33.07	18.73	7.52	0.23	0.39	126 – 148
***Archaeolemur* (DPC 11835)**	130	NA	1.20	25.77	16.79	NA	0.19	0.34	NA
Paleopropithecus kelyus	26	17.11	1.93	5.87	15.57	1.34	0.20	0.38	18 – 42
Megaladapis	30	16.67	1.81	10.79	20.77	1.31	0.28	0.36	38 – 68
Epipliopithecus vindobonensis	55	7.06	2.56	11.69	14.36	3.15	0.06	0.16	29 – 58
Proconsul	NA	29.30	2.14	2.02	3.90	NA	NA	NA	-38 (i.e., 0)

[1]Predicted RTL range values represent lower and upper values derived from the regression models. They do not include the standard error of the estimate (SEE) used to determine 95% confidence limits for *each* lower and upper value. See text for descriptions of which models values are derived from. See also Table 3.6 for SEE values.

Table 3.3 PGLS regression results for external sacral morphometric variables on RTL. Boldfaced text indicates significant result.

All Mammals	Body mass slope	Body mass p-value	λ	RTL slope	RTL p-value	Adjusted R-squared	p-value (model)	Included in PCA?
Sacral Index	-7.993	0.071	0.000	4.851	**<0.001**	0.519	**<0.001**	**Y**
Degree of tapering	0.330	0.731	0.328	-2.219	**<0.001**	0.269	**<0.001**	**Y**
CAS Shape Index	-0.029	0.535	0.685	-0.119	**<0.001**	0.284	**<0.001**	**Y**
CAS Area	-0.694	0.272	0.926	1.639	**<0.001**	0.296	**<0.001**	**Y**
Transverse Process Breadth	-1.265	**<0.001**	0.973	0.675	**<0.001**	0.307	**<0.001**	**Y**
Spinous Process Length	-0.298	0.370	0.854	0.443	**<0.001**	0.558	**<0.001**	**Y**
Primates	Body mass slope	Body mass p-value	λ	RTL slope	RTL p-value	Adjusted R-squared	p-value (model)	Included in PCA?
Sacral Index	-4.521	0.382	0.000	5.412	**<0.001**	0.596	**<0.001**	**Y**
Degree of tapering	2.165	0.126	0.173	-2.482	**<0.001**	0.320	**<0.001**	**Y**
CAS Shape Index	-0.063	0.468	0.685	-0.131	**<0.001**	0.223	**<0.001**	**Y**
CAS Area	-1.162	0.210	0.903	1.660	**<0.001**	0.325	**<0.001**	**Y**
Transverse Process Breadth	-1.271	**0.011**	0.943	0.678	**<0.001**	0.335	**<0.001**	**Y**
Spinous Process Length	-0.421	0.328	0.884	0.453	**<0.001**	0.541	**<0.001**	**Y**
Nonprehensile-tailed primate taxa	Body mass slope	Body mass p-value	λ	RTL slope	RTL p-value	Adjusted R-squared	p-value (model)	Included in PCA?
Sacral Index	-5.200	0.612	0.000	2.990	0.199	0.044	0.313	N
Degree of tapering	2.820	0.105	0.000	-1.961	0.083	0.148	**0.010**	N
CAS Shape Index	0.075	0.194	0.871	-0.030	0.135	0.085	0.053	N
CAS Area	-2.821	**0.024**	0.715	1.654	**<0.001**	0.377	**<0.001**	**Y**
Transverse Process Breadth	-2.326	**<0.001**	0.908	0.709	**<0.001**	0.497	**<0.001**	**Y**
Spinous Process Length	-1.564	**0.023**	1.000	0.341	**0.007**	0.620	**<0.001**	**Y**

Table 3.4 PGLS regression results for internal sacral morphometric variables on RTL. Boldfaced text indicates significant result.

Primates	Body mass slope	Body mass p-value	λ	RTL slope	RTL p-value	Adjusted R-squared	p-value (model)	Included in PCA?
BV/TV	0.007	0.663	0.528	-0.007	0.249	0.046	0.279	N
Tb.N	-0.170	**0.006**	0.000	-0.025	0.125	0.339	**0.010**	N
DA	-0.296	0.236	0.000	-0.075	0.307	-0.020	0.497	N
E	-0.046	0.196	0.000	0.005	0.765	0.047	0.276	N
Tb.Th (size-corrected)	-0.001	**<0.000**	0.000	0.005	**0.012**	0.287	**0.004**	**Y**

Nonprehensile-tailed primate taxa	Body mass slope	Body mass p-value	λ	RTL slope	RTL p-value	Adjusted R-squared	p-value (model)	Included in PCA?
BV/TV	0.005	0.882	1.000	0.024	**0.041**	0.450	**0.029**	**Y**
Tb.N	-0.157	0.221	0.477	0.119	0.091	0.304	0.077	N
DA	0.792	0.092	0.000	0.485	0.192	0.250	0.211	N
E	0.043	0.589	0.000	0.080	0.095	0.294	0.082	N
Tb.Th (size-corrected)	-0.003	**0.013**	0.000	0.001	0.095	0.347	**0.085**	N

Table 3.5 Summary of principal components analyses

	Dataset	PC1 %	Eigenvalue
External sacral morphology	All Mammals Dataset #1	61.461	2.458
	Dataset #2	70.67	4.240
	Primates Dataset #1	65.272	2.611
	Dataset #2	70.786	4.247
	Nonprehensile-tailed taxa		
	Dataset #1	91.834	1.837
	Dataset #2	88.525	2.656
External sacral morphology + internal sacral morphology	Primates (All external variables & size-corrected Tb.Th)	69.224	4.846
	Nonprehensile-tailed primate taxa (CAS area, transverse process breadth, spinous process length & BV/TV)	73.701	2.948

Table 3.6 Least-squares regression coefficients and model summaries for RTL on PC1 species mean scores.

Dataset		R^2	Adjusted R^2	Pearson's *r*	SEE	slope	constant
External morphology	All Mammals Dataset #1	0.66	0.67	0.81	30.94	46.80	58.59
	Dataset #2	0.82	0.81	0.91	23.63	51.59	50.10
	Primates Dataset #1	0.86	0.85	0.92	21.80	55.92	57.77
	Dataset #2	0.87	0.86	0.93	20.19	51.67	45.48
	Nonprehensile-tailed taxa Dataset #1	0.75	0.74	0.87	26.39	46.43	74.63
	Dataset #2	0.54	0.51	0.74	35.55	37.85	56.79
External sacral morphology + internal sacral morphology	Primates (All external variables & Tb.Th)	0.94	0.93	0.97	16.38	51.32	36.16
	Nonprehensile-tailed primate taxa (CAS area, transverse process breadth, spinous process length & BV.TV)	0.87	0.83	0.93	22.26	38.46	49.82

REFERENCES

Abitbol, M. 1989. Sacral curvature and supine posture. Am. J. Phys. Anthropol. 80, 379–89.

Andrews, P. 1992. Evolution and environment in the Hominoidea. Nature 360, 641.

Ankel, F., 1965. Der canalis sacralis als indikator für die länge der caudal region der primaten. Folia Primatol. 3, 263-276.

Ankel, F., 1972. Vertebral morphology of fossil and extant primates. In: Tuttle, R.(Ed.), The Functional and Evolutionary Biology of Primates. Aldine, Chicago, pp. 223-240.

Begun, D.R., Ward, C.V., Rose, M.D., 1997. Events in hominoid evolution. In: Begun, D.R.,Ward, C.V., Rose, M.D. (Eds.), Function, Phylogeny, and Fossils: Miocene Hominoid Evolution and Adaptations. Plenum Press, New York, pp. 389-416.

Begun, D., Teaford, M., Walker, A., 1994. Comparative and functional anatomy of *Proconsul* phalanges from the Kaswanga primate site, Rusinga Island, Kenya. J. Hum. Evol. 26, 89-165.

Bernstein, P., Smith, W., Krensky, A., and Rosene, K. 1978. Tail positions of *Cercopithecus aethiops*. Zeitschrift für Tierpsychologie 46, 268–278.

Bezanson, M.F. 2004. Ontogenetic influences on prehensile-tail use in *Cebus capucinus.* Am. J. Phys. Anthropol. 123:63.

Bezanson, M.F. 2005. Leap bridge or ride? Ontogenetic influences on positional behavior in Cebus and Alouatta. In: Estrada A, Garber PA, Pavelka MSM, Luecke L, editors. New perspectives in the study of Mesoamerican primates: distribution, ecology, behavior and conservation. New York: Springer. p 333–348.

Bezanson, M.F. 2006. Ontogenetic patterns of positional behavior in Cebus capucinus and Alouatta palliata. PhD dissertation, University of Arizona, Tucson, AZ.

Bezanson MF. 2009. Life history and locomotion in *Cebus capucinus* and *Alouatta palliata*. Am. J. Phys .Anthropol. 140,508– 517.

Bininda-Emonds, O.R.P., Cardillo, M., Jones, K.E., MacPhee, R.D.E., Beck, R.M.D., Grenyer, R., Price, S.A., Vos, R.A., Gittleman, J.L., and Purvis, A. 2007. The delayed rise of present-day mammals. Nature 446, 507–512.

Buck, C., Tolman, N., Tolman, W., 1925. The tail as a balancing organ in mice.

J. Mammal 6, 267-271.

Chang, H.T., and Ruch, T.C. 1947. Morphology of the spinal cord, spinal nerves, caudal plexus, tail segmentation, and caudal musculature of the spider monkey. The Yale Journal of Biology and Medicine 19, 345-377.

Coleman, M.N., and Colbert, M.W. 2007. Technical note: CT thresholding protocols for taking measurements on three-dimensional models. Am. J. Phys. Anthropol. 133, 723–725.

Cotter, M.M., Simpson, S.W., Latimer, B.M., and Hernandez, C.J. 2009. Trabecular microarchitecture of hominoid thoracic vertebrae. Anat. Rec. 292, 1098–1106.

Cotter, M.M., Loomis, D.A., Simpson, S.W., Latimer, B.,Hernandez, C.J. 2011. Human evolution and osteoporosis-related spinal fractures. PLoS ONE 6, e26658.

Deinard, A., and Smith, D.G. 2001. Phylogenetic relationships among the macaques: evidence from the nuclear locus NRAMP1. J. Hum. Evol. 41,45–59.

Demes, B., Jungers, W.L., Fleagle, J.G., Wunderlich, R.E., Richmond, B.G., and Lemelin P. 1996. Body size and leaping kinematics in Malagasy vertical clingers and leapers. J. Hum. Evol. 31,367–388.

Doube, M., Klosowski, M.M., Wiktorowicz-Conroy, A.M.,Hutchinson, J.R., Shefelbine S.J. 2011 Trabecular bone scales allometrically in mammals and birds. Proc. R. Soc.B 278, 3067–3073.

Elftman, H., 1932. The evolution of the pelvic floor of primates. Am. J. Anat. 51, 307-346.

Emerson, S.B., 1985. Jumping and leaping. In: Hildebrand, M., Bramble, D.M., Liem, K.F., Wake, D.B. (Eds.), Functional Vertebrate Morphology. Belknap Press, Cambridge, pp. 58e72.

Emmons, L.H., and Gentry, A.H. 1983. Tropical forest structure and the distribution of gliding and prehensile-tailed vertebrates. Am. Nat. 121,513–524.

Essner, Jr., R.L., 2002. Three-dimensional launch kinematics in leaping, parachuting and gliding squirrels. J. Exp. Biol. 205, 24-69.

Fa, J.E., 1985. Baby care in barbary macaque. In: Macdonald, D. (Ed.), Primates. Torstar Books, New York, pp. 92-93.

Fa, J.E., 1989. The genus *Macaca*: a review of taxonomy and evolution. Mammal Rev.

19, 45-81.

Fajardo, R.J., and Müller, R. 2001. Three dimensional analysis of nonhuman primate trabecular architecture using micro computed tomography. Am. J. Phys. Anthropol. 115,327–336.

Fajardo,R.J., Desilva, J.M., Manoharan, R.K., Schmitz, J.E., Maclatchy, L.M., and Bouxsein, M.L. 2013. Lumbar Vertebral Body Bone Microstructural Scaling in Small to Medium-Sized Strepsirhines. Anat. Rec. 296, 210–226.

Fleagle, J.G. 1984. Size and adaptation in primates. In: Jungers WL, editor. Size and scaling in primate biology. New York: Plenum Press. p 1–19.

Fleagle, J.G. 2013. Primate Adaptation and Evolution: 3rd Edn. Academic Press.

Fooden, J. 1988. Taxonomy and evolution of the sinica group of macaques: 6. Interspecific comparisons and synthesis. Fieldiana Zool 45:1–44

Fooden, J., 1997. Tail length variation in Macaca fascicularis and M. mulatta. Primates 38, 221-232

Fooden, J., Albrecht, G.H., 1999. Tail length evolution in fascicularis group macaques (Cercopithecidae: Macaca). Int. J. Primatol. 20, 431-440.

Fooden, J., 2006. Comparative review of fascicularis-group species of macaques (Primates: Macaca). Fieldiana Zool. 107, 1-44.

Fooden, J., 2007. Systematic review of the barbary macaque, Macaca sylvanus (Linnaeus, 1758). Fieldiana Zool. 113, 1-58.

Francis, C.M., 2008. A Field Guide to the Mammals of Southeast Asia. New Holland.

Freckleton, R.P, Harvey, P.H., and Pagel, M. 2002. Phylogenetic analysis and comparative data: a test and review of evidence. Am. Nat. 160,712–726.

Garber, P.A., and Rehg, J.A. 1999. The ecological role of the prehensile tail in white-faced capuchins (*Cebus capucinus*). Am. J. Phys. Anthropol. 110,325–339.

Gebo, D.L. 1992. Locomotor and postural behavior in *Alouatta palliata* and *Cebus capucinus*. *Am. J. Primatol*. 26,277–290.

German, R.Z. 1982. The functional morphology of caudal vertebrae in New World monkeys. Am. J. Phys. Anthropol. 58,453–459.

Gibson, L.J. 1985. The mechanical behaviour of cancellous boneJ. Biomech. 18,317.

Godfrey, L.R., and Jungers, W.L. 2002. Quaternary Fossil Lemurs. In The Primate Fossil Record. W. Hartwig (ed.). Cambridge: Cambridge University Press, pp. 97-121.

Godfrey, L.R., and Jungers, W.L. 2003. The extinct sloth lemurs of Madagascar. Evo. Anthropol. 12,252–263.

Godfrey, L.R., Jungers, W.L., Simons, E.L., Chatrath, P.S. and Berthe Rakotosamimanana. 1999. Past and present distributions of lemurs in Madagascar. In B. Rakotosamimanana, H. Rasaminmanana, J. Ganzhorn, and S. Goodman. (Eds.) New Directions in Lemur Studies. New York: Plenum Press. pp. 19-53.

Godfrey, L.R., Jungers, W.L., Burney, D.A., Vasey, N., Wheeler, W., Lemelin, P., Shapiro, L.J., Schwartz, G.T., King, S.J, et al. 2006. New discoveries of skeletal elements of *Hadropithecus stenognathus* from Andrahomana Cave, southeastern Madagascar. J. Hum. Evol. 51,395–410.

Goldstein, S.A., Matthews, L.S., Kuhn, J.L, and Hollister, S.J. 1991. Trabecular bone remodeling: an experimental model. J. Biomech. 24,135–150.

Goldstein, S.A., Goulet, R., and McCubbrey, D. 1993. Measurement and significance of three-dimensional architecture to the mechanical integrity of trabecular bone. Calc. Tiss. Intl. 53,S127–S133.

Gommery, D., Ramanivosoa, B., Tombomiadana-Raveloson, S., Randrianantenaina, H., & Kerloc'h, P. 2009. Une nouvelle espèce de lémurien géant subfossile du Nord-Ouest de Madagascar (*Palaeopropithecus kelyus*, Primates). Comptes Rendus Palevol, 8(5), 471-480.

Gosman, J.H., and Ketcham, R.A. 2009. Patterns in ontogeny of human trabecular bone from SunWatch Village in the prehistoric Ohio Valley: general features of microarchitectural change. Am. J. Phys. Anthropol. 138, 318–332.

Groves, C.P. 2001. Primate taxonomy. Washington, DC: Smithsonian Institution Press.

Groves, C.P. 2005. Order primates. In: Wilson DE, Reeder DM, editors. Mammal species of the world: a taxonomic and geographic reference, 3rd ed. Baltimore: Johns Hopkins University Press. p 111–184, Vol.1.

Günther, M.M., Ishida, H., Kumakura, H., Nakano, Y., 1991. The jump as a fast mode of locomotion in arboreal and terrestrial biotopes. Z. Morphol. Anthropol. 78, 341-372.

Hamada, Y., Yamamoto, A., Kunimatsu, Y., Tojima, S., Mouri, T., and Kawamoto, Y. 2012. Variability of tail length in hybrids of the Japanese macaque (Macaca fuscata) and the Taiwanese macaque (Macaca cyclopis). Primates:1–15.

Harrigan, T.P., Jasty, M., Mann ,R.W., and Harris, W.H. 1988. Limitations of the continuum assumption in cancellous bone. Journal of Biomechanics 21:269–275.

Harrison, T., 1987. The phylogenetic relationships of the early catarrhine primates: a review of the current evidence. J. Hum. Evol. 16, 41-80.

Harrison, T., 1998. Evidence for a tail in *Proconsul heseloni*. Am. J. Phys. Anthropol. 26, 93-94.

Harrison, T., 1993. Cladistic concepts and the species problem in hominoid evolution. In: Kimbel, W.H., Martin, L.B. (Eds.), Species, Species Concepts and Primate Evolution. Plenum Press, New York, pp. 345-371.

Harrison, T., 2002. Late Oligocene to middle Miocene catarrhines from Afro-Arabia. In: Hartwig, W.C. (Ed.), The Primate Fossil Record. Cambridge University Press, Cambridge, pp. 311e338.

Hartman, C.G., and Straus, W.L. 1933. The anatomy of the rhesus monkey (Macaca mulatta). The Williams & Wilkins Company.

Horner, B., 1954. Arboreal adaptations of Peromyscus, with special reference to use of the tail. Contrib. Lab. Vert. Biol. 61, 1-84.

Hürzeler, J. 1958. *Oreopithecus bambolii* Gervais: A preliminary report. Verh. naturf. Ges. Basel. 69, 1-48.

Huq, E. and Jungers, W. 2009. Tail length and the sacral index in living and subfossil Malagasy prosimians. Am. J. Phys. Anthropol. 138:231 (abstract).

Ishida, H., Kunimatsu, Y., Takano, T., Nakano Y, and Nakatsukasa, M. 2004. Nacholapithecus skeleton from the Middle Miocene of Kenya. J. Hum. Evol. 46,69–103.

Johanson, D.C., Lovejoy, C.O., Kimbel, W.H., White, T.D., Ward, S.C., Bush, M.E., Latimer, B.M., Coppens, Y. 1982. Morphology of the Pliocene partial hominid skeleton (AL 288-1) from the Hadar formation, Ethiopia. Am. J. Phys. Anthropol. 57, 403–451.
Igarashi, M., and Levy, J. 1981. Locomotor balance performance of short-tailed squirrel monkeys. J. Med. Primatol. 10, 136.

Ihaka, R., and Gentleman, R. 1996. R: A language for data analysis and graphics. J. Comp. Graph Stat. 5, 299–314.

Jenkins, P.D., 1990. Catalogue of Primates in the British Museum (Natural History) and Elsewhere in the British Isles. Part V: The Apes, Superfamily Hominoidea. The British Museum (Natural History), London.

Jungers, W.L. 1988. Relative joint size and hominoid locomotor adaptations with implications for the evolution of hominid bipedalism. J. Hum. Evol. 17,247–265.

Jungers, W.L., 1991. Scaling of postcranial joint size in hominoid primates. J. Hum. Evol. 6, 391-399.

Jungers, W.L., Godfrey LR, Simons EL, Wunderlich RE, Richmond BG, Chatrath PS, Plavcan JM, Kay RF, Jungers WL, et al. 2002. In: Ecomorphology and behavior of giant extinct lemurs from Madagascar. Reconstructing behavior in the primate fossil record. pp. 371–411.

Jungers, W.L., Godfrey, L.R., Simons, E.L., Wunderlich, R.E., Richmond, B.G., Chatrath, P.S., Plavcan, J.M., Kay, R.F. 2002. Ecomorphology and behavior of giant extinct lemurs from Madagascar. Reconstructing behavior in the primate fossil record:371–411.

Kapandji, I.A., 2008. The Physiology of the Joints (V3): The Spinal Column, Pelvic Girdle and Head. Lavoisier, Paris.

Kelley, J., 1997. Paleobiological and phylogenetic significance of life history in Miocene Hominoidea. In: Begun, D.R., Ward, C.V., Rose, M.D. (Eds.), Function, Phylogeny, and Fossils: Miocene Hominoid Evolution and Adaptations. Plenum Press, New York, pp. 173-208.

Ketcham RA, and Carlson WD. 2001. Acquisition, optimization and interpretation of X-ray computed tomographic imagery: applications to the geosciences. Computers & Geosciences 27:381–400.

Ketcham, R., and Ryan, T. 2004. Quantification and visualization of anisotropy in trabecular bone. Journal of Microscopy 213:158–171.

Kim, D. G., Christopherson, G. T., Dong, X. N., Fyhrie, D. P., & Yeni, Y. N. (2004). The effect of microcomputed tomography scanning and reconstruction voxel size on the accuracy of stereological measurements in human cancellous bone. Bone, *35*(6), 1375-1382.

Kothari, M., Keaveny, T.M., Lin, J.C., Newitt, D.C., Genant, H.K., Majumdar, S. Impact of spatial resolution on the prediction of trabecular architecture parameters. Bone. 22(5), 437-443.

Lazenby, R.A., Skinner, M.M., Kivell TL, and Hublin, J.J. 2011. Scaling VOI size in 3D CT studies of trabecular bone: A test of the over sampling hypothesis. Am. J. Phys. Anthropol. 144, 196-203.

Larson, S., Stern Jr., J., 2006. Maintenance of above-branch balance during primate arboreal quadrupedalism: coordinated use of forearm rotators and tail motion. Am. J. Phys. Anthropol. 129, 71-81.

Lemelin, P. 1995. Comparative and functional myology of the prehensile tail in New World monkeys. J. Morphol. 224,351– 368.

Leutenegger, W., 1970. Das Becken der rezenten Primaten. Morph. Jahrb. 115, 1-101.

MacLatchy, L., 2004. The oldest ape. Evol. Anthropol. 13, 90-103.

MacLatchy, L., Müller, R. 2002. A comparison of the femoral head and neck trabecular architecture of *Galago* and *Perodicticus* using micro-computed tomography (mCT). J. Hum. Evol. 43, 89–105.

Maga, M., Kappelman, J., Ryan, T.M., and Ketcham. R.A. 2006. Preliminary Observations on the Calcaneal Trabecular Microarchitecture of Extant Large-Bodied Hominoids. Am. J. Phys. Anthropol. 129,410–417.

Martin, R. 1968. Reproduction and Ontogeny in tree shrews (*Tupaia belangeri*), with reference to their general behaviour and taxonomic relationships1. Zeitschrift für Tierpsychologie 25,409–495.

Martins, E.P., and Hansen, T.F. 1997. Phylogenies and the comparative method: a general approach to incorporating phylogenetic information into the analysis of interspecific data. Am. Nat. 149,646–667.

McCrossin, M.L., and Benefit, B.R. 1992. Comparative assessment of the ischial morphology of Victoriapithecus macinnesi. Am. J. Phys. Anthropol. 87,277–290.

McCrossin, M.L. 1994. The phylogenetic relationships, adaptations, and ecology of *Kenyapithecus*. Ph.D. Dissertation. University of California, Berkeley.

Miller, G.S. 1900. Key to the land mammals of northeastern North America. University of the State of New York.

Moyà Solà, S., and Kohler, M. 1996. A *Dryopithecus* skeleton and the origins of great-ape locomotion. Nature 379:156–159.

Moyà Solà, S., Köhler, M., Alba, D.M., Casanovas-Vilar, I., Galindo, J., 2004. *Pierolapithecus catalaunicus*, a new Middle Miocene great ape from Spain. Science 306, 1339-1344.

Nakatsukasa, M., Tsujikawa, H., Shimizu, D., Takano, T., Kunimatsu, Y., Nakano, Y., Ishida, H., 2003. Definitive evidence for tail loss in *Nacholapithecus*, an East African Miocene hominoid. J. Hum. Evol. 45, 179-186.

Nakatsukasa, M., Ward, C.V., Walker, A., Teaford, M., Kunimatsu, Y., Ogihara, N., 2004. Tail loss in *Proconsul heseloni*. J. Hum. Evol. 46, 777-784.

Nakatsukasa, M., and Kunimatsu, Y. 2009. *Nacholapithecus* and its importance for understanding hominoid evolution. Evol. Anthropol. 18,103–119.

Napier, P.H., 1981. Catalogue of Primates in the British Museum (Natural History) and Elsewhere in the British Isles, Part 2: Family Cercopithecidae, Subfamily: Cercopithecinae. British Museum (Natural History), London.

Nowak, R.M., 1991. Walker's Mammals of the World, fifth ed., vol. 1. J. Hopkins University Press, Baltimore and London.

Organ, J.M. 2007. The functional anatomy of prehensile and non- prehensile tails of the Platyrrhini (Primates) and Procyonidae (Carnivora). PhD Dissertation. The Johns Hopkins University, Baltimore, MD.

Organ, J.M. 2010. Structure and function of platyrrhine caudal vertebrae. Anat. Rec. 293:730–745.

Organ, J.M., Teaford, M.F., Taylor, A.B. 2009. Functional correlates of fiber architecture of the lateral caudal musculature in pr hensile and nonprehensile tails of the Platyrrhini (Primates) and Procyonidae (Carnivora). Anat. Rec. 292,827–841.

Organ, J.M., Muchlinski, M.N., Deane, A.S. 2011. Mechanoreceptivity of prehensile tail skin varies between atelines and Cebus. Anat. Rec. 294, 2064–2072.

Pagel, M. 1999. Inferring the historical patterns of biological evolution. Nature 401,877–884.

Paradis E., Claude, J., and Strimmer, K. 2004. APE: analyses of phylogenetics and evolution in R language. Bioinformatics 20,289–290.

Parker, S.P. 1990. Grzimek's Encyclopedia of Mammals, vol. 2. McGraw Hill, New York.

Procter-Gray, E., and Ganslosser, U. 1986. The individual behaviors of Lumholtz's tree-kangaroo: repertoire and taxonomic implications. J. Mammal. 343–352.

Ramanivosoa, B., and Gommery, D. 2011. Les lémuriens subfossiles dans le Nord-Ouest de Madagascar, du terrain à la diffusion des connaissances ou 15 ans de recherches franco-malgaches. Revue de primatologie 3.

Ridler, T. W., and Calvard, S. 1978. Picture thresholding using an iterative selection method. IEEE transactions on Systems, Man and Cybernetics, 8(8), 630-632.

Robinson, J.T. 1972. Early hominid posture and locomotion. University of Chicago Press, Chicago.

Rose, M.D., 1993. Locomotor anatomy of Miocene hominoids. In: Gebo, D. (Ed.), Postcranial Adaptation in Nonhuman Primates. Northern Illinois University Press, DeKalb, pp. 252-272.

Rose, M.D., 1997. Functional and phylogenetic features of the forelimb in Miocene hominoids. In: Begun, D.R., Ward, C.V., Rose, M.D. (Eds.), Function, Phylogeny, and Fossils: Miocene Hominoid Evolution and Adaptations. Plenum Press, New York, pp. 79-100.

Rose, M.D., Nakano, Y., and Ishida, H. 1996. *Kenyapithecus* postcranial specimens from Nachola, Kenya. Afr. Stud. Monogr. 24,3–56.

Rosenberger, A.L., and Matthews, L.J. 2008. *Oreonax*—not a genus. Neotrop. Primates 15:8–12.

Rowe, N., 1996. The Pictorial Guide to the Living Primates. Pogonias Press, New York.

Russo, G.A., Shapiro, L.J. 2011. Morphological correlates of tail length in the catarrhine sacrum. J. Hum. Evol. 30, 223–232.

Russo, G.A., Shapiro, L.J. 2013. Reevaluation of the lumbosacral region of *Oreopithecus bambolii.* J. Hum. Evol. (doi: 10.1016/j.jhevol.2013.05.004)

Russo, G.A., Fajardo, R.J., Schmitz, J.E. 2012. Internal bone structure of the last sacral vertebra and its relationship to tail length. Am. J. Phys. Anthropol. 147 (S52), 255-256.

Ryan, T.M., and Ketcham, R.A. 2002a. The three-dimensional structure of trabecular bone in the femoral head of strepsirrhine primates. J. Hum. Evol. 43,1–26.

Ryan, T.M., and Ketcham, R.A. 2002b. Femoral head trabecular bone structure in two omomyid primates. J. Hum. Evol 43,241–263.

Ryan, T.M., and Ketcham R.A. 2005. Angular Orientation of Trabecular Bone in the Femoral Head and Its Relationship to Hip Joint Loads in Leaping Primates. J. Morpol. 265:249.

Ryan, T.M., Krovitz, G.E. 2006 Trabecular bone ontogeny in the human proximal femur. J. Hum. Evol. 51, 591–602.

Ryan, T.M., and Shaw, C.N. 2012 Unique suites of trabecular bone features characterize locomotor behavior in human and non-human anthropoid primates. PLoS ONE 7, e41037.

Ryan, T.M., and Walker, A. 2010 Trabecular bone structure in the humeral and femoral heads of anthropoid primates. Anat. Rec. 293, 719–729.

Rylands, A.B., Mittermeier, R.A. 2009. The diversity of the New World primates (Platyrrhini): an annotated taxonomy. In: Garber, P.A., Estrada, A., Bicca-Marques, J.C., Heymann, E.W., Strier, K.B. (Eds.). South American primates: comparative perspectives in the study of behavior, ecology, and conservation. New York: Springer. pp 23–54.

Schmidt-Nielsen, K. 1984. Scaling: why is animal size so important? Cambridge: Cambridge University Press.

Schmitt, D., Rose, M.D., Turnquist, J.E., Lemelin, P., 2005. Role of the prehensile tail during ateline locomotion: experimental and osteological evidence. Am. J. Phys. Anthropol. 126, 435-446.

Schultz, A.H. 1930. The skeleton of the trunk and limbs of higher primates. Wayne State University Press.

Schultz, A.H., Straus Jr., W.L., 1945. The number of vertebrae in primates. Proc. Am. Phil. Soc. 89, 601-626.

Schultz, A. 1961. Vertebral column and thorax. S. Karger.

Shapiro, L.J. 2007. Morphological and functional differentiation in the lumbar spine of lorisids and galagids. Am. J. Phys. Anthropol. 69,86–102.

Shapiro, L.J., Seiffert, C., Godfrey, L., Jungers, W.L., Simons, E., Randria, G. 2005. Morphometric analysis of lumbar vertebrae in extinct Malagasy strepsirrhines. Am. J. Phys. Anthropol. 128, 823-839.

Shaw, C.N., Ryan, T.M. 2012 Does skeletal anatomy reflect adaptation to locomotor patterns? Cortical and trabecular architecture in human and nonhuman anthropoids. Am. J. Phys. Anthropol. 147, 187–200.

Siegel, M., 1970. The tail, locomotion and balance in mice. Am. J. Phys. Anthropol. 33, 101-102.

Silva, M., and Downing, J.A. 1995. CRC handbook of mammalian body masses. CRC press Boca Raton, Florida.

Simpson, S.W., Quade, J. Levin, N.E., Butler, R. et al. 2008. A female *Homo erectus* Pelvis from Gona, Ethiopia. Science 322, 1089-1092.

Smith, R., and Jungers, W. 1997. Body mass in comparative primatology. J. Hum. Evol. 32,523–559.

Sokal. R., Rohlf, S. 1995. Biometry. New York: WH Freeman.

Spoor, C.F., Zonneveld, F.W., and Macho, G.A. 1993. Linear measurements of cortical bone and dental enamel by computed tomography: applications and problems. Am. J. Phys. Anthropol. 91,469–484.

Stevens, N., Wright, K., Covert, H., Nadler, T., 2008. Tail postures of four quadrupedal leaf monkeys (Pygathrix nemaeus, P. cinerea, Trachypithecus delacouri and T. hatinhensis) at the Endangered Primate Rescue Center, Cuc Phuong National Park, Vietnam. Viet. J. Primatol 2, 13-24.

Straus, W.L. 1963. The classification of *Oreopithecus*. In: Washburn, S.L. (ed.), Classification and Human Evolution. Aldine Pub. Co., Chicago. pp, 146–177.

Su, A., Wallace, I.J., Nakatsukasa, M. Trabecular anisotropy and orientation in an Early Pleistocene hominin talus from East Turkana, Kenya. J. Hum. Evol. 64 (6), 667-677.

Sueur, C., Salze, P., Weber, C., and Petit, O. 2011. Land use in semi-free ranging Tonkean macaques *Macaca tonkeana* depends on environmental conditions: A geographical information system approach. Zool. 57:1.

Tito, G. 2008. New remains of *Eremotherium laurillardi* (Lund, 1842)(Megatheriidae, Xenarthra) from the coastal region of Ecuador. Journal of South American Earth Sciences 26,424–434.

Ulrich, D., van Rietbergen, B., Laib A, Ruegsegger P. 1999. The ability of three-dimensional structural indices to reflect mechanical aspects of trabecular bone. Bone 25:55–60.

Ulrich, D., Binet, M.G., Sanecki, M.G., Kieffer, S.A. 1980. Quantitative assessment of the lumbar spinal canal by computed tomography. Radiology 134,137–143.

Wada, N., Hori, H., Tokuriki, M., 1993. Electromyographic and kinematic studies of tail movements in dogs during treadmill locomotion. J. Morph. 217, 105-113.

Walker, A.C. 1974. Locomotor adaptations in past and present prosimian primates. In: Jenkins, F.A. (Ed.) Primate locomotion. pp 349–381.

Walker, A.C., and Pickford, M. 1983. New postcranial fossils of *Proconsul africanus* and *Proconsul nyanzae*. In Ciochon, R.L. and Corruccini, R.S. (Eds.) New interpretations of ape and human ancestry. New York : Plenum Press, pp. 325–351.

Walker A.C. and Leakey R. 1993. The postcranial bones. In: Walker, A. and Leakey, R. (Eds.) The Nariokotome *Homo erectus* Skeleton. Harvard University Press, Cambridge. pp, 95–160.

Ward, C.V. 1993. Torso morphology and locomotion in *Proconsul nyanzae*. Am. J. Phys. Anthropol. 92, 291–328.

Ward, C.V., 1997. Functional anatomy and phyletic implications of the hominoid trunk and hindlimb. In: Begun, D.R., Ward, C.V., Rose, M.D. (Eds.), Function, Phylogeny, and Fossils: Miocene Hominoid Evolution and Adaptations. Plenum Press, New York, pp. 101-130.

Ward, C.V., 2007. Postcranial and locomotor adaptations of hominoids. In: Henke, W., Tattersall, I. (Eds.), Handbook of Paleoanthropology. Primate Evolution and Human Origins, vol. 2. Springer, Heidelberg, pp. 1011-1030.

Ward, C.V., Walker, A., Teaford, M.F., 1991. *Proconsul* did not have a tail. J. Hum. Evol. 21, 215-220.

Ward, C.V., Walker, A., Teaford, M.F., 1999. Still no evidence for a tail in *Proconsul* heseloni. Am. J. Phys. Anthropol. 28, 273.

Ward, C.V., Walker, A., Teaford, M., and Odhiambo, I. 1993. Partial skeleton of *Proconsul nyanzae* from Mfangano Island, Kenya. Am. J. Phys. Anthropol. 90,77–111.

Ward, C.V. 1997. Functional anatomy and phyletic implications of the hominoid trunk and hindlimb. In: Begun D, Ward C, Rose M, editors. Function, Phylogeny, and Fossils: Miocene Hominoid Evolution and Adaptations. New York, Plenum. pp 101–130.

Wilson, D.R., 1972. Tail reduction in Macaca. In: Tuttle, R. (Ed.), The Functional and Evolutionary Biology of Primates. Aldine Press, New York, pp. 241-261.

Youlatos, D. 2003. Osteological correlates of tail prehensility in carnivorans. J. Zool. 259:423–430.

Zapfe, H. 1958. The skeleton of Pliopithecus (Epipliopithecus) vindobonensis (Zapfe and Hürzeler). Am. J. Phys. Anthropol. 16:441–457.

Zapfe, H. 1960. A new fossil anthropoid from the Miocene of Austria. Curr. Anthropol. 1:428–429.

Chapter 4: Functional morphology of proximal caudal vertebrae in nonprehensile-tailed primates

ABSTRACT

Researchers interested in tail functional morphology have focused primarily on mammalian prehensile tails. By contrast, far fewer workers have endeavored to examine the functional morphology of nonprehensile tails, despite the fact that this tail type characterizes the majority of mammalian taxa. Further, tail length reduction/ loss has evolved independently in a number of mammalian lineages, several of which occur within primates. In this study, caudal/coccygeal vertebral anatomy among living primates known to differ in tail length was quantitatively evaluated in the context of a comparative mammalian sample (Carnivora, Diprotodontia, Pilosa, Rodentia, and Scandentia) to offer functional insight into the anatomy associated with tail length reduction/loss. Vertebral variables with known or suspected biomechanical significance were collected on the first postsacral, mid-proximal, and transition proximal caudal vertebrae for 333 individuals. Results demonstrate that longer-tailed primates generally exhibit a greater number of features associated with increased proximal tail mobility, increased range of motion, and increased muscular mechanical advantage, compared to shorter-tailed primates. Variables were further evaluated using multivariate analyses to predict the tail lengths of two subfossil lemurs (*Archaeolemur* and *Palaeopropithecus*) with associated caudal vertebral specimens. *Archaeolemur* was predicted to have a long, with a relative tail length (tail length/[head+body length] x 100) of between 109 and 143. The predicted relative tail length for *Palaeopropithecus* is 36, suggesting it possessed a relatively short tail.

Predicted relative tail lengths for the subfossil lemur sample accord with previous inferences concerning their tail length based on other regions of the skeleton.

INTRODUCTION

Background

Researchers interested in tail functional morphology have focused primarily on mammalian prehensile tails (Dor, 1937; German, 1982; Rosenberger, 1983; Bergeson, 1992, 1995, 1996; Gebo, 1992; Lemelin, 1995; Meldrum, 1998; Garber and Rehg, 1999; Lawler and Stamps, 2002; Youlatos, 1999, 2003; Bezanson, 2004, 2005, 2006, 2009; Schmitt et al., 2005; Organ, 2006, 2007, 2010; Organ et al., 2009, 2011; Russo and Young, 2011). Although prehensile tails independently evolved in several mammalian taxa (e.g., carnivores, marsupials; Youlatos, 1999, 2003; Emmons and Gentry, 1983), they characterize just six primate genera from two platyrrhine clades: *Alouatta, Ateles*, *Brachyteles, Lagothrix* (Atelidae), and *Cebus* and *Sapajus* (Cebinae) (Groves, 2001, 2005; Ryland and Mittermeier, 2009; see also Rosenberger and Matthews, 2008). Functionally, prehensile tails are capable of providing sole support for an animal's body weight, and assist in travel and foraging activities by allowing animals to distribute their weight over a greater number of supports and access food resources located in terminal branch settings (Emmons and Gentry, 1983; Gebo, 1992; Garber and Rehg, 1999; Bezanson, 2004, 2005, 2006, 2009). Structurally, prehensile tails are distinguished from nonprehensile tails by a number of osteological features associated with their specialized function. The neural arches of proximal caudal vertebrae (and the distal sacrum) in prehensile tails are relatively higher than those in nonprehensile tails in order to

accommodate increased innervation to well-developed tail musculature (Ankel, 1965, 1972; see also Grand, 1977). In addition, the proximal caudal vertebrae in prehensile tails are more numerous and exhibit craniocaudally shorter vertebral bodies than those of nonprehensile tails (Ankel, 1972). A vertebral sequence comprised of a greater number of shorter elements can be bent into more acute angles, permitting a greater degree of proximal tail flexibility in prehensile tails than can be achieved by nonprehensile tails (or prehensile-tailed taxa that rely on tail-only suspensory behaviors to a lesser degree, e.g., *Lagothrix*) (Lemelin, 1995; Schmitt et al., 2005). The proximal articular surface of the first caudal vertebra in prehensile-tailed taxa also exhibits more pronounced mediolateral (convex) curvature than in nonprehensile-tailed taxa, which likely enhances the range of mediolateral motion permitted at the sacrocaudal joint in the former, according with their greater emphasis on varied movements at this joint (Deane et al., in prep; see also Schmitt et al., 2005). In the distal region of the tail, caudal vertebrae in prehensile tails have more expanded bony attachment points, including the laterally projecting transverse processes and ventrally projecting hemal processes, than those in nonprehensile tails, affording the former increased muscular mechanical advantage of the tail abductor (e.g., *intertransversarii caudae* mm.) and ventrodorsal flexor (e.g., *flexor caudae brevis et longus* mm.) musculature (Organ et al., 2010). In all three tail regions (as represented by the transition vertebra [proximal region], longest vertebra [transition region] and the mid-distal vertebra [distal region]; see Figure 4.1), the caudal vertebrae in prehensile tails generally exhibit greater average bending strength (approximated by polar section modulus standardized by craniocaudal vertebral length) than those in nonprehensile tails,

reflecting their increased structural resistance to high magnitudes of loading engendered during tail-suspension behaviors (Organ, 2010; see also German, 1982). The functional association between bending strength and prehensile tail use is supported by ontogenetic work on caudal vertebral structure in the context of age-related differences in tail-suspensory positional behaviors (Russo and Young, 2011).

In contrast to the extensive research devoted to prehensile tail function and structure, far fewer workers have endeavored to examine the functional morphology of nonprehensile tails, despite the fact that this tail type characterizes the majority of mammalian taxa. Further, tail length reduction/ loss has evolved independently in a number of mammalian lineages (e.g., pilosans, diprotodonts, rodents), several of which occur within primates (e.g., some species of macaque, mandrills, lorises, *Indri,* and living and extinct hominoids). Some studies of nonprehensile tail function have demonstrated that arboreal animals with shortened or reduced tail lengths cannot attain the same level of locomotor competence as their counterparts with longer length tails (rodents, Buck et al., 1925; Horner, 1954; Siegel, 1970; primates, Igarashi and Levy, 1981). In the study by Siegel (1970:101), mice with surgically-removed tails made to walk on small poles showed an increase in their degree of "hind limb prehension" (i.e., foot grasping) for maintaining balance, and reportedly fell from the poles significantly more often, compared to control mice (see also Igarashi and Levy, 1981). Arboreal primates have been observed to emphasize lateral (i.e., abduction) tail movements during quadrupedal progression (Larson and Stern, 2006), likely to create oppositely-directed angular momentum to stabilize the body's center of gravity over the substrate during moments of

imbalance (Horner, 1954; Fredrickson, 1989; Wada et al., 1993; Walker, 1998; Larson and Stern, 2006). Additionally, it has been suggested that dorsally extended tail positions help to reorient the body to prepare for landing when leaping between discontinuous substrates (Hildebrand, 1974; Emerson, 1985; Demes et al., 1996; Essner, 2002). Moreover, in nonprehensile-tailed mice trained to climb, the tail is engaged in order to stabilize the body, resulting in more expanded caudal vertebral transverse processes compared to nonclimbing mice (Byron et al., 2010). Consistent with these observations, anatomical data demonstrates that arboreal mammals tend to have longer, heavier tails than their terrestrial, close phyletic relatives (e.g., rodents; Horner, 1954; tree shrews, Martin, 1968; primates, Grand, 1977; see also Fleagle, 1999; but see Larson and Stern, 2006), which presumably do not require the tail as much for balance (but see Wada et al., 1993). Though the tail has a number of other functions (e.g., social and auto-communication, defense, see Hickman, 1979 for a review), taken together, these aforementioned studies indicate that variation in tail length impacts an animal's ability to maintain balance and successfully navigate an arboreal environment (see also Jusufi et al., 2008).

Although nonprehensile tails have clear functional importance for mammalian locomotion, little research has examined how caudal vertebral anatomy differs among mammals that vary in tail length. Some previous workers have focused on how to distinguish between coccygeal and caudal vertebral anatomy (i.e., tail absence vs. tail presence, respectively). For example, Nakatsukasa and colleagues (2003) specified a series of traits that, collectively, distinguish the morphology of hominoid coccygeal

vertebrae from that of first caudal vertebrae in nonhominoid primates and other mammals possessing very short or nearly absent tails. In addition to the absence of a neural arch and prezygapophyses, Nakatsukasa et al. (2003:180) noted that coccygeal vertebrae are also characterized by an overall "T-shape", reduced transverse processes, and dorsoventral compression of the vertebral body. Using these traits, they identified and attributed a coccygeal vertebra to the Middle Miocene (ca. 15Ma) hominoid *Nacholapithecus kerioi.* The applicability of this analysis to other studies is limited, however, as these comparisons were qualitative and based on an unspecified number of individuals as representatives for the mammalian sample (Nakatsukasa et al., 2003). More recently, Hamada et al. (2012; see also Tojima, 2012) examined the caudal vertebrae from a sample of hybridized long-tailed *Macaca cyclopsis* (relative tail length [RTL] =83) and short-tailed *M. fuscata* (RTL=15). They demonstrated that vertebral craniocaudal length decreases as tail length decreases (see also Fooden, 1975, 1988), though variation in the craniocaudal length of the first vertebral body was not as pronounced as that of other caudal vertebrae (Hamada et al., 2012). While the study by Hamada and colleagues (2012) expands our knowledge of how caudal vertebral structure differs among primates that vary in tail length, it quantified only one of many known biomechanically informative aspects of vertebral morphology.

Objectives

The primary goal of this study is to offer additional functional insight into the anatomy associated with tail length reduction/loss by quantitatively evaluating proximal caudal/coccygeal vertebral anatomy among living primates known to differ in tail length.

This study focuses on proximal caudal vertebrae because the bulk of the caudal musculature responsible for moving the tail is near the tail base in nonprehensile-tailed primates (Lemelin, 1995). Generally, it is expected that primates with longer tails will possess a greater number of features associated with increased proximal tail flexibility, increased range of motion, and increased muscular mechanical advantage, compared to shorter-tailed primates. It is reasonable to expect variation in caudal/coccygeal vertebral anatomy as tail length is likely proportional to tail mass (Organ, 2007). Grand (1977) demonstrated that the tail of *M. fascicularis* (RTL =108) comprises 3.6% of total body weight, while the tail of *M.nemestrina* (RTL = 37) comprises just 0.2% of total body weight. Therefore, longer-tailed primates should have to accommodate and move a more heavily-muscled tail than shorter-tailed primates, in which a reduction in tail length is presumably associated with reduction in tail musculature. In order to assess potentially functionally relevant variation, aspects of vertebral anatomy and functional predictions are delineated based on previous studies of vertebrae from other spinal regions (Ankel, 1965, 1972; Ward et al., 1991, 1993; Shapiro, 1993, 2007; Sanders and Bodenbender, 1994; Shapiro and Simons, 2002; Argot, 2003; Shapiro et al., 2005; Organ, 2007, 2010; Organ et al., 2009; Russo and Shapiro, 2011; Russo et al., 2012).

Primate proximal caudal vertebrae are evaluated in the context of a comparative mammalian sample chosen based on phylogenetic relatedness and variation in tail length and/or function. Tail length reduction/loss has evolved independently in a number of distantly-related nonprimate mammals (e.g., koalas, sloths), offering a valuable

opportunity to draw on the strength of a comparative sample to validate form-function links by detecting instances of morphological convergence.

A second goal of this study is to predict the tail lengths of extinct primates with known associated caudal/coccygeal vertebrae using the extant primate data. Subfossil lemurs are excellent test subjects because they likely exhibited considerable tail length diversity, as revealed by previous studies of their sacral anatomy (Godfrey and Jungers, 2002, 2003; Godfrey et al., 2006; Huq and Jungers, 2009). For example, most *Archaeolemur* sacra are comprised of three vertebrae, have large caudal neural apertures relative to the cranial neural apertures (Ankel, 1965; Godfrey et al., 2006) and nearly circularly-shaped (i.e., approximately equal mediolateral and dorsoventral dimensions) caudal articular surfaces (Chapter 3; see also Russo and Shapiro, 2011), suggesting that *Archaeolemur* possessed a long tail. *Palaeopropithecus* sacra are generally comprised of four sacral vertebrae, exhibit small caudal neural apertures relative to cranial neural apertures (Ankel, 1965; Huq and Jungers, 2009), and caudal articular surfaces somewhat elliptical in shape (i.e., more mediolaterally than dorsoventrally expanded; Chapter 3; see also Russo and Shapiro, 2011), suggesting that *Palaeopropithecus* exhibited a short to nearly-absent tail (Godfrey and Jungers, 2002, 2003). In addition to sacral specimens, caudal vertebral specimens are also known for *Archaeolemur* (e.g., DPC 12890) and *Palaeopropithecus* (e.g., DPC 17201). However, the anatomy of these caudal vertebrae has not been quantitatively examined for determining tail length. This study will reconstruct the tail lengths of these two subfossil lemurs (*Archaeolemur* and *Palaeopropithecus*) from their associated caudal vertebral specimens.

METHODS

Extant Mammal Sample

Measurements (Figure 4.2) on proximal caudal/coccygeal vertebrae were collected for 81 species from six mammalian Orders: Primates, Carnivora, Diprotodonia, Rodentia, Pilosa and Scandentia (Table 4.1). The sample derives from osteological collections at the American Museum of Natural History (New York, NY, USA), the Natural Museum of Natural History (Washington D.C., USA), and the Field Museum of Natural History (Chicago, IL, USA). The comparative sample includes 211 primates (46 species), 23 carnivores (10 species), 39 diprotodonts (11 species), 21 pilosans (five species), 32 rodents (six species) and seven tree shrews (three species) (Total N = 333 individuals) (Table 4.1). This study endeavored to examine six to ten specimens per species where sufficient material was available and time permitted. Small sample numbers per taxon reflect the poor preservation of caudal vertebral elements in museum collections. Nonetheless, the sample sizes in this study are within the range of those examined in other studies of caudal vertebrae (e.g., German, 1982; Organ, 2010). Due to small sample sizes and the large number of unknown sex cases, it was not possible to separate data collection equally across the sexes in order to statistically test for sex differences. Accordingly, pooled-sex species averages were used for analyses. Though tail and body length measurements may vary between sexes of a single species, Fooden (1997; see also Fooden and Albrecht, 1999) has demonstrated that among macaques, for example, corresponding tail length indices do not. All examined individuals were wild-captured and classified as adult based on long bone epiphyseal fusion or dental eruption.

Caudal vertebral specimens exhibiting substantial damage, malformation, and/or markers indicating bone disorders (e.g., osteophytes) were excluded from the study.

Taxa for the comparative sample were chosen based on phylogenetic relatedness and variation in tail length and/or function (Table 4.1). For each extant taxon, a relative tail length index (Fooden, 1997) was calculated (as defined earlier: RTL = tail length / [head + trunk length] x 100) using morphometric data collected from the literature (Table 4.1). Previous studies have calculated RTL using the literature cited here (e.g., Youlatos, 2003) and employed this index for quantifying tail length (Fooden, 1997; Youlatos, 2003; Russo and Shapiro, 2011; Hamada et al., 2012). All hominoid primates were assigned a RTL of 0 because they lack an external tail. Nonprimate mammalian taxa described in the literature as vestigial-tailed or as possessing diminutive tails, and thus without associated tail length measurements, were also assigned a RTL of 0 (Table 4.1). Although this study is focused on nonprehensile-tailed taxa, prehensile-tailed taxa were included for comparative purposes because the functional morphology of their caudal vertebrae is well understood (citations above). Additionally, for some clades, prehensile-tailed taxa possess the longest tails (e.g., Primates: *Ateles*, RTL = 158). Among the primates sampled, *Indri*, lorises (e.g., *Nycticebus*), some macaques (e.g., *Macaca arctoides*), and all hominoids represent taxa with reduced tail lengths. *Macaca* is a particularly useful taxonomic group for comparative purposes as tail length reduction occurs within several species groups (e.g., *sinica* species group, Fooden, 1988; Deinard and Smith, 2001). Carnivores, diprotodonts, rodents, pilosans, and tree shrews were also chosen for comparison because these clades that contain species characterized by reduced tail

lengths (Table 4.1). Carnivores include short-tailed felids (e.g., *Lynx*) and mustelids (e.g., *Gulo*), and long nonprehensile- (e.g., *Genetta*) or prehensile- tailed (e.g., *Arctictis*) viverrids. Diprotodontia includes short-tailed vombatiformes (*Phascolarctos* and *Vombatus*), and long-tailed macropodiformes (e.g., *Dendrolagus*) and phalangeriformes (e.g., *Trichosurus*). Within Pilosa, modern two- (*Choloepus*) and three- (*Bradypus*) toed sloths have likely independently evolved tail loss as these living taxa are distantly related and all known fossil genera have long tails (Tito, 2008). Other modern representatives of Pilosa include anteaters, some of which have long nonprehensile (e.g., *Myrmecophaga*) or long partially prehensile (e.g., *Tamandua*) tails. Rodentia includes tailless caviids (e.g., *Hydrochaeris*), short-tailed North American beavers (*Castor*) and common porcupines (*Erethizon*), and long-tailed heteromyids (e.g., *Dipodomys*).

Extinct Primate Sample

The extinct primate sample included three caudal vertebrae from the extinct subfossil lemurs *Archaeolemur* (DPC 12890A and DPC 12890F) and *Palaeopropithecus* (DPC 17201) (Figure 4.3), which are housed at the Duke University Primate Center Division of Fossil Primates (Durham, NC, USA). The *Archaeolemur* caudal specimens belong to a series of at least 12 vertebrae attributed to DPC 12890, though it is possible that they may not all belong to the same individual (see below). To facilitate quantification, an attempt was made to seriate (using vertebral body craniocaudal length) and then assign these caudal vertebrae a letter (placed after the specimen number), denoting their probable position in the caudal sequence.

There are at least six proximal caudal vertebrae present for DPC 12890. DPC 12890A (Figure 4.3A) is the craniocaudally longest and most robust vertebra in the series and thus was designated as the first postsacral vertebra. This specimen lacks a left transverse process, however a reasonable estimate of transverse process breadth can be obtained from the right side, which preserves a complete transverse process. The ventral aspect of the cranial articular surface is slightly eroded at midline, and so the dorsoventral dimension of this surface was taken lateral and right to midline where the ventral surface is better preserved. DPC 12890F (Figure 4.3B) is well preserved and could be easily identified as the transition vertebra because it possesses zygapophyses on its proximal end but lacks them on its distal end. The neural arches and zygapophyses of the caudal vertebrae situated between 12890A and 12890F are variously preserved. To be conservative, only 12890A and 12890F were included in the study because they could be confidently identified. DPC 12890M, a distal caudal vertebra, exhibits differently-shaped centra (both cranial and caudal end) and different apparent surface curvature than the other vertebrae in the series, signifying that it may not be a part of the DPC 12890 caudal vertebral sequence. The species attribution of the *Archaeolemur* specimens was less certain that that of the *Palaeopropithecus* specimen (see below). DPC 12890 was attributed to *A. edwardsi* as this was the only species with known associated vertebrae housed at Duke. As such, a body mass of 25kg was used for size adjustments (Jungers et al., 2002).

The overall morphology of the *Palaeopropithecus* postsacral vertebral specimen (DPC 17201; Figure 4.3C) specimen resembles a robust coccygeal vertebra. In

hominoids, the first coccygeal is typically the largest, and subsequent coccygeal vertebrae quickly diminish in size (Woon and Stringer, 2012). The size of the cranial articular surface of the *Palaeopropithecus* specimen nearly approximates the caudal articular surface dimensions of known *Palaeopropithecus* sacral specimens (personal observations). The specimen also lacks a neural arch (and associated zygapophyses) and the body appears dorsoventrally compressed. As such, the *Palaeopropithecus* postsacral vertebral specimen (DPC 17201) was designated as the first postsacral vertebra. As with the *Archaeolemur* first postsacral, the right transverse process of this specimen is better preserved than the left. Thus, measurements for transverse process breadth were taken on the right side and multiplied by two to obtain a reasonable estimate of this measure. The *Palaeopropithecus* specimen was attributed to the *P. ingens* species based on its locality data, which matches that of other *Palaeopropithecus ingens* vertebral specimens from the same locality and housed at Duke (see Shapiro et al., 2005). As such, a body mass of 45kg was used for size adjustments (Jungers et al., 2002).

Measurements

This study examined the first postsacral vertebra, the mid-proximal, and transition vertebra (Figure 4.1) for each individual in the extant mammal sample. Herein, the first postsacral vertebra refers to the vertebra immediately subjacent to the distal sacrum regardless of form, and thus represents first caudal and coccygeal vertebrae. Analyses of hominoid taxa and other mammalian taxa possessing proximal caudal vertebrae without neural arches were thus restricted to the first postsacral vertebra. By the same token, analyses at the levels of the mid-proximal and transition vertebrae were

restricted to those taxa whose postsacral vertebrae could be confidently identified as caudal (i.e., they bear a neural arch). The mid-proximal vertebra is defined by its position in the tail sequence (as halfway through the proximal caudal vertebral sequence), following Organ's (2010) definition of the mid-distal vertebra. The transition vertebra is recognized as the last vertebra in the proximal caudal vertebral sequence and is designated TV in Figure 4.1.

The measurements obtained in this study are illustrated and described in Figure 4.2). Measures of cranial articular surface dimensions, craniocaudal vertebral body length and transverse process breadth were taken using digital calipers linked to a laptop and recorded to the nearest 0.01mm. For cases where one transverse process was broken, the lateral projection of the complete transverse process from the midline was measured and multiplied by two to obtain a reasonable estimate of total breadth. In cases where the transverse processes had bifurcated at the level of the transition vertebra, maximum transverse process breadth was obtained. Typically, the distalmost pair of transverse processes are most laterally expanded. For cases where caudal vertebrae were articulated, vertebral body length was measured at the ventral surface. A Panasonic Lumix DMC-G2 12.1 MP (SLR) digital camera was used to photograph caudal vertebral specimens in dorsal, cranial and lateral views to obtain additional linear and angular measurements (Figure 4.2) and for general documentation purposes. A 1cm scale and a dry erase marker board denoting species, museum identification number, sex, and vertebral element were placed in the camera frame. To ensure consistent orientation, vertebrae were oriented using the following guidelines: 1) In dorsal and lateral views, the cranial articular surface

of each specimen was placed flush against a flat rod attached perpendicular to the end of the board such that the cranial articular surface is also perpendicular to the camera lens; 2) In cranial views, the cranial articular surface of each specimen was positioned upright and thus parallel with the camera lens. All measurements from photographs were obtained using the "line tool" in ImageJ v1.42j software (http://rsbweb.nih.gov/ij/).

Functional Rationale and Predictions for Vertebral Variables

Vertebral Body Craniocaudal Length

In a given spinal region, the interaction between the number of vertebrae, the region's total length, and craniocaudal length of the vertebral bodies in the sequence is important for understanding the spine's potential range of motion (Ward, 1993; Shapiro and Simons, 2002). In a comparison of two spinal regions with the same total length but different numbers of vertebrae, the sequence with the greater number of relatively shorter (i.e., reduced craniocaudal length) vertebral bodies can achieve a greater arc of flexion; in a comparison of two spinal regions with different total lengths and different vertebral body craniocaudal lengths, the longer vertebral sequence achieves a greater arc of flexion irrespective of vertebral number (Ward, 1993; Shapiro and Simons, 2002). It is worth noting that these functional comparisons assume comparable mediolateral vertebral body widths and intervertebral disk thickness (Ward, 1993; Shapiro and Simons, 2002).

Based on Hamada et al. (2012), it is predicted that as tail length increases, linear measures of craniocaudal length of the proximal caudal vertebral bodies (Measurement 1; Figure 4.2), relative to body mass$^{1/3}$ (i.e., divided by), will also increase. Primates with different tail lengths may exhibit similar numbers of proximal caudal vertebrae (Table

4.1; Russo and Shapiro, 2011; Hamada et al., 2012). Functionally, assuming similar proximal caudal vertebral numbers, a proximal tail sequence characterized by longer vertebral bodies affords greater proximal tail mobility than a shorter tail sequence. Alternatively, proximal tail flexibility may also be increased by assuming a greater number of craniocaudally shorter vertebral elements, as in *Ateles* (Lemelin, 1995).

Cranial Articular Surface Shape

In primates with long tails, the sacrum's caudal articular surface is circularly shaped, whereas primates with reduced tail lengths (and humans, Kapandji, 2008) exhibit more elliptically-shaped (i.e., mediolaterally wide, dorsoventrally narrow) caudal articular surfaces (Russo and Shapiro, 2011). Functionally, a more circular sacrocaudal/coccygeal joint articular surface permits an increased range of movement that allows for multidirectional movements (Russo and Shapiro, 2011). In humans, the more dorsoventrally compressed sacrococcygeal joint is associated with a reduced range of motion (Saluja, 1998; Kapandji, 2008; Woon and Stringer, 2012). A greater range of motion in the proximal tail would enhance the ability to actively extend, flex, abduct, and rotate the tail during locomotion (Bernstein et al., 1978; Hickman, 1979; Schmitt et al., 2005; Larson and Stern, 2006; Stevens et al., 2008; Organ et al., 2009). The cranial articular surfaces of the subjacent caudal vertebrae should reflect the caudal articular surface of the sacrum, and so it is expected that as tail length increases, proximal caudal/coccygeal cranial articular surface shape will become increasingly circularly shaped. This measure can be estimated by a ratio of the mediolateral articular surface breadth (Measurement 2) to dorsoventral articular surface breadth (Measurement 3)

(Figure 4.2). A ratio value greater than 1 indicates greater mediolateral than dorsoventral dimensions, and thus more elliptically-shaped cranial articular surface, whereas a ratio value closer to 1 indicates more equal mediolateral and dorsoventral dimensions, and thus more circularly-shaped cranial articular surface.

Cranial Articular Surface Area

If tail length is proportional to tail mass (Organ, 2007), the proximal tail region should be subject to greater loads in primates with long tails compared to primates with reduced tail lengths. Preliminary data from trabecular and cortical bone analyses of the last sacral vertebra (near the sacro- caudal/coccygeal joint) generally support this idea (Russo et al., 2012). For example, the distal sacra of primates with longer tails exhibit features associated with increased bone strength, such as thicker cortical bone and more numerous trabeculae compared to primates with shorter tails (Russo et al., 2012; see Chapter 3). Functionally, relatively large vertebral articular surface dimensions serve to distribute high loads over a wider area, thereby reducing axial compressive forces (the primary loads acting on the vertebral column; see Chapter 2) (Schultz, 1930; Jungers, 1988; Kapandji, 2008). It is thus predicted that as tail length increases, the cranial articular surface areas of proximal caudal vertebrae will also increase. Articular surface area is calculated using the formula for an ellipse: π * ½ mediolateral breadth (Measurement 2)* ½ dorsoventral breadth (Measurement 3), relative to body mass $^{2/3}$ (Figure 2). A higher value indicates a relatively larger articular surface area than a lower value, which indicates a smaller surface area.

Transverse Processes

The *abductor caudae lateralis* and *medialis* mm., and the *ischio-* and *ilio-caudalis* mm., attach to the dorsolateral aspects of the proximal caudal vertebral transverse processes and serve to laterally abduct and rotate the tail (Hartman and Strauss, 1933; Lemelin, 1995). The leverages of these muscles depend on the length (Measurement 6), orientation (craniocaudal [Measurement 7], dorsoventral [Measurement 8]), and dorsoventral position (Measurement 9) of the proximal caudal vertebral transverse processes (Figure 4.2). It is predicted that relative to body mass$^{1/3}$, lateral projection of the transverse processes will increase as tail length increases. It is also predicted that the transverse processes will become increasingly more ventrally located, and more ventrally (i.e., dorsoventral angle is more acute) and caudally (i.e., craniocaudal angle is more acute) oriented as tail length increases. Functionally, these morphologies would enlarge the size of the dorsal compartment for extensor musculature, improve muscular leverage, and increase sagittal plane range of motion.

Area of Cranial Neural Aperture

The size of the distal sacrum's neural aperture relative to its cranial neural aperture is an indicator of tail length and function (Ankel, 1965, 1972). Specifically, a reduction in tail length or tail loss is associated with a concomitant reduction in the relative area of the sacrum's caudal neural aperture (Ankel, 1965, 1972). Functionally, a reduction in the area of the sacrum's caudal neural aperture reflects reduced innervation to a nearly diminished caudal region (i.e., no or shorter tail), while an increase in the area of the sacrum's caudal neural aperture reflects enhanced innervation to a robust caudal

region (i.e., longer tail, prehensile tail) (Ankel, 1965, 1972). Since the proximal caudal vertebrae articulate with the distal sacrum and serve as a passageway for innervation to the tail, it is predicted that the area of the cranial neural aperture will increase in area as tail length increases. This measure is calculated as the formula for an ellipse: π * ½ cranial neural aperture mediolateral breadth (Measurement 4)* ½ cranial neural aperture dorsoventral breadth (Measurement 5), relative to body mass $^{2/3}$ (Figure 4.2). A higher value indicates a larger neural aperture area, while a lower value indicates a smaller neural aperture area.

Spinous Processes

The *extensor caudae medialis* mm. and *interspinales caudae* mm. are the caudal extension of the lumbar spine's *multifidus lumborum* mm. and *interspinales lumborum* mm. (Hartman and Strauss, 1933; Lemelin, 1995). These caudal muscles attach to the spinous processes in the proximal caudal sequence and serve to dorsally extend the tail. Therefore, the leverages of these muscles depend on the length (Measurement 10) and craniocaudal orientation (Measurement 11) of the proximal caudal vertebral spinous processes (Figure 4.2). It is predicted that relative to body mass$^{1/3}$, dorsal projection of the spinous processes will increase as tail length increases. It is also predicted that the spinous processes will become more caudally oriented (i.e., craniocaudal angle is more obtuse) as tail length increases. Functionally, more dorsally projected and caudally oriented spinous processes would increase the leverage and surface area for attachment of tail musculature.

Prezygapophyseal orientation

Spinal movements are influenced in part by the orientation and shape of the spine's zygapophyseal synovial joints (Shapiro, 1993; Bogduk and Twomey, 2005; Russo, 2010). Zygapophyses oriented in the sagittal plane (with medially facing articular facets) allow for sagittal bending and resist rotation and lateral flexion; coronally oriented zygapophyses (with dorsally facing articular facets) allow rotation and lateral bending while resisting sagittal bending and ventral displacement; and intermediate or obliquely oriented zygapophyses (with dorsomedially facing facets) resist sagittal bending, ventral displacement, and rotation to some extent (Shapiro, 1993; Bogduk and Twomey, 2005; Russo, 2010). It is predicted that as tail length increases, caudal vertebral prezygapophyses will become increasingly obliquely oriented (i.e., articular facets rotate from the sagittal plane into the dorsal plane, with facet surfaces facing dorsally) (Measurement 12; Figure 4.2). Functionally, this orientation would permit greater lateral tail flexion movements, which long-tailed primates may employ for producing counterbalancing movements during arboreal locomotion (Larson and Stern, 2006).

Size Adjustments

Body mass, an appropriate proxy of body size (Fleagle, 1984; Schmidt-Nielsen, 1984), varies greatly across the taxa in this study. Therefore, variables need to be size-adjusted prior to comparative analyses. Previous studies of vertebral morphology often standardize measurements by the geometric mean of (nonangular) variables (e.g., Shapiro, 2007). However, caudal vertebral sequences in museum collections are often partially/fully articulated, or vertebrae are missing or damaged, hindering the ability to

obtain all measurements on all three vertebrae for each individual. To exclude such cases from the analysis would have drastically reduced the study's sample size. Therefore, body mass data from museum records and the literature were used to make size-adjustments so that partial datasets could be retained for analyses. Body mass data were available for some individual specimens from museum documents and applied where possible. However, this information was absent for the majority of specimens, and so body masses were obtained from the literature (primates: Smith and Jungers, 1997; nonprimate mammals: Silva and Downing, 1995; Nowak, 1991) and applied on a by-species (or by-subspecies when possible) and by-sex basis. In cases where sex was unknown, the average of male and female body mass values was applied. Linear measurements (mm) were standardized (i.e., divided by) by body mass$^{1/3}$; area measurements (mm^2) were standardized by body mass $^{2/3}$; angular measurements (°) were not subject to standardization.

Datasets

In order to facilitate data collection, the extant mammal sample was partitioned into two datasets. Dataset #1 is comprised of all mammals in the sample (Table 4.1). For all mammals in the sample, measurements were obtained to calculate vertebral body craniocaudal length, cranial articular surface area, cranial articular surface shape, and transverse process breadth. Because these variables derive from measurements taken on the vertebral body, they are more likely to be preserved in the fossil record. Additionally, these measurements can be obtained using standard digital calipers. In these ways, variables in Dataset #1 may be more readily applicable to studies of fossil caudal

vertebrae. Dataset #2 contains a subset of the total mammal sample (boldfaced taxa in Table 4.1). For mammals in Dataset #2, measurements were obtained to calculate an additional seven variables: transverse process craniocaudal and dorsoventral angles, transverse process position, area of the cranial neural aperture, spinous process length and craniocaudal orientation, and prezygapophyseal orientation. These variables derive from measurements obtained using calipers and digital photographs of specimens in multiple views.

Statistical Analysis

Data were analyzed using species means for each variable at each vertebral level. Each variable was examined within all mammals and among only primates. The relationship between each trait and RTL was evaluated using a phylogenetic generalized least-squares (pGLS) regression technique. The pGLS method is generalized least-squares regression model that incorporates an error term in order to consider covariation among taxa on the basis of phylogenetic similarity (Martins and Hansen, 1997). Using a measure of phylogenetic correlation, λ (Pagel 1999; see also Freckleton et al. 2002), the covariance matrix accounts for the degree to which trait evolution deviates from the Brownian motion model of evolution. The Brownian motion model of evolution predicts that $\lambda = 1$, assuming closely-related species (using the inferred phylogeny) are anatomically similar and thus traits are proportional to phylogenetic relatedness. In other words, variation in a trait is a sole function of evolutionary distance among taxa. Models that assume phylogenetic independence predict that $\lambda = 0$, indicating the absence of a relationship between the trait and phylogenetic relatedness. In other words, variation in a

trait is independent of evolutionary distance among taxa. For this study, mammalian phylogenetic information and branch lengths were taken from Bininda-Emonds et al. (2007). Branch length data were not available for *Papio cynocephalus* (n = 6) or *Gulo luscus* (n=1). Therefore, *Papio cynocephalus* and *Gulo luscus* were reclassified as *P. hamadryas* and *Gulo gulo,* taxa for which branch length data were available. The impact of this adjustment is likely negligible as the taxa in question are more closely related to their alternative taxonomic classifications than to any other taxon in the sample.

Because linear and area measurements were size-standardized prior to analysis (i.e., were rendered "dimensionless"), the relationship between body mass and each variable should be nonsignificant unless allometric effects remain. Multiple regression PGLS was employed to test for allometry, wherein each vertebral variable was evaluated as a function of both log-transformed RTL and log-transformed body mass. Where the influence of body mass on the variable was nonsignificant, body mass was removed from the PGLS regression model and the model was reevaluated with RTL as the only predictive factor (Table 4.2). All PGLS analyses were conducted in the R Statistical Package (Ihaka and Gentleman, 1996) using Analysis of Phylogenetics and Evolution (APE) package (Paradis et al., 2004) and nlme, with code provided by W.A. Barr.

Where RTL was a significant predictor of a given variable (Table 4.2), this variable was subsequently included in principal components analyses (PCAs). PCAs were conducted for each vertebral level across all mammalian taxa and for only primate taxa using both Datasets #1 and #2. PC1 scores were then extracted from the PCA

models and used to predict RTL for the extinct primate taxa using the regression equation model:

$$Y = mX + b,$$

where *Y* represents the predicted RTL, m is the slope, X is the extracted PC1 score, and b is the constant or *Y*-intercept.

The standard error of the estimate (SEE), calculated as:

$$SEE = sdY\sqrt{1-r^2},$$

where sd*Y* is the standard deviation of the *Y*-variable and r is the correlation between the X and *Y* variables, was used to provide 95% confidence limits (i.e., +/- 2 SEE) for the predictions. All PCAs were conducted in SPSS (IBM, Chicago, IL). For PGLS and PCA analyses, significance was recognized at $p<0.05$.

RESULTS

Postsacral Vertebral Numbers

Across the mammals sampled in this study, the number of proximal caudal vertebrae was significantly correlated with RTL (Pearson's two-tailed, r = 0.496, p < 0.01). The mammal exhibiting the greatest number of proximal caudal vertebrae (n=18) in the sample is the northern tamandua (*Tamandua mexicana*: Pilosa). The two primates exhibiting the greatest number of proximal caudal vertebrae (n=8) in the sample are both spider monkeys (*Ateles fusciceps* and *A. geoffroyi*). These mammalian taxa all possess prehensile tails. The nonprehensile-tailed mammal exhibiting the greatest number of proximal caudal vertebrae (n=16) is the giant anteater (*Myrmecophaga tridactyla*: Pilosa). All seven squirrel monkey (*Saimiri boliviensis*) individuals exhibited 6 proximal

caudal vertebrae, the greatest number observed in the nonprehensile-tailed primate sample.

PGLS

Figures 4.3-4.13 depict size-corrected vertebral variables on RTL and a fitted line (with 95% confidence intervals) for the model that includes all mammalian taxa. PGLS results for all mammals and for only primate taxa are provided in Table 4.2. Below, the PGLS results are discussed for each of the vertebral variables examined.

Vertebral Body Craniocaudal Length

As predicted, size-corrected vertebral body craniocaudal length increased as tail length increased at all three vertebral levels (Figure 4.4; Table 4.2). RTL was a significant predictor of vertebral body craniocaudal length ($p<0.05$) at all three vertebral levels among all mammals and among only primates. Among all mammalian taxa, RTL accounted for 40%, 23% and 39% of variation in vertebral body craniocaudal length at the levels of the first postsacral, mid-proximal, and transition vertebrae, respectively. Among only primate taxa, RTL accounted for 57%, 36% and 66% of variation in vertebral body craniocaudal length at the levels of the first postsacral, mid-proximal, and transition vertebrae, respectively.

The influence of body size on vertebral body craniocaudal length was significant at the level of the first postsacral vertebra among all mammals ($p<0.05$), and at the level of the first postsacral and mid-proximal vertebrae among primates ($p <0.00$), suggesting allometric effects remained. There was an intermediate phylogenetic signal for this variable at all three vertebral levels among all mammals (Table 4.2). Among primates,

phylogenetic signal was low at the level of the first postsacral vertebra ($\lambda = 0.32$), absent at the level of the mid-proximal vertebra ($\lambda = 0.00$), and highest at the level of the TV ($\lambda = 0.48$).

Cranial Articular Surface Shape

As predicted, the ratio of mediolateral to dorsoventral breadth decreased as tail length increased at all three vertebral levels (Figure 4.5; Table 4.2), indicating that the cranial articular surface becomes more circularly shaped as tail length increases. RTL was a significant predictor of cranial articular surface shape ($p<0.05$) at all three vertebral levels among all mammals and among only primates (Table 4.2). Among all mammalian taxa, RTL accounted for 62%, 44% and 59% of variation in cranial articular surface shape at the levels of the first postsacral, mid-proximal, and TV, respectively. Among only primate taxa, RTL accounted for 68%, 56% and 52% of variation in cranial articular surface shape at the levels of the first postsacral, mid-proximal, and TV, respectively.

Among all mammals, body mass was also a significant predictor of cranial articular surface shape ($p<0.05$), though only at the level of the mid-proximal vertebra, suggesting allometric effects remained. The influence of body mass was nonsignificant ($p>0.05$) for all models in the primate sample. Among all mammals, a phylogenetic signal was absent the level of the first postsacral ($\lambda = 0.00$), intermediate at the mid-proximal caudal vertebrae ($\lambda = 0.62$), and high ($\lambda = 1.00$) at the level of the transition vertebra. Among only primates, a phylogenetic signal was absent ($\lambda = 0.00$) the levels of the first postsacral and transition vertebrae, but high ($\lambda = 0.86$) at the level of the mid-proximal vertebra.

Cranial Articular Surface Area

As predicted, size-corrected cranial articular surface area increased as tail length increased at all three vertebral levels (Figure 4.6; Table 4.2). RTL was a significant predictor of cranial articular surface area ($p<0.05$) across all three vertebral levels among all mammals and among only primates. Among all mammalian taxa, RTL accounted for 31%, 32% and 25% of variation in this variable at the levels of the first postsacral, mid-proximal, and transition vertebrae, respectively. Among only primates, RTL accounted for 31%, 61% and 68% of variation in this variable at the levels of the first postsacral, mid-proximal, and transition vertebrae, respectively.

At all three caudal vertebral levels among all mammals and among only primates, the influence of body mass was nonsignificant ($p>0.05$). Among all mammals (first postsacral, $\lambda = 0.88$; midproximal, $\lambda =0.87$; transition, $\lambda =1.00$) and among only primates (first postsacral, $\lambda = 0.89$, midproximal, $\lambda =0.77$, transition, $\lambda = 0.70$) all three vertebral levels, results demonstrated somewhat high phylogenetic signals (Table 4.2).

Transverse Process Breadth

As predicted, size-corrected transverse process breadth increased as tail length increased at all three vertebral levels (Figure 4.7; Table 4.2). RTL was a significant predictor of transverse process breadth ($p<0.05$) at all vertebral levels among all mammals and among only primates (Table 4.2). Among all mammalian taxa, RTL accounted for 44%, 19%, and 14% of variation in transverse process breadth at the levels of the first postsacral, mid-proximal, and TV, respectively (Table 4.2). Among only primate taxa, RTL accounted for 47%, 12%, and 59% of variation in transverse process

breadth at the levels of the first postsacral, mid-proximal, and transition vertebra, respectively (Table 4.2).

Among all mammals, the influence of body mass on transverse process breadth was significant ($p<0.05$) at the levels of the first postsacral and the mid-proximal vertebrae, but not at the level of the transition vertebra (Table 4.2). Among only primates, body mass had a significant effect size ($p<0.05$) on transverse process breadth at the levels of the first postsacral and the TV, but not at the level of the mid-proximal vertebra (Table 4.2). Among all mammals, high phylogenetic signals were detected at all three vertebral levels (first postsacral, $\lambda=0.95$; mid-proximal, $\lambda=0.93$, and transition, $\lambda=0.92$; Table 4.2). Among only primates, PGLS results demonstrated a high phylogenetic signal for the first postsacral ($\lambda=0.87$), a lower phylogenetic signal at the level of the mid-proximal caudal vertebra ($\lambda=0.67$) and the absence of a phylogenetic at the level of the TV ($\lambda=0.00$).

Transverse Process Craniocaudal Angle

As predicted, the craniocaudal angle of the transverse processes decreased (i.e., became more acute) as tail length increased at the levels of the first postsacral and mid-proximal vertebrae (the only vertebrae for which this measurement could be reliably obtained; Figure 4.8; Table 4.2), indicating that as tail length increases the transverse processes become relatively more caudally angled. RTL was a significant predictor of transverse process craniocaudal angle ($p<0.05$) at the levels of the first postsacral and the mid-proximal caudal vertebrae among all mammals and among only primates. Among all mammalian taxa, RTL accounted for 76% and 52% of variation in transverse process

craniocaudal angle at the levels of the first postsacral and the mid-proximal caudal vertebra, respectively (Table 4.2). Among only primates, RTL accounted for 78% and 59% of variation in transverse process craniocaudal angle at the levels of the first postsacral and the mid-proximal caudal vertebrae, respectively (Table 4.2).

The influence of body mass on transverse process craniocaudal angle was nonsignificant ($p>0.05$) at both vertebral levels among all mammals and among only primates (Table 4.2). A phylogenetic signal for this variable was absent ($\lambda = 0.0$) at both vertebral levels among all mammals and among only primates.

Transverse Process Dorsoventral Angle

As predicted, the dorsoventral angle of the transverse processes decreased (i.e., became more acute) as tail length increased at the level of the first postsacral and the mid-proximal vertebrae (the only vertebrae for which this measurement could be reliably obtained; Figure 4.9; Table 4.2), indicating that transverse processes become more ventrally angled as tail length increases. RTL was a significant predictor of transverse process dorsoventral angle ($p<0.05$) at the levels of the first postsacral and the mid-proximal vertebrae among all mammals and among only primates. Among all mammalian taxa, RTL accounted for 27% and 38% variation in transverse process craniocaudal angle at the levels of the first postsacral and the mid-proximal vertebrae, respectively (Table 4.2). Among only primates, RTL accounted for 22% and 50% variation in transverse process dorsoventral angle at the levels of the first postsacral and the mid-proximal caudal vertebrae, respectively (Table 4.2).

The influence of body mass on transverse process dorsoventral angle was nonsignificant ($p>0.05$) at both vertebral levels among all mammals and among only primates (Table 4.2). Among all mammals, a phylogenetic signal was intermediate at the level of the first postsacral ($\lambda = 0.56$) and absent ($\lambda = 0.0$) at the level of the mid-proximal caudal vertebra. Among only primates, there was a high phylogenetic signal at the level of the first postsacral ($\lambda = 0.93$) and a phylogenetic signal was absent ($\lambda = 0.0$) at the level of mid-proximal caudal vertebra.

Transverse Process Position

Contrary to predictions, values for the position of the transverse processes relative to the ventral edge of the vertebral body increased as tail length increased at the levels of the first postsacral and the mid-proximal vertebra (the only vertebrae on which this measurement was obtained; Figure 4.10; Table 4.2), indicating that transverse processes become increasingly dorsally positioned on the vertebral body as tail length increases. RTL was a significant predictor of transverse process position ($p<0.05$) at the level of the first postsacral vertebra, but not at the level of the mid-proximal caudal vertebrae, among all mammals and among only primates. Among all mammalian taxa, RTL accounted for 48% and 9% of variation in transverse process position at the levels of the first postsacral and the mid-proximal vertebrae, respectively (Table 4.2). Among only primates, RTL accounted for 57% and 9% of variation in transverse process position at the levels of the first postsacral and the mid-proximal caudal vertebrae, respectively (Table 4.2).

The influence of body mass was nonsignificant ($p>0.05$) on transverse process position at both vertebral levels among all mammals and among only primates (Table

4.2). Among all mammals and among only primates, PGLS results demonstrated the absence ($\lambda = 0.0$) of a phylogenetic signal this variable at both vertebral levels.

Area of Cranial Neural Aperture

Not all taxa possess neural arches, and thus it should be noted that hominoid primates and other mammals possessing coccygeal-like postsacral vertebrae are inherently excluded from this analysis and subsequent (spinous process length, spinous process craniocaudal angle and prezygapophyseal orientation) analyses.

As predicted, size-corrected area of cranial neural aperture increased as tail length increased at the levels of the first postsacral and the mid-proximal vertebrae (Figure 4.11; Table 4.2). RTL was a significant predictor of the area of the cranial neural aperture at the level of the first postsacral ($p<0.05$) and a nonsignificant predictor at the level of the mid-proximal caudal vertebra ($p>0.05$), among all mammals and among only primates (Table 4.2). Among all mammalian taxa, RTL accounted for 27% of variation in the area of the cranial neural aperture at the level of the first postsacral vertebra (Table 4.2). Among only primates, RTL accounted for 44% of variation in the area of the cranial neural aperture at the level of the first postsacral vertebra (Table 4.2).

The influence of body mass was nonsignificant ($p>0.05$) on the area of the cranial neural aperture at the levels of both the first postsacral and the mid-proximal caudal vertebrae among all mammals and among only primates (Table 4.2). High phylogenetic signals were detected at both vertebral levels among all mammals (first postsacral, $\lambda = 1.00$; mid-proximal, $\lambda =0.87$) and among only primates (first postsacral, $\lambda = 0.79$; mid-proximal, $\lambda =0.97$) (Table 4.2).

Spinous Process Length

As predicted, the length of the spinous process increased as tail length increased (Figure 4.12; Table 4.2). RTL was a significant predictor of spinous process length at both caudal vertebral levels ($p<0.05$) among all mammals and among only primates. Among all mammalian taxa, RTL accounted for 54% and 49% of variation in spinous process length at the level of the first postsacral and the mid-proximal caudal vertebrae, respectively (Table 4.2). Among only primates, RTL accounted for 77% and 54% of variation in spinous process length at the level of the first postsacral and the mid-proximal caudal vertebrae, respectively (Table 4.2).

The influence of body mass on spinous process length was nonsignificant ($p>0.05$) at both vertebral levels among all mammals and among only primates (Table 4.2). A strong phylogenetic signal was detected at both caudal vertebral levels among all mammals (first postsacral, $\lambda = 1.00$; mid-proximal, $\lambda =1.00$) and among only primates (first postsacral, $\lambda = 0.87$; mid-proximal, $\lambda =1.00$) (Table 4.2).

Spinous Process Craniocaudal Angle

Results were somewhat consistent with predictions. At the level of the first postsacral vertebra, spinous process craniocaudal angle decreased (i.e., became more acute) as tail length increased (Figure 4.13; Table 4.2), suggesting that spinous processes become more cranially oriented as tail length increases at this vertebral level. However, at the level of the mid-proximal caudal vertebra, spinous process craniocaudal angle increased (i.e., became more obtuse) as tail length increased, suggesting spinous processes become more caudally oriented as tail length increases. Nonetheless, the effect

of RTL (and body mass) was nonsignificant ($p>0.05$) at both vertebral levels among all mammals and among only primates.

Prezygapophyseal orientation

Results were inconsistent with predictions. At both vertebral levels, prezygapophyseal articular facet orientation decreased (i.e., angle became more acute) as tail length increased (Figure 2.14; Table 2.2), suggesting that prezygapophyses become more sagittally oriented as tail length increases. RTL was a nonsignificant ($p>0.05$) predictor of this variable at the level of the first postsacral vertebra, and a significant ($p<0.05$) predictor at the level of the mid-proximal caudal vertebra, among all mammals and among only primates. RTL accounted for 18% and 29% of variation in prezygapophyseal orientation at the level of the mid-proximal caudal vertebra among all mammals and among only primates, respectively.

The influence of body mass on prezygapophyseal orientation was nonsignificant ($p>0.05$) at the level of the mid-proximal caudal vertebra among all mammals and among only primates (Table 2). PGLS results demonstrated that a phylogenetic signal was present only among all mammals at the level of the mid-proximal caudal vertebra ($\lambda = 0.61$; Table 2).

Principal Components Analyses

The variables included in the PCA are listed in Table 4.2. The PCA results are presented in Table 4.3. As with the PGLS analyses, the PCAs were conducted among all mammals and among only primates for both Datasets #1 and #2 at the levels of the first postsacral and mid-proximal caudal vertebra. For the TV, PCA include only Dataset #1

as the variables obtained in Dataset #2 are variably present (e.g., neural arches) at this vertebral level.

Dataset #1

At all three vertebral levels, Dataset #1 included four variables for which RTL had a significant effect size (Table 4.2): vertebral body craniocaudal length, cranial articular surface shape and area, and transverse process breadth. At the level of the first postsacral vertebra, PC1 accounted for approximately 74% and 77% of variation among all mammals and among only primates, respectively. At the level of the mid-proximal caudal vertebra, PC1 accounted for approximately 64% and 65% of variation among all mammals and among only primates, respectively. At the level of the TV, PC1 accounted for approximately 53% and 66% of variation among all mammals and among only primates, respectively.

Dataset #2

At the level of the first postsacral vertebra, Dataset #2 included 9 variables for which RTL had a significant effect size (Table 4.2): vertebral body craniocaudal length, cranial articular surface shape and area, area of the cranial neural aperture, transverse process breadth, position, and dorsoventral and craniocaudal angles, and spinous process length. PC1 accounted for approximately 57% and 62% of variation among all mammals and among only primates, respectively. PCA at the level of the mid-proximal caudal vertebra included the same variables as that at the level of the first postsacral with the exception of transverse process position, which was excluded because RTL did not have

a significant effect size on this variable (Table 4.2). PC1 accounted for approximately 42% and 50% of variation among all mammals and among only primates, respectively.

RTL on PC1 Scores

Figures 4.15 -4.17 depict bivariate plots of RTL on PC1 species mean scores for all mammals and only primates for both datasets at all three caudal vertebral levels. A morphocline is provided below the primate graphs to illustrate the anatomical changes associated with changing PC1 scores. Regression equation coefficients and model summaries are provided in Table 4.4.

Figures 4.15A and 4.15B show RTL on species mean PC1 scores for the first postsacral vertebra in Dataset #1 for all mammals and only primates, respectively. For all mammals in Dataset #1, 62% of the variation in RTL is accounted for by species mean PC1 scores (Figure 4.15A). For only primates in Dataset #1, 80% of the variation in RTL is accounted for by species mean PC1 scores (Figure 4.15B). The PC1 score for the *Archaeolemur* first postsacral specimen at this level using Dataset #1 predicts a RTL of 143 (95% confidence limits of 91 - 195) (Table 4.4). The PC1 score for the *Palaeopropithecus* first postsacral specimen at this level using Dataset #1 predicts a RTL of 36 (95% confidence limits of -16 to 88) (Figure 4.15B, Table 4.4).

Figures 4.15C and 4.15D show RTL on species mean PC1 scores for the first postsacral vertebra in Dataset #2 at the level of the first postsacral vertebra for all mammals and only primates, respectively. For all mammals in Dataset #2, 68% of the variation in RTL can be explained by species mean PC1 scores (Figure 4.15C). For only primates in Dataset #2, 94% of the variation in RTL can be explained by species mean

PC1 scores (Figure 4.15D). The PC1 score for the *Archaeolemur* first postsacral specimen at this level predicts a RTL of 120 (95% confidence limits of 92 - 148) (Table 4.4). The *Palaeopropithecus* specimen was not included in Dataset #2 because the neural arch is not completely formed. The standard error of the estimate for Dataset #2 (95% confidence intervals = +/-28) is nearly half that of Dataset #1 (95% confidence intervals= +/- 52).

Figures 4.16A and 4.16B show RTL on species mean PC1 scores for the mid-proximal caudal vertebra in Dataset #1 for all mammals and only primates, respectively. For all mammals in Dataset #1, 49% of the variation in RTL can be explained by species mean PC1 scores (Figure 4.16A). For only primates in Dataset #1, 78% of the variation in RTL can be explained by species mean PC1 scores (Figure 4.15B).

Figures 4.16C and 4.16D show RTL on species mean PC1 scores for the mid-proximal caudal vertebra in Dataset #2 for all mammals and only primates, respectively. For all mammals in Dataset #2, 70% of the variation RTL can be explained by species mean PC1 scores (Figure 4.16C). For only primates in Dataset #2, 93% of the variation in RTL is explained by species mean PC1 scores (Figure 4.16D). *Archaeolemur* and *Palaeopropithecus* either did not preserve, or elements could not be confidently identified as, caudal vertebral specimens. Thus, they were excluded from these predictions at the level of the mid-proximal caudal vertebra.

Figures 4.17A and 4.17B show RTL on species mean PC1 scores for the transition vertebra in Dataset #1 for all mammals and only primates, respectively. For all mammals, 38% of the variation in RTL is explained by species mean PC1 scores (Figure

4.17A). For only primates, 86% of the variation in RTL can be explained by species mean PC1 scores (Figure 4.17B). The PC1 score for the *Archaeolemur* transition vertebra at this level predicts a RTL of 109 (95% confidence limits 71 - 147) (Table 4.4). *Palaeopropithecus* does not preserve a transition vertebra.

DISCUSSION

The findings presented here demonstrate that caudal/coccygeal vertebral anatomy varies among primates that differ in relative tail length. Among primates, the vertebral features examined here accounted for 94%, 93% and 86% of the variation in RTL at the levels of the first postsacral (Dataset #2), mid-proximal (Dataset #2) and transition (Dataset #1) vertebrae, respectively. Additionally, by using a broad comparative mammalian sample to examine changes in tail length, this study demonstrates that some of these morphological changes are observed in other mammalian lineages thereby supporting functional links with tail length reduction (Figure 4.18). Generally, changes in vertebral features along a relative tail length continuum were consistent with the study's predictions: shorter-tailed primates exhibit a greater number of features associated with reduced proximal tail mobility, reduced range of motion and reduced leverage of basal tail musculature compared to longer-tailed primates.

Vertebral body craniocaudal length decreased as tail length decreased. Hamada et al. (2012) found that variation in the craniocaudal length of the first vertebral body was not as pronounced as that of other caudal vertebrae in their sample of hybridized macaques. Consistent with their findings, our study demonstrated that even in the context of the larger sample of primates employed here, the influence of RTL on craniocaudal

vertebral body length was smallest at the level of the first postsacral, followed by the mid-proximal, and then the transition vertebra. However, the results show that RTL was a significant predictor of RTL all three vertebral levels. Functionally, craniocaudal length of the vertebral bodies must be considered in the context of its interaction with the number of vertebrae in a given region and that spinal region's total length in order to understand the spine's potential range of motion (Ward, 1993; Shapiro and Simons, 2002). Although shorter-tailed macaques may have nearly as many proximal caudal vertebrae as macaques with longer tails (Table 4.1), the summed length of craniocaudally shorter caudal vertebrae produces an absolutely shorter proximal tail region. Consequently, the proximal tail region of a longer-tailed primate should theoretically achieve a greater arc of flexion than that of a shorter-tailed primate (Ward, 1993; Shapiro and Simons, 2002).

This study also demonstrated that that the articular surfaces of proximal caudal and coccygeal vertebrae became increasingly elliptically shaped (i.e., wider mediolaterally than dorsoventrally) and decreased in surface area relative to body mass, as tail length decreased (Figure 4.18), indicating that that tail reduction is associated with increasing dorsoventral vertebral body compression and reduced surface area for distributing forces across joints. Similar articular surface shape trends have been reported for the caudal articular surface of the sacrum in catarrhine primates (Russo and Shapiro, 2011). Though they did not provide quantitative measures of these articular surface dimensions for their mammalian sample, Nakatsukasa and colleagues (2003) asserted that dorsoventral compression of the caudal vertebral body is rare in nonhominoid

anthropoids, and that even among short-tailed cercopithecoids the cranial articular surface is wider dorsoventrally than mediolaterally. Yet, the results presented here show that values for the cranial articular surface shape ratio (mediolateral width/dorsoventral width) are above 1 for all caudal/coccygeal vertebrae, with the exception of the TV, among the mammal sample. Thus, the cranial articular surfaces of the first postsacral and mid-proximal caudal vertebrae among all primates (and mammals) are actually slightly wider mediolaterally than dorsoventrally. Moreover, since hominoids do not possess "mid-proximal" or "transition" caudal vertebrae, that the high cranial articular surface shape ratio values have an inverse relationship to tail length at all three vertebral levels suggest that dorsoventral vertebral body compression is not necessarily unique to hominoid primates (Figure 4.18). Notably, however, hominoid primates exhibited the highest values, and thus the most dorsoventrally compressed vertebral bodies, at the level of the first postsacral (Figure 4.5), and, among mammals there is a considerable amount of scatter in the data.

Functionally, changes in cranial articular surface shape and surface area likely influence the potential range of motion at, and ability to distribute forces across, intervertebral joint surfaces. Clinical work demonstrates that in humans, the range of extension movement at the (unfused) sacrococcygeal joint is between 5-15° (with average total mobility [extension and flexion] of 9°) (Maigne and Bertrand, 1996; Woon and Stringer, 2012). By contrast, Wilson (1972) has shown that macaques (*Macaca*: Primates) can dorsally extend their tails up to at least 155°, and Russo and Shapiro (2011; see also Schmitt et al., 2005) demonstrated that longer-tailed catarrhine primates have more

dorsally-tilted sacrocaudal articular surfaces than shorter-tailed catarrhines, which would facilitate dorsal extension in the former group. Nonetheless, Wilson (1972) suggested that short-tailed macaques should be able to achieve a greater degree of extension than long-tailed macaques. With respect to articular surface area, relatively smaller joint surfaces suggest a reduced ability to distribute high loads over a wider area, suggesting lower force magnitudes may transmitted across the caudal/coccygeal joint surfaces of shorter-tailed primates (see also Nakatsukasa et al., 2003; Russo et al., 2012).

Taken together, these results suggest that proximal caudal or coccygeal vertebrae having shorter vertebral bodies, along with more elliptically-shaped cranial articular surfaces, likely reduces the range of proximal tail movements in shorter-tailed primates, whereas proximal caudal or coccygeal vertebrae having longer vertebral bodies, along with more circularly-shaped cranial articular surfaces (Figure 4.5), likely permit longer-tailed primates a greater range of proximal tail movements. Nonetheless, comparative kinematic analyses of the sacrocaudal joint and proximal tail region among tail-bearing primates are needed to verify the functional hypotheses concerning tail movement proposed here.

Shorter-tailed primates are further characterized by proximal caudal vertebrae having smaller cranial neural apertures, shorter spinous processes, and less laterally projected transverse processes that are angled more dorsally, projected less caudally, and positioned more dorsally on the vertebral body, compared to longer-tailed primates (Figure 4.18). Contrary to predictions, the dorsal position of the transverse processes increased (i.e., became more dorsally positioned) as tail length increased. Transverse

processes that are positioned more dorsally should enhance leverage for dorsal extension (Shapiro, 1993). However, their positioning as it is observed here is also likely due to changes in dorsoventral height of the body. That is, as tail length decreases, dorsoventral compression of the vertebral body likely reduces the available space for the origin of the transverse processes. Given changes in articular surface dimensions, it is possible that future measures of transverse process position should consider it relative to dorsoventral breadth of the cranial articular surface.

Smaller neural apertures likely reflect a decrease in the size of the pathway for innervation to the tail (Ankel, 1965; 1972), and a reduction in the projection of the spinous and transverse processes decreases the leverage of, and surface area of attachment for, the basal tail musculature. Because hominoids lack external tails, much of the musculature associated with the tail (e.g., *abductor caudae lateralis* mm., *interspinalis caudae* mm.) is entirely absent. However, some basal tail musculature has become reduced and reorganized in the hominoid pelvis. Though their exact origins vary, the *ilio*-, *ischio*- and the *pubo- caudalis* are three pelvicaudal muscles that arise from the ventral surface of the ilium, ischial spine and adjacent surfaces, and the inner surface of the pubic symphysis, respectively, in tailed primates (Elftman, 1932; Hartmann and Straus, 1933). The *ilio*- and *ischio- caudalis* insert onto the ventrolateral surfaces of the transverse processes of the first few caudal vertebrae, as do some fibers of the *pubocaudalis*, though ventral slips of this latter muscle attach to the rectum (Elftman, 1932; Hartmann and Straus, 1933). These basal tail muscles act chiefly as abductor-flexors in tailed primates (Hartmann and Straus, 1933). In hominoids, the *ilio*- and *pubo-*

coccygeas mm. (homologs of *ilio* – and *pubo* – *caudalis* mm.) are reorganized on each side of the pelvic floor to make up the *levator ani* mm. (along with the *puborectalis* mm). The *levator ani* mm. attach to the ventral and lateral surfaces of the coccyx (Gray, 1977). The *ischiococcygeus* mm. (homolog of *ischiocaudalis* mm.) remain distinct from the levator ani group, but are reduced to a tendinous sheath (Elftman, 1932). The *ischiococcygeus* mm. attach to the lateral aspects of the last sacral vertebra and the coccygeal vertebrae (Gray, 1977). Right and left sides taken together, the *levator ani* mm. and the *ischiococcygeus* mm. form a hammock-like pelvic diaphragm, which supports the abdominal and pelvic viscera (Elftman, 1932; Wood, 1985; Woon and Stringer, 2012). It is unknown whether any other tailless mammals reorganize their tail musculature similarly. However, as tail length is likely proportional to tail mass (Organ, 2007), the proximal caudal and coccygeal anatomy observed here to characterize short or absent-tailed primates appears related to a reduction in tail length and its associated musculature.

Overall, the morphology of the sacro-caudal/coccygeal transition across mammals with reduced tail lengths varied considerably, often complicating counts of proximal caudal vertebrae in the species with very-short or absent tails. Some slow lorises (*Nycticebus*: Primates) possessed coccygeal-like vertebrae. Neural arches were partially formed with the laminae appearing as two bony ridges along the dorsal aspect of the body (Figure 4.19). Zygapophyses were absent, and in many cases the postsacral vertebral series were fully ankylosed. Where the laminae did appear fused, a neural aperture was compressed (i.e., closed off). Other mammalian taxa had postsacral vertebrae without mobile zygapophyseal facets, but bearing fully formed neural arches (e.g., *Hydrochaeris,*

Rodentia; Figure 4.19). The neural arches of the first postsacral vertebrae of several short-tailed macaques, including the Barbary macaque (*Macaca sylvanus*; RTL = 0) and the Tonkean macaques (*Macaca tonkeana*; RTL =8), were only partially formed and exhibited a deep groove between two laminar ridges (Figure 4.19; *contra* Nakatsukasa et al., 2003). Among nearly absent-tailed nonhominoid mammalian taxa, the presence of postzygapophyseal facets on the distal sacrum was variable, and there were a number of instances of absent sacral postzygapophyses/ present first postsacral prezygapophyses or present sacral postzygapophyses/ absent first postsacral prezygapophyses. This variation should be taken into consideration when attributing tail morphology to fossil primates on the basis of individual vertebrae.

Extinct Primates

The results of the extant mammal sample were used to reconstruct the tail lengths of two subfossil lemurs: *Archaeolemur* and *Palaeopropithecus*. The estimated RTLs of *Archaeolemur* and *Palaeopropithecus* calculated using the extant primate data are consistent with previous inferences concerning their tail lengths. For example, both the first postsacral and the transition vertebra for *Archaeolemur* predicted its relative tail length as over 100, or longer than the total length of its body and head. This generally accords with previous interpretations that *Archaeolemur* possessed a "long" tail (e.g., Godfrey et al., 2006). Specifically, the extant primate data here reconstructed the *Archaeolemur* tail length at between 109 (using the transition vertebra) and 143 (using the first postsacral Dataset #1). In comparison to primates in the extant study, the high estimated RTL for *Archaeolemur* of 143 falls closest to that of *Saguinus sp.* (RTL = 142),

while the low estimated RTL fall near *Macaca fascicularis* and *Sapajus apella* (both taxa, RTL= 107). However, Dataset #2, which contained the greatest number of variables and exhibited the highest R^2 and correlation (between PC1 species means scores and RTL), predicted the *Archaeolemur* RTL as 120, a value identical to that of *Varecia variegata* (Table 4.1).

The RTL estimate for *Palaeopropithecus* obtained in this study supports previous inferences that this taxon had a "short" tail (e.g., Godfrey et al., 2006). The reconstructed RTL of *Palaeopropithecus* using Dataset #1 is 36. This reconstructed RTL for *Palaeopropithecus* is identical to that of *Macaca assamensis* (Table 4.1). That the RTL reconstructions for the subfossil lemurs accord with previous interpretations of the tail lengths based on sacral anatomy, supports the utility of the extant primate caudal vertebral data presented here for making inferences about tail length from caudal vertebral anatomy.

Significance

The data presented in this study represent the first attempt at a quantitative examination of how caudal vertebral anatomy differs among nonprehensile-tailed primates that vary in tail length. This research has significance for our understanding of primate postcranial functional anatomy and evolution. First, this study provides an anatomical basis for research on nonprehensile tail kinematics and behavior. Only recently have researchers begun to devote attention to how nonprehensile-tailed primates use these appendages to maintain balance in arboreal settings (e.g., Larson and Stern, 2006; Stevens et al., 2008; Chadwell et al., 2013). A complete understanding of

nonprehensile tail functional morphology requires both the anatomical component (now provided by this results of this study), and the behavioral component.

Second, this research will enhance our understanding of tail loss in the primate fossil record. Complete caudal vertebral sequences are rarely found in the fossil record. As such, researchers cannot rely on straightforward counts of caudal vertebrae to make inferences about the tail lengths of extinct primates. Indeed, the ability to confidently attribute tail length to extinct primates, and perhaps more importantly, to track evolutionary changes in tail length within specific lineages, requires a better understanding of the aspects of caudal vertebral morphology associated with tail reduction. The mechanisms by which tails were lost in different primate clades, including the Hominoidea, are also unclear. It is likely that each mammalian lineage evolved taillessness for a different reason; however, the ability to appropriately contextualize its occurrence, either ecologically or behaviorally, cannot be ascertained until there is a better understanding of which fossil taxa are actually characterized by reduced tail lengths. Thus, a prerequisite to generating testable hypotheses for evaluating the evolutionary timing and functional significance of tail length reduction is the ability to confidently identify it in the fossil record. By identifying morphological correlates of tail length in caudal vertebrae among nonprehensile-tailed primates, this study now permits inferences concerning the tail lengths of fossil primates represented by only one, or few, caudal vertebral elements present.

CONCLUSIONS

Tail morphology varies greatly among primates. Much emphasis has been placed on the specialized prehensile-tails that characterize just six genera of platyrrhines. This study is the first to comprehensively examine caudal vertebral anatomy among nonprehensile-tailed primates that vary in tail length. The results of this study demonstrate that generally, longer-tailed taxa exhibit caudal vertebrae that are structured to permit increased proximal tail flexibility and increased range of intervertebral movement compared to primates with shorter tails or having no tail, which possess caudal/coccygeal vertebrae exhibiting reduced surface area for attachment of caudal musculature and a reduced range of motion and more restricted intervertebral movements. These form-function links are generally supported by the use of a broad comparative mammalian sample, in which similar morphological trends in relation to tail length are observed (Figure 4.18). The results of the extant primate caudal vertebral sample produced RTL predictions for *Archaeolemur* and *Palaeopropithecus* that were consistent with previous interpretations of their tail lengths based on sacral anatomy, suggesting that, using the anatomical correlates of tail length identified here, researchers can more accurately reconstruct the tail lengths of fossil primates beyond a simple present vs. absent dichotomy.

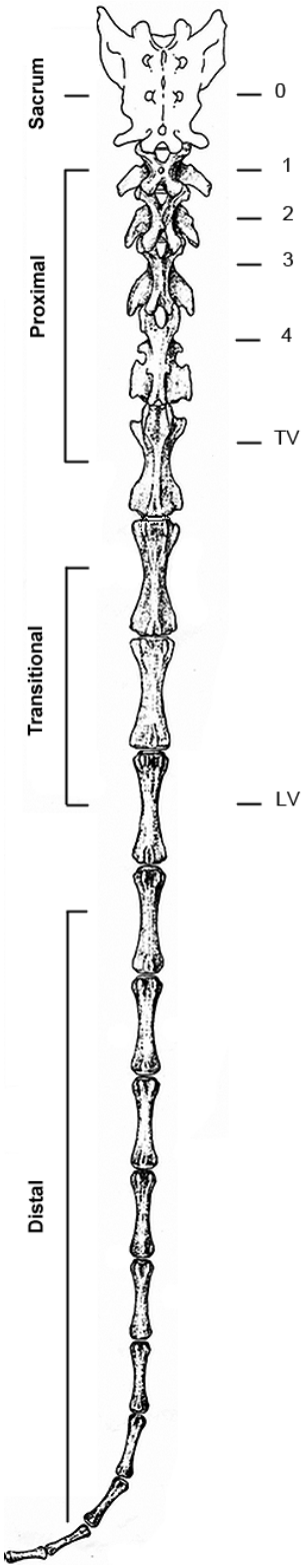

Figure 4.1 Illustration of the primate sacrocaudal region showing regional distinctions along the tail. Starting with the sacrum(0), proximal caudal vertebrae are numbered progressing distally until reaching the last proximal caudal vertebra known as the transition vertebra (TV). The craniocaudal length of caudal vertebral bodies increases until reaching a longest vertebra (LV). Thereafter, caudal vertebrae decrease in craniocaudal vertebral body length until reaching the tail's end. See text for more detail. Figure adapted from Kimura et al. (1986), modified in Russo and Young (2011).

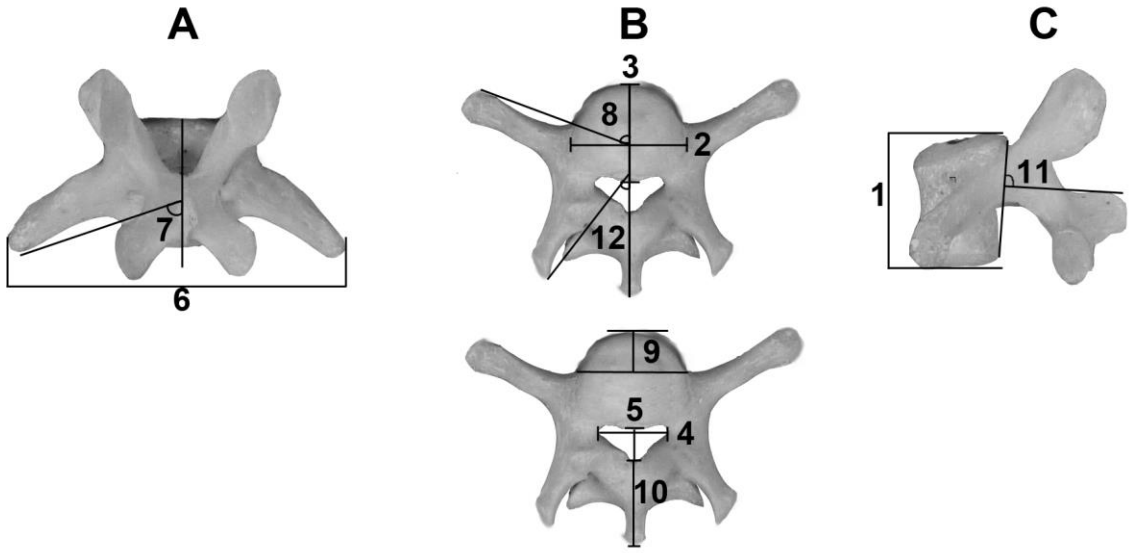

Figure 4.2 Measurements collected on proximal caudal vertebrae. Views are dorsal view (A), cranial (B) and lateral (C). 1) Maximum craniocaudal vertebral body length (mm) of caudal vertebral body in the midsagittal plane; 2) Cranial articular surface mediolateral breadth (mm): maximum mediolateral diameter of the cranial articular surface; 3) Cranial articular surface dorsoventral breadth (mm): maximum dorsoventral diameter of the cranial articular surface; 4) Neural aperture mediolateral breadth (mm): maximum breadth of the neural aperture in the transverse plane; 5) Neural aperture dorsoventral breadth (mm): maximum height of the neural aperture from the dorsal edge of the vertebral body to the dorsal edge of the neural canal in the midsagittal plane; 6) Transverse process breadth (mm): maximum lateral expansion of transverse processes measured from the lateralmost point of the left transverse process to the lateralmost point on the right transverse process; 7) Transverse process craniocaudal orientation (°): measured in the coronal plane as the angle between the caudal edge of the transverse process (defined as a line connecting the caudalmost point of the transverse process to the point of attachment on the vertebral body) and the midsagittal plane of the vertebra; 8) Transverse process dorsoventral orientation (°): measured in the transverse plane as the angle between the ventral edge of the transverse process (defined as a line connecting the ventralmost point on the tip of the transverse process and the point of attachment on the vertebral body) and the midsagittal plane of the vertebra; 9) Transverse process dorsoventral position (mm): distance between a line connecting the ventralmost attachment points of the transverse processes to the vertebral body and a line drawn tangent to the ventral surface of the vertebral body; 10) Spinous process length (mm): maximum distance from the dorsal edge of the vertebral canal to the apex of the spinous process; 11) Spinous process craniocaudal orientation (°): angle between the cranial edge of the spinous process (defined as a line connecting the cranialmost point on the spinous process and the point of attachment on the dorsal edge of the neural canal) and a line connecting the dorsocranial and dorsocaudal most points on the vertebral body; 12) Prezygapophyseal orientation (°): the angle formed between the chord of the arc formed by the prezygapophyseal articular surface and a sagittal plane through the vertebra). See text for some variable calculations. Adapted from Shapiro, 2007.

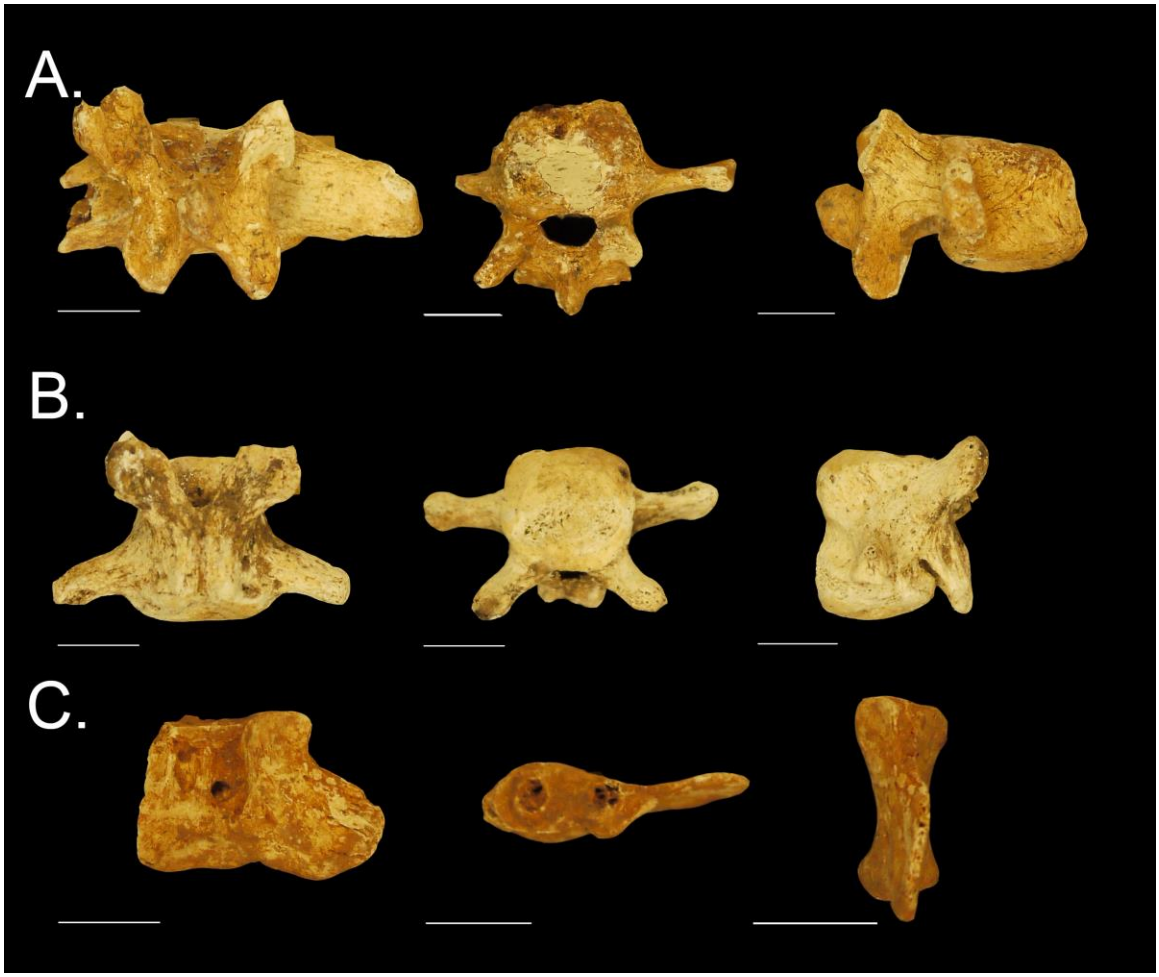

Figure 4.3 Subfossil lemur caudal vertebrae sample. A) *Archaeolemur* DPC 12890A, first postsacral vertebra; B) *Archaeolemur* DPC 12890F, transition vertebra; C) *Palaeopropithecus* DPC 17201, first postsacral. Views are (from left to right) dorsal, cranial and lateral. In dorsal view, cranial is up. In cranial view, ventral is up. In lateral view, ventral is right except for *Archaeolemur* DPC 12890A.

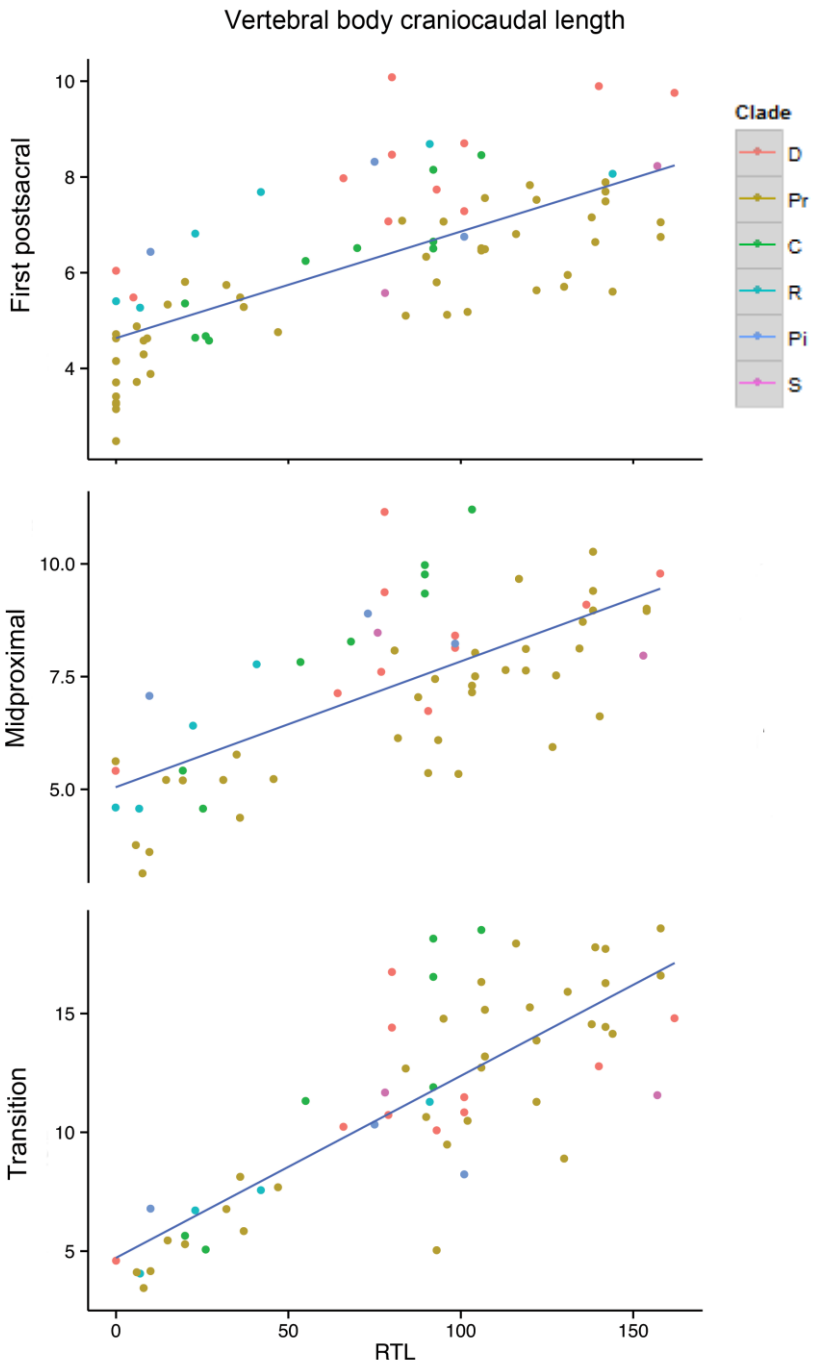

Figure 4.4 Size-corrected vertebral body craniocaudal length on RTL. A) first postsacral B) mid-proximal and C) transition vertebrae. Legend: D = Diprotodontia; Pr = Primates; R= Rodentia; C= Carnivora; Pi = Pilosa; S= Scandentia.

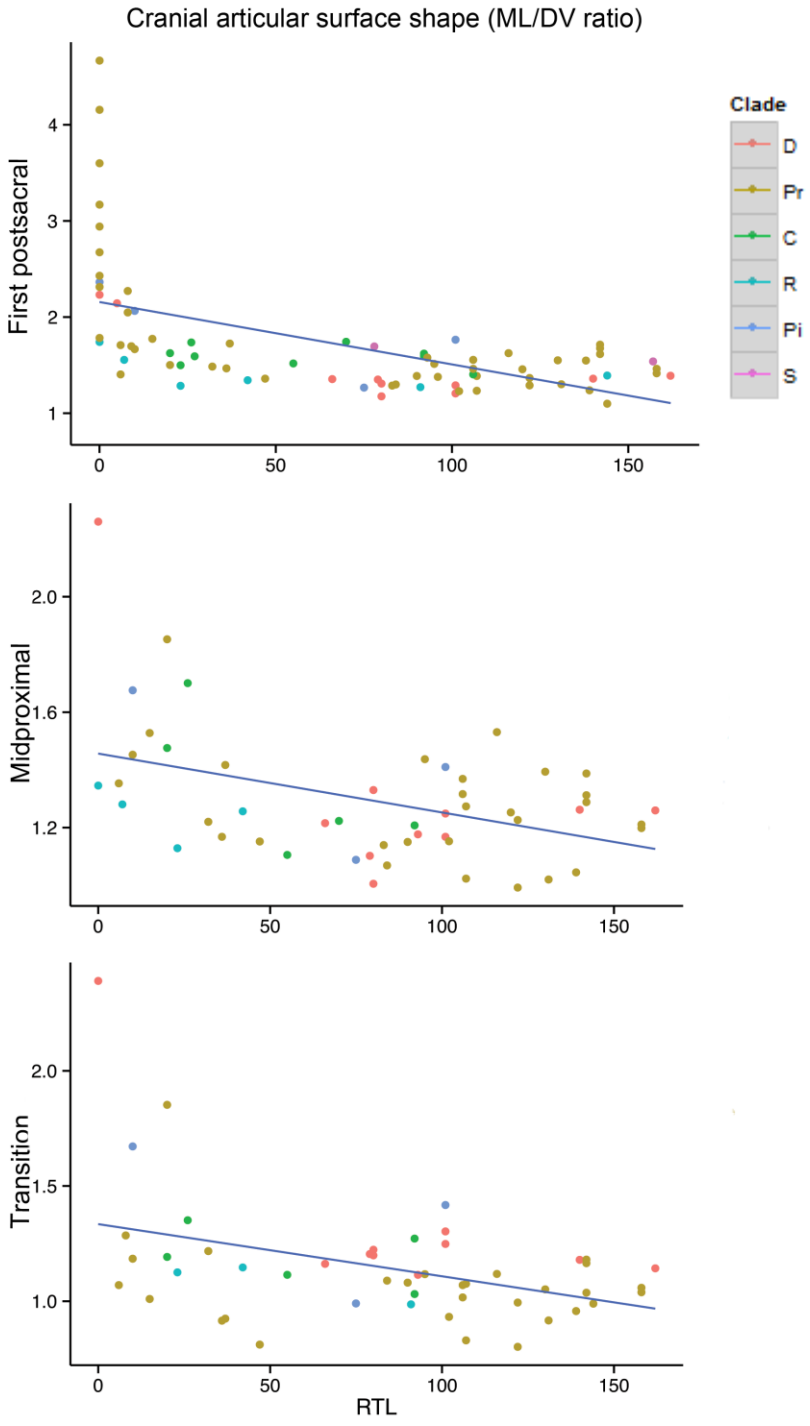

Figure 4.5 Cranial articular surface shape (mediolateral breadth/dorsoventral breadth) on RTL. A) first postsacral vertebra B) mid-proximal and C) transition vertebrae. Legend: D = Diprotodontia; Pr = Primates; R= Rodentia; C= Carnivora; Pi = Pilosa; S= Scandentia.

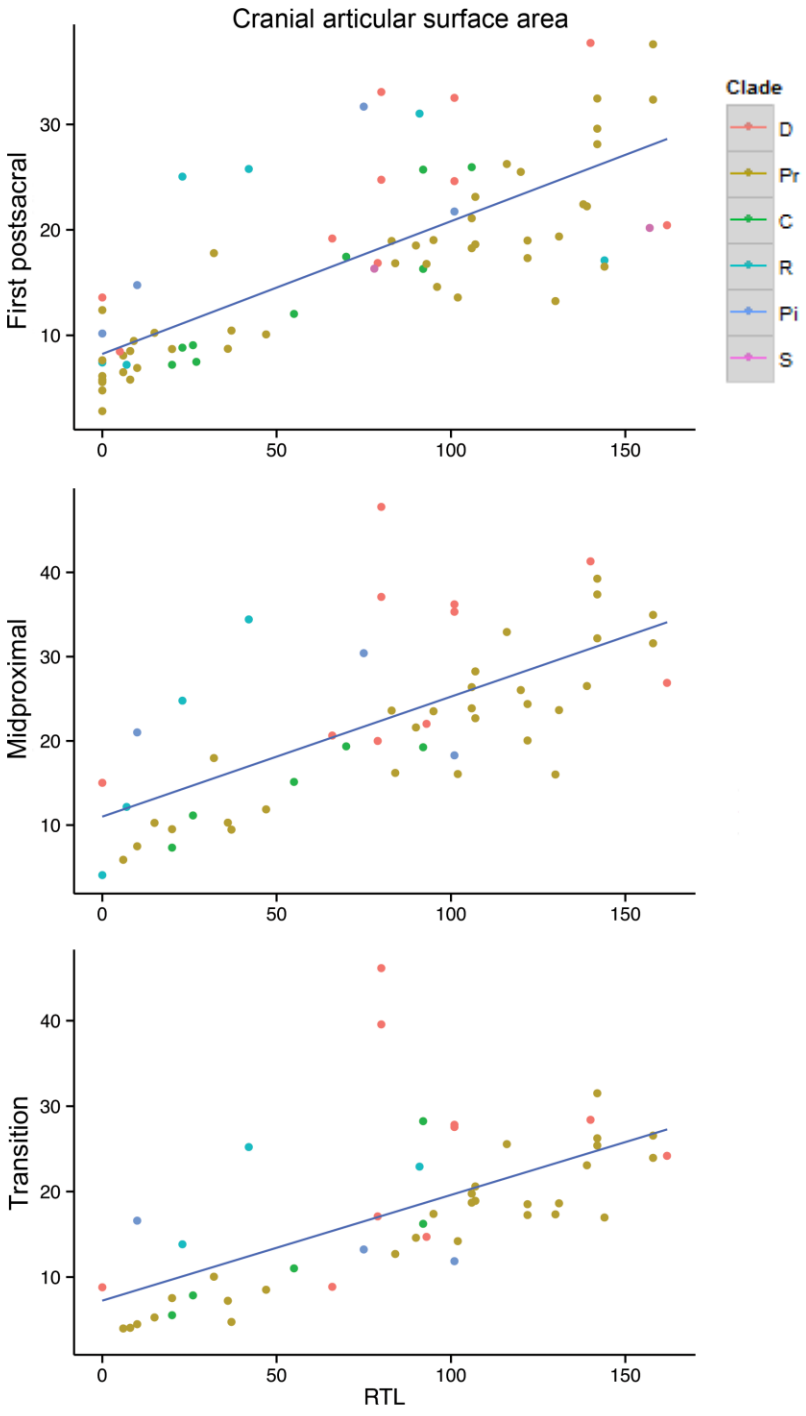

Figure 4.6 Size-corrected cranial articular surface area on RTL. A) first postsacral B) mid-proximal and C) transition vertebrae. Legend: D = Diprotodontia; Pr = Primates; R= Rodentia; C= Carnivora; Pi = Pilosa; S= Scandentia.

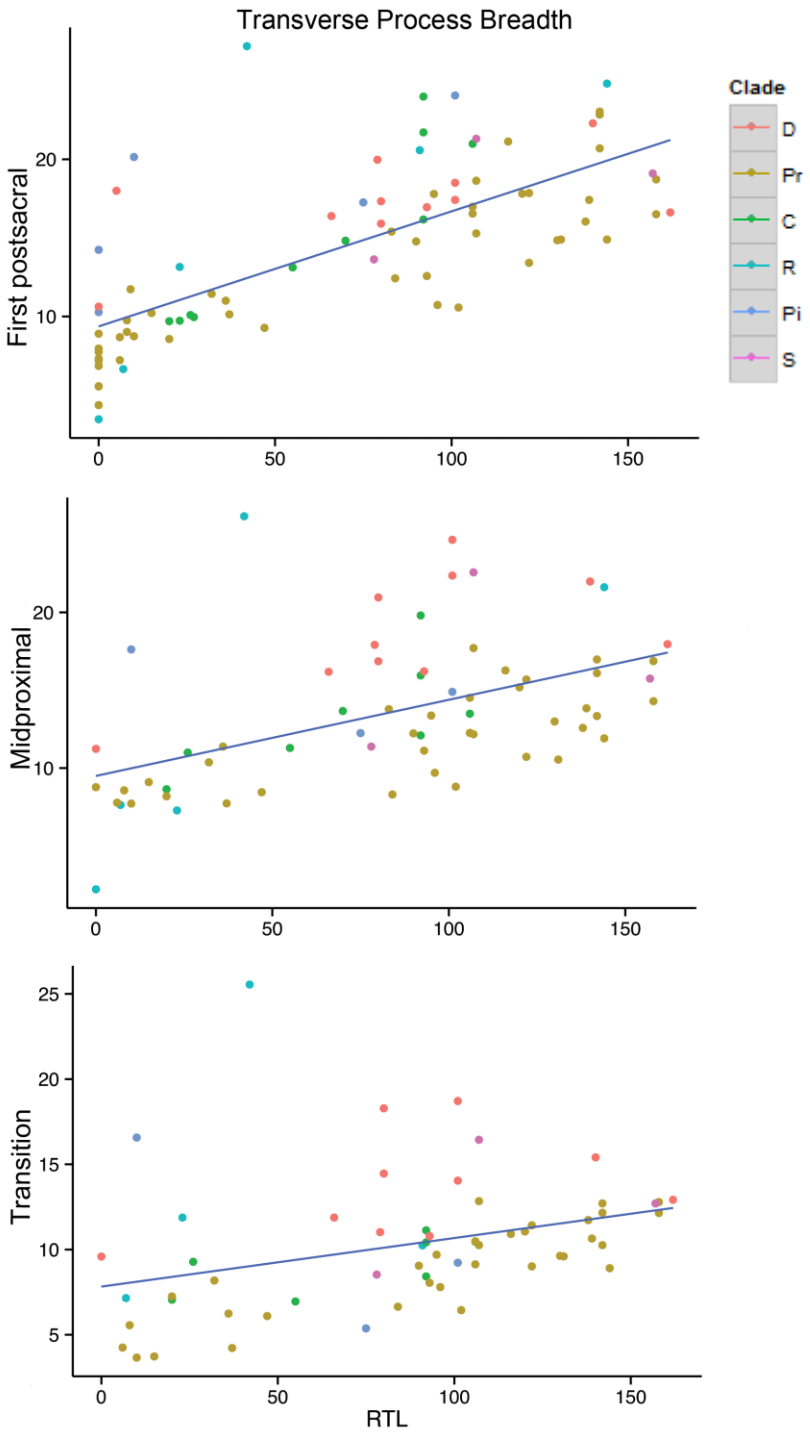

Figure 4.7 Size-corrected transverse process breadth on RTL. A) first postsacral vertebra B) mid-proximal and C) transition vertebrae. Legend: D = Diprotodontia; Pr = Primates; R= Rodentia; C= Carnivora; Pi = Pilosa; S= Scandentia.

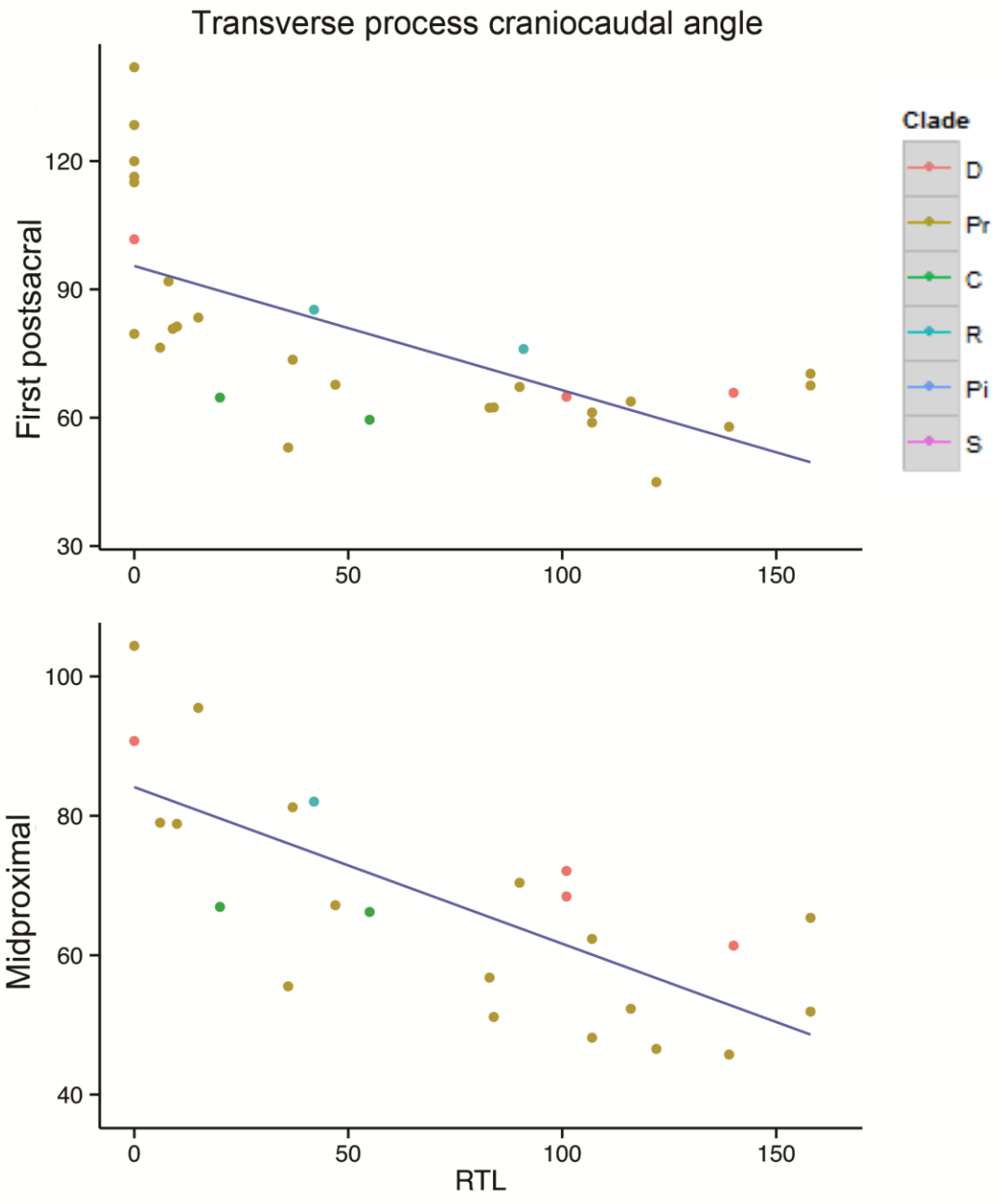

Figure 4.8 Transverse process craniocaudal angle on RTL. A) the first postsacral vertebra and B) mid-proximal. Legend: D = Diprotodontia; Pr = Primates; R= Rodentia; C= Carnivora; Pi = Pilosa; S= Scandentia.

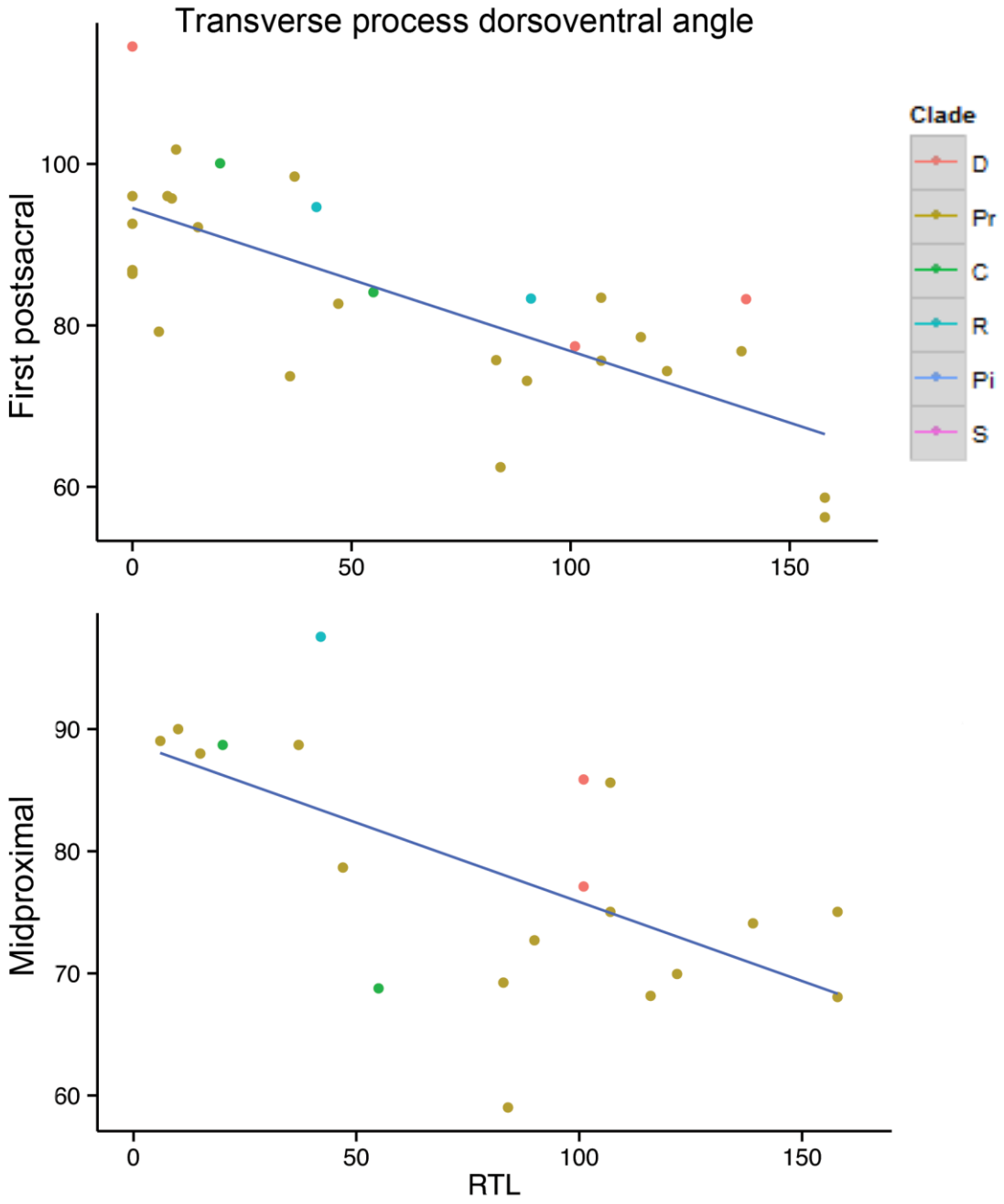

Figure 4.9 Transverse process dorsoventral angle on RTL. A) the first postsacral vertebra and B) mid-proximal. Legend: D = Diprotodontia; Pr = Primates; R= Rodentia; C= Carnivora; Pi = Pilosa; S= Scandentia.

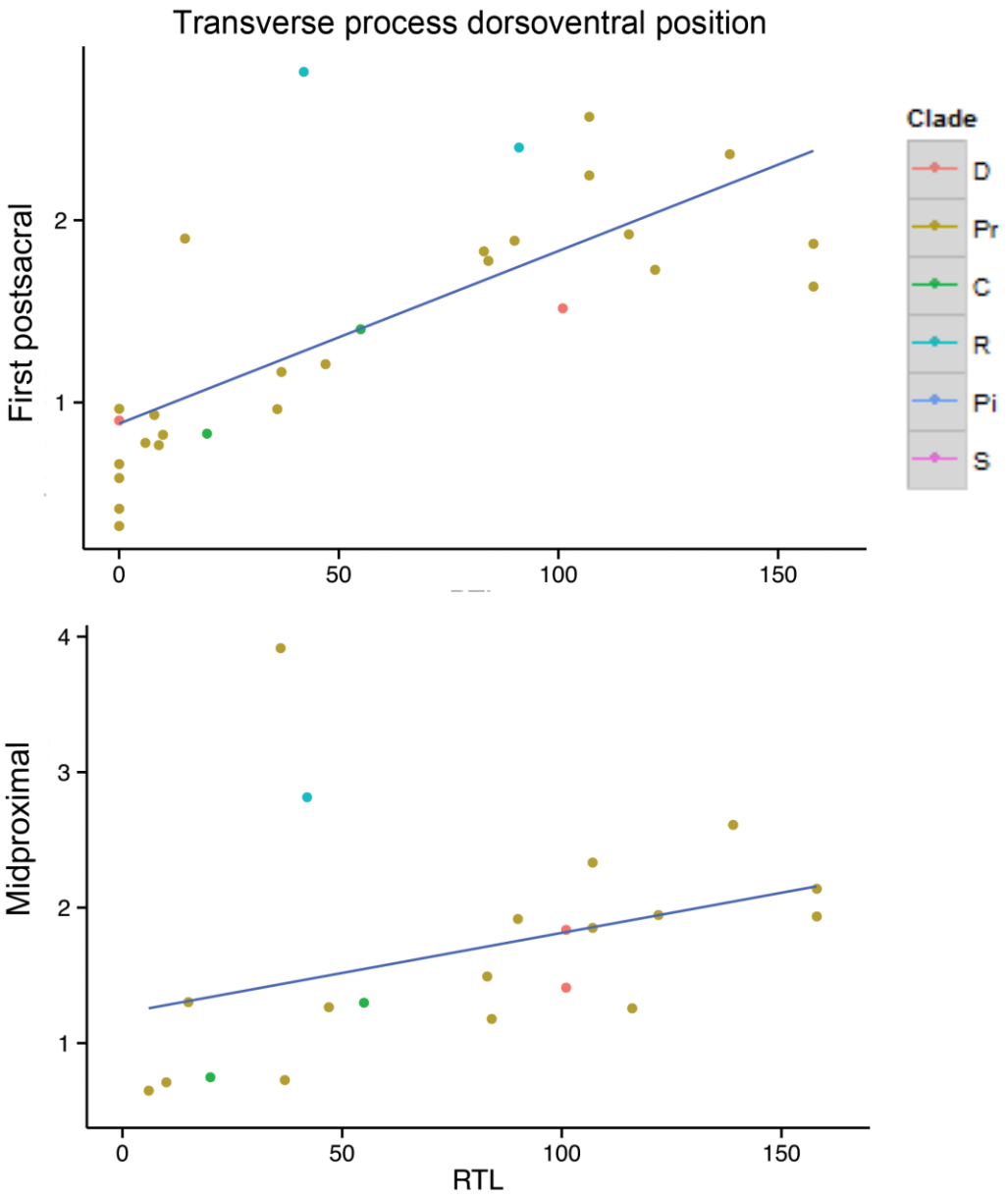

Figure 4.10 Size-corrected transverse process position on RTL. A) the first postsacral vertebra and B) mid-proximal. Legend: D = Diprotodontia; Pr = Primates; R= Rodentia; C= Carnivora; Pi = Pilosa; S= Scandentia.

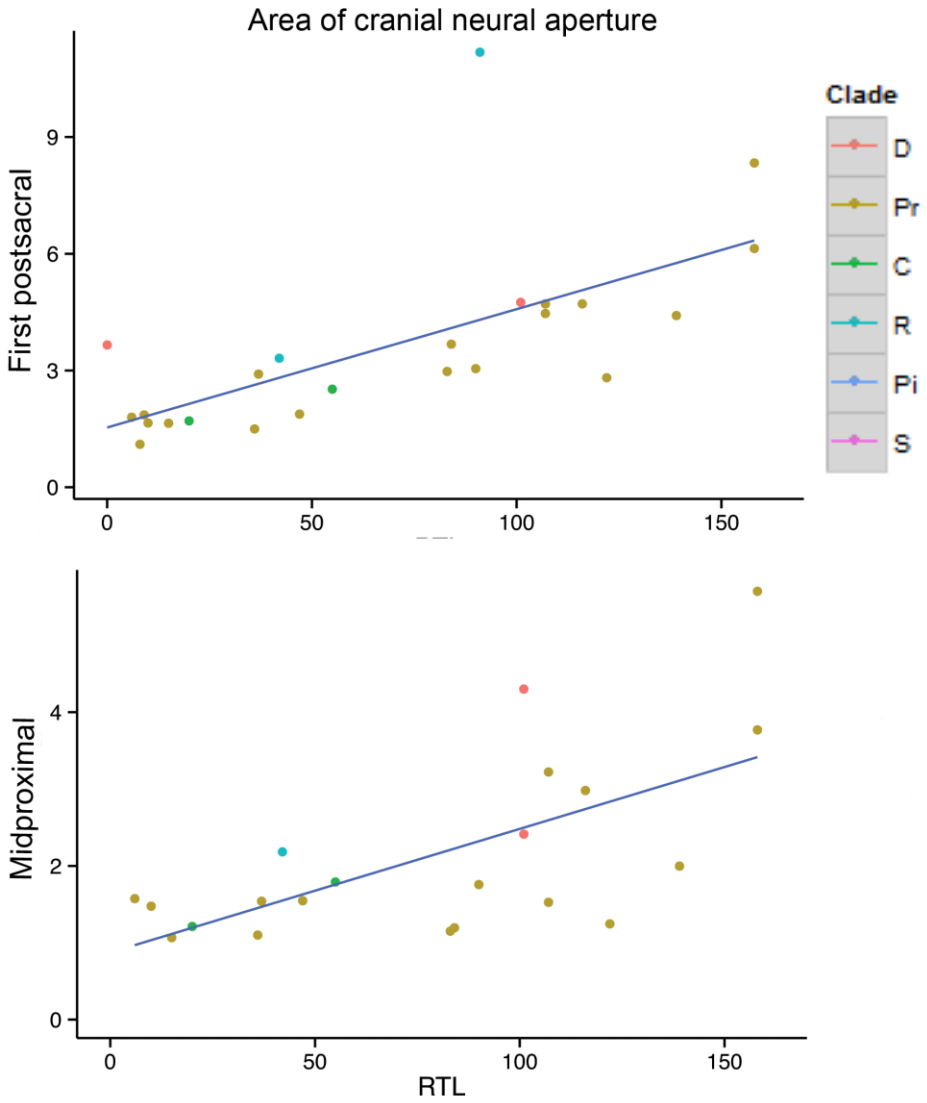

Figure 4.11 Size-corrected area of cranial neural aperture on RTL. A) the first postsacral vertebra and B) mid-proximal. Legend: D = Diprotodontia; Pr = Primates; R= Rodentia; C= Carnivora; Pi = Pilosa; S= Scandentia.

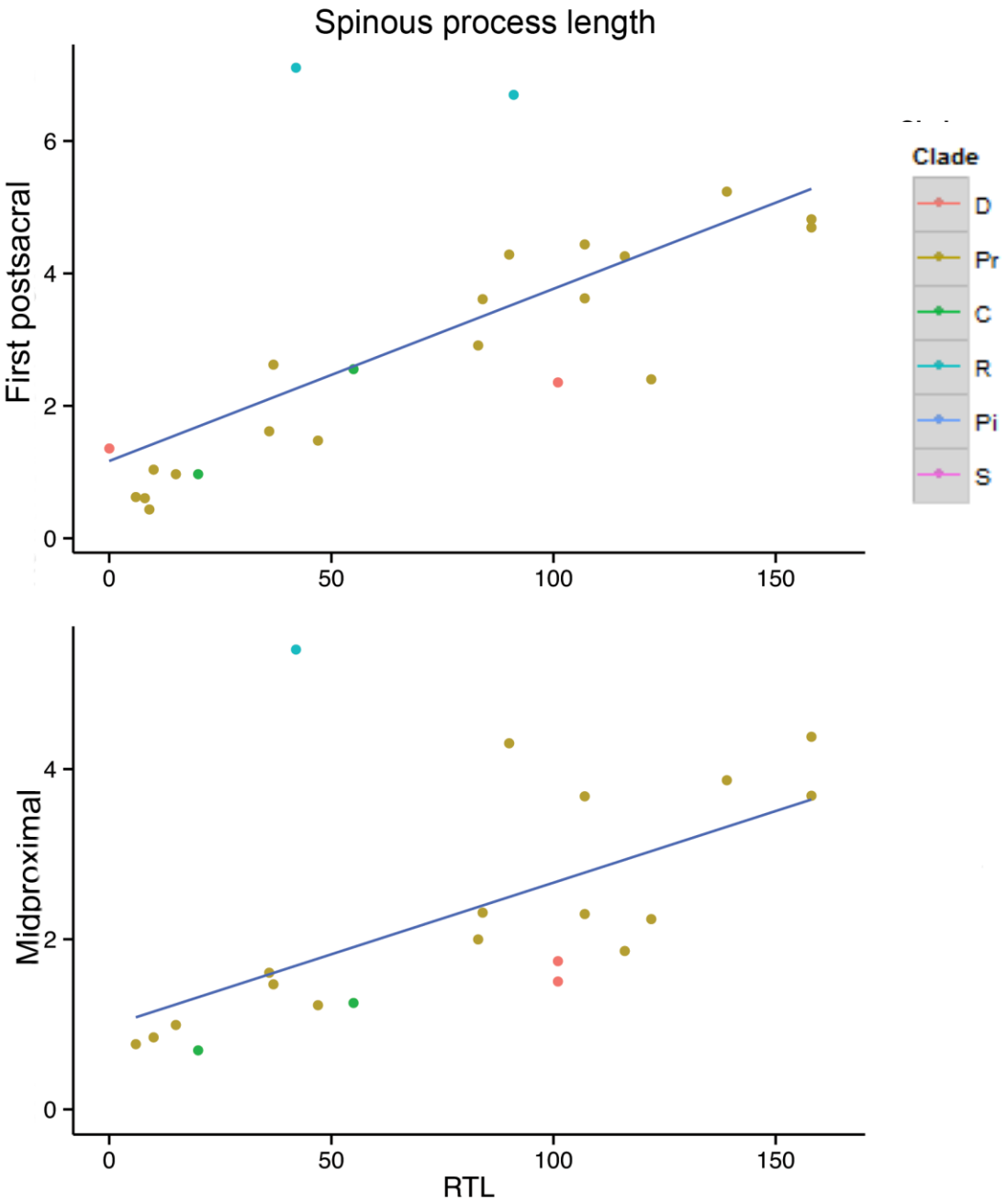

Figure 4.12 Size-corrected spinous process length on RTL. A) the first postsacral vertebra and B) mid-proximal. Legend: D = Diprotodontia; Pr = Primates; R= Rodentia; C= Carnivora; Pi = Pilosa; S= Scandentia.

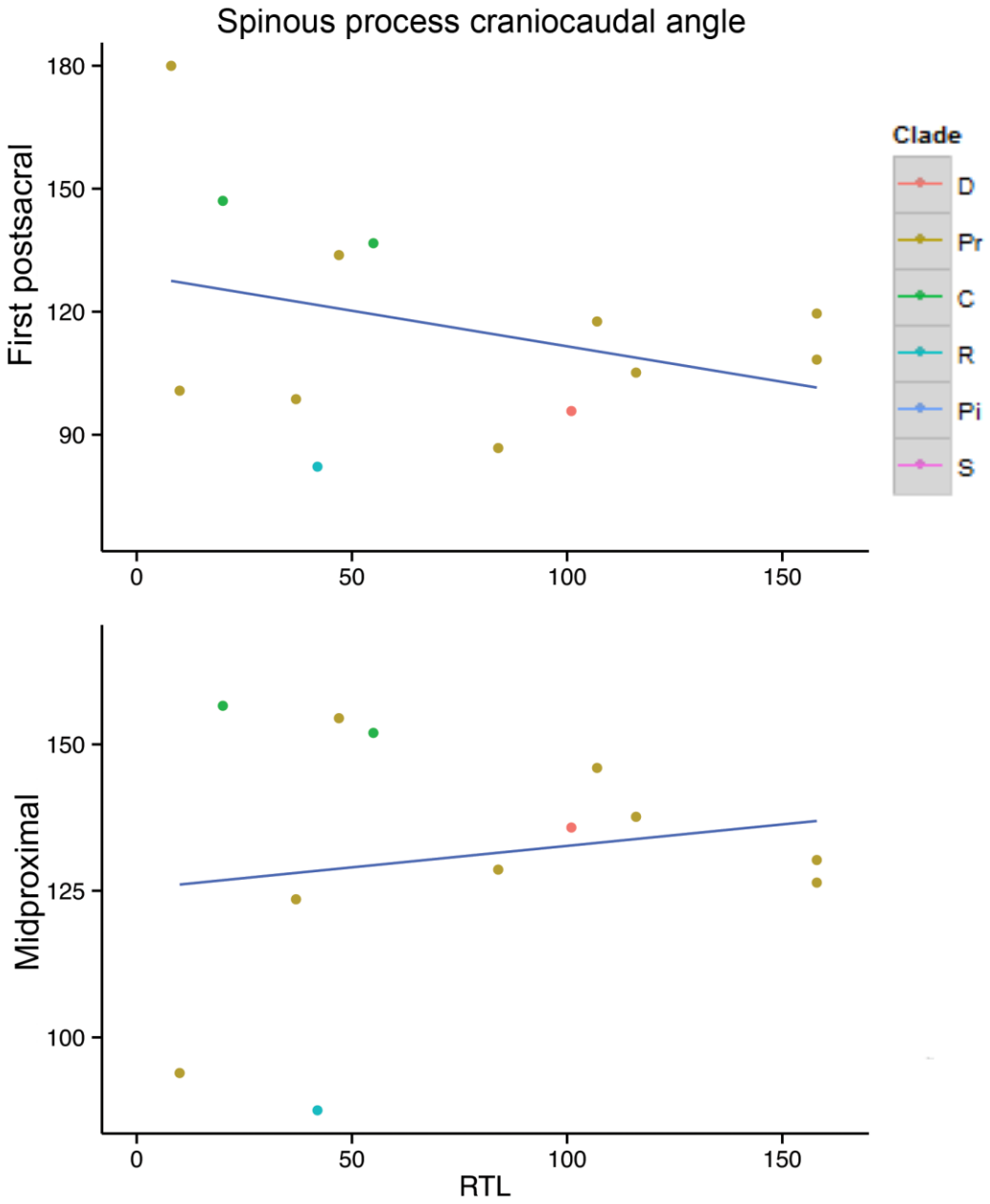

Figure 4.13 Spinous process craniocaudal angle on RTL. A) the first postsacral vertebra and B) mid-proximal. Legend: D = Diprotodontia; Pr = Primates; R= Rodentia; C= Carnivora; Pi = Pilosa; S= Scandentia.

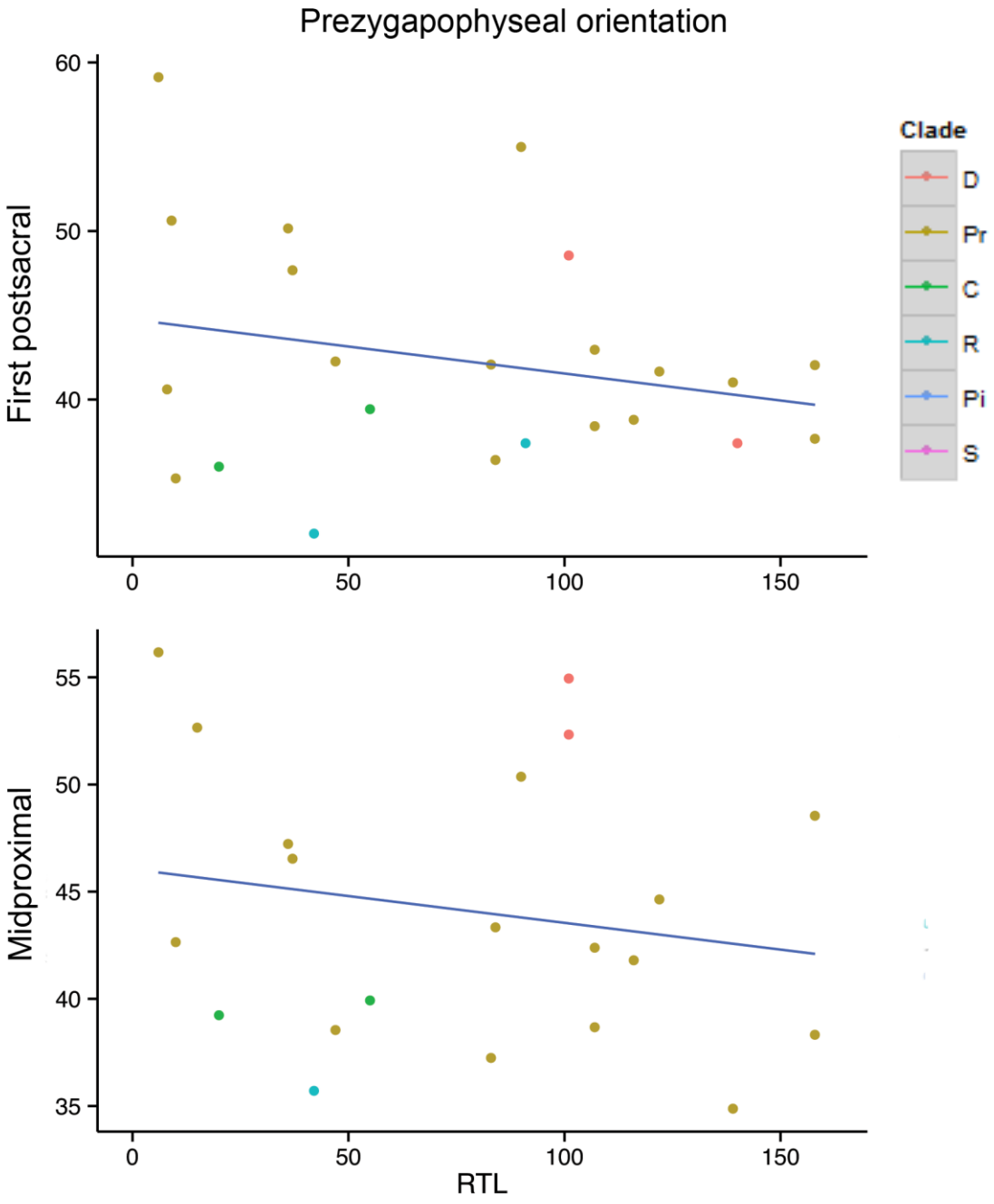

Figure 4.14 Prezygapophyseal orientation on RTL. A) the first postsacral vertebra and B) mid-proximal. Legend: D = Diprotodontia; Pr = Primates; R= Rodentia; C= Carnivora; Pi = Pilosa; S= Scandentia.

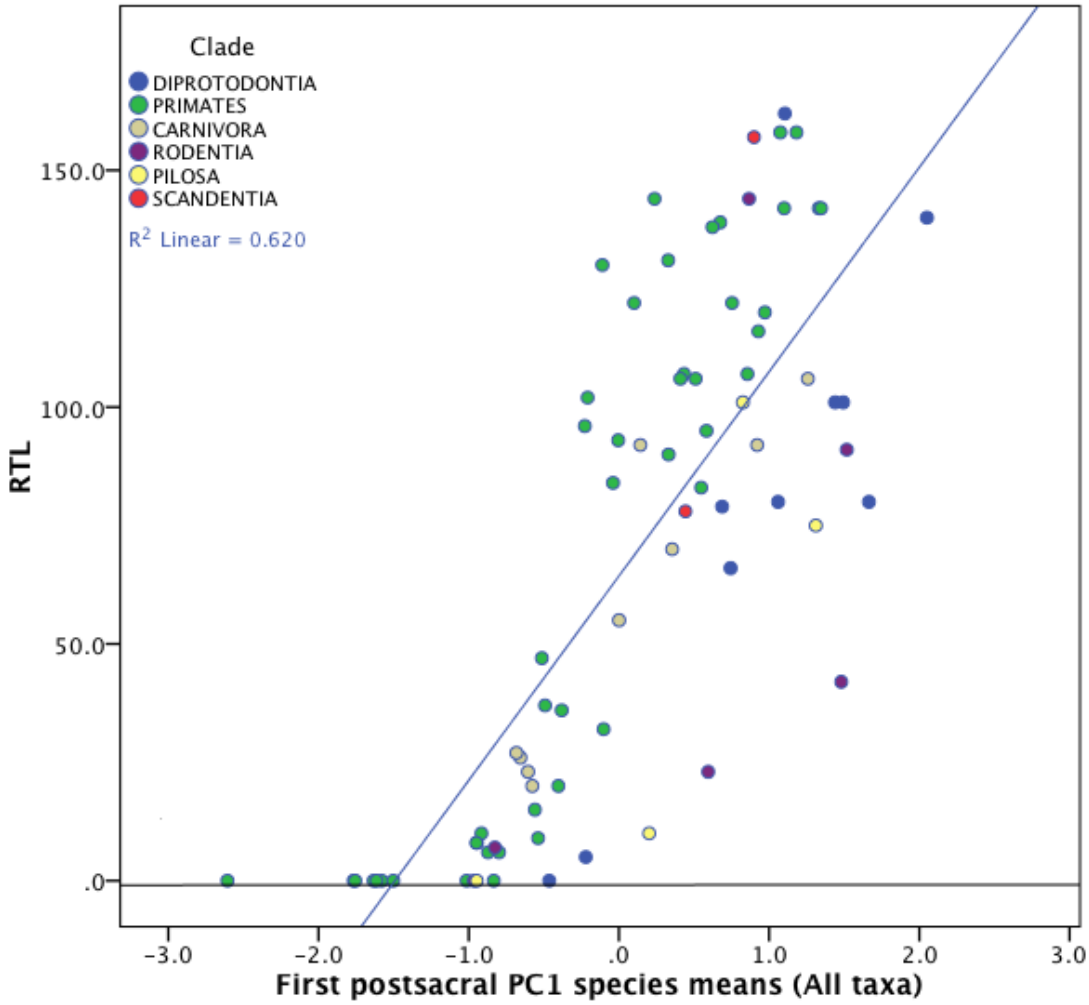

Figure 4.15A Species mean PC1 scores for the first postsacral vertebra on RTL for Dataset 1 among all mammals. R^2=0.62.

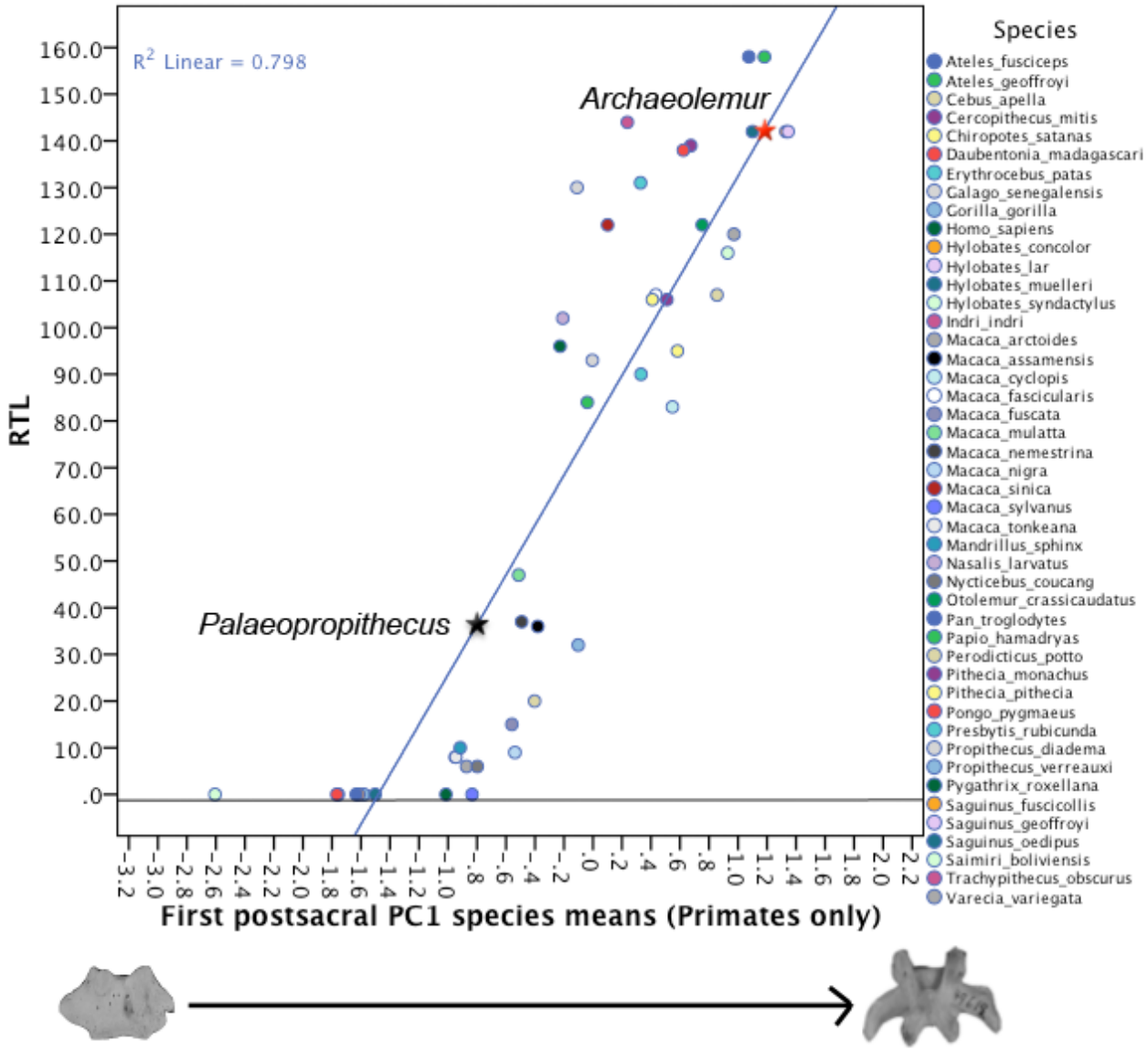

Figure 4.15B Species mean PC1 scores for the first postsacral vertebra on RTL for Dataset 1 in primates. A morphocline is provided below the graph depicting primates only to illustrate the anatomical changes associated with PC1 scores. R^2=0.80.

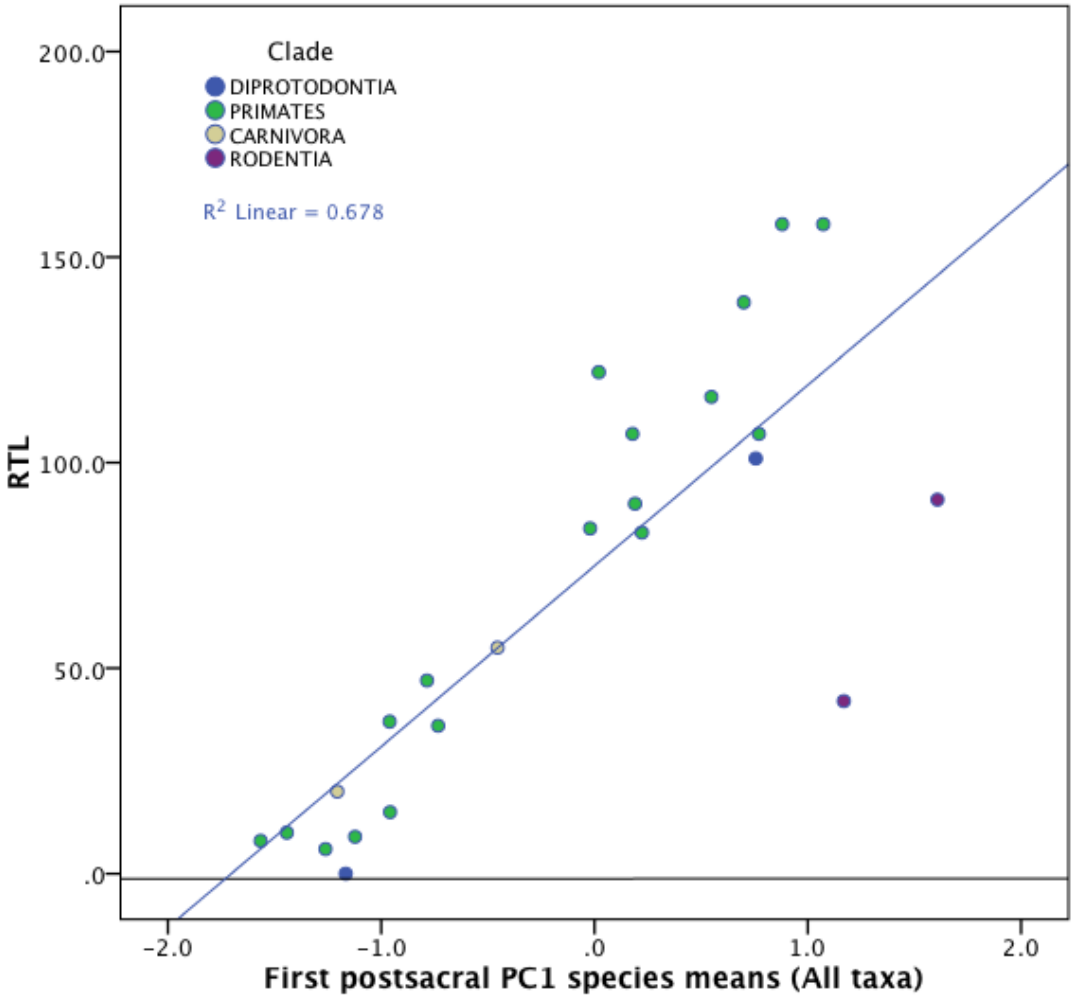

Figure 4.15C Species mean PC1 scores for the first postsacral vertebra on RTL for Dataset 2 among all mammals. R^2=0.68.

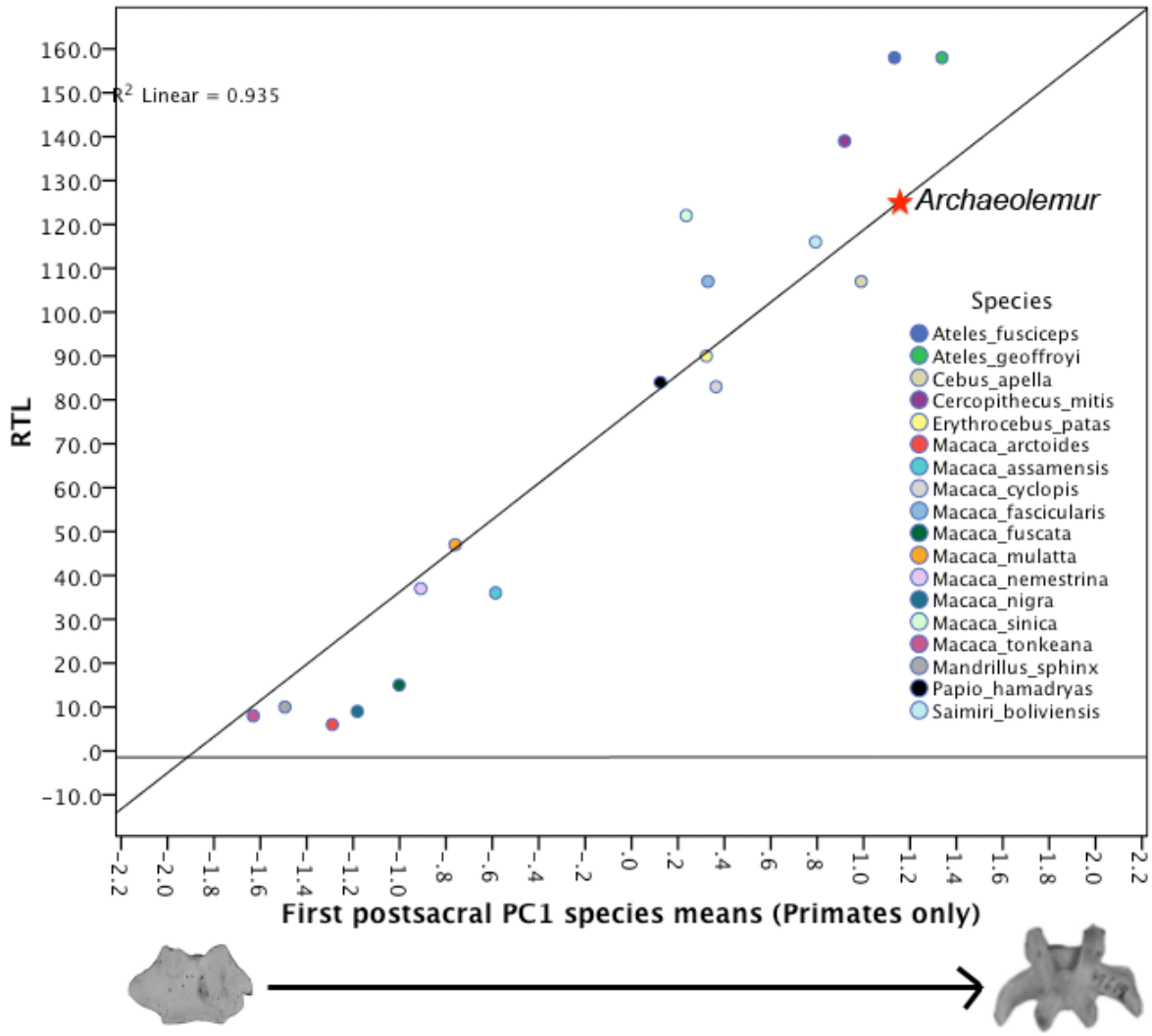

Figure 4.15D Species mean PC1 scores for the first postsacral vertebra on RTL for Dataset 2 in primates. A morphocline is provided below the graph depicting primates only to illustrate the anatomical changes associated with PC1 scores. R^2=0.94.

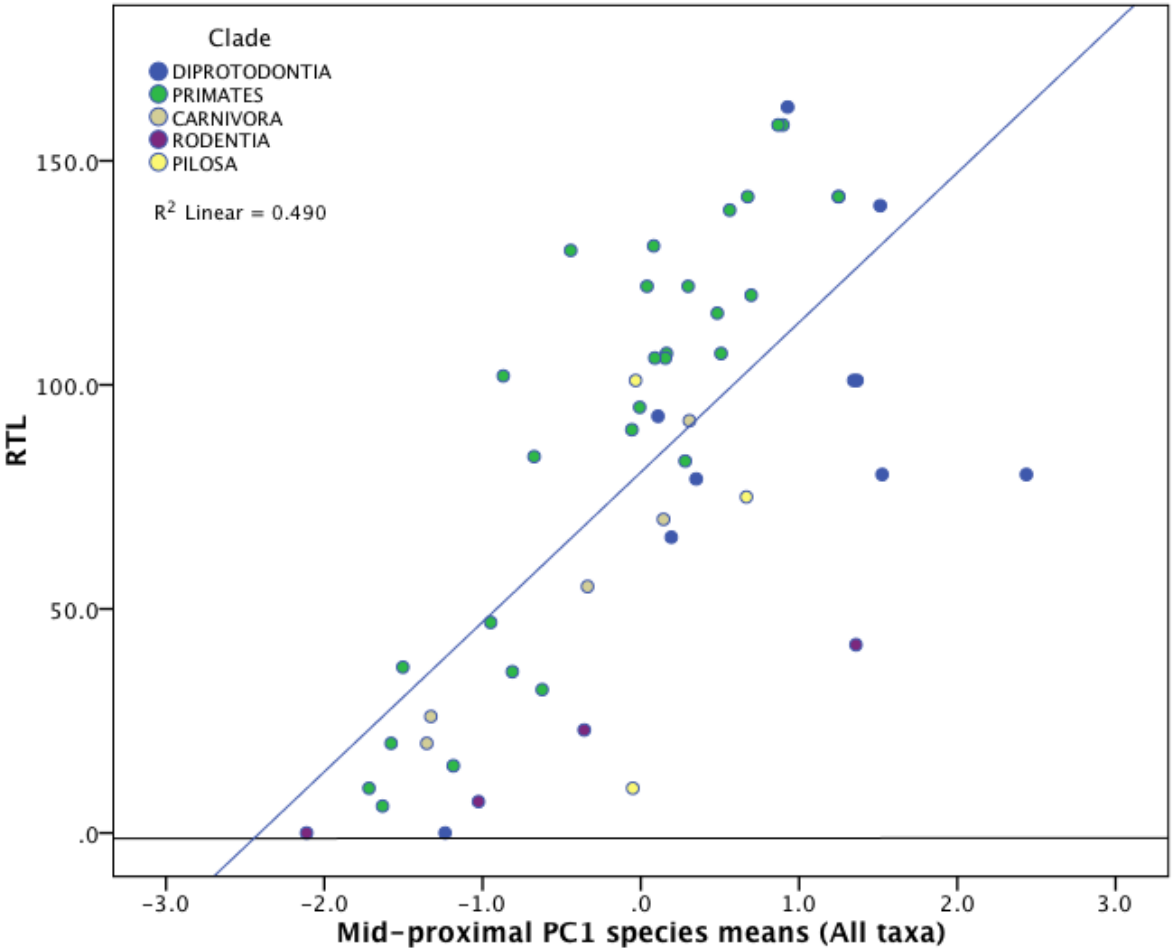

Figure 4.16A Species mean PC1 scores for the mid-proximal caudal vertebra on RTL for Dataset 1 in all mammals. R^2=0.49.

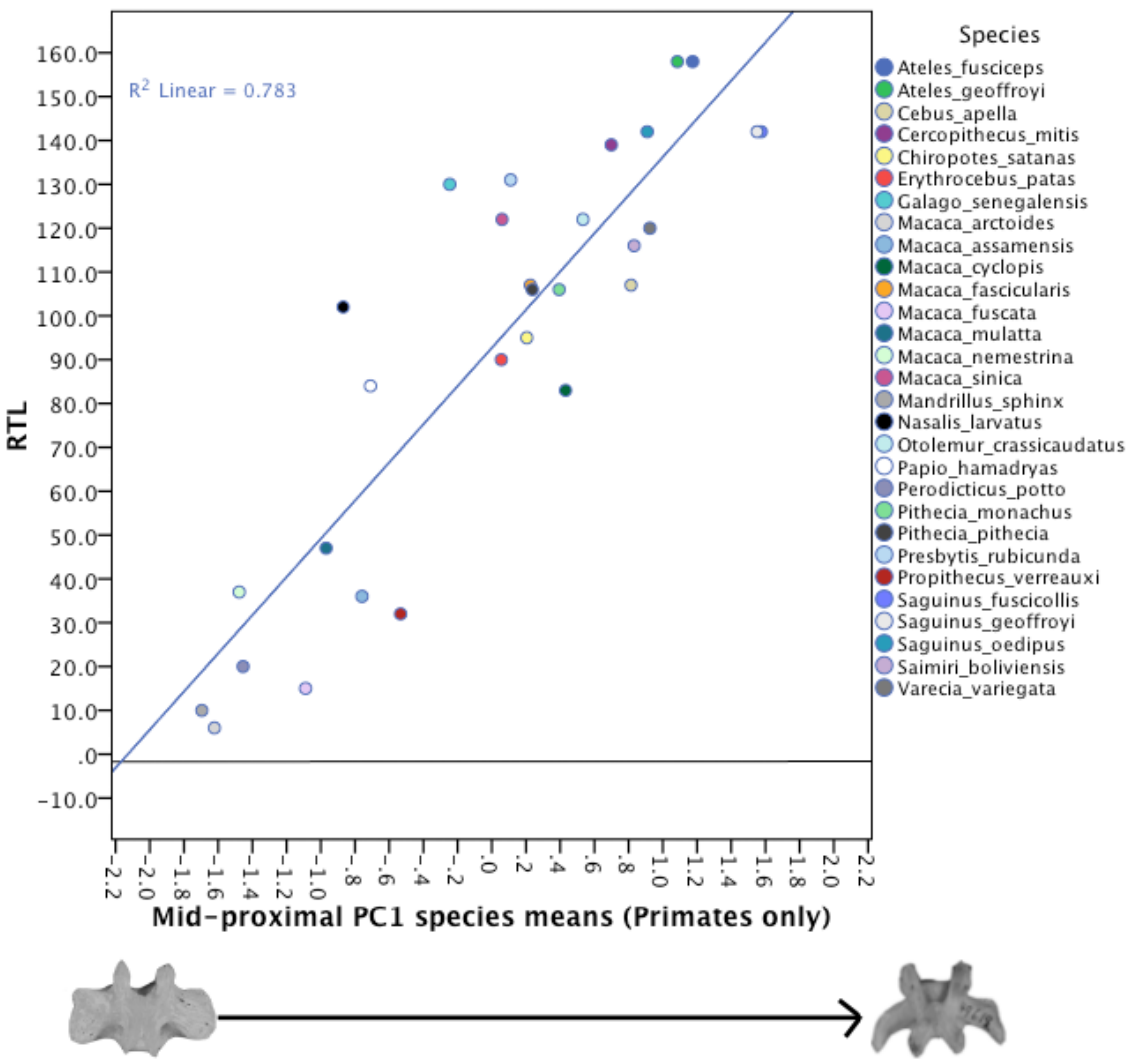

Figure 4.16B. Species mean PC1 scores for the mid-proximal caudal vertebra on RTL for Dataset 1 in primates. A morphocline is provided below the graph depicting primates only to illustrate the anatomical changes associated with PC1 scores. R^2=0.78.

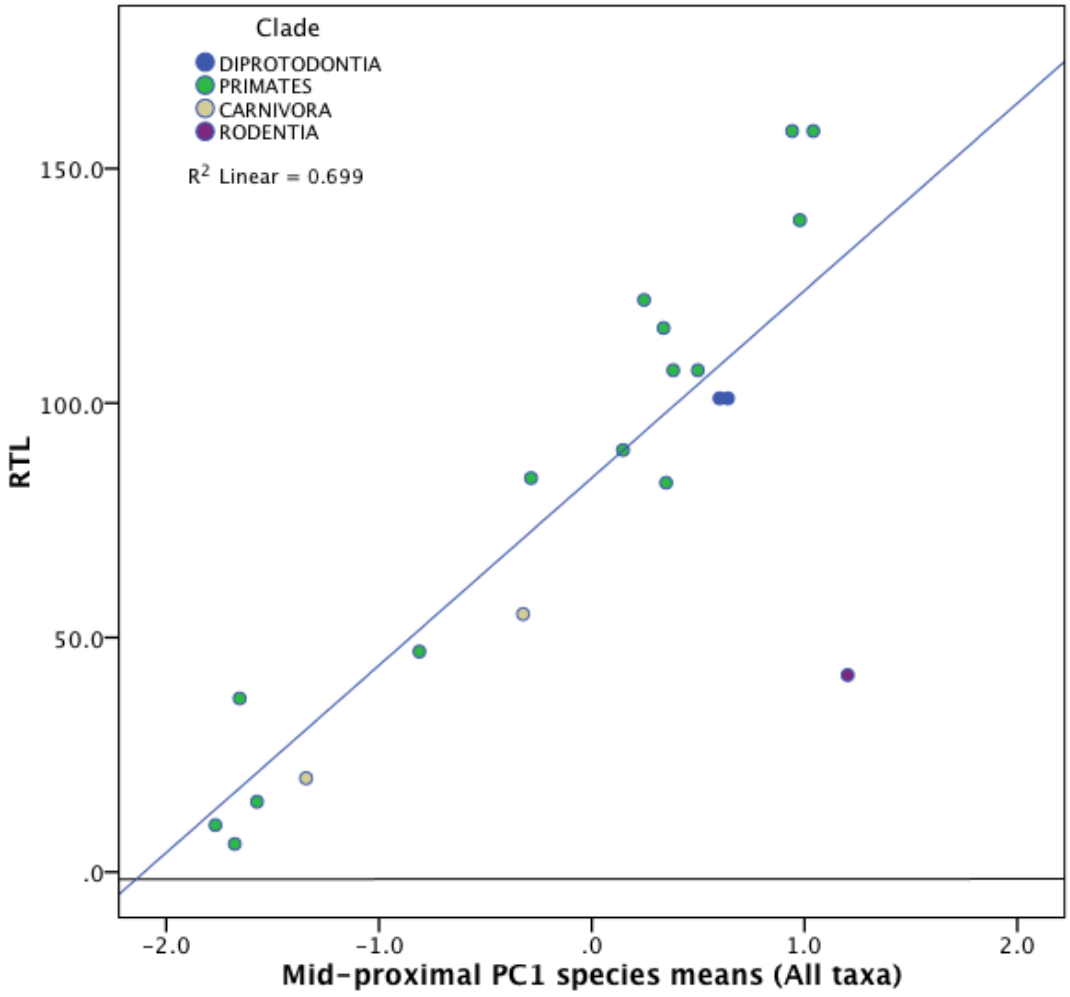

Figure 4.16C. Species mean PC1 scores for the mid-proximal caudal vertebra on RTL for Dataset 2 among all mammals. R^2=0.70.

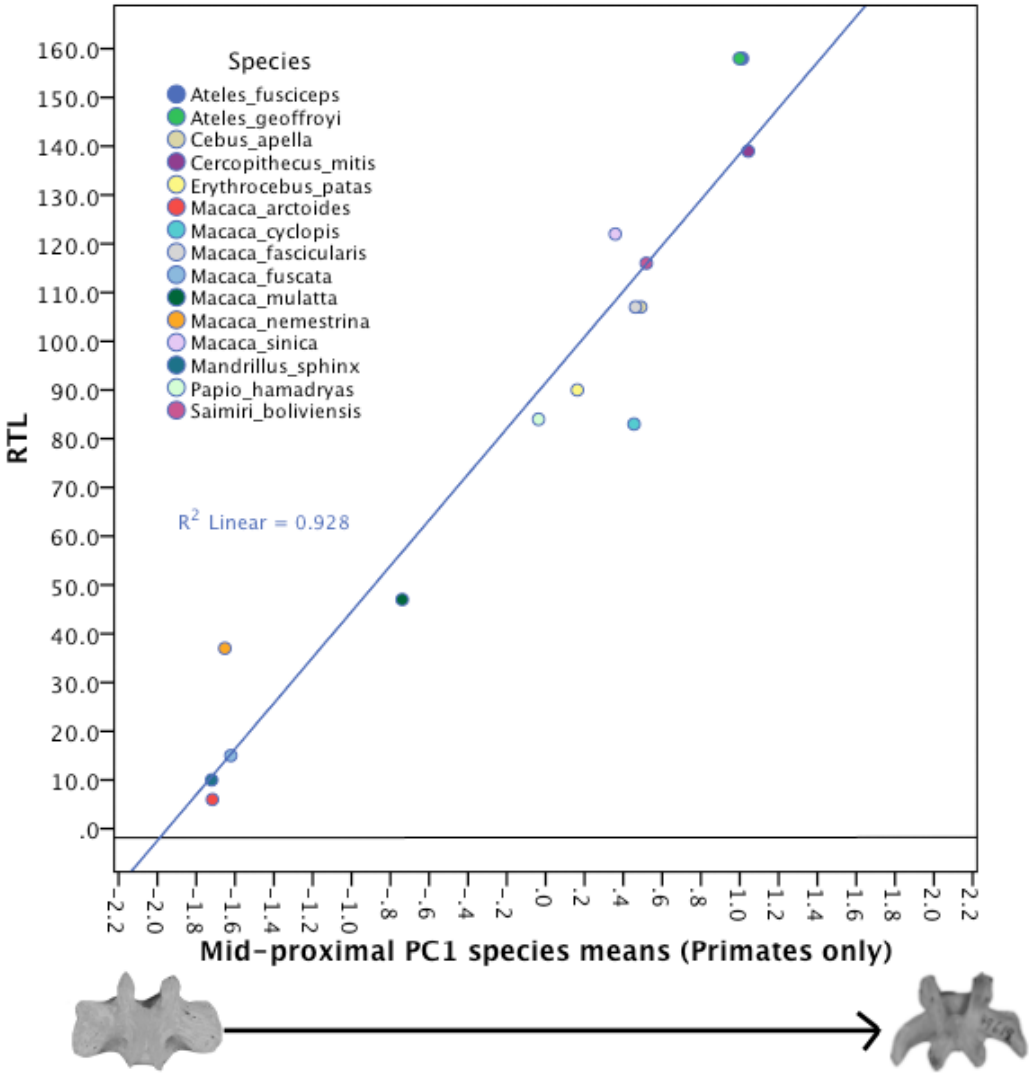

Figure 4.16D. Species mean PC1 scores for the mid-proximal caudal vertebra on RTL for Dataset 2 in primates. A morphocline is provided below the graph depicting primates only to illustrate the anatomical changes associated with PC1 scores. R^2=0.93.

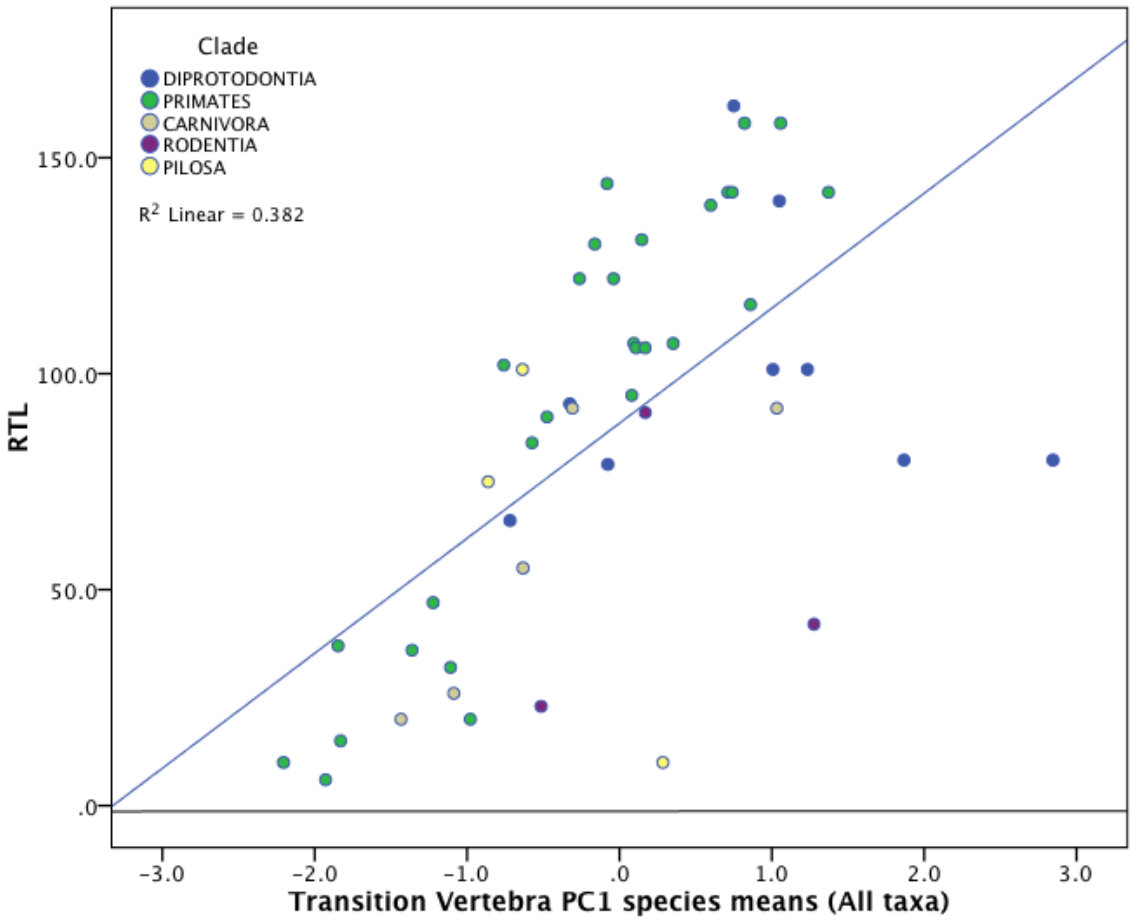

Figure 4.17A Species mean PC1 scores for the TV on RTL for Dataset 1 among all mammals. R^2=0.38.

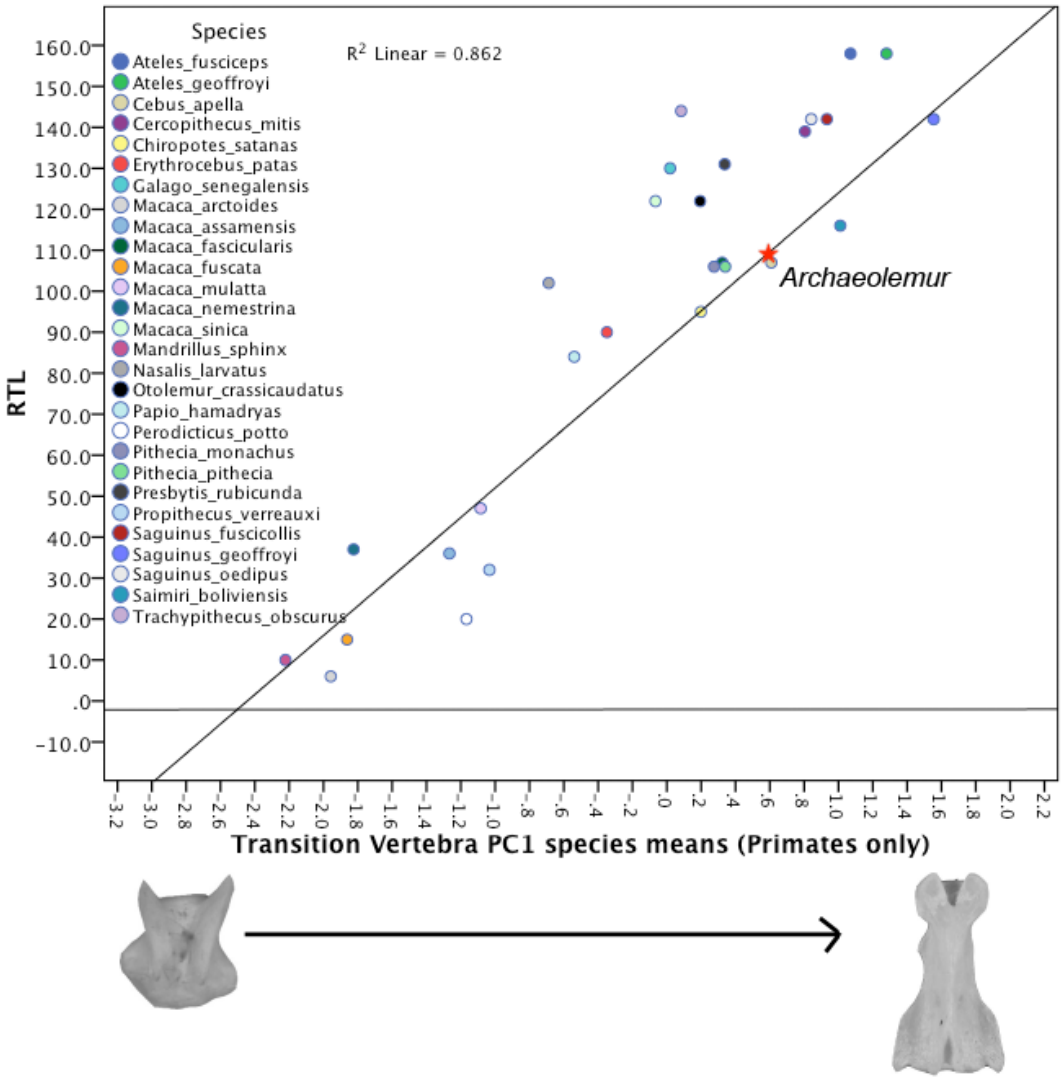

Figure 4.17B. Species mean PC1 scores for the TV on RTL for Dataset 1 in primates. A morphocline is provided below the graph depicting primates only to illustrate the anatomical changes associated with PC1 scores. R^2=0.86.

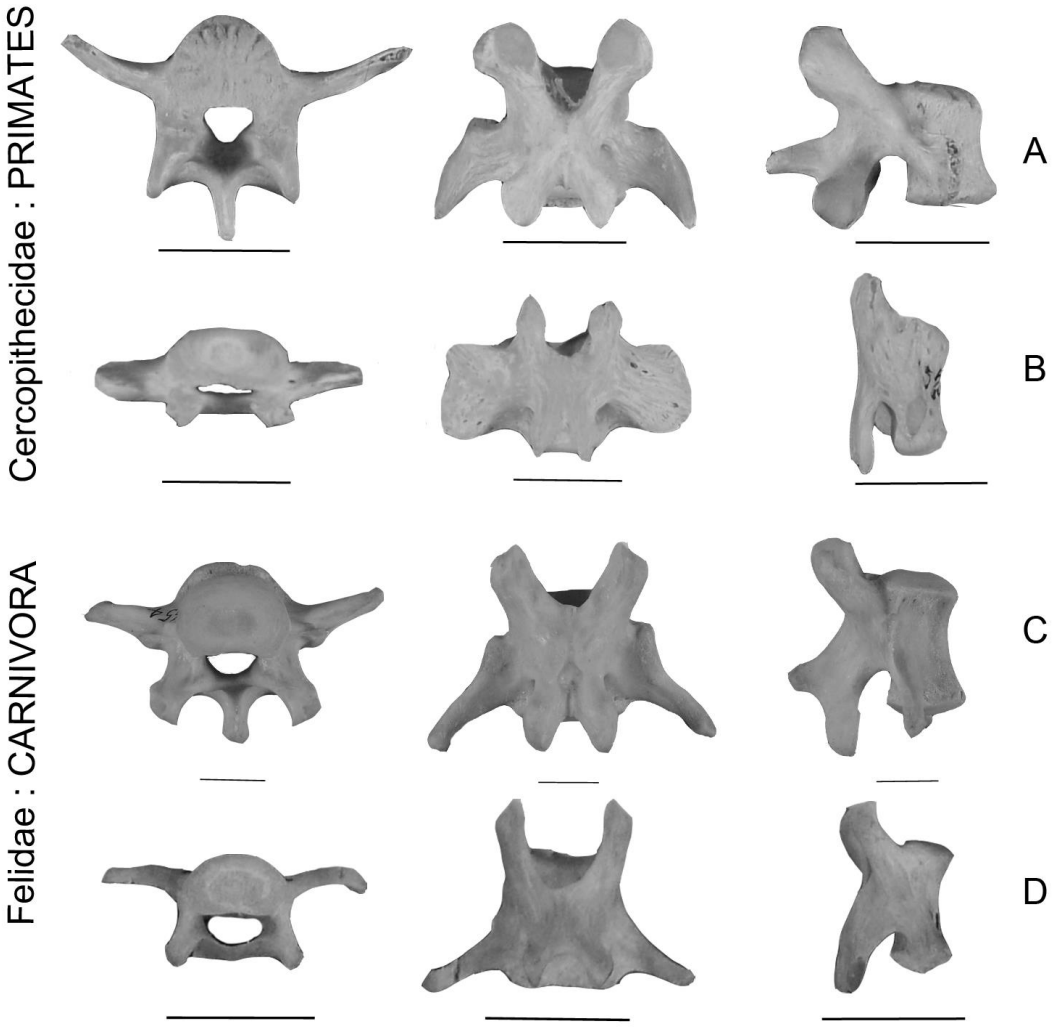

Figure 4.18 First postsacral vertebrae of A) crab-eating macaque (*Macaca fascicularis*; RTL =107); B) crested macaque (*Macaca nigra*, RTL = 9); C) cheetah (*Acinonyx jubatus*; RTL = 55) and D) lynx (*Lynx rufus;* RTL = 20) in (from left to right) cranial, dorsal and lateral views. Illustration exemplifies the morphological differences between closely-related longer-tailed and shorter-tailed taxa, and morphological convergences between distantly-related longer-tailed and shorter-tailed taxa. Scale bar = 1cm.

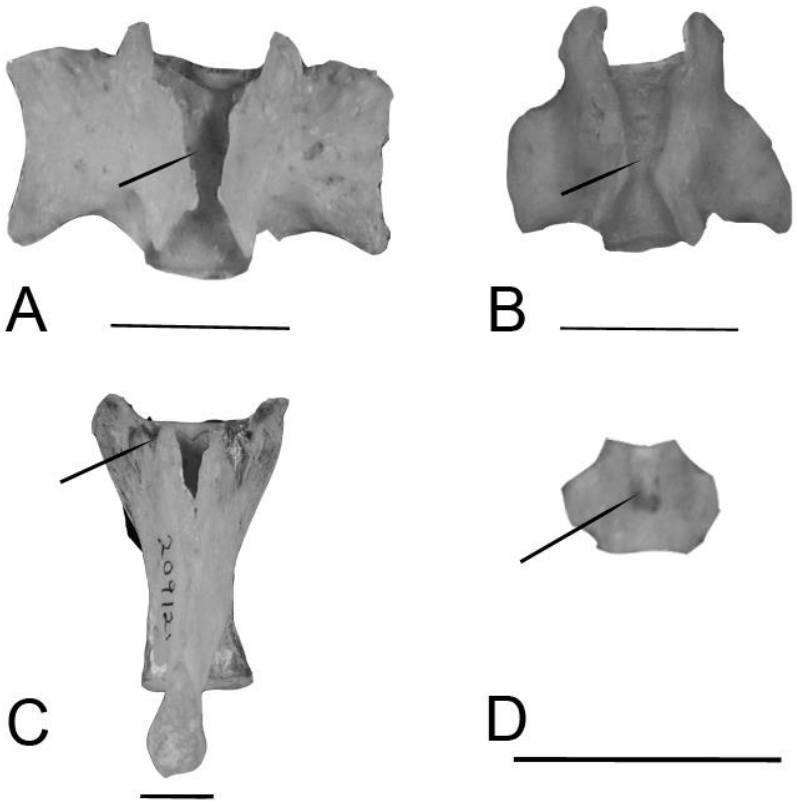

Figure 4.19 First postsacral vertebrae in dorsal views of A) Tonkean macaque (*Macaca tonkeana,* RTL =8); B) Barbary macaque (*Macaca sylvanus*, RTL = 0); C) capybara (*Hydrochaeris hydrochaeris*, RTL= 0); and D) slow loris (*Nycticebus coucang;* RTL =6). Illustration exemplifies the variation in first postsacral vertebral anatomy among the mammals sampled. In the macaques (A and B), arrows point to grooves formed by partially developed neural arches, prezygapophyseal articulations are retained; In the capybara (C), a neural arch is fully developed, but zygapophyseal articulations are absent; In the slow loris (D), the neural arch is not fully formed, and the prezygapophyses (or cornuae) are absent. Scale bar = 1cm.

Table 4.1 Extant mammal sample and relative tail lengths (RTL). In alphabetical order by Order, Family, then Species.

Order	Family	Species[a]	N	Range (Mean) no. proximal caudal vertebrae	RTL[b]
Carnivora	Felidae	***Acinonyx jubatus***	5	5-6 (6)	55
		Lynx rufus	5	3-4 (3)	20
	Hyaenidae	*Crocuta crocuta*	1	3	27
	Viverridae	*Arctictis binturong*	3	9-11 (10)	92&
		Genetta servalina	2	7	92
		Genetta victoriae	1	6	92
		Nandinia binotata	2	8	106
		Arctonyx collaris	1	2	23
	Mustelidae	*Eira barbara*	2	5	70
		Gulo luscus	1	3	26
Diprotodontia	Macropodidae	***Dendrolagus goodfellowi***	1	5	101
		Dendrolagus lumholtzi	4	5-6 (6)	140
		Dendrolagus matschiei	4	4-5 (5)	101
		Macropus giganteus	3	5-6 (5)	80
		Macropus robustus	2	5	80
	Phascolarctidae	***Phascolarctos cinereus***	10	2-3 (2)	3 or 0
	Phalangeridae	*Caluromys lanatus*	2	5	162&
		Spilocuscus maculatus	3	8	93
		Trichosurus vulpecula	4	6-7 (7)	66&
	Potoroidae	*Potorous tridactylus*	1	4	79
	Vombatiidae	*Vombatus ursinus*	5	4-6 (5)	5
Pilosa	Bradypodidae	***Bradypus tridactylus***	5	1-4 (2)	10
	Megalonychidae	***Choloepus didactylus***	3	0-2 (1)	0
		Choloepus hoffmanni	2	1-2 (2)	0
	Myrmecophagidae	***Myrmecophaga tridactyla***	4	15-18 (16)	75
		Tamandua mexicana	7	16-19 (18)	101&
Primates	Atelidae	***Ateles fusciceps***	6	8-9 (8)	158&
		Ateles geoffroyi	1	8	158&
	Callitrichidae	*Saguinus fuscicollis*	2	5	142
		Saguinus geoffroyi	3	5	142
		Saguinus oedipus	1	5	142
	Cebidae	***Cebus apella***	8	5-6 (6)	107&
		Saimiri boliviensis	7	6	116
	Cercopithecidae	***Cercopithecus mitis***	6	5	139
		Erythrocebus patas	4	4-5 (4)	90
		Macaca arctoides	7	3-4 (3)	6

Table 4.1 continued...

		Macaca assamensis	1	4	36
		Macaca cyclopis	1	4	83
		Macaca fascicularis	11	4-5 (5)	107
		Macaca fuscata	2	4	15
		Macaca mulatta	7	4-5 (4)	47
		Macaca nemestrina	8	4-5 (5)	37
		Macaca nigra	8	0-2 (1)	9
		Macaca tonkeana	8	3-4 (3)	8
		Macaca sinica	3	4-5 (5)	122
		Macaca sylvanus	1	1	0
		Mandrillus sphinx	6	2-4 (4)	10
		Nasalis larvatus	6	4	102
		Papio cynocephalus	6	6-7 (6)	84
		Presbytis rubicunda	2	4-5 (5)	131
		Pygathrix roxellana	2	5	96
		Trachypithecus obscurus	2	4-5 (5)	144
	Daubentoniidae	*Daubentonia madagascariensis*	1	5	138
	Galagidae	*Galago senegalensis*	7	3-4 (3)	130
		Otolemur crassicaudatus	6	4-5 (4)	122
	Hominidae	***Gorilla gorilla***	7	0	0
		Homo sapiens	6	0	0
		Hylobates concolor	2	0	0
		Hylobates lar	2	0	0
		Hylobates muelleri	2	0	0
		Hylobates syndactylus	5	0	0
		Pan troglodytes	8	0	0
		Pongo pygmaeus	6	0	0
	Indriidae	*Indri indri*	2	3	8
		Propithecus diadema	1	5	93
		Propithecus verreauxi	6	5-6 (5)	32
	Lemuridae	*Varecia variegata*	2	5-6 (6)	120
	Lorisidae	*Nycticebus coucang*	10	0-2?	6
		Perodicticus potto	7	2-5 (5)	20
	Pitheciidae	*Chiropotes satanas*	5	5-6 (6)	95
		Pithecia monachus	3	4	106
		Pithecia pithecia	4	5	106
Rodentia	Castoridae	***Castor canadensis***	7	4-5 (4)	42
		Aplodontia rufa	4	4-5 (4)	7

Table 4.1 continued...

	Caviidae	*Hydrochaeris hydrochaeris*	6	2-4 (3)	0
	Erethizontidae	***Coendou prehensilis***	6	12-15 (13)	91&
		Erethizon dorsatum	3	6-10 (9)	23
	Heteromyidae	*Dipodomys merriami*	6	4-5 (4)	144
Scandentia		*Tupaia glis*	1	5	157
		Tupaia gracilis	1	6	107
		Tupaia tana	5	5	78

[a]boldface indicates that species is also part of Dataset#2
[b]Data compiled from: Miller, 1900; Martin, 1968; Fooden, 1969, 2006, 2007; Wilson, 1972; Napier, 1981; Fa, 1985, 1989; Procter Gray and Ganslosser, 1986; Fooden and Albrecht, 1999; Jenkins, 1990; Parker, 1990; Nowak, 1991; Rowe, 1996; Francis, 2008
N = maximum number of individuals sampled
& = prehensile-tailed

Table 4.2 Results for PGLS regressions for sample of all mammals and only primates. Significant values indicated by boldface.

All Mammals

First postsacral	Body mass slope	Body mass p-value	λ	RTL slope	RTL p-value	Adjusted R-squared	p-value (model)	Included in PCA?
Vertebral body craniocaudal length	-0.19	**0.05**	0.64	0.27	**<0.00**	0.40	**<0.00**	Y
Cranial articular surface shape	-0.05	0.15	0.00	-0.15	**<0.00**	0.62	**<0.00**	Y
Cranial articular surface area	-0.90	0.34	0.88	1.46	**<0.00**	0.31	**<0.00**	Y
Area of cranial neural aperture	-0.37	0.32	1.00	0.45	**<0.00**	0.27	**<0.00**	Y
Transverse process breadth	-1.16	**<0.00**	0.94	0.91	**<0.00**	0.44	**<0.00**	Y
Transverse process craniocaudal angle	2.71	0.29	0.00	-5.52	**<0.00**	0.76	**<0.00**	Y
Transverse process dorsoventral angle	-3.20	0.23	0.56	-2.13	**<0.00**	0.27	**<0.00**	Y
Transverse process position	-0.13	0.26	0.00	0.13	**<0.00**	0.48	**<0.00**	Y
Spinous process length	-0.27	0.47	1.00	0.75	**<0.00**	0.54	**<0.00**	Y
Spinous process craniocaudal angle	-5.23	0.56	0.00	-15.03	0.10	0.10	0.24	N
Prezygapophyseal orientation	-1.66	0.41	0.00	-2.39	0.12	0.03	0.30	N
Mid-proximal caudal vertebra								
Vertebral body craniocaudal length	-0.19	0.26	0.51	0.41	**<0.00**	0.23	**<0.00**	Y
Cranial articular surface shape	-0.05	**0.03**	0.62	-0.09	**<0.00**	0.44	**<0.00**	Y
Cranial articular surface area	0.94	0.34	0.87	2.91	**<0.00**	0.32	**<0.00**	Y
Area of cranial neural aperture	0.12	0.59	0.87	0.14	0.36	-0.01	0.43	N
Transverse process breadth	-0.78	**0.04**	0.93	0.57	**0.01**	0.19	**<0.00**	Y
Transverse process craniocaudal angle	4.82	0.24	0.00	-4.45	**<0.00**	0.52	**<0.00**	Y
Transverse process dorsoventral angle	-1.22	0.64	0.00	-6.81	**<0.00**	0.38	**<0.00**	Y
Transverse process position	0.01	0.96	0.00	0.37	0.08	0.09	0.15	N
Spinous process length	0.33	0.26	1.00	0.65	**<0.00**	0.49	**<0.00**	Y

Table 4.2 continued...

Spinous process craniocaudal angle	-7.90	0.19	0.92	11.85	0.09	0.32	0.06	N
Prezygapophyseal orientation	-0.08	0.96	0.61	-3.13	**0.03**	0.18	**0.01**	Y
Transition vertebra (Last proximal)								
Vertebral body craniocaudal length	-0.44	0.26	0.72	1.93	**<0.00**	0.39	**<0.00**	Y
Cranial articular surface shape	-0.03	0.14	1.00	-0.12	**<0.00**	0.59	**<0.00**	Y
Cranial articular surface area	0.44	0.65	0.89	2.96	**<0.00**	0.25	**<0.00**	Y
Transverse process breadth	-0.06	0.87	0.95	0.92	**<0.00**	0.14	**<0.00**	Y

Primates

First postsacral	**Body mass slope**	**Body mass p-value**	**λ**	**RTL slope**	**RTL p-value**	**Adjusted R-squared**	**p-value (model)**	**Included in PCA?**
Vertebral body craniocaudal length	-0.33	**<0.00**	0.32	0.24	**<0.00**	0.57	**<0.00**	Y
Cranial articular surface shape	-0.08	0.14	0.00	-0.18	**<0.00**	0.68	**<0.00**	Y
Cranial articular surface area	-0.90	0.35	0.89	1.47	**<0.00**	0.31	**<0.00**	Y
Area of cranial neural aperture	0.16	0.68	0.79	0.65	**<0.00**	0.44	**<0.00**	Y
Transverse process breadth	-1.24	**<0.00**	0.86	0.77	**<0.00**	0.47	**<0.00**	Y
Transverse process craniocaudal angle	2.66	0.44	0.00	-5.90	**<0.00**	0.78	**<0.00**	Y
Transverse process dorsoventral angle	-3.06	0.37	0.93	-2.24	**0.01**	0.22	**<0.00**	Y
Transverse process position	-0.18	0.18	0.00	0.14	**<0.00**	0.57	**<0.00**	Y
Spinous process length	0.10	0.75	0.87	1.07	**<0.00**	0.77	**<0.00**	Y
Spinous process craniocaudal angle	-8.17	0.50	0.00	-14.94	0.17	0.05	0.39	N
Prezygapophyseal orientation	-1.10	0.67	0.00	-2.67	0.12	0.05	0.27	N

Table 4.2 continued...

Mid-proximal caudal vertebra								
Vertebral body craniocaudal length	-0.58	**0.01**	0.00	0.42	**0.01**	0.36	**<0.00**	Y
Cranial articular surface shape	-0.05	0.08	0.86	-0.16	**<0.00**	0.56	**<0.00**	Y
Cranial articular surface area	-1.32	0.20	0.77	6.34	**<0.00**	0.61	**<0.00**	Y
Area of cranial neural aperture	0.06	0.83	0.97	0.05	0.71	-0.06	0.87	N
Transverse process breadth	-0.82	0.07	0.69	0.49	**0.02**	0.12	**0.01**	Y
Transverse process craniocaudal angle	4.82	0.24	0.00	-5.88	**<0.00**	0.59	**<0.00**	Y
Transverse process dorsoventral angle	-1.85	0.50	0.00	-6.71	**<0.00**	0.50	**<0.00**	Y
Transverse process position	-0.04	0.91	0.00	0.36	0.14	0.09	0.22	N
Spinous process length	0.46	0.21	1.00	0.66	**<0.00**	0.54	**<0.00**	Y
Spinous process craniocaudal angle	-6.74	0.34	0.44	12.30	0.14	0.41	0.11	N
Prezygapophyseal orientation	0.15	0.94	0.00	-3.39	**0.02**	0.29	**0.01**	Y
Transition vertebra (Last proximal)								
Vertebral body craniocaudal length	-0.36	0.48	0.48	3.89	**<0.00**	0.66	**<0.00**	Y
Cranial articular surface shape	-0.00	0.97	0.00	-0.12	**<0.00**	0.52	**<0.00**	Y
Cranial articular surface area	-1.41	0.06	0.70	5.50	**<0.00**	0.68	**<0.00**	Y
Transverse process breadth	-0.42	0.13	0.00	1.96	**<0.00**	0.59	**<0.00**	Y

Table 4.3 Summary of principal components analyses

Caudal vertebra	Dataset		PC1 %	Eigenvalue
First postsacral	All Taxa	Dataset 1	74.12	2.97
		Dataset 2	57.38	5.16
	Primates	Dataset 1	77.09	3.08
		Dataset 2	62.32	5.61
Mid-proximal caudal vertebra	All Taxa	Dataset 1	64.18	2.57
		Dataset 2	41.68	3.33
	Primates	Dataset 1	65.24	2.61
		Dataset 2	50.13	4.01
Transition vertebra (Last proximal)	All Taxa	Dataset 1	52.75	2.11
	Primates	Dataset 1	66.20	2.65

Table 4.4 Least-squares regression coefficients and model summaries for RTL on PC1 species mean scores.

Caudal vertebra	Dataset	R^2	Adjusted R^2	Pearson's *r*	SEE	slope	constant
First postsacral	All Taxa Dataset 1	0.62	0.62	0.79	33.37	43.15	64.36
	Dataset 2	0.68	0.66	0.82	29.48	43.97	74.91
	Primates Dataset 1	0.80	0.79	0.89	26.20	53.41	79.07
	Dataset 2	0.94	0.93	0.97	14.19	53.11	80.81
Mid-proximal caudal vertebra	All Taxa Dataset 1	0.49	0.48	0.70	34.58	33.43	80.52
	Dataset 2	0.70	0.68	0.84	27.22	39.95	84.05
	Primates Dataset 1	0.78	0.78	0.89	22.42	43.55	92.70
	Dataset 2	0.93	0.92	0.96	14.39	46.96	91.48
Transition vertebra (Last proximal)	All Taxa Dataset 1	0.38	0.37	0.62	36.10	26.63	88.54
	Primates Dataset 1	0.86	0.86	0.93	18.46	42.75	100.89

REFERENCES

Andrews, P., 1992. Evolution and environment in the Hominoidea. Nature 360, 641.

Ankel, F., 1965. Der canalis sacralis als indikator für die länge der caudal region der primaten. Folia Primatol. 3, 263-276.

Ankel, F., 1972. Vertebral morphology of fossil and extant primates. In: Tuttle, R.(Ed.), The Functional and Evolutionary Biology of Primates. Aldine, Chicago, pp. 223-240.

Argot, C. 2003. Functional-adaptive anatomy of the axial skeleton of some extant marsupials and the paleobiology of the paleocene marsupials *Mayulestes ferox* and *Pucadelphys andinus*. J. Morph. 255,279–300.

Begun, D.R., Ward, C.V., Rose, M.D., 1997. Events in hominoid evolution. In: Begun, D.R.,Ward, C.V., Rose, M.D. (Eds.), Function, Phylogeny, and Fossils: Miocene Hominoid Evolution and Adaptations. Plenum Press, New York, pp. 389-416.

Bergeson, D.J. 1992. The use of the prehensile tail in Alouatta and Cebus. Am J Phys Anthropol 14:48.

Bergeson, D.J. 1995. The ecological role of the platyrrhine pre- hensile tail. Am J Phys Anthropol 20:64–65.

Bergeson, D.J. 1996. The positional behavior and prehensile tail use of Alouatta paliatta, Ateles geoffrroyi, and Cebus capucinus. PhD Dissertation, Washington University, St. Louis.

Bernstein, P., Smith, W., Krensky, A., and Rosene, K. 1978. Tail positions of *Cercopithecus aethiops*. Zeitschrift für Tierpsychologie 46:268–278.

Bezanson, M.F. 2004. Ontogenetic influences on prehensile-tail use in *Cebus capucinus.* Am. J. Phys. Anthropol. 123:63.

Bezanson, M.F. 2005. Leap bridge or ride? Ontogenetic influences on positional behavior in Cebus and Alouatta. In: Estrada A, Garber PA, Pavelka MSM, Luecke L, editors. New perspectives in the study of Mesoamerican primates: distribution, ecology, behavior and conservation. New York: Springer. p 333–348.

Bezanson, M.F. 2006. Ontogenetic patterns of positional behavior in Cebus capucinus and Alouatta palliata. PhD dissertation, University of Arizona, Tucson, AZ.

Bezanson MF. 2009. Life history and locomotion in *Cebus capucinus* and *Alouatta palliata*. Am. J. Phys .Anthropol. 140,508– 517.

Bininda-Emonds ORP, Cardillo M, Jones KE, MacPhee RDE, Beck RMD, Grenyer R, Price SA, Vos RA, Gittleman JL, and Purvis A. 2007. The delayed rise of present-day mammals. Nature 446, 507–512.

Bogduk N, Twomey L. 2005. Clinical anatomy of the lumbar spine and sacrum. Livingstone: Churchill.

Buck, C., Tolman, N., Tolman, W., 1925. The tail as a balancing organ in mice. J. Mammal 6, 267e271.

Byron, C., Kunz, H., Matuszek, H., Lewis, S., and Van Valkinburgh D. 2011. Rudimentary pedal grasping in mice and implications for terminal branch arboreal quadrupedalism. J. Morph. 272,230–240.

Cartmill M, and Milton K. 1977. The lorisiform wrist joint and the evolution of "'brachiating'"adaptations in the Hominoidea. Am. J. Phys. Anthropol. 47,249–272.

Chadwell, BA, Young, JW, Shapiro, LJ. 2013. A comparative look at tail movement during narrow branch locomotion. Society of Integrative and Comparative Biology 2013 Annual Meeting. San Franciso, CA.

Deane, A.S., Russo, G.A., Muchlinski, M., Organ, J.M. *in prep*. Functional correlates of caudal vertebral body articular surface size and shape in prehensile- and nonprehensile-tailed anthropoids.

Deinard. A., and Smith, D.G. 2001. Phylogenetic relationships among the macaques: evidence from the nuclear locus NRAMP1. J. Hum. Evol. 41,45–59.

Demes, B., Jungers, W.L., Fleagle, J.G., Wunderlich, R.E., Richmond, B.G., and Lemelin, P. 1996. Body size and leaping kinematics in Malagasy vertical clingers and leapers. Journal of Human Evolution 31:367–388.

Dor, M. 1937. La morphologie de la queue des mammiferes. Paris: Pierre Andre.

Elftman, H., 1932. The evolution of the pelvic floor of primates. Am. J. Anat. 51, 307e346.

Emerson, S.B., 1985. Jumping and leaping. In: Hildebrand, M., Bramble, D.M., Liem, K.F., Wake, D.B. (Eds.), Functional Vertebrate Morphology. Belknap Press, Cambridge, pp. 58e72.

Essner Jr., R.L., 2002. Three-dimensional launch kinematics in leaping, parachuting and gliding squirrels. J. Exp. Biol. 205, 24e69.

Fa, J.E., 1985. Baby care in barbary macaque. In: Macdonald, D. (Ed.), Primates. Torstar Books, New York, pp. 92-93.

Fa, J.E., 1989. The genus *Macaca*: a review of taxonomy and evolution. Mammal Rev. 19, 45-81.

Fleagle JG. 1984. Size and adaptation in primates. In: Jungers WL, editor. Size and scaling in primate biology. New York: Plenum Press. p 1–19.

Flower WH. 1876. An Introduction to the Osteology of the Mammalia: Being the Substance of the Course of Lectures Delivered at the Royal College of Surgeons of England in 1870. Macmillan.

Fooden, J. 1988. Taxonomy and evolution of the sinica group of macaques: 6. Interspecific comparisons and synthesis. Fieldiana Zool 45:1–44

Fooden, J., 1997. Tail length variation in Macaca fascicularis and M. mulatta. Primates 38, 221-232

Fooden, J., Albrecht, G.H., 1999. Tail length evolution in fascicularis group macaques (Cercopithecidae: Macaca). Int. J. Primatol. 20, 431-440.

Fooden, J., 2006. Comparative review of fascicularis-group species of macaques (Primates: Macaca). Fieldiana Zool. 107, 1-44.

Fooden, J., 2007. Systematic review of the barbary macaque, Macaca sylvanus (Linnaeus, 1758). Fieldiana Zool. 113, 1-58.

Francis, C.M., 2008. A Field Guide to the Mammals of Southeast Asia. New Holland.

Freckleton RP, Harvey PH, and Pagel M. 2002. Phylogenetic analysis and comparative data: a test and review of evidence. The American Naturalist 160:712–726.

Fredrickson J. 1989. The tailless cat in free-fall. The Physics Teacher 27:620.

Garber, P.A., and Rehg, J.A. 1999. The ecological role of the prehensile tail in white-faced capuchins (*Cebus capucinus*). Am. J. Phys. Anthropol. 110,325–339.

Gebo, D.L. 1992. Locomotor and postural behavior in *Alouatta palliata* and *Cebus capucinus*. *Am. J. Primatol*. 26,277–290.

Gebo DL, and Sargis EJ. 1994. Terrestrial adaptations in the postcranial skeletons of guenons. Am. J. Phys. Anthropol. 93:341–371.

German, R.Z. 1982. The functional morphology of caudal vertebrae in New World monkeys. Am. J. Phys. Anthropol. 58,453–459.

Godfrey, L.R., and Jungers, W.L. 2002. Quaternary Fossil Lemurs. In The Primate Fossil Record. W. Hartwig (ed.). Cambridge: Cambridge University Press, pp. 97-121.

Godfrey, .LR., and Jungers, W.L. 2003. The extinct sloth lemurs of Madagascar. Evo. Anthropol. 12,252–263.

Grand, T., 1977. Body weight: its relation to tissue composition, segment distribu- tion, and motor function. I. Interspecific comparisons. Am. J. Phys. Anthropol. 47, 211e239.

Groves, C.P. 2001. Primate taxonomy. Washington, DC: Smithsonian Institution Press.

Groves, C.P. 2005. Order primates. In: Wilson DE, Reeder DM, editors. Mammal species of the world: a taxonomic and geographic reference, 3rd ed. Baltimore: Johns Hopkins University Press. p 111–184, Vol.1.

Hamada, Y., Yamamoto, A., Kunimatsu, Y., Tojima, S., Mouri, T., and Kawamoto, Y. 2012. Variability of tail length in hybrids of the Japanese macaque (Macaca fuscata) and the Taiwanese macaque (Macaca cyclopis). Primates:1–15.

Harrison, T., 1987. The phylogenetic relationships of the early catarrhine primates: a review of the current evidence. J. Hum. Evol. 16, 41-80.

Harrison, T., 1993. Cladistic concepts and the species problem in hominoid evolution. In: Kimbel, W.H., Martin, L.B. (Eds.), Species, Species Concepts and Primate Evolution. Plenum Press, New York, pp. 345-371.

Harrison, T., 2002. Late Oligocene to middle Miocene catarrhines from Afro-Arabia. In: Hartwig, W.C. (Ed.), The Primate Fossil Record. Cambridge University Press, Cambridge, pp. 311-338.

Hartman, C.G., and Straus, W.L. 1933. The anatomy of the rhesus monkey (Macaca mulatta). The Williams & Wilkins Company.

Hickman, G., 1979. The mammalian tail: a review of functions. Mammal Rev. 9, 143-157.

Hildebrand M. 1974. Analysis of vertebrate structure. Wiley, New York, NY.

Horner, B., 1954. Arboreal adaptations of Peromyscus, with special reference to use of the tail. Contrib. Lab. Vert. Biol. 61, 1-84.

Igarashi, M., and Levy, J. 1981. Locomotor balance performance of short-tailed squirrel monkeys. J. Med. Primatol. 10:136.

Jenkins, P.D., 1990. Catalogue of Primates in the British Museum (Natural History) and Elsewhere in the British Isles. Part V: The Apes, Superfamily Hominoidea.

The British Museum (Natural History), London.

Jungers, W.L. 1988. Relative joint size and hominoid locomotor adaptations with implications for the evolution of hominid bipedalism. J. Hum. Evol. 17,247–265.

Jungers, W.L., Godfrey LR, Simons EL, Wunderlich RE, Richmond BG, Chatrath PS, Plavcan JM, Kay RF, Jungers WL, et al. 2002. In: Ecomorphology and behavior of giant extinct lemurs from Madagascar. Reconstructing behavior in the primate fossil record. pp. 371–411.

Kapandji, I.A., 2008. The Physiology of the Joints (V3): The Spinal Column, Pelvic Girdle and Head. Lavoisier, Paris.

Kelley, J., 1997. Paleobiological and phylogenetic significance of life history in Miocene Hominoidea. In: Begun, D.R., Ward, C.V., Rose, M.D. (Eds.), Function, Phylogeny, and Fossils: Miocene Hominoid Evolution and Adaptations. Plenum Press, New York, pp. 173-208.

Larson, S., Stern Jr., J., 2006. Maintenance of above-branch balance during primate arboreal quadrupedalism: coordinated use of forearm rotators and tail motion. Am. J. Phys. Anthropol. 129, 71e81.

Lawler, R.R., and Stamps, C. 2002. The relationship between tail use and positional behavior in Alouatta palliata. Primatol. 43,147–152.

Lemelin, P. 1995. Comparative and functional myology of the prehensile tail in New World monkeys. J. Morphol. 224,351– 368.

Maigne, J.Y., and Tamalet, B. 1996. Standardized radiologic protocol for the study of common coccygodynia and characteristics of the lesions observed in the sitting position: Clinical elements differentiating luxation, hypermobility, and normal mobility. Spine 21,2588–2593.

Martin, R. 1968. Reproduction and Ontogeny in tree–shrews (*Tupaia belangeri*), with reference to their general behaviour and taxonomic relationships1. Zeitschrift für Tierpsychologie 25,409–495.

Martins, E.P., and Hansen, T.F. 1997. Phylogenies and the comparative method: a general approach to incorporating phylogenetic information into the analysis of interspecific data. Am. Nat. 149:646–667.

Meldrum, D.J. 1998. Tail-assisted hind limb suspension as a transitional behavior in the evolution of the platyrrhine prehensile tail. In: Strasser E, et al., editors. Primate locomotion: recent advances. New York: Plenum. p 145–156.

Miller, G.S. 1900. Key to the land mammals of northeastern North America. University of the State of New York.

Nakatsukasa, M., Tsujikawa, H., Shimizu, D., Takano, T., Kunimatsu, Y., Nakano, Y., Ishida, H., 2003. Definitive evidence for tail loss in Nacholapithecus, an East African Miocene hominoid. J. Hum. Evol. 45, 179-186.

Nakatsukasa, M., Ward, C.V., Walker, A., Teaford, M., Kunimatsu, Y., Ogihara, N., 2004. Tail loss in Proconsul heseloni. J. Hum. Evol. 46, 777-784.

Napier, P.H., 1981. Catalogue of Primates in the British Museum (Natural History) and Elsewhere in the British Isles, Part 2: Family Cercopithecidae, Subfamily: Cercopithecinae. British Museum (Natural History), London.

Nowak, R.M., 1991. Walker's Mammals of the World, fifth ed., vol. 1. J. Hopkins University Press, Baltimore and London.

Organ, J.M. 2006. To grasp or not to grasp? Structure and func- tion of platyrrhine caudal vertebrae. Am J Phys Anthro- pol(S42):142.

Organ, J.M. 2007. The functional anatomy of prehensile and non- prehensile tails of the Platyrrhini (Primates) and Procyonidae (Carnivora). PhD Dissertation. The Johns Hopkins University, Baltimore, MD.

Organ, J.M. 2010. Structure and function of platyrrhine caudal vertebrae. Anat. Rec. 293:730–745.

Organ, J.M., Teaford, M.F., Taylor, A.B. 2009. Functional correlates of fiber architecture of the lateral caudal musculature in pr hensile and nonprehensile tails of the Platyrrhini (Primates) and Procyonidae (Carnivora). Anat. Rec. 292,827–841.

Organ, J.M., Muchilinski, M.N., Deane, A.S. 2011. Mechanoreceptivity of prehensile tail skin varies between atelines and Cebus. Am. J. Phys. Anthropol. 144,230.

Pagel, M. 1999. Inferring the historical patterns of biological evolution. Nature 401,877–884.

Paradis E., Claude, J., and Strimmer, K. 2004. APE: analyses of phylogenetics and evolution in R language. Bioinformatics 20:289–290.

Parker, S.P., 1990. Grzimek's Encyclopedia of Mammals, vol. 2. McGraw Hill, New York.

Procter-Gray, E., and Ganslosser, U. 1986. The individual behaviors of Lumholtz's tree-kangaroo: repertoire and taxonomic implications. J. Mammal. 343–352.

Rodman, P.S. 1979. Skeletal differentiation of Macaca fascicularis and Macaca nemestrina in relation to arboreal and terrestrial quadrupedalism. Am. J. Phys. Anthropol. 51,51–62.

Rose, M.D., 1993. Locomotor anatomy of Miocene hominoids. In: Gebo, D. (Ed.), Postcranial Adaptation in Nonhuman Primates. Northern Illinois University Press, DeKalb, pp. 252e272.

Rose, M.D., 1997. Functional and phylogenetic features of the forelimb in Miocene hominoids. In: Begun, D.R., Ward, C.V., Rose, M.D. (Eds.), Function, Phylogeny, and Fossils: Miocene Hominoid Evolution and Adaptations. Plenum Press, New York, pp. 79-100.

Rose, M.D., Nakano, Y., Ishida, H., 1996. Kenyapithecus postcranial specimens from Nachola, Kenya. Afr. Stud. Monogr. 24, 3e56.

Rosenberger, A.L. 1983. Tale of tails: parallelism and prehensility. Am. J. Phys. Anthropol. 60,103–107.

Rosenberger, A.L., and Matthews L.J. 2008. Oreonax—not a genus. Neotrop. Primates. 15,8–12.

Rowe, N., 1996. The Pictorial Guide to the Living Primates. Pogonias Press, New York.

Russo, G.A. 2010. Prezygapophyseal articular facet shape in the catarrhine thoracolumbar vertebral column. Am. J. Phys. Anthropol. 142,600–612.

Russo, G.A., Shapiro, L.J. 2011. Morphological correlates of tail length in the catarrhine sacrum. J. Hum. Evol. 30, 223–232.

Russo, G.A., and Young, J.W. 2011. Tail growth tracks the ontogeny of prehensile tail use in capuchin monkeys (*Cebus albifrons* and *C. apella*). Am. J. Phys. Anthropol. 146:465–473.

Russo, G.A., Fajardo, R.J., Schmitz, J.E. 2012. Internal bone structure of the last sacral vertebra and its relationship to tail length. Am. J. Phys. Anthropol. 147 (S52): 255-256

Rylands, A.B., Mittermeier, R.A. 2009. The diversity of the New World primates (Platyrrhini): an annotated taxonomy. In: Garber PA, Estrada A, Bicca-Marques JC, Heymann EW, Strier KB, editors. South American primates: comparative perspectives in the study of behavior, ecology, and conservation. New York: Springer. p 23–54.

Saluja, P.G. 1988. The incidence of ossification of the sacrococcygeal joint. J. Anat. 156:11.

Sanders WJ, Bodenbender BE. 1994. Morphometric analysis of lumbar vertebra UMP 67–28: implications for spinal function and phylogeny of the Miocene Moroto hominoid. J. Hum. Evol. 26:203–237.

Schmidt-Nielsen K. 1984. Scaling: why is animal size so important? Cambridge: Cambridge University Press.

Schmitt, D., Rose, M.D., Turnquist, J.E., Lemelin, P., 2005. Role of the prehensile tail during ateline locomotion: experimental and osteological evidence. Am. J. Phys. Anthropol. 126, 435e446.

Schultz, A.H. 1930. The skeleton of the trunk and limbs of higher primates. Wayne State University Press.

Schultz, A.H. 1941. Chevron bones in adult man. Am. J. Phys. Anthropol. 28,91–97.

Schultz, A.H., Straus Jr., W.L., 1945. The number of vertebrae in primates. Proc. Am. Phil. Soc. 89, 601-626.

Shapiro, L.J. 1993. Functional morphology of the vertebral col- umn in primates. In: Gebo D, editor. Postcranial adaptation in nonhuman primates. DeKalb: Northern Illinois University Press. p 121–149.

Shapiro, L.J. 2007. Morphological and functional differentiation in the lumbar spine of lorisids and galagids. Am. J. Primatol. 69,86–102.

Shapiro, L.J., and Simons, C. 2002. Functional aspects of strepsirrhine lumbar vertebral bodies and spinous processes. J. Hum. Evol. 42:753–783.

Shapiro, L.J., Seiffert, C., Godfrey, L., Jungers, W., Simons, E, Randria G. 2005. Morphometric analysis of lumbar vertebrae in extinct Malagasy strepsirrhines. Am. J. Phys. Anthropol. 128,823.

Siegel, M., 1970. The tail, locomotion and balance in mice. Am. J. Phys. Anthropol. 33, 101-102.

Silva, M., and Downing, J.A. 1995. CRC handbook of mammalian body masses. CRC press Boca Raton, Florida.

Smith R, and Jungers W. 1997. Body mass in comparative primatology. Journal of Human Evolution 32:523–559.

Stevens, N., Wright, K., Covert, H., Nadler, T., 2008. Tail postures of four quadrupedal leaf monkeys (Pygathrix nemaeus, P. cinerea, Trachypithecus delacouri and T. hatinhensis) at the Endangered Primate Rescue Center, Cuc Phuong National Park, Vietnam. Viet. J. Primatol 2, 13-24.

Tito, G. 2008. New remains of *Eremotherium laurillardi* (Lund, 1842)(Megatheriidae, Xenarthra) from the coastal region of Ecuador. Journal of South American Earth Sciences 26,424–434.

Tojima, S. 2012. Tail length estimation from sacrocaudal skeletal morphology in catarrhines. Anthropological Science.

Wada, N., Hori, H., Tokuriki, M., 1993. Electromyographic and kinematic studies of tail movements in dogs during treadmill locomotion. J. Morph. 217, 105-113.

Walker C, Vierck C, and Ritz L. 1998. Balance in the cat: role of the tail and effects of sacrocaudal transection. Behav. Brain. Res. 91:41–47.

Ward CV. 1993. Torso morphology and locomotion in Proconsul nyanzae. Am J Phys Anthropol 92:291–328.

Ward, C.V., 1997. Functional anatomy and phyletic implications of the hominoid trunk and hindlimb. In: Begun, D.R., Ward, C.V., Rose, M.D. (Eds.), Function, Phylogeny, and Fossils: Miocene Hominoid Evolution and Adaptations. Plenum Press, New York, pp. 101-130.

Ward, C.V., 2007. Postcranial and locomotor adaptations of hominoids. In: Henke, W., Tattersall, I. (Eds.), Handbook of Paleoanthropology. Primate Evolution and Human Origins, vol. 2. Springer, Heidelberg, pp. 1011-1030.

Ward, C.V., Walker, A., Teaford, M.F., 1991. Proconsul did not have a tail. J. Hum. Evol. 21, 215-220.

Ward, C.V., Walker, A., Teaford, M.F., 1999. Still no evidence for a tail in Proconsul heseloni. Am. J. Phys. Anthropol. 28, 273.

Wilson, D.R., 1972. Tail reduction in Macaca. In: Tuttle, R. (Ed.), The Functional and Evolutionary Biology of Primates. Aldine Press, New York, pp. 241-261.

Woon, J.T., and Stringer, M.D. 2011. Clinical anatomy of the coccyx: A systematic review. Clin. Anat. 25,158–167.

Youlatos, D. 1999. Tail-use in capuchins. Neotrop. Prim. 7,16–20.

Youlatos, D. 2003. Osteological correlates of tail prehensility in carnivorans. J. Zool. 259,423–430

Chapter 5: Conclusions and Future Directions

CONCLUSIONS AND FUTURE DIRECTIONS

The goals of this dissertation study were to 1) *identify* anatomical correlates of tail length and positional behaviors from the external and internal bony morphology of the sacrocaudal region using a diverse comparative mammalian sample, and then 2) *apply* the identified anatomical correlates to reconstructions of the tail lengths and positional behaviors of extinct primates. The study presented in Chapter 2 examined the relationship between trabecular bone structure in the first sacral vertebra among living primates and positional behaviors, and then used these results to interpret the sacral anatomy of *Archaeolemur, Palaeopropithecus, Megaladapis, Proconsul* and *Nacholapithecus*. In Chapter 3, the relationship between the internal and external bony anatomy of the sacrum, particularly at its distal end, and relative tail length, was quantified in mammals and then used to reconstruct the tail lengths of *Archaeolemur, Palaeopropithecus, Megaladapis, Epipliopithecus,* and *Proconsul*. Finally, in Chapter 4, the functional morphology of caudal vertebral anatomy in nonprehensile-tailed taxa known to vary in tail length reduction was comprehensively evaluated among mammals in order to offer additional insight into the anatomy associated with tail loss. Results from this final chapter were used to reconstruct the tail lengths of *Archaeolemur* and *Palaeopropithecus* from associated caudal vertebrae. Below, the results of these studies are discussed in the context of sacrocaudal functional anatomy and primate evolution.

Positional Behaviors

The quantification of trabecular bone morphology in the proximal sacrum did not distinguish among living primates that differ in positional behaviors in a consistent or predictable manner (Chapter 2). The ability of verterbral trabecular morphological parameters to successfully distinguish among taxa differing in positional behaviors has received mixed support in the literature (e.g., Smit, 2002; Oxnard and Yang, 1981; Fajardo et al., 2010). One explanation for the unclear results of this study could be that a functional signal exists, but the specific methodology employed here (e.g., placement or scaling of the volume of interest) failed to capture the biological phenomenom. Alternatively, the use a broader taxonomic sample may have obscured functional signals. For example, in the analysis restricted to hominoids, some taxonomic trends were present and humans differed significantly from some other apes, suggesting that bipeds might be readily distinguished from nonbiped hominoids. Such a finding would be of great importance for palaeoanthropologists as a number of sacra are known for hominin taxa and analysis of their sacral trabecular morphology could inform inferences concerning the nature of their bipedal locomotion. Yet, when the sample is broadened beyond hominoids, the distributions of most hominoid taxa are indistinguishable from those of nonhominoid taxa that rely on fundamentally different postural and locomotor behaviors (e.g., *Mandrillus* and *Macaca*), suggesting that the functional signal is not as straightforward. Finally, it is possible that the methodology employed and results captured are precise, and that a functional signal is not present at this vertebral level (S1).

Additional work will be required to further elucidate the functional morphology of the proximal sacrum among living primates.

Unique Aspects of Hominoid Sacrococcygeal Anatomy

Previous research seeking to attribute tail lengths to extinct catarrhines has focused primarily on examining the extent to which the sacral anatomy of extinct apes resembles that of living apes (e.g., Ward et al., 1991). Yet, as discussed, the sacral anatomy of extant hominoids also reflects adaptations to orthograde posture, making unclear to what extent specific aspects of hominoid sacral anatomy reflects tail loss, upright posture, or some combination of both factors. For example, though increased sacral numbers in most primates occurs via sacralization of the caudal vertebrae, it instead occurs in living hominoids through sacralization of the lower lumbar vertebrae, which functions to shorten the lumbar vertebral column and increase its resistance to intervertebral bending moments induced by upright trunk postures (Cartmill and Milton, 1977; Ward, 1993; Lovejoy, 2005). The torso morphology characteristic of living hominoids (e.g., lumbar reduction and orthogrady) does not become frequent in the fossil record until the mid to late Miocene (Moyà Solà and Köhler, 1996; Moyà Solà et al., 2004; Ward, 2007; but see MacLatchy, 2004). Although *Nacholapithecus kerioi* and *Proconsul heseloni* were tailless (Ward et al., 1991; Nakatsukasa et al., 2003; Chapter 3), they exhibited anthropoid-like numbers of lumbar and sacral vertebrae, and emphasized predominantly pronograde postures (Ward, 1993; Ishida et al., 2004; Nakatsukasa and Kunimatsu, 2009).

By emphasizing a broad comparative mammalian sample to identify instances of morphological convergence, the results of Chapter 3 help elucidate what aspects of hominoid sacral anatomy are associated with tail loss independent of posture. The nonhominoid primate and mammalian sample employed in this dissertation rely on a variety of postures, though importantly, most of these taxa exhibiting reduced tail lengths are predominantly pronograde (e.g., *Macaca, Lynx, Hydrochaeris*). Like orthograde-adapted hominoids, pronograde primates and mammals with reduced tail lengths exhibit sacra with smaller caudal neural apertures than cranial neural apertures and last sacral vertebrae with mediolaterally tapered distal ends (relative to the mediolateral with of the proximal end of the vertebral body), smaller caudal articular surfaces, and reduced transverse and spinous processes (Chapter 3), in comparison to mammals possessing longer tails. That these features are characteristic of pronograde primates and mammals possessing reduced tail lengths, and orthograde-adapted hominoids, suggests that they can be confidently functionally linked with tail loss. The one exception to these observed morphological trends appears to be the shape of the caudal articular surface, which is extremely dorsoventrally compressed among hominoids, but shows a less consistent trend with tail length among other primates and mammals (Chapter 3; but see also Chapter 4). It is possible that the shape of the sacrum's caudal articular surface may reflect the joint influence of tail loss (e.g., greater mediolateral than dorsoventral breadth is related to articulation with a similarly dorsoventrally compressed first coccygeal vertebra; Chapter 4) and adaptations to upright trunk posture (e.g., greater mediolateral than dorsoventral breadth may offer increased surface area for attachment of *levator ani* mm. and sacro-

tuberous and spinous ligaments; Chapter 3), however the early hominoid postcranial axial skeleton exhibits adaptations to pronograde posture, and so this idea does not receive support from the fossil record.

The results of Chapter 4 have additional importance for our understanding of the unique aspects of coccygeal vertebral anatomy. Designation of "coccygeal" vertebrae is generally restricted to the postsacral vertebrae in hominoid taxa, probably by extension from the clinical literature (Woon and Stringer, 2011). Nakatsukasa et al. (2003) identified a series of traits that they argued, collectively, distinguish the morphology of hominoid coccygeal vertebrae from that of first caudal vertebrae in nonhominoid primates and other mammals possessing very short or nearly absent tails. These features include absence of a neural arch and its associated structures (e.g., zygapophyses), an overall "T-shape", reduced transverse processes, and dorsoventral compression of the vertebral body. Indeed, the results of Chapter 4 lend support to the idea that these features are specifically associated with tail length reduction/loss. For instance, as tail length decreases, the transverse processes of first postsacral vertebrae become less laterally projected and less caudally oriented, reflecting a decrease in the anatomical mechanical advantage of the tail's abductor musculature, and contributing to an overall "T-shaped" appearance. Though the *combination* of these features are most consistently observed in hominoid taxa, nonhominoid primate and nonprimate mammalian taxa were also observed to exhibit the entire suite of features.

Morphological/Functional Specializations of Caudal Vertebrae in Mammals

This dissertation emphasized a taxonomically and morphologically diverse comparative mammalian sample in order to identify correlates of relative tail length in caudal/coccygeal morphology. The results presented in Chapter 4 suggest that differences in caudal/coccygeal vertebral anatomy, including, for example, transverse process breadth, cranial articular surface shape and area, and vertebral body craniocaudal height, can be related to tail length variation among mammals. Nonetheless, in some cases, the examined caudal vertebral morphological features may additionally (or instead) relate to specializations in tail function (other than prehensility). For example, that the vertebral bodies of the caudal vertebrae in *Castor* (North American beaver; RTL=42, Table 4.1) are dorsoventrally flattened may reflect the dorsoventral movements required to create propulsive movements under water (Ji et al., 2006). In *Castor,* caudal vertebral transverse processes are very broad and, in the mid-proximal region, they may begin to bifurcate (Ji et al., 2006). Together, the flat caudal vertebral bodies and laterally expanded transverse processes create a distinct shape that has been suggested to represent a "key feature in… tails specialized for swimming", as it is also observed in other aquatic mammals such as otters (Ji et al., 2006).

The tail serves a number of non-locomotor functions that, while not considered here, may have bony anatomical correlates. For example, some animals use the position of their tails to display social status or warning. Ojha (1974) found a correlation between tail carriage and dominance in *Macaca mulatta.* Dominant males carry the tail upright, with the distal part arched over the back, whereas subordinate males carried their tails

closer to the ground (Ojha, 1974). When the dominant male is absent, or removed from the troop, the beta or gamma male assumed the tail positions characteristic of the dominant male to assert their new status (Ojha, 1974). Though morphological correlates related to the use of the tail in social communication may more evident in its external structure than in its internal structure (i.e., the ability to use the tail to communicate a message to other individuals may rely in part on its coloration, or the arrangement/display of the hair), at least one bony anatomical correlate may relate to tail posture in baboons. Baboons exhibit a distinct proximal tail "kink" that has been suggested to distinguish among species (Virchow, 1914), and may be related to social display or other factors, including the stabilization of infants during transportation ("rump riding"). Located near the transition vertebra, a shelf-like bony plate formed by either an osteophytic development from the prezygapophyses (Figure 1, top image) or proximal cornuae of the vertebra, or the extreme coronal plane flattening of the prezygapophyses (Figure 1, bottom image), is sometimes observed on baboon caudal vertebral specimens (*Papio cynocephalus;* RTL = 84). Results presented in Chapter 4 for prezygapophyseal orientation demonstrate that for all taxa examined, mean prezygapophyseal orientation did not exceed 60 degrees, and it decreased (i.e., near the transition vertebra prezygapophyses were more acutely angled relative to the sagittal plane than more proximal caudal vertebrae) as tail length increased, though notably it was only a significant predictor of tail length at the level of the mid-proximal caudal vertebra. The atypical nearly flattened prezygapophyses (Figure 5.1, bottom image) of the transition and near-transition vertebrae in *P. cynocephalus* could be related to its inclusion in the

formation of the tail kink. That is, the bony plate could form a rigid plate-like surface that limits tail rotation and creates a hinge at this joint. Nonetheless, only a small sample of baboons was examined (N=9), and a more thorough anatomical and behavioral investigation will be required to understand the functional significance, if any, of this unusual anatomy.

The loss of the tail (i.e., tail autotomy) as an escape mechanism is an additional non-locomotor function that has been shown to have anatomical correlates. At least fifteen species of rodents use tail autonomy (Mohr, 1941), where the tail skin, the tail tip, or the entire tail itself is lost to evade predator capture. Studies demonstrate that in some pocket mouse genera, such as *Perognathus*, the tail is lost mid-caudal vertebra (Sumner and Collins, 1918; Hatt, 1932). The caudal vertebrae of these rodents exhibit "fracture lines" across their vertebral bodies to facilitate breakage and thus the loss of the tail (Hatt, 1932). Though this defense mechanism has not been observed or suggested for primates, it is presented as another example of tail function reflected in tail anatomy. These abovementioned examples all strongly suggest that future tail research should attempt to examine how variation in caudal vertebral anatomy may be related to other specializations in tail function among mammals beyond a nonprehensile vs. prehensile dichotomy.

Chevron bones are inverted v-shaped bony arches that are situated on the ventral surface of the caudal vertebrae opposite intervertebral spaces, such that they often articulate with two adjacent caudal vertebrae (though this is not always the case) (Flower, 1876). Chevron bones articulate with caudal vertebral bodies via bony prominences

called hemal processes (Flower, 1876). The primary function of the chevron bones is to protect caudal vasculature, in particular the caudal artery, which passes through the arches of the chevron bones and sends branches to the tail musculature (Hongo and Luck, 1953). They are located primarily in the proximal caudal region and their presence dissipates travelling caudally (Flower, 1876). Variation in chevron bone anatomy was not considered in this study. Chevron bone anatomy is difficult to quantify, chiefly because they are poorly preserved in museum collections. Further, preserved chevron bones are challenging to seriate and cannot easily be associated with specific caudal vertebrae (i.e., caudal vertebral number) in the tail sequence. Nonetheless, several observations regarding variation in chevron bone anatomy were made during the course of data collection for this project that may be functionally significant.

A number of mammals use their tails as props or supports during various positional behaviors (Hickman, 1979). For example, giant anteaters employ their heavy tail to facilitate a bipedal stance and counterweight their long heavy fore claws (Hickman, 1979), but it can also be used as a grasping organ when climbing (Hildebrand and Goslow, 1974). At slower speeds, macropodids may incorporate their forelimbs or tails to assume a 'pentapedal' posture (Windsor and Dagg, 1971; Dawson and Taylor, 1973). Use of the tail as a prop or support has also been noted for *Tarsius,* which additionally bears a roughened pad on its distal tail to help maintain their upright trunk posture on tree trunks (Sprankel, 1965).

In the macropods sampled here, *Macropus* exhibited a unusual chevron bone morphology that could be related to its use of the tail as a prop or support during slow "pentapedal' locomotion. Figure 5.2 shows a comparison of chevron bones belonging to *Macropus giganteus* and *Dendrolagus sp. Dendrolagus* is the only macropodid that employs predominantly pronograde, quadrupedal walking gaits (Windsor and Dagg, 1971). In *M. giganteus*, the ventral surface of the chevron bones are flattened in the mediolateral plane, and additional surface area is provided by bilaterally flaring bony prominences. By contrast, the ventral surface of the chevron bones in *Dendrolagus* is not flattened, and does not possess bilaterally flaring bony prominences (Figure 5.2). Instead, the two centers of ossification meet at midline to form a narrow ridge (Flower, 1876). Whereas the morphology of the chevron bones observed for *Dendrolagus* closely resembles that of, and appears to be the typical condition for, other mammalian taxa (Flower, 1876), that observed for *M. giganteus* could reflect its specialized use of the tail. That is, the mediolaterally flattened, broad ventral surface might provide a "pedestal"-like surface that serves to support body weight and dissipate the forces encountered when the tail is employed during "pentapedal" locomotion. Due to time constraints and the difficulties in quantifying chevron bony anatomy mentioned above, the chevron bones of the majority of primate taxa sampled in this study, including vertical clinger and leaper primates known to use their tails as a props (e.g., *Tarsius*), were not examined here. However, it is possible that the chevron bone anatomy of these primates, in comparison to their non-vertical clinger and leaper close phyletic relatives, may also differ, reflecting potentially important functional information regarding tail use.

In addition to a "pedestal"-like ventral surface, variation in other aspects of chevron bone anatomy could be functionally informative. The tail's primary ventral flexors (e.g., *flexor caudae longus mm*.) send tendinous insertions distally to the ventrolateral surfaces of the chevron bones (Figure 5.3). Therefore, total chevron bone length (dorsoventrally) and the craniocaudal angle at which they articulate with the ventral surface of the caudal vertebral bodies (in addition to hemal process length, which also contributes to their projection from the ventral caudal vertebral bodies; Organ, 2010) should determine the mechanical advantage of the tail's ventral flexors. Future research should attempt to examine how variation in caudal vertebral anatomy may be related to other specializations in tail function, and seek out ways to accurately quantify chevron bone anatomy.

Extinct Primates and the Evolution of Tail Loss

Only results from the living taxa examined in Chapters 3 (distal sacrum) and 4 (caudal/coccygeal vertebrae) provided a sound functional context for evaluating the sacra of extinct primates. The tail lengths for *Archaeolemur* and *Palaeopropithecus* (the only two primates included in the extinct primate sample for both Chapters 3 and 4) reconstructed from the sacral data presented in Chapter 3 are largely consistent with those reconstructed from the caudal vertebrae data presented in Chapter 4. For example, the extant primate sacral data predicted *Archaeolemur* to have a relative tail length of between 126 and 148 (Chapter 3), while the extant primate caudal vertebrae data predicted *Archaeolemur* to have a relative tail length of between 109 and 143 (Chapter 4). In addition, the predicted relative tail lengths for *Palaeopropithecus* using the sacral

data are between 18 and 42, while the predicted tail length for *Palaeopropithecus* using the caudal vertebrae data is 36 (though it should be noted that the *Palaeopropithecus* specimens were attributed to different species having different body weights; sacrum, *P. kelyus.*; caudal vertebra, *P. ingens*). Thus, sacral and caudal vertebrae data produce comparable tail length reconstructions, supporting the use of both skeletal regions for making tail length inferences in extinct primates.

These reconstructions of *Archaeolemur* as having a tail longer than its combined head and body length, and *Palaeopropithecus* having a tail shorter than ½ its combined head and body length, generally accord with previous inferences that *Archaeolemur* had a "long" tail (Godfrey et al., 2006) and *Palaeopropithecus* had a "short" tail (Godfrey and Jungers, 2003). *Megaladapis* was reconstructed as having a tail length generally intermediate between those of *Archaeolemur* and *Palaeopropithecus,* with a predicted RTL range of 38 to 68, the lower end of which overlaps with the predicted RTL of *Palaeopropithecus.* Results from analysis of the distal sacrum suggest that *Epipliopithecus* possessed a relative tail length of between 29 and 58, which is comparable to that of some living macaques such as *M. mulatta*. These findings do not necessarily transform our understanding of the evolutionary relationships among these extinct primates. Rather, the inclusion of distantly-related extinct primate taxa is important for evaluating the context of, and for validating the anatomy associated with, tail length reduction in primate evolution. For example, though, as a clade, living hominoids are uniquely characterized by complete loss of an external tail, it should be acknowledged that a number of extant and extinct primates exhibit variation in tail

length. That two subfossil lemurs and an extinct pliopithecoid exhibit tail length reduction, in addition to the tail absence observed for *Proconsul,* indicates that tail length reduction occurred independently, multiple times, in primate evolution.

Moreover, given the anatomical parallels between *Palaeopropithecus* and extant sloths (and living lorises) and *Megaladapis* and extant koalas (Godfrey and Jungers, 2002), which includes but is not limited to extreme reduction of the tail, it is probable that tail length reduction is probably somehow related to inverted suspensory postures and/or slow, deliberate climbing activities. *Proconsul*, generally reconstructed as lacking a tail in this study, has also been reconstructed as a slow, deliberate climber (e.g., Begun et al., 1994). Researchers have hypothesized that the slow, deliberate climbing locomotion characteristic of *Proconsul* may be related to the combination of large body size and tail loss (Cartmill and Milton, 1977; Walker and Pickford, 1983; Begun et al., 1994). A number of studies have demonstrated the importance of the mammalian tail for maintaining balance during pronograde quadrupedal progression or assisting in feeding postures in arboreal settings (e.g., Buck et al., 1925; Horner, 1954; Siegel, 1970; Grand, 1977; Hickman, 1979; Hildebrand and Goslow, 1982; Peters and Preuschoft, 1984; Wada et al., 1993; Dunbar and Badam, 2000; Stevens et al., 2008). Given the relatively large body sizes estimated for *Proconsul* individuals (10.9 kg: *P. heseloni*, 75.1 kg: *Proconsul major*, 35.6 kg: *P. nyanzae* [Rafferty et al., 1995]; 9.3 kg, *P. africanus* [Ruff et al., 1989]), the possession of a tail for maintaining arboreal stability on smaller branches (relative to body size) would seemingly confer an adaptive advantage. Some researchers speculate that, when the tail is absent, “the torso and limbs must meet certain

requirements of movement formerly executed by the tail" (Begun, 2003: 78). Kelley (1997) suggested that enhanced grasping abilities and limb mobility were compensatory mechanisms for tail loss and permitted maneuvering of the body over secure hand and foot holds (but see MacLatchy, 2004). Thus, the evolution of more modern ape-like grasping and tail loss may be functionally linked (see also Almécija et al., 2007).

It is likely that mammalian lineages evolve tail length reduction and/or loss for different reasons. Among mammals, hypotheses put forth to explain tail length reduction include, but are not limited to, terrestriality (Wilson, 1972), increased body size (e.g., Preuschoft et al., 1995; MacKenzie and Begun, 2009), and climate (i.e., Allen's rule; Fooden, 1980) in Primates, carnivory in Chiroptera (Coleman, 2009), and fossoriality in Insectivora and Xenarthra (Hildebrand and Goslow, 1982). The ability to appropriately contextualize its evolutionary occurrence, either ecologically or behaviorally, is not possible until there is a better understanding of which fossil taxa are actually characterized by reduced tail lengths. Thus, a prerequisite to generating testable hypotheses for evaluating the evolutionary timing and functional significance of tail length reduction is the ability to confidently identify it in the fossil record.

Figure 5.1 Baboon caudal vertebrae. Top image is of the caudal vertebra immediately distal to the transition vertebra. Bottom image of a transition caudal vertebra. Note the osteophytic lipping (arrow) on the top caudal vertebra, and the broad, flattened prezygapophyses on the bottom caudal vertebra (arrow). It is possible that these morphologies are partly related to formation of the tail "kink" characteristic of baboon tail carriage.

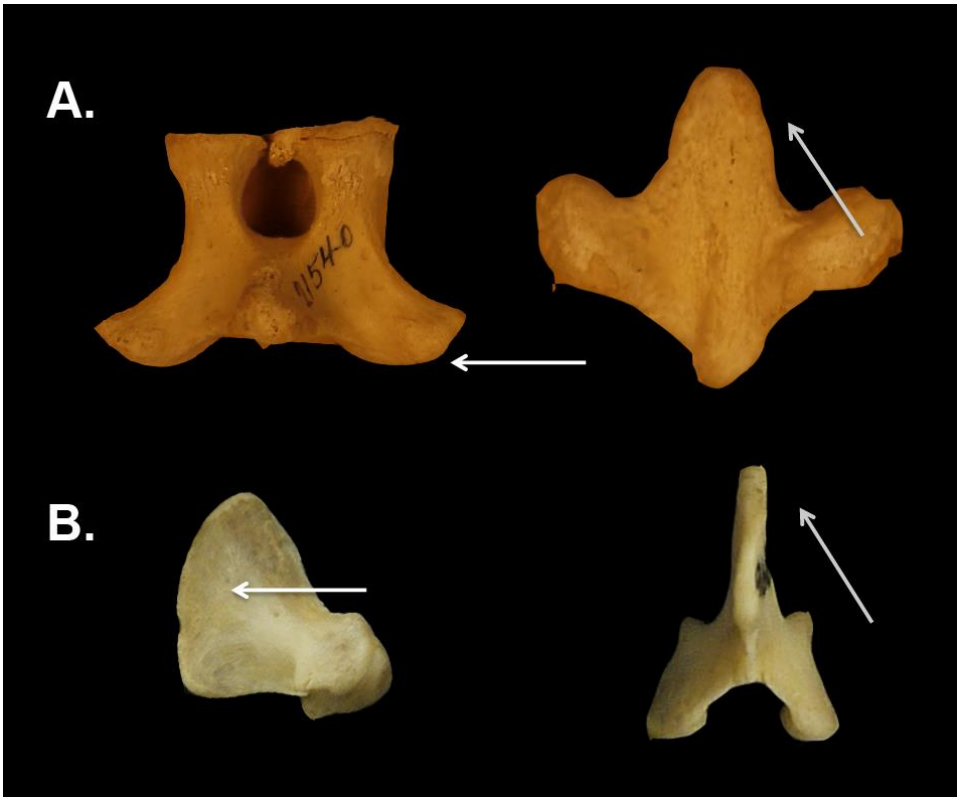

Figure 5.2 Comparison of chevron bone anatomy between *Macropus giganteus* (A) and *Dendrolagus sp.* (B). For *Macropus giganteus,* left image shows a cranial view of the chevron bone, ventral is down, right image shows a ventral view of the bone, proximal is up. The white arrow points to the bilateral bony prominences that protrude from the ventrolateral surface, contributing to the broad flat, ventral surface of the bone. The left image for *Dendrolagus* shows a lateral view of the chevron bone. A cranial view was not taken, however, the white arrow in the lateral view shows the absence of the bilateral processes observed for *Macropus*. The condition observed in *Dendrolagus* is more consistent with the chevron bone anatomy typical of other mammals than *Macropus*.

Figure 5.3 Ventral surface of the proximal tail musculature of *Sapajus apella*. Proximal is up. Distal tendons are from ventral flexor musculature.

REFERENCES

Almécija, S., Alba, D.M., Moyà-Solà, S., and Kohler. 2007. Orang-like manual adaptations in the fossil hominoid *Hispanopithecus laietanus*: first steps towards great ape suspensory behaviours. Proc. R. Soc. 274, 2375–2384.

Begun, D., Teaford, M., Walker, A., 1994. Comparative and functional anatomy of *Proconsul* phalanges from the Kaswanga primate site, Rusinga Island, Kenya. J. Hum. Evol. 26, 89-165.

Begun, D.R. 2003. Planet of the apes. Sci. Am. 289,74–83.

Buck, C., Tolman, N., Tolman, W., 1925. The tail as a balancing organ in mice. J. Mammal 6, 267-271.

Cartmill, M., and Milton, K. 1977. The lorisiform wrist joint and the evolution of "'brachiating'"adaptations in the Hominoidea. Am. J. Phys. Anthropol. 47, 249–272.

Coleman, J. L. 2009. A strange tale of taillessness in a vespertilionid bat. Acta Chiropterologica, 11, 212-215.

Dawson, T.J., Taylor, C.R., 1973. Energetic cost of locomotion in kangaroos. Nature 246, 313– 314.

Dunbar, D., Badam, G., 2000. Locomotion and posture during terminal branch feeding. Int. J. Primatol. 21, 649-669.

Fajardo, R.J., De Silva, J., and MacLatchy, L. 2010. Does the amount of bone dictate the trabecular bone structure in strepsirhine lumbar vertebrae? Am. J. Phys. Anthropol. S50:102.

Flower, W.H. 1876. An Introduction to the Osteology of the Mammalia: Being the Substance of the Course of Lectures Delivered at the Royal College of Surgeons of England in 1870. Macmillan.

Fooden, J. 1980. Classification and distribution of living macaques (Macaca Lace´pe`de, 1799). In: Lindburg DG (Ed.) The macaques: studies in ecology, behavior and evolution. Van Nostrand Reinhold, New York, pp 1–9.

Godfrey, L.R., and Jungers, W.L. 2003. The extinct sloth lemurs of Madagascar. Evo. Anthropol. 12,252–263.

Godfrey, L.R., Jungers, W.L., Burney, D.A., Vasey, N., Wheeler, W., Lemelin, P., Shapiro, L.J., Schwartz, G.T., King, S.J, et al. 2006. New discoveries of skeletal elements of *Hadropithecus stenognathus* from Andrahomana Cave, southeastern Madagascar. J. Hum. Evol. 51,395–410.

Grand, T., 1977. Body weight: its relation to tissue composition, segment distribu- tion, and motor function. I. Interspecific comparisons. Am. J. Phys. Anthropol. 47, 211-239.

Hatt, R. 1932. The vertebral columns of ricochetal rodents. Bulletin of the American Museum of Natural History.

Hickman G. 1979. The mammalian tail: a review of functions. Mamm. Rev. 9:143–157.

Hildebrand, M., Goslow, G.E., 1982. Analysis of Vertebrate Structure. Wiley, New York.

Hongo, T., and Luck, C. 1953. The circulation in the tail of a monkey (*Cercopithecus pygerythrus*). J. Physiol. 122, 570-581.

Horner, B., 1954. Arboreal adaptations of Peromyscus, with special reference to use of the tail. Contrib. Lab. Vert. Biol. 61, 1-84.

Ishida, H., Kunimatsu, Y., Takano, T., Nakano Y, and Nakatsukasa, M. 2004. *Nacholapithecus* skeleton from the Middle Miocene of Kenya. J. Hum. Evol. 46,69–103.

Ji, Q., Luo, Z.X., Yuan, C.X., and Tabrum, A.R. 2006. A swimming mammaliaform from the Middle Jurassic and ecomorphological diversification of early mammals. Science 311, 1123.

Kelley, J., 1997. Paleobiological and phylogenetic significance of life history in Miocene Hominoidea. In: Begun, D.R., Ward, C.V., Rose, M.D. (Eds.), Function, Phylogeny, and Fossils: Miocene Hominoid Evolution and Adaptations. Plenum Press, New York, pp. 173-208.

Lovejoy, C.O. 2005. The natural history of human gait and posture: Part 1. Spine and pelvis. Gait & Posture 21, 95–112.

MacKenzie, A.E. and Begun, D.R. 2009. The ancestor's tail: evolution of taillessness. am. J. Phys. Anthropol. 138 (48) 245-246.

MacLatchy, L., 2004. The oldest ape. Evol. Anthropol. 13, 90-103.

Mohr, E. 1941. Schwanzverlust und Schwanzregenerationbei Nagetieren. Zool. Anzeiger, 135:49-65.

Moyà Solà, S., and Kohler, M. 1996. A *Dryopithecus* skeleton and the origins of great-ape locomotion. Nature 379, 156–159.

Moyà Solà, S., Köhler, M., Alba, D.M., Casanovas-Vilar, I., Galindo, J., 2004. *Pierolapithecus catalaunicus*, a new Middle Miocene great ape from Spain. Science 306, 1339-1344.

Nakatsukasa, M., Tsujikawa, H., Shimizu, D., Takano, T., Kunimatsu, Y., Nakano, Y., Ishida, H. 2003. Definitive evidence for tail loss in *Nacholapithecus*, an East African Miocene hominoid. J. Hum. Evol. 45, 179-186.

Nakatsukasa, M., Ward, C.V., Walker, A., Teaford, M., Kunimatsu, Y., Ogihara, N., 2004. Tail loss in *Proconsul heseloni*. J. Hum. Evol. 46, 777-784.

Nakatsukasa, M., and Kunimatsu, Y. 2009. *Nacholapithecus* and its importance for understanding hominoid evolution. Evol. Anthropol. 18, 103–119.

Ojha, P.R. 1974. Tail carriage and dominance in the rhesus monkey, *Macaca mulatta*. Mammalia 38, 163–170.

Organ JM. 2010. Structure and function of platyrrhine caudal vertebrae. The Anatomical Record: Advances in Integrative Anatomy and Evolutionary Biology 293:730–745.

Oxnard CE, and Yang HCL. 1981. Beyond biometrics: studies of complex biological patterns. In: Symp Zool Soc Lond. Vol. 46. . p 127–167.

Peters, A., Preuschoft, H., 1984. External biomechanics of leaping in *Tarsius* and its morphological and kinematic consequences. In: Niemitz, C. (Ed.), Biology of Tarsiers. Gustav Fischer, Stuttgart, pp. 303e318.

Preuschoft, H., Witte, H. and Fischer, M. 1995. Locomotion in nocturnal prosimians. In: Doyle, G.A., Alterman, l. and Izard, M. Creatures of the Dark. Plenum Press: New York. pp 453-472.

Rafferty, K.L., Walker, A., Ruff, C.B., Rose, M.D., Andrews, P.J., 1995. Postcranial estimates of body weight in Proconsul, with a note on a distal tibia of P. major from Napak, Uganda. Am. J. Phys. Anthropol. 97, 391-402.

Ruff, C.B., Walker, A., Teaford, M.F., 1989. Body mass, sexual dimorphism and femoral proportions of Proconsul from Rusinga and Mfangano Islands, Kenya.
J. Hum. Evol. 18, 515-536.

Siegel, M., 1970. The tail, locomotion and balance in mice. Am. J. Phys. Anthropol. 33, 101-102.

Smit, T.H. 2002. The use of a quadruped as an in vivo model for the study of the spine-biomechanical considerations. European Spine Journal 11, 137–144.

Sprankel, H. 1965. Untersuchungen an Tarsius. I. Morphologie des Schwanzes nebstethologischen Bemerkungen. Folia Primatol. 3, 135-188

Stevens, N., Wright, K., Covert, H., Nadler, T., 2008. Tail postures of four quadrupedal leaf monkeys (Pygathrix nemaeus, P. cinerea, Trachypithecus delacouri and T. hatinhensis) at the Endangered Primate Rescue Center, Cuc Phuong National Park, Vietnam. Viet. J. Primatol 2, 13-24.

Sumner, F.B., and Collins, H.H. 1918. Autotomy of the tail in rodents. Biological Bulletin 34:1–6.

Wada, N., Hori, H., Tokuriki, M., 1993. Electromyographic and kinematic studies of tail movements in dogs during treadmill locomotion. J. Morph. 217, 105-113.

Walker, A.C., and Pickford, M. 1983. New postcranial fossils of *Proconsul africanus* and *Proconsul nyanzae*. In Ciochon, R.L. and Corruccini, R.S. (Eds.) New interpretations of ape and human ancestry. New York : Plenum Press, pp. 325–351.

Ward, C.V. 1993. Torso morphology and locomotion in *Proconsul nyanzae*. Am. J. Phys. Anthropol. 92, 291–328.

Ward, C.V., 1997. Functional anatomy and phyletic implications of the hominoid trunk and hindlimb. In: Begun, D.R., Ward, C.V., Rose, M.D. (Eds.), Function, Phylogeny, and Fossils: Miocene Hominoid Evolution and Adaptations. Plenum Press, New York, pp. 101-130.

Ward, C.V., Walker, A., Teaford, M.F., 1991. *Proconsul* did not have a tail. J. Hum. Evol. 21, 215-220.

Windsor, D.E., and Dagg, A.I. 1971. The gaits of the Macropodinae (Marsupialia). J. Zool. 163,165–175.

Woon, J.T., and Stringer, M.D. 2011. Clinical anatomy of the coccyx: A systematic review. Clin. Anat. 25,158–167.

Virchow, B. 1914. 9.82 Papio: 14.71 1913. Dio Mechanik der Schwanzwirbelsäule von *Papio olivaceus*. Sitz. Ber. Ges. nat. Freundelierlin:181—186.

References

Abitbol, M. 1987a. Evolution of the lumbosacral angle. Am. J. Phys. Anthropol. 72, 361–72.

Abitbol, M. 1987b. Evolution of the sacrum in hominoids. Am. J. Phys. Anthropol. 74, 65–81.

Abitbol, M. 1989. Sacral curvature and supine posture. Am. J. Phys. Anthropol. 80, 379–89.

Alba, D.M., Almécija, S., and Moyà-Solà, S. 2010. Locomotor inferences in *Pierolapithecus* and *Hispanopithecus*: Reply to Deane and Begun (2008). J. Hum. Evol. 59:143–149.

Andrews, P. 1992. Evolution and environment in the Hominoidea. Nature 360, 641.

Ankel, F., 1965. Der canalis sacralis als indikator für die länge der caudal region der primaten. Folia Primatol. 3, 263-276.

Ankel, F., 1972. Vertebral morphology of fossil and extant primates. In: Tuttle, R.(Ed.), The Functional and Evolutionary Biology of Primates. Aldine, Chicago, pp. 223-240.

Argot, C. 2003. Functional-adaptive anatomy of the axial skeleton of some extant marsupials and the paleobiology of the paleocene marsupials *Mayulestes ferox* and *Pucadelphys andinus*. J. Morph. 255, 279–300.

Begun, D.R., Ward, C.V., Rose, M.D., 1997. Events in hominoid evolution. In: Begun, D.R.,Ward, C.V., Rose, M.D. (Eds.), Function, Phylogeny, and Fossils: Miocene Hominoid Evolution and Adaptations. Plenum Press, New York, pp. 389-416.

Begun, D., Teaford, M., Walker, A., 1994. Comparative and functional anatomy of *Proconsul* phalanges from the Kaswanga primate site, Rusinga Island, Kenya. J. Hum. Evol. 26, 89-165.

Begun, D.R. 2002. European hominoids. In: Hartwig, W. (Ed.) Cambridge Studies in Biological and Evolutionary Anthropology. Cambridge University Press. pp 339–368.

Benefit, B.R., and McCrossin, M.L. 1995. Miocene Hominoids and Hominid Origins. Ann. Rev. Anthropol. 24, 237–256.

Benn, D.I., 1994. Fabric shape and the interpretation of sedimentary fabric data. J. Sediment. Res. A 64, 910-915.

Benton R. 1967. Morphological evidence for adaptations within the epaxial region of the primates. In: Vagtborg, H (Ed.) The Baboon in Medical Research. pp 201–216.

Bergeson, D.J. 1992. The use of the prehensile tail in Alouatta and Cebus. Am. J. Phys. Anthropol. 14, 48.

Bergeson, D.J. 1995. The ecological role of the platyrrhine prehensile tail. Am. J. Phys. Anthropol. 20, 64–65.

Bergeson, D.J. 1996. The positional behavior and prehensile tail use of *Alouatta paliatta, Ateles geoffrroyi,* and *Cebus capucinus*. PhD Dissertation, Washington University, St. Louis.

Bernstein, P., Smith, W., Krensky, A., and Rosene, K. 1978. Tail positions of *Cercopithecus aethiops*. Zeitschrift für Tierpsychologie 46, 268–278.

Bezanson, M.F. 2004. Ontogenetic influences on prehensile-tail use in *Cebus capucinus.* Am. J. Phys. Anthropol. 123:63.

Bezanson, M.F. 2005. Leap bridge or ride? Ontogenetic influences on positional behavior in Cebus and Alouatta. In: Estrada A, Garber PA, Pavelka MSM, Luecke L, editors. New perspectives in the study of Mesoamerican primates: distribution, ecology, behavior and conservation. New York: Springer. p 333–348.

Bezanson, M.F. 2006. Ontogenetic patterns of positional behavior in Cebus capucinus and Alouatta palliata. PhD dissertation, University of Arizona, Tucson, AZ.

Bezanson MF. 2009. Life history and locomotion in *Cebus capucinus* and *Alouatta palliata*. Am. J. Phys .Anthropol. 140,508– 517.

Biewener, A., Fazzalari, N., Konieczynski, D., and Baudinette, R. 1996. Adaptive changes in trabecular architecture in relation to functional strain patterns and disuse. Bone 19, 1–8.

Bininda-Emonds, O.R.P., Cardillo, M., Jones, K.E., MacPhee, R.D.E., Beck, R.M.D., Grenyer, R., Price, S.A., Vos, R.A., Gittleman, J.L., and Purvis, A. 2007. The delayed rise of present-day mammals. Nature 446, 507–512.

Bogduk N, Twomey L. 2005. Clinical anatomy of the lumbar spine and sacrum. Livingstone: Churchill.

Buck, C., Tolman, N., Tolman, W. 1925. The tail as a balancing organ in mice. J. Mammal 6, 267-271.

Burr, D.B., Robling, A.G., C.H. Turner. 2002. Effects of Biomechanical Stress on Bones in Animals. Bone 30(5): 781-786.

Byron, C., Kunz, H., Matuszek, H., Lewis, S., and Van Valkinburgh D. 2011. Rudimentary pedal grasping in mice and implications for terminal branch arboreal quadrupedalism. J. Morph. 272, 230–240.

Cant, J.G. 1987. Positional behavior of female Bornean orangutans (*Pongo pygmaeus*). Am. J. Primatol. 12, 71–90.

Carter, D.R., Fyhrie, D.P., and Whalen, R.T. 1987. Trabecular bone density and loading history: regulation of connective tissue biology by mechanical energy. J. Biomech. 20, 785-794.

Cartmill, M., and Milton, K. 1977. The lorisiform wrist joint and the evolution of "'brachiating'"adaptations in the Hominoidea. Am. J. Phys. Anthropol. 47, 249–272.

Chadwell, B.A., Young, J.W., Shapiro, L.J. 2013. A comparative look at tail movement during narrow branch locomotion. Society of Integrative and Comparative Biology 2013 Annual Meeting. San Franciso, CA.

Chang, H.T., and Ruch, T.C. 1947. Morphology of the spinal cord, spinal nerves, caudal plexus, tail segmentation, and caudal musculature of the spider monkey. The Yale Journal of Biology and Medicine 19, 345-377.

Coleman, M.N., and Colbert, M.W. 2007. Technical note: CT thresholding protocols for taking measurements on three-dimensional models. Am. J. Phys. Anthropol. 133, 723–725.

Cotter, M.M., Simpson, S.W., Latimer, B.M., and Hernandez, C.J. 2009. Trabecular microarchitecture of hominoid thoracic vertebrae. Anat. Rec. 292, 1098–1106.

Cotter, M.M., Loomis, D.A., Simpson, S.W., Latimer, B.,Hernandez, C.J. 2011. Human evolution and osteoporosis-related spinal fractures. PLoS ONE 6, e26658.

Currey, J.D. 1975. The effects of strain rate, reconstruction and mineral content on some mechanical properties of bovine bone. J.Biomech. 8, 81–86.

Currey, J.D. 1984. The mechanical adaptations of bones. Princeton University Press Princeton, NJ.

Deane, A.S., and Begun, D.R. 2010. *Pierolapithecus* locomotor adaptations: a reply to Alba et al.'s comment on Deane and Begun (2008). J. Hum. Evol. 59, 150–154.

Deane, A.S., Russo, G.A., Muchlinski, M., Organ, J.M. *in prep*. Functional correlates of caudal vertebral body articular surface size and shape in prehensile- and nonprehensile-tailed anthropoids.

Deinard, A., and Smith, D.G. 2001. Phylogenetic relationships among the macaques: evidence from the nuclear locus NRAMP1. J. Hum. Evol. 41, 45–59.

Demes, B., Jungers, W.L., Fleagle, J.G., Wunderlich, R.E., Richmond, B.G., and Lemelin P. 1996. Body size and leaping kinematics in Malagasy vertical clingers and leapers. J. Hum. Evol. 31, 367–388.

Ding, M., and Hvid, I. 2000. Quantification of age-related changes in the structure model type and trabecular thickness of human tibial cancellous bone. Bone 26, 291–295.

Dor, M. 1937. La morphologie de la queue des mammiferes. Paris: Pierre Andre.
Doran, D. 1989. Chimpanzee and pygmy chimpanzee positional behavior: the influence of environment, body size, morphology and ontogeny on locomotion and posture, Ph.D. dissertation, The State University of New York, Stony Brook, NY.

Doube, M., Klosowski, M.M., Wiktorowicz-Conroy, A.M.,Hutchinson, J.R., Shefelbine S.J. 2011 Trabecular bone scales allometrically in mammals and birds. Proc. R. Soc.B 278, 3067–3073.

Elftman, H., 1932. The evolution of the pelvic floor of primates. Am. J. Anat. 51, 307-346.

Emerson, S.B., 1985. Jumping and leaping. In: Hildebrand, M., Bramble, D.M., Liem, K.F., Wake, D.B. (Eds.), Functional Vertebrate Morphology. Belknap Press, Cambridge, pp. 58-72.

Emmons, L.H., and Gentry, A.H. 1983. Tropical forest structure and the distribution of gliding and prehensile-tailed vertebrates. Am. Nat. 121, 513–524.

Essner, Jr., R.L., 2002. Three-dimensional launch kinematics in leaping, parachuting and gliding squirrels. J. Exp. Biol. 205, 24-69.

Fa, J.E., 1985. Baby care in barbary macaque. In: Macdonald, D. (Ed.), Primates. Torstar Books, New York, pp. 92-93.

Fa, J.E., 1989. The genus *Macaca*: a review of taxonomy and evolution. Mammal Rev. 19, 45-81.

Fajardo, R.J., De Silva, J., and MacLatchy, L. 2010. Does the amount of bone dictate the trabecular bone structure in strepsirhine lumbar vertebrae? Am. J. Phys. Anthropol. S50,102.

Fajardo, R.J., Desilva, J.M., Manoharan, R.K., Schmitz, J.E., Maclatchy, L.M., and Bouxsein, M.L. 2013. Lumbar Vertebral Body Bone Microstructural Scaling in Small to Medium-Sized Strepsirhines. Anat. Rec. 296, 210–226.

Fajardo, R.J., and Müller, R. 2001. Three dimensional analysis of nonhuman primate trabecular architecture using micro computed tomography. Am. J. Phys. Anthropol. 115, 327–336.

Fajardo, R.J., Müller, R., Ketcham, R.A., and Colbert, M. 2007. Nonhuman anthropoid primate femoral neck trabecular architecture and its relationship to locomotor mode. Anat. Rec. 290, 422–436.

Fajardo, R.J., Ryan, T.M., and Kappelman, J. 2002. Assessing the accuracy of high-resolution X-ray computed tomography of primate trabecular bone by comparisons with histological sections. Am. J. Phys. Anthropol. 118:1–10.

Fleagle, J.G. 1976. Locomotion and posture of the Malayan siamang and implications for hominoid evolution. Folia Primatol. (Basel) 26, 245–269.

Fleagle, J.G. 1984. Size and adaptation in primates. In: Jungers W.L. (Ed.). Size and scaling in primate biology. New York: Plenum Press. pp 1–19.

Fleagle, J.G. 2013. Primate Adaptation and Evolution: 3rd Edn. Academic Press.

Flower, W.H. 1876. An Introduction to the Osteology of the Mammalia: Being the Substance of the Course of Lectures Delivered at the Royal College of Surgeons of England in 1870. Macmillan.

Fooden, J. 1988. Taxonomy and evolution of the sinica group of macaques: 6. Interspecific comparisons and synthesis. Fieldiana Zool 45:1–44

Fooden, J., 1997. Tail length variation in Macaca fascicularis and M. mulatta. Primates 38, 221-232

Fooden, J., Albrecht, G.H., 1999. Tail length evolution in fascicularis group macaques (Cercopithecidae: Macaca). Int. J. Primatol. 20, 431-440.

Fooden, J., 2006. Comparative review of fascicularis-group species of macaques (Primates: Macaca). Fieldiana Zool. 107, 1-44.

Fooden, J., 2007. Systematic review of the barbary macaque, Macaca sylvanus (Linnaeus, 1758). Fieldiana Zool. 113, 1-58.

Francis, C.M., 2008. A Field Guide to the Mammals of Southeast Asia. New Holland.

Freckleton, R.P, Harvey, P.H., and Pagel, M. 2002. Phylogenetic analysis and comparative data: a test and review of evidence. Am. Nat. 160,712–726.

Fredrickson J. 1989. The tailless cat in free-fall. The Physics Teacher 27, 620.

Fyhrie, D.P., and Schaffler, M.B. 1995. The adaptation of bone apparent density to applied load. J. Biomech. 28:135–146.

Games, P., and Howell, J. 1976. Pairwise Multiple Comparison Procedures with Unequal N's and/or Variances: A Monte Carlo Study. J. Ed. Behav. Stat. 1, 113.

Garber, P.A., and Rehg, J.A. 1999. The ecological role of the prehensile tail in white-faced capuchins (*Cebus capucinus*). Am. J. Phys. Anthropol. 110, 325–339.

Gebo, D.L. 1992. Locomotor and postural behavior in *Alouatta palliata* and *Cebus capucinus*. Am. J. Primatol. 26, 277–290.

Gebo, D.L., and Sargis, E.J. 1994. Terrestrial adaptations in the postcranial skeletons of guenons. Am. J. Phys. Anthropol. 93, 341–371.

German, R.Z. 1982. The functional morphology of caudal vertebrae in New World monkeys. Am. J. Phys. Anthropol. 58, 453–459.

Gibson, L.J. 1985. The mechanical behaviour of cancellous bone. J. Biomech. 18,317.

Godfrey, L.R., and Jungers, W.L. 2002. Quaternary Fossil Lemurs. In The Primate Fossil Record. W. Hartwig (Ed.). Cambridge: Cambridge University Press, pp. 97-121.

Godfrey, .LR., and Jungers, W.L. 2003. The extinct sloth lemurs of Madagascar. Evo. Anthropol. 12,252–263.

Godfrey, L.R., Jungers, W.L., Simons, E.L., Chatrath, P.S. and Berthe Rakotosamimanana. 1999. Past and present distributions of lemurs in Madagascar. In B. Rakotosamimanana, H. Rasaminmanana, J. Ganzhorn, and S. Goodman. (Eds.) New Directions in Lemur Studies. New York: Plenum Press. pp. 19-53.

Godfrey, L.R., Jungers, W.L., Burney, D.A., Vasey, N., Wheeler, W., Lemelin, P., Shapiro, L.J., Schwartz, G.T., King, S.J, et al. 2006. New discoveries of skeletal elements of *Hadropithecus stenognathus* from Andrahomana Cave, southeastern Madagascar. J. Hum. Evol. 51,395–410.

Goldstein, S.A., Matthews, L.S., Kuhn, J.L, and Hollister, S.J. 1991. Trabecular bone remodeling: an experimental model. J. Biomech. 24,135–150.

Goldstein, S.A., Goulet, R., and McCubbrey, D. 1993. Measurement and significance of three-dimensional architecture to the mechanical integrity of trabecular bone. Calc. Tiss. Intl. 53, S127–S133.

Gommery, D., Ramanivosoa, B., Tombomiadana-Raveloson, S., Randrianantenaina, H., & Kerloc'h, P. 2009. Une nouvelle espèce de lémurien géant subfossile du Nord-Ouest de Madagascar (*Palaeopropithecus kelyus*, Primates). Comptes Rendus Palevol, 8(5), 471-480.

Gosman, J.H., and Ketcham, R.A. 2009. Patterns in ontogeny of human trabecular bone from SunWatch Village in the prehistoric Ohio Valley: general features of microarchitectural change. Am. J. Phys. Anthropol. 138, 318–332.

Graham, D.J., Midgley, N.G., 2000. Graphical representation of particle shape using triangular diagrams: an excel spreadsheet method. Earth Surf. Proc. Landf. 25, 1473-1477.

Granhed H, Jonson R, and Hansson T. 1987. The loads on the lumbar spine during extreme weight lifting. Spine 12:146–149.

Grand, T., 1977. Body weight: its relation to tissue composition, segment distribu- tion, and motor function. I. Interspecific comparisons. Am. J. Phys. Anthropol. 47, 211e239.

Gregory, W.K. 1928. The upright posture of man: A review of its origin and evolution. Proc. Am. Phil. Soc. 67, 339–377.

Groves, C.P. 2001. Primate taxonomy. Washington, DC: Smithsonian Institution Press.

Groves, C.P. 2005. Order primates. In: Wilson DE, Reeder DM, editors. Mammal species of the world: a taxonomic and geographic reference, 3rd ed. Baltimore: Johns Hopkins University Press. p 111–184, Vol.1.

Günther, M.M., Ishida, H., Kumakura, H., Nakano, Y., 1991. The jump as a fast mode of locomotion in arboreal and terrestrial biotopes. Z. Morphol. Anthropol. 78, 341-372.

Hamada, Y., Yamamoto, A., Kunimatsu, Y., Tojima, S., Mouri, T., and Kawamoto, Y. 2012. Variability of tail length in hybrids of the Japanese macaque (Macaca fuscata) and the Taiwanese macaque (Macaca cyclopis). Primates:1–15.

Hammer, Ø., Harper, D.A.T., Ryan, P.D. 2001. PAST: Paleontological statistics software package for education and data analysis. Palaeontologia Electronica 4(1): 9pp.

Harrigan, T.P., Jasty, M., Mann ,R.W., and Harris, W.H. 1988. Limitations of the continuum assumption in cancellous bone. Journal of Biomechanics 21:269–275.

Harrison, T., 1987. The phylogenetic relationships of the early catarrhine primates: a review of the current evidence. J. Hum. Evol. 16, 41-80.

Harrison, T. 1987. A reassessment of the phylogenetic relationships of *Oreopithecus bambolii* Gervais 1872. J. Hum. Evol. 15, 541–583.

Harrison, T., 1993. Cladistic concepts and the species problem in hominoid evolution. In: Kimbel, W.H., Martin, L.B. (Eds.), Species, Species Concepts and Primate Evolution. Plenum Press, New York, pp. 345-371.

Harrison, T., 1998. Evidence for a tail in *Proconsul heseloni*. Am. J. Phys. Anthropol. 26, 93-94.

Harrison, T. 1991. The implications of *Oreopithecus bambolii* for the origins of bipedalism. In: Coppens, Y., Senut, B. (Eds.), Origine (s) de la bipédie chez les hominidés, Cahiers de Paléoanthropologie. Paris: Editions du CNRS. pp. 235–244.

Harrison, T., 2002. Late Oligocene to middle Miocene catarrhines from Afro-Arabia. In: Hartwig, W.C. (Ed.), The Primate Fossil Record. Cambridge University Press, Cambridge, pp. 311e338.

Harrison T, and Rook L. 1997. Enigmatic anthropoid or misunderstood ape? The phylogenetic status of Oreopithecus bambolii reconsidered. In: Begun, D.R., Ward, C.V., Rose, M.D. (Eds.), Function, Phylogeny, and Fossils: Miocene Hominoid Evolution and Adaptations. Plenum Press, New York, pp. 327–362.

Hartman, C.G., and Straus, W.L. 1933. The anatomy of the rhesus monkey (*Macaca mulatta*). The Williams & Wilkins Company.

Hickman, G., 1979. The mammalian tail: a review of functions. Mammal Rev. 9, 143-157.

Hildebrand, M. 1974. Analysis of vertebrate structure. Wiley, New York, NY.

Horner, B., 1954. Arboreal adaptations of Peromyscus, with special reference to use of the tail. Contrib. Lab. Vert. Biol. 61, 1-84.

Hürzeler, J. 1958. *Oreopithecus bambolii* Gervais: A preliminary report. Verh. naturf. Ges. Basel. 69, 1-48.

Huq, E. and Jungers, W. 2009. Tail length and the sacral index in living and subfossil Malagasy prosimians. Am. J. Phys. Anthropol. 138:231 (abstract).

Hunt, K. 1989. Positional behavior in Pan troglodytes at the Mahale Mountains and the Gombe stream national parks, Tanzania, Ph.D. dissertation, University of Michigan, Ann Arbor, Michigan.

Hunt, K. 1991. Positional behavior in the Hominoidea. Int. J. Primatol. 12, 95–118.

Igarashi M, and Levy J. 1981. Locomotor balance performance of short-tailed squirrel monkeys. J. Med. Primatol. 10,136.

Ihaka, R., and Gentleman, R. 1996. R: A language for data analysis and graphics. J. Comp. Graph Stat. 5, 299–314.

Ishida, H., Kunimatsu, Y., Takano, T., Nakano Y, and Nakatsukasa, M. 2004. *Nacholapithecus* skeleton from the Middle Miocene of Kenya. J. Hum. Evol. 46,69–103.

Jenkins, P.D., 1990. Catalogue of Primates in the British Museum (Natural History) and Elsewhere in the British Isles. Part V: The Apes, Superfamily Hominoidea. The British Museum (Natural History), London.

Johanson, D.C., Lovejoy, C.O., Kimbel, W.H., White, T.D., Ward, S.C., Bush, M.E., Latimer, B.M., Coppens, Y. 1982. Morphology of the Pliocene partial hominid skeleton (AL 288-1) from the Hadar formation, Ethiopia. Am. J. Phys. Anthropol. 57, 403–451.

Johnson S, and Shapiro L. 1998. Positional behavior and vertebral morphology in atelines and cebines. Am. J. Phys. Anthropol. 105, 333–354.

Jenkins, P.D., 1990. Catalogue of Primates in the British Museum (Natural History) and Elsewhere in the British Isles. Part V: The Apes, Superfamily Hominoidea. The British Museum (Natural History), London.

Judex, S., Garman, R., Squire, M., Donahue, L.R., Rubin, C., 2004. Genetically based influences on the site-specific regulation of trabecular and cortical bone morphology. J. Bone Miner. Res. 19, 600-606.

Jungers, W.L. 1988. Relative joint size and hominoid locomotor adaptations with implications for the evolution of hominid bipedalism. J. Hum. Evol. 17, 247–265.

Jungers, W.L., 1991. Scaling of postcranial joint size in hominoid primates. J. Hum. Evol. 6, 391-399.

Jungers, W.L., Godfrey LR, Simons EL, Wunderlich RE, Richmond BG, Chatrath PS, Plavcan JM, Kay RF, Jungers WL, et al. 2002. Ecomorphology and behavior of giant extinct lemurs from Madagascar. In: Plavcan, J.M. (Ed.) Reconstructing behavior in the primate fossil record. Plenum Press: New York. pp. 371–411.

Kapandji, I.A., 2008. The Physiology of the Joints (V3): The Spinal Column, Pelvic Girdle and Head. Lavoisier, Paris.

Keaveny, T.M., Morgan, E.F., Niebur, G.L., and Yeh, O.C. 2001. Biomechanics of trabecular bone. Ann. Rev. Bio. Eng. 3, 307–333.

Kelley, J., 1997. Paleobiological and phylogenetic significance of life history in Miocene Hominoidea. In: Begun, D.R., Ward, C.V., Rose, M.D. (Eds.), Function, Phylogeny, and Fossils: Miocene Hominoid Evolution and Adaptations. Plenum Press, New York, pp. 173-208.

Ketcham, R.A., and Carlson, W.D. 2001. Acquisition, optimization and interpretation of X-ray computed tomographic imagery: applications to the geosciences. Computers & Geosciences 27, 381–400.

Ketcham, R.A., and Ryan, T. 2004. Quantification and visualization of anisotropy in trabecular bone. J. Microscop. 213, 158–171.

Kim, D. G., Christopherson, G. T., Dong, X. N., Fyhrie, D. P., & Yeni, Y. N. (2004). The effect of microcomputed tomography scanning and reconstruction voxel size on the accuracy of stereological measurements in human cancellous bone. Bone, *35*(6), 1375-1382.

Kirk E.C., and Gosselin-Ildari A.D. 2009. Cochlear labyrinth volume and hearing abilities in primates. Anat. Rec. 292, 765–776.

Köhler, M., and Moyà-Solà, S. 1997. Ape-like or hominid-like? The positional behavior of *Oreopithecus bambolii* reconsidered. Proc. Natl. Acad. Sci. 94, 11747-11750.

Kothari, M., Keaveny, T.M., Lin, J.C., Newitt, D.C., Genant, H.K., Majumdar, S. Impact of spatial resolution on the prediction of trabecular architecture parameters. Bone. 22(5), 437-443.

Larson, S. 1998. Parallel evolution in the hominoid trunk and forelimb. Evol. Anthropol. 6, 87–99.

Larson, S., and Stern Jr., J., 2006. Maintenance of above-branch balance during primate arboreal quadrupedalism: coordinated use of forearm rotators and tail motion. Am. J. Phys. Anthropol. 129, 71-81.

Lazenby, R.A., Skinner, M.M., Kivell TL, and Hublin, J.J. 2011. Scaling VOI size in 3D CT studies of trabecular bone: A test of the over sampling hypothesis. Am. J. Phys. Anthropol. 144, 196-203.

Lawler, R.R., and Stamps, C. 2002. The relationship between tail use and positional behavior in *Alouatta palliata*. Primatol. 43,147–152.

Lemelin P. 1995. Comparative and functional myology of the prehensile tail in New World monkeys. J. Morphol. 224:351– 368.

Leutenegger, W., 1970. Das Becken der rezenten Primaten. Morph. Jahrb. 115, 1-101.

Leutenegger, W. 1977. A functional interpretation of the sacrum of *Australopithecus africanus*. S. Afr. J. Sci. 73, 308–10.

Lieberman, D.E., Devlin, M.J., and Pearson, O.M. 2001. Articular area responses to mechanical loading: effects of exercise, age and skeletal location. Am. J. Phys. Anthropol. 116, 266-277.

Lieberman, D.E., Polk, J.D., and Demes B. 2004. Predicting long bone loading from cross-sectional geometry. Am. J. Phys. Anthropol. 123, 156-171.

Lovejoy, C.O. 1988. Evolution of human walking. Sci. Am. 259, 82–89.

Lovejoy, C.O., McCollum, M.A., Reno, P.L., and Rosenman, B.A. 2003. Developmental biology and human evolution. Ann. Rev. Anthropol. 32, 85–109.

Macchiarelli, R., Rook, L., Bondioli, L. 2001. Comparative analysis of the iliac trabecular architecture in extant and fossil primates by means of digital image processing techniques: implications for the reconstruction of fossil locomotor behaviours. In: Agusti, J., Rook, L., Andrews, P. (Eds.), Hominoid Evolution and Climatic Change in Europe. Cambridge University Press, U.K. pp 60–101.

Machida, A., and Inoue, T. 1994. The effect of weight-bearing on the bone tissue of bipedal rats. J. Bone Min. Met. 12, 15–29.

MacLatchy, L., 2004. The oldest ape. Evol. Anthropol. 13, 90-103.

MacLatchy, L., Gebo, D., Kityo, R., and Pilbeam, D. 2000. Postcranial functional morphology of *Morotopithecus bishopi*, with implications for the evolution of modern ape locomotion. J. Hum. Evol. 39, 159–183.

MacLatchy, L., Müller, R. 2002 A comparison of the femoral head and neck trabecular architecture of *Galago* and *Perodicticus* using micro-computed tomography (mCT). J. Hum. Evol. 43, 89–105.

Maga, M., Kappelman, J., Ryan, T.M., and Ketcham. R.A. 2006. Preliminary Observations on the Calcaneal Trabecular Microarchitecture of Extant Large-Bodied Hominoids. Am. J. Phys. Anthropol. 129, 410–417.

Mahato, N.K. 2010. Trabecular architecture in human sacra: patterns observed in complete sacralisation and accessory articulation with the fifth lumbar vertebrae. J. Morphol. 27, 19–22.

Maigne, J.Y., and Tamalet, B. 1996. Standardized radiologic protocol for the study of common coccygodynia and characteristics of the lesions observed in the sitting position: Clinical elements differentiating luxation, hypermobility, and normal mobility. Spine 21,2588–2593.

Martin, R. 1968. Reproduction and Ontogeny in tree shrews (*Tupaia belangeri*), with reference to their general behaviour and taxonomic relationships1. Zeitschrift für Tierpsychologie 25,409–495.

Martins, E.P., and Hansen, T.F. 1997. Phylogenies and the comparative method: a general approach to incorporating phylogenetic information into the analysis of interspecific data. Am. Nat. 149, 646–667.

Meldrum, D.J. 1998. Tail-assisted hind limb suspension as a transitional behavior in the evolution of the platyrrhine prehensile tail. In: Strasser, E. (Ed.) Primate locomotion: recent advances. Plenum Press: New York. pp 145–156.

McCrossin, M.L., and Benefit, B.R. 1992. Comparative assessment of the ischial morphology of *Victoriapithecus macinnesi*. Am. J. Phys. Anthropol. 87,277–290.

McCrossin, M.L. 1994. The phylogenetic relationships, adaptations, and ecology of *Kenyapithecus*. Ph.D. Dissertation. University of California, Berkeley.

Miller, G.S. 1900. Key to the land mammals of northeastern North America. University of the State of New York.

Moyà Solà, S., and Kohler, M. 1996. A *Dryopithecus* skeleton and the origins of great-ape locomotion. Nature 379, 156–159.

Moyà Solà, S., Köhler, M., Alba, D.M., Casanovas-Vilar, I., Galindo, J., 2004. *Pierolapithecus catalaunicus*, a new Middle Miocene great ape from Spain. Science 306, 1339-1344.

Mullender, M.G., Huiskes, R., Versleyen, H., Burma, P.1996. Osteocyte density and histomorphometric parameters in cancellous bone of the proximal femur in five mammalian species. J. Orthop. Res. 14, 972–979.

Nakatsukasa, M., Tsujikawa, H., Shimizu, D., Takano, T., Kunimatsu, Y., Nakano, Y., Ishida, H., 2003. Definitive evidence for tail loss in *Nacholapithecus*, an East African Miocene hominoid. J. Hum. Evol. 45, 179-186.

Nakatsukasa, M., Ward, C.V., Walker, A., Teaford, M., Kunimatsu, Y., Ogihara, N., 2004. Tail loss in *Proconsul heseloni*. J. Hum. Evol. 46, 777-784.

Nakatsukasa, M., and Kunimatsu, Y. 2009. *Nacholapithecus* and its importance for understanding hominoid evolution. Evol. Anthropol. 18, 103–119.

Napier, P.H., 1981. Catalogue of Primates in the British Museum (Natural History) and Elsewhere in the British Isles, Part 2: Family Cercopithecidae, Subfamily: Cercopithecinae. British Museum (Natural History), London.

Nowak, R.M., 1991. Walker's Mammals of the World, fifth ed., vol. 1. J. Hopkins University Press, Baltimore and London.

Odgaard A. 1997. Three-dimensional methods for quantification of cancellous bone architecture. Bone. 20, 315–328.

Organ, J.M. 2006. To grasp or not to grasp? Structure and function of platyrrhine caudal vertebrae. Am. J. Phys. Anthropol. (S42):142.

Organ, J.M. 2007. The functional anatomy of prehensile and non- prehensile tails of the Platyrrhini (Primates) and Procyonidae (Carnivora). PhD Dissertation. The Johns Hopkins University, Baltimore, MD.

Organ, J.M. 2010. Structure and function of platyrrhine caudal vertebrae. Anat. Rec. 293:730–745.

Organ, J.M., Teaford, M.F., Taylor, A.B. 2009. Functional correlates of fiber architecture of the lateral caudal musculature in pr hensile and nonprehensile tails of the Platyrrhini (Primates) and Procyonidae (Carnivora). Anat. Rec. 292, 827–841.

Organ, J.M., Muchlinski, M.N., Deane, A.S. 2011. Mechanoreceptivity of prehensile tail skin varies between atelines and Cebus. Anat. Rec. 294, 2064–2072

Oxnard CE, and Yang HCL. 1981. Beyond biometrics: studies of complex biological patterns. Symp. Zool. Soc. Lond. 46, 127–167.

Pagel, M. 1999. Inferring the historical patterns of biological evolution. Nature 401,877–884.

Paradis E., Claude, J., and Strimmer, K. 2004. APE: analyses of phylogenetics and evolution in R language. Bioinformatics 20:289–290.

Parker, S.P., 1990. Grzimek's Encyclopedia of Mammals, vol. 2. McGraw Hill, New York.

Pearson, O.M., Lieberman, D.E. 2004. The aging of Wolff's "law": ontogeny and responses to mechanical loading in cortical bone. Am. J. Phys. Anthropol. 125, 63-99.

Pilbeam, D., and Young, N. 2004. Hominoid evolution: synthesizing disparate data. Comptes. Rendus. Palevol. 3, 305–321.

Peretz, A.M., Hipp, J.A., and Heggeness, M.H. 1998. The internal bony architecture of the sacrum. Spine 23, 971-974.

Procter-Gray, E., and Ganslosser, U. 1986. The individual behaviors of Lumholtz's tree-kangaroo: repertoire and taxonomic implications. J. Mammal. 343–352.

Rafferty, K.L. 1998. Structural design of the femoral neck in primates. J. Hum. Evol. 34, 361–383.

Rafferty, K.L., and Ruff, C. 1994. Articular structure and function in *Hylobates*, *Colobus*, and *Papio*. Am. J. Phys. Anthropol. 94, 395–408.

Ramanivosoa, B., and Gommery, D. 2011. Les lémuriens subfossiles dans le Nord-Ouest de Madagascar, du terrain à la diffusion des connaissances ou 15 ans de recherches franco-malgaches. Revue de primatologie 3.

Rice, J.C., Cowin, S.C., and Bowman, J.A. 1988. On the dependence of the elasticity and strength of cancellous bone on apparent density. J. Biomech. 21, 155-168.

Ridler, T. W., and Calvard, S. 1978. Picture thresholding using an iterative selection method. IEEE transactions on Systems, Man and Cybernetics, 8(8), 630-632.

Robinson, J.T. 1972. Early hominid posture and locomotion. University of Chicago Press, Chicago.

Robson-Brown, K., Katharine, A., Davies, E.N., and McNally, D.S. 2002. The angular distribution of vertebral trabeculae in modern humans, chimpanzees and the Kebara 2 Neanderthal. J. Hum. Evol.43:189–205.
Rodman, P.S. 1979. Skeletal differentiation of Macaca fascicularis and Macaca nemestrina in relation to arboreal and terrestrial quadrupedalism. Am. J. Phys. Anthropol. 51, 51–62.

Rook, L., Bondioli, L., Köhler, M., Moyà-Solà, S., and Macchiarelli, R. 1999. *Oreopithecus* was a bipedal ape after all: evidence from the iliac cancellous architecture. Proc. Natl. Acad. Sci. 96, 8795-8799.

Rook, L., Oms, O., Benvenuti, M.G., Papini, M. 2011. Magnetostratigraphy of the Late Miocene Baccinello–Cinigiano basin (Tuscany, Italy) and the age of *Oreopithecus bambolii* faunal assemblages. Palaeogeogr. Palaeoclimatol. Palaeoecol. 305, 286–294.

Rook, L., Renne, P., Benvenuti, M., Papini, M. 2000. News and Views Geochronology of *Oreopithecus*-bearing succession at Baccinello (Italy) and the extinction pattern of European Miocene hominoids. J. Hum. Evol. 39, 577–582.

Rose, M.D., 1993. Locomotor anatomy of Miocene hominoids. In: Gebo, D. (Ed.), Postcranial Adaptation in Nonhuman Primates. Northern Illinois University Press, DeKalb, pp. 252-272.

Rose, M.D., 1997. Functional and phylogenetic features of the forelimb in Miocene hominoids. In: Begun, D.R., Ward, C.V., Rose, M.D. (Eds.), Function, Phylogeny, and Fossils: Miocene Hominoid Evolution and Adaptations. Plenum Press, New York, pp. 79-100.

Rose, M.D., Nakano, Y., and Ishida, H. 1996. *Kenyapithecus* postcranial specimens from Nachola, Kenya. Afr. Stud. Monogr. 24, 3–56.

Rosenberger, A.L. 1983. Tale of tails: parallelism and prehensility. Am. J. Phys. Anthropol. 60,103–107.

Rosenberger, A.L., and Matthews, L.J. 2008. *Oreonax*—not a genus. Neotrop. Primates 15, 8–12.

Rosenman, B. (2008). Triangulating the evolution of the vertebral column in the last common ancestor: thoracolumbar transverse process homology in the Hominoidea. Ph.D. Dissertation. Kent State University, Kent, Ohio.

Rowe, N., 1996. The Pictorial Guide to the Living Primates. Pogonias Press, New York.

Rubin, C.T., and Lanyon, L.E. 1985. Regulation of bone mass by mechanical strain magnitude. Calc. Tiss. Intl. 37, 411–417.

Ruff, C.B. 1999. Skeletal structure and behavioral patterns of prehistoric Great Basin populations. In: Hemphill, B.E., Larsen, C.S. (Eds.) Prehistoric Lifeways in the Great Basin Wetlands: Bioarchaeological Reconstruction and Interpretation. Salt Lake city: University Utah Press. pp. 290-320.

Ruff, C. B. 2008. Biomechanical analyses of archaeological human skeletons. In: Katzenberg, M.A. and S.R. Saunders (Eds). Biological Anthropology of the Human Skeleton, Second Edition. John Wiley & Sons, Inc. pp 183-206.

Ruff, C., Holt, B., & Trinkaus, E. 2006. Who's afraid of the big bad Wolff?:"Wolff's law" and bone functional adaptation. Am. J. Phys. Anthropol. 129, 484-498.

Russo, G.A. 2010. Prezygapophyseal articular facet shape in the catarrhine thoracolumbar vertebral column. Am. J. Phys. Anthropol. 142, 600–612.

Russo, G.A., Shapiro, L.J. 2011. Morphological correlates of tail length in the catarrhine sacrum. J. Hum. Evol. 30, 223–232.

Russo, G.A., Shapiro, L.J. 2013. Reevaluation of the lumbosacral region of *Oreopithecus bambolii.* J. Hum. Evol. (doi: 10.1016/j.jhevol.2013.05.004)

Russo, G.A., Fajardo, R.J., Schmitz, J.E. 2012. Internal bone structure of the last sacral vertebra and its relationship to tail length. Am. J. Phys. Anthropol. 147 (S52), 255-256

Russo, G.A., and Young, J.W. 2011. Tail growth tracks the ontogeny of prehensile tail use in capuchin monkeys (*Cebus albifrons* and *C. apella*). Am. J. Phys. Anthropol. 146, 465–473.

Ryan, T.M., and Ketcham, R.A. 2002a. The three-dimensional structure of trabecular bone in the femoral head of strepsirrhine primates. J. Hum. Evol. 43,1–26.

Ryan, T.M., and Ketcham, R.A. 2002b. Femoral head trabecular bone structure in two omomyid primates. J. Hum. Evol. 43,241–263.

Ryan, T.M., and Ketcham R.A. 2005. Angular Orientation of Trabecular Bone in the Femoral Head and Its Relationship to Hip Joint Loads in Leaping Primates. J. Morpol. 265:249.

Ryan, T.M., Krovitz, G.E. 2006. Trabecular bone ontogeny in the human proximal femur. J. Hum. Evol. 51, 591–602.

Ryan, T.M., and Shaw, C.N. 2012 Unique suites of trabecular bone features characterize locomotor behavior in human and non-human anthropoid primates. PLoS ONE 7, e41037.

Ryan, T.M., and Walker, A. 2010 Trabecular bone structure in the humeral and femoral heads of anthropoid primates. Anat. Rec. 293, 719–729.

Rylands, A.B., Mittermeier, R.A. 2009. The diversity of the New World primates (Platyrrhini): an annotated taxonomy. In: Garber, P.A., Estrada, A., Bicca-Marques, J.C., Heymann, E.W., Strier, K.B. (Eds.). South American primates: comparative perspectives in the study of behavior, ecology, and conservation. New York: Springer. pp 23–54.

Saluja, P.G. 1988. The incidence of ossification of the sacrococcygeal joint. J. Anat. 156:11.

Sanders, W.J., Bodenbender, B.E. 1994. Morphometric analysis of lumbar vertebra UMP 67–28: implications for spinal function and phylogeny of the Miocene Moroto hominoid. J. Hum. Evol. 26, 203–237.

Scherf, H., Harvati, K., and Hublin, J.J. 2013. A comparison of proximal humeral cancellous bone of great apes and humans. J. Hum. Evol. 65: 29-38.

Schmidt-Nielsen, K. 1984. Scaling: why is animal size so important? Cambridge: Cambridge University Press.

Schmitt, D. 2010. Primate locomotor evolution: Biomechanical studies of primate locomotion and their implications for understanding primate neuroethology. In: Platt, M.L. and Ghazanfar, A.A. (Eds.) Primate neuroethology. pp 31-63.

Schmitt, D., Rose, M.D., Turnquist, J.E., Lemelin, P., 2005. Role of the prehensile tail during ateline locomotion: experimental and osteological evidence. Am. J. Phys. Anthropol. 126, 435-446.

Schultz, A. 1930. The skeleton of the trunk and limbs of higher primates. Wayne State University Press.

Schultz, A.H. 1941. Chevron bones in adult man. Am. J. Phys. Anthropol. 28, 91–97.

Schultz, A.H., Straus Jr., W.L., 1945. The number of vertebrae in primates. Proc. Am. Phil. Soc. 89, 601-626.

Schultz, A.H. 1960. Einige Beobachtungen und Maße am Skelett von *Oreopithecus*: im Vergleich mit anderen catarrhinen Primaten. Z. Morph. Anthropol. 50, 136–149.

Schultz, A. 1961. Vertebral column and thorax. S. Karger.

Shapiro, L.J. 1993. Functional morphology of the vertebral col- umn in primates. In: Gebo D. (Ed.) Postcranial adaptation in nonhuman primates. DeKalb: Northern Illinois University Press. p 121–149.

Shapiro, L.J. 2007. Morphological and functional differentiation in the lumbar spine of lorisids and galagids. Am. J. Phys. Anthropol. 69,86–102.

Shapiro, L.J., and Simons, C. 2002. Functional aspects of strepsirrhine lumbar vertebral bodies and spinous processes. J. Hum. Evol. 42:753–783.

Shapiro, L.J., Seiffert, C., Godfrey, L., Jungers, W.L., Simons, E., Randria, G. 2005. Morphometric analysis of lumbar vertebrae in extinct Malagasy strepsirrhines. Am. J. Phys. Anthropol. 128, 823-839.

Shaw, C.N., Ryan, T.M. 2012 Does skeletal anatomy reflect adaptation to locomotor patterns? Cortical and trabecular architecture in human and nonhuman anthropoids. Am. J. Phys. Anthropol. 147, 187–200.

Siegel, M., 1970. The tail, locomotion and balance in mice. Am. J. Phys. Anthropol. 33, 101-102.

Silva, M., and Downing, J.A. 1995. CRC handbook of mammalian body masses. CRC press Boca Raton, Florida.

Simpson, S.W., Quade, J. Levin, N.E., Butler, R. et al. 2008. A female *Homo erectus* Pelvis from Gona, Ethiopia. Science 322, 1089-1092.

Slijper, E. 1946. Comparative biologic-anatomical investigations on the vertebral column and spinal musculature of mammals. Verh. K. Ned. Akad. Wet. Afd. Natuurkd. Tweede Reeks 42:1–128

Smit, T.H. 2002. The use of a quadruped as an in vivo model for the study of the spine-biomechanical considerations. European Spine Journal 11, 137–144.

Smit, T.H., Odgaard, A., and Schneider, E. 1997. Structure and function of vertebral trabecular bone. Spine 22, 2823-2833.

Smith, R., and Jungers, W. 1997. Body mass in comparative primatology. J. Hum. Evol. 32, 523–559.

Sneed, E.D., and Folk, R.L. 1958. Pebbles in the lower Colorado River, Texas, a study in particle morphogenesis. J. Geol. 66, 114-150.

Sode, M., Burghardt, A. J., Nissenson, R. A., & Majumdar, S. (2008). Resolution dependence of the non-metric trabecular structure indices. Bone. 42, 728-736.

Sokal. R., Rohlf, S. 1995. Biometry. New York: WH Freeman.

Spoor, C.F., Zonneveld, F.W., and Macho, G.A. 1993. Linear measurements of cortical bone and dental enamel by computed tomography: applications and problems. Am. J. Phys. Anthropol. 91, 469–484.

Stevens, N., Wright, K., Covert, H., Nadler, T., 2008. Tail postures of four quadrupedal leaf monkeys (*Pygathrix nemaeus, P. cinerea, Trachypithecus delacouri* and *T. hatinhensis*) at the Endangered Primate Rescue Center, Cuc Phuong National Park, Vietnam. Viet. J. Primatol 2, 13-24.

Stern, Jr., J.T., and Susman, R. 1983. The locomotor anatomy of *Australopithecus afarensis*. Am. J. Phys. Anthropol. 60, 279–317.

Straus, W.L. 1963. The classification of *Oreopithecus*. In: Washburn, S.L. (Ed.), Classification and Human Evolution. Aldine Pub. Co., Chicago. pp, 146–177.

Su, A., Wallace, I.J., Nakatsukasa, M. Trabecular anisotropy and orientation in an Early Pleistocene hominin talus from East Turkana, Kenya. J. Hum. Evol. 64, 667-677.

Sueur, C., Salze, P., Weber, C., and Petit, O. 2011. Land use in semi-free ranging Tonkean macaques *Macaca tonkeana* depends on environmental conditions: A geographical information system approach. Zool. 57:1.

Susman, R.L. 2004. *Oreopithecus bambolii*: an unlikely case of hominid like grip capability in a Miocene ape. J. Hum. Evol. 46, 105–117.

Susman, R.L. 2005. *Oreopithecus*: still apelike after all these years. J. Hum. Evol. 49, 405–411.

Swartz, S.M., Parker, A., Huo, C. 1998. Theoretical and empirical scaling patterns and topological homology in bone trabeculae. J. Exp. Biol. 201, 573–590.

Thompson, D.W. 1919. On Growth and Form. University Press, Cambridge.

Tito, G. 2008. New remains of *Eremotherium laurillardi* (Lund, 1842)(Megatheriidae, Xenarthra) from the coastal region of Ecuador. Journal of South American Earth Sciences 26, 424–434.

Tojima, S. 2012. Tail length estimation from sacrocaudal skeletal morphology in catarrhines. Anthropological Science.

Turner, C..H. 1992. On Wolff's law of trabecular architecture. J. Biomech. 25,1–9.

Turner, C.H. 1992. Functional determinants of bone structure: beyond Wolff's law of bone transformation. Bone 13, 403-409.

Tuttle, R.H., Watts, D.P. 1985. The positional behavior and adaptive complexes of *Pan gorilla*. In: Kondo S, (Ed.). Primate morphophysiology, locomotor analyses, and human bipedalism. pp 261–288.

Ulrich, D., van Rietbergen, B., Laib A, and Ruegsegger P. 1999. The ability of three-dimensional structural indices to reflect mechanical aspects of trabecular bone. Bone 25:55–60.

Ulrich, D., Binet, M.G., Sanecki, M.G., and Kieffer, S.A. 1980. Quantitative assessment of the lumbar spinal canal by computed tomography. Radiol. 134, 137–143.

Wada, N., Hori, H., Tokuriki, M., 1993. Electromyographic and kinematic studies of tail movements in dogs during treadmill locomotion. J. Morph. 217, 105-113.

Wainwright, S. A., W. D. Biggs, J, D. Currey, and J. M. Gosline. 1976. Mechanical Design in Organisms. Princeton University Press, Princeton, NJ.

Walker, A.C. 1974. Locomotor adaptations in past and present prosimian primates. In: Jenkins, F.A. (Ed.) Primate locomotion. pp 349–381.

Walker, A.C., and Pickford, M. 1983. New postcranial fossils of *Proconsul africanus* and *Proconsul nyanzae*. In Ciochon, R.L. and Corruccini, R.S. (Eds.) New interpretations of ape and human ancestry. New York : Plenum Press, pp. 325–351.

Walker A.C. and Leakey R. 1993. The postcranial bones. In: Walker, A. and Leakey, R. (Eds.) The Nariokotome *Homo erectus* Skeleton. Harvard University Press, Cambridge. pp, 95–160.

Walker, C., Vierck, C., and Ritz, L. 1998. Balance in the cat: role of the tail and effects of sacrocaudal transection. Behav. Brain. Res. 91, 41–47.

Wallace, I.J., Tommasini, S.M., Judex, S., Garland Jr., T., Demes, B., 2012. Genetic variations and physical activity as determinants of limb bone morphology: an experimental approach using a mouse model. Am. J. Phys. Anthropol. 148, 24-35.

Ward, C.V. 1993. Torso morphology and locomotion in *Proconsul nyanzae*. Am. J. Phys. Anthropol. 92, 291–328.

Ward, C.V., 1997. Functional anatomy and phyletic implications of the hominoid trunk and hindlimb. In: Begun, D.R., Ward, C.V., Rose, M.D. (Eds.), Function, Phylogeny, and Fossils: Miocene Hominoid Evolution and Adaptations. Plenum Press, New York, pp. 101-130.

Ward, C.V., 2007. Postcranial and locomotor adaptations of hominoids. In: Henke, W., Tattersall, I. (Eds.), Handbook of Paleoanthropology. Primate Evolution and Human Origins, vol. 2. Springer, Heidelberg, pp. 1011-1030.

Ward, C.V., Walker, A., Teaford, M.F., 1991. Proconsul did not have a tail. J. Hum. Evol. 21, 215-220.

Ward, C.V., Walker, A., Teaford, M.F., 1999. Still no evidence for a tail in Proconsul heseloni. Am. J. Phys. Anthropol. 28, 273.

Ward, C.V., Walker, A., Teaford, M., and Odhiambo, I. 1993. Partial skeleton of *Proconsul nyanzae* from Mfangano Island, Kenya. Am. J. Phys. Anthropol. 90,77–111.

Ward, C.V. 1997. Functional anatomy and phyletic implications of the hominoid trunk and hindlimb. In: Begun D, Ward C, Rose M, editors. Function, Phylogeny, and Fossils: Miocene Hominoid Evolution and Adaptations. New York, Plenum. pp 101–130.

Weidenreich, F. 1913. Uber das Huftbein und das Becken der Primaten und ihre Umformung durch den aufrechten Gang. Anat. Anz. 44, 497–513.

Weisl, H. 1954. The ligaments of sacroiliac joint examined with their particular reference to function. Acta. Anat. 20, 201–213.

Welch, J., Turner, C., Devareddy, L., Arjmandi, B., and Weaver, C. 2008. High impact exercise is more beneficial than dietary calcium for building bone strength in the growing rat skeleton. Bone. 42, 660–668.

Whitcome, K. 2006. Obstetric load and the evolution of human lumbopelvic sexual dimorphism. Ph.D. Dissertation. The University of Texas at Austin, Austin, TX.

Wilke, H.J, Kettler, A., and Claes, L.E. 1997. Are sheep spines a valid biomechanical model for human spines? Spine 22, 2365-2374.

Wilson, D.R., 1972. Tail reduction in Macaca. In: Tuttle, R. (Ed.), The Functional and Evolutionary Biology of Primates. Aldine Press, New York, pp. 241-261.

Wolff, J. 1892. The law of bone transformation. Berlin: Hirschwald.

Woon, J.T., and Stringer, M.D. 2011. Clinical anatomy of the coccyx: A systematic review. Clin. Anat. 25,158–167.

Wunderlich, R..E., Walker, A., Jungers, W.L. 1999. Rethinking the positional repertoire of *Oreopithecus*. Am. J. Phys. Anthropol. S108, 528.

Youlatos, D. 1999. Tail-use in capuchins. Neotrop. Prim. 7, 16–20.

Youlatos, D. 2003. Osteological correlates of tail prehensility in carnivorans. J. Zool. 259,423–430.

Young, N.M. 2003. A reassessment of living hominoid postcranial variability: implications for ape evolution. J. Hum. Evol. 45, 441–464.

Zapfe, H. 1958. The skeleton of Pliopithecus (Epipliopithecus) vindobonensis (Zapfe and Hürzeler). Am. J. Phys. Anthropol. 16, 441–457.

Zapfe, H. 1960. A new fossil anthropoid from the Miocene of Austria. Curr. Anthropol. 1, 428–429.